UNIVERSITY OF
ARIZONA LIBRARY
Documents Collection
MAY 22 1964

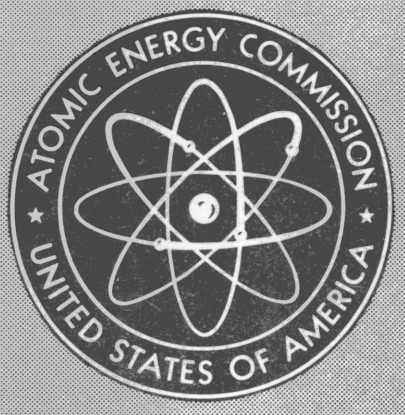

GEAP-3971

VBWR STABILITY TEST REPORT

June 1963

Atomic Power Equipment Department
General Electric Company
San Jose, California

metadc101077

UNITED STATES ATOMIC ENERGY COMMISSION • DIVISION OF TECHNICAL INFORMATION

LEGAL NOTICE

This report was prepared as an account of Government sponsored work. Neither the United States, nor the Commission, nor any person acting on behalf of the Commission:

A. Makes any warranty or representation, expressed or implied, with respect to the accuracy, completeness, or usefulness of the information contained in this report, or that the use of any information, apparatus, method, or process disclosed in this report may not infringe privately owned rights; or

B. Assumes any liabilities with respect to the use of, or for damages resulting from the use of any information, apparatus, method, or process disclosed in this report.

As used in the above, "person acting on behalf of the Commission" includes any employee or contractor of the Commission, or employee of such contractor, to the extent that such employee or contractor of the Commission, or employee of such contractor prepares, disseminates, or provides access to, any information pursuant to his employment or contract with the Commission, or his employment with such contractor.

This report has been reproduced directly from the best available copy.

Printed in USA. Price $4.50. Available from the Office of Technical Services, Department of Commerce, Washington, D. C. 20230

USAEC Division of Technical Information Extension, Oak Ridge, Tennessee

GEAP-3971
REACTOR TECHNOLOGY
(TID-4500, 28th Ed.)

VBWR STABILITY TEST REPORT

By

Members of
Engineering Development

June 1963

U. S. Atomic Energy Commission
Contract AT(04-3)-189
Project Agreement 11

ATOMIC POWER EQUIPMENT DEPARTMENT

GENERAL ELECTRIC

SAN JOSE, CALIFORNIA

TABLE OF CONTENTS

PAGE

SECTION I

INTRODUCTION 1

SECTION II

SUMMARY 6

A. Rod Oscillator Tests 7

1. Power Responses with Well-Damped Loop Hydrodynamics 7

2. Power and Flow Responses with Under-Damped Hydraulic Natural Circulation and Forced Circulation By-Pass Flow 9

B. Transient Tests 10

C. Steady-State Tests 10

D. Conclusions 12

1. Absolute Stability 12

2. Operational Noise and its Effect on BWR Stability 14

SECTION III

OBJECTIVES OF VBWR STABILITY STUDIES 16

1. VBWR Stability Data 17

2. Test Data Analysis 17

a. Objectives of this Report 17

b. Objectives of Fuel Cycle Stability Task 18

1. Model Analysis 19

2. Hydrodynamic Model Evaluation by Means of Stability Loop 21

3. Model Improvement 21

4. Application to Other Reactors 21

SECTION IV

TEST FACILITY 27

Coolant Circulation 27

Core Composition and Power Distribution 27

Control Rods 28

Instrumentation 28

SECTION V

TEST PROCEDURES 31

TABLE OF CONTENTS (Cont'd)

PAGE

SECTION VI

DATA REDUCTION 32

A. Instrument Calibration 32

B. Frequency Response of Instrumentation 33

C. Experimental Accuracy 34

D. Data Analysis Use of a Band Pass Filter Network 35

SECTION VII

TEST RESULTS 36

VII-A Steady-State Noise 39

A-1 Operational Parameters 39

A-2 Neutron Flux Traces 48

Phase Relationships 48

Amplitudes 49

Spatial Flux Study 49

Character of Traces 51

Frequency Analysis of Steady-State Recordings 52

A-3 Flow Trace Analysis 79

Phase Relationships 80

Fundamental Frequencies 80

Amplitudes 80

Character of Traces 81

Effect of Flow Changes and Orificing 85

Band Pass Filter Output Spectra for Steady-State Runs 87

Steady-State Flow Analysis Discussions and Conclusions 88

VII-B Rod Oscillator Test Analysis 100

1. Control Rod Responses from Pen Recorder Traces 101

2. Method of Data Reduction 106

a. Rod Oscillator Flux Response Description 107

b. Band Pass Filter Techniques 109

c. Experimental Amplitude and Phase Relationships 112

TABLE OF CONTENTS (Cont'd)

		PAGE
VII-B	Rod Oscillator Test Analysis (Cont'd)	
	3. Data Analysis and Results	114
	A. Neutron Flux from ΔK Transfer Functions	114
	1. Reactor System Relationship	114
	2. Rod Worth Normalization	118
	3. Power Reactivity Feedback Determination	122
	4. Power Transfer Function Curve Interpretation	125
	5. Gain Margin Determination	128
	6. Steady-State Peak-to-Peak Flux Noise and System Stability	132
	B. Core Coolant Flow from ΔK Transfer Functions	133
	4. Conclusions and Summary of Results	135
VII-C	Consideration of Noise Phenomena	153
	1. Itemized Observations of Noise Properties from 15 MWt Runs	155
	2. Relationship of Steady-State Flux Noise to Rod Oscillator Measurements	156
	3. Measurements of Possible Flux Noise Excitations	157
	4. A Propagation of Disturbance Theory for Noise Responses of a Boiling Water Reactor	158
	5. VBWR Data Compared to Theory	160
	a. Variation of Frequencies with Flow	160
	b. Noise Amplitude Variation with Flow	161
	c. Increases in Amplitude of High Frequency Flux Noise with Elevation in Core	163
	d. Effect of Orificing in High Frequency Noise	163
	e. No Phase Relationship Seen Between Flows and Fluxes	164
	6. Summary of Interpretation of Noise by the Propagation of Disturbances	164
VII-D	Transient Tests	168
	Test Description and Test Parameters	168
	Results	170

TABLE OF CONTENTS (Cont'd)

PAGE

SECTION VIII

COMPARISON TO PREDICTED RESULTS 175

A. Pre-Test Analysis of the VBWR Stability Tests 175

1. The Analytical Model 176

Reactor Kinetics Simulation 176
Fuel Element Thermal Time Constant Simulation 177
The Hydrodunamics Model Simulation 177
Void Reactivity Model Simulation 178

2. Analytical Model Solution 179

Rod Oscillator Test (Reactor Power and Flow Transfer Function) 179

Noise (Spectral Power and Flow Density) 180

Pre-Test Analysis Prediction 180

B. Comparison of Analysis and Test Results 186

1. Pre-Test Predictions and Experimental Results 186

2. Test Observation and the Analytical Model 191

3. Predicted and Measured Power Transfer Functions 198

a. High Flow Forced Circulation 198

b. Low Flow Forced Circulation - Loop Hydrodynamics 199

c. Low Flow Forced Circulation - Parallel Channel Hydrodynamics 201

d. Natural Circulation 202

SECTION IX

FUTURE WORK 218

A. Improved Data Retrieval 219

B. Improved Analysis of VBWR Test Points 220

C. Data Contributing to Model Analysis Improvement - Derived From APED Hydraulic Stability Loop 222

D. Improved Analytical Model 223

E. Generalization to the Design of Large Plants 225

TABLE OF CONTENTS (Cont'd)

PAGE

APPENDIX A

TEST FACILITY 227

1. Reactor System 227
2. Core Composition and Characteristics 229
3. Rod Oscillator System 236
   a. General 236
   b. Description of Equipment 236
      1. Normal Operation and Scram Control 237
      2. Rod Oscillator Mechanism 237
      3. Rod Oscillator Control System 238
   c. Pre-Test Operational Check-Out 239
4. Instrumented Assemblies 240
5. Readout Instrumentation 242
   a. Readout System Description 242

APPENDIX B

TEST PROCEDURES 262

A. Overall Description 262
B. Choice of Test Conditions 263
C. Steady-State Tests 264
D. Rod Oscillator Tests 264
E. Transient Tests 264

APPENDIX C

DATA REDUCTION 265

1. Instrument Calibration 265
   a. Initial Transducer Calibration 265
   b. Maintenance of Calibration 266
   c. Calibration Equation 270

TABLE OF CONTENTS (Cont'd)

PAGE

Instrument Calibration (Cont'd)

d. Special Calibration Problems 272
1. In-Core Flowmeters 272
2. In-Core Ion Chambers 272
3. In-Core Thermocouples 273
4. Fuel and Riser Pressure Drop 273
5. Overall Channel Gains 273
6. Sixty-Cycle Filter 274

2. Frequency Response of Instrumentation 274
a. Readout System 274
b. Transducers 276

3. Experimental Accuracy 276
a. Approach to Error Analysis 276
1. Personal Errors 276
2. Fixed Errors 277
3. Accidental Errors 278
b. Estimating Errors Propagated Through Readout System 278
c. Frequency Analysis 282

4. Data Analysis Use of a Band Pass Filter Network 285
a. Equipment 285
b. Procedure 286
1. Steady-State Data 286
2. Rod Oscillator Data - Amplitude 290
3. Rod Oscillator Data - Phase Shift 291
c. Calibrations 291
1. Band Pass Filter Calibration 292
a. Gain vs. Frequency Calibrations 292
b. Filter Bandwidth 293
c. Transient Response 294
2. Chart Recorder Calibration 295
3. Integrating Amplifiers 295
d. Time Requirements 295

TABLE OF CONTENTS (Cont'd)

PAGE

APPENDIX D

PROPAGATION OF A FLOW DISTURBANCE 323

APPENDIX E

STATISTICAL AND MATHEMATICAL ASPECTS OF DATA ANALYSIS 327

1. Objective 327
2. Definitions 327
3. Methods of Approach to Mathematical Handling of Data 328
   a. Band Pass Filter 334
   b. Digital Auto Correlation Code 336
   c. Basis for Further Revisions in Digital Auto Correlation Codes 338
   d. Digital Filtering 341
   e. Timed Circuit Analogue Filter 342
   f. Fourier Spectrum Analyzer 342
4. Conclusions 344

APPENDIX F

INDEX OF INSTRUMENT HOOK-UPS AND REACTOR OPERATING PARAMETERS FOR FUEL CYCLE STABILITY TESTS 347

NOMENCLATURE 351

REFERENCES 353

LIST OF ILLUSTRATIONS

FIGURE	TITLE	PAGE
IV-1	Schematic Diagram - Reactor Circulation System	30
VII-1	External Flux Peak-to-Peak vs. Flow for Forced Circulation	43
VII-2	External ($\mu\mu$A) Flux Peak-to-Peak vs. Flow for Forced Circulation	44
VII-3	External Flux Peak-to-Peak Percentage Variation vs. Power (Natural Circulation Case)	45
VII-4	Instrumented Assembly Flow vs. Power	46
VII-5	Instrumented Assembly Flow vs. Reactor Flow	47
VII-6	Run 15-1-1,2 Forced Circulation 15 MWt - 20,000 gpm	57
VII-7	Run 15-9-1a,1b Forced Circulation 15 MWt - 4,000 gpm	58
VII-8	Run 15-19-2,3 Forced Circulation 15 MWt - 4,400 gpm	59
VII-9	Run 15-16-1,2 Forced Circulation, Baffles Open 15 MWt - 4,000 gpm	60
VII-10	Run 15-18-1,2 Natural Circulation 15 MWt - 4,300 gpm	61
VII-11	Forced Circulation Run 15-1-2, 20,000 gpm, Steady-State Noise	62
VII-12	Forced Circulation Run 15-1-4-15, 20,000 gpm, Rod Oscillator	63
VII-13	Natural Circulation Run 15-18-2, Steady-State Noise	64
VII-14	Natural Circulation Run 15-18-2, Rod Oscillator	65
VII-15	Forced Circulation Run 15-19-3, Steady-State Noise	66
VII-16	Forced Circulation Run 15-19-4-15, Rod Oscillator	67
VII-17	Forced Circulation, Baffles Open, Run 15-16-2, Steady-State Noise	68
VII-18	Forced Circulation, Baffles Open, Rod Oscillator	69
VII-19	Forced Circulation Run 15-19-1b, 4,000 gpm, Steady-State Noise	70
VII-20	Forced Circulation Run 15-9, 4,000 gpm, Rod Oscillator	71
VII-21	Forced Circulation Run 0-2-2, 10,000 gpm, Steady-State Noise	72
VII-22	Forced Circulation Run 0-2, 10,000 gpm, Rod Oscillator	73
VII-23	Forced Circulation Run 15-11-36, 2,600 gpm Steady-State	74
VII-24	Forced Circulation Run 15-3, 2,600 gpm, Rod Oscillator	75
VII-25	Forced Circulation Run 15-3-14b, 10,000 gpm, Steady-State	76
VII-26	Comparison of Noise Spectrum at Three Elevations in Core and at External Ion Chamber	77

LIST OF ILLUSTRATIONS (Cont'd)

FIGURE	TITLE	PAGE
VII-27	Comparison of Noise Spectrum for Neutron Flux at Different Flow Conditions	78
VII-28	Flow-Pump Head Relationship for VBWR Recirculation Pumps 1 and 2	93
VII-29	Steady-State Flow Noise Effect of Flow, Orificing on Noise	94
VII-30	Steady-State Flow μμA Run 15-1	95
VII-31	Steady-State Flow μμA Run 15-19	96
VII-32	Flow Spectra Run 15-16	97
VII-33	Steady-State Flow μμA Run 15-18	98
VII-34	Frequency Comparison	99
VII-35	Natural Circulation, Rod Oscillator Test, Run 15-18-7 0.5 cps Record Data Trace	141
VII-36	Natural Circulation, Rod Oscillator Test, Control Data Trace	142
VII-37	Natural Circulation, Rod Oscillator Test, Run 15-18-6 Control Data Trace	143
VII-38	Band Pass Analysis of Natural Circulation Rod Oscillator Test, Run 15-18-4, 0.05 cps	144
VII-39	Logic Block Diagram for Response of the VBWR	114
VII-40	Zero Power Reactor Kinetics Function	145
VII-41	Example: Feedback Function for Reactor Kinetics	116
VII-42	Dimensionless Frequency Characteristic BWR Power Transfer Function	117
VII-43	Rod Oscillator Response for Natural Circulation Test Series	146
VII-44	Normalized Rod Oscillator Response Curve for Natural Circulation Test Series	147
VII-45	Normalized Rod Oscillator Response Curve for Forced Circulation, Baffle Doors Open, Test Series	148
VII-46	Normalized Rod Oscillator Response Curve for Valve-Controlled, Forced Circulation, 4,000 gpm Test Series	149
VII-47	Normalized Rod Oscillator Response Curve for Speed-Controlled, 4,000 gpm Test Series	150
VII-48	Normalized Rod Oscillator Response Curve for 20,000 gpm, Forced Circulation Test Series	151
VII-49	Power Transfer Function of Test Series 15-9	152
VII-50	Power Transfer Function of Test Series 15-1	153

LIST OF ILLUSTRATIONS (Cont'd)

FIGURE	TITLE	PAGE
VII-51	Noise Comparison 20,000, 4,000, and Natural Circulation Conditions - Control data Trace	154
VII-52	Comparison of Theoretical Transit Times with Experimental Points for VBWR at 15 MWt	166
VII-53	Density Change Response to Channel ΔP Change	167
VII-54	Response of the System to Recirculation Flow Transient	173
VII-55	Nomenclature of Transient	174
VIII-1	Logic Model for VBWR Stability Analysis	175
VIII-2	Frequency Response of Inlet Water Velocity (V*) to Cyclical Variation in ΔK	210
VIII-3	Frequency Response of Reactor Flux (N*) to Cyclical Variation in ΔK	211
VIII-4	Frequency Response of Reactor Flux (N*) to Cyclical Variation in ΔK - Effect of Inlet Orificing Upon Parallel Flow Channel Stability	212
VIII-5	Frequency Response of Reactor Flux (N*) to Cyclical Variation in ΔK - Effect of Power and Core Flow Upon Parallel Flow Channel Stability	213 214
VIII-6	Reactor Power Transfer Function Comparison of Prediction With Experiment High Flow - Forced Circulation	
VIII-7	Reactor Power Transfer Function Comparison of Prediction With Experiment Low Flow - Forced Circulation Loop Hydrodynamics	215
VIII-8	Reactor Power Transfer Function Comparison of Prediction With Experiment Low Flow - Forced Circulation, Parallel Channel Hydrodynamics	216
VIII-9	Reactor Power Transfer Function Comparison of Prediction With Experiment - Natural Circulation	217
A-1	VBWR Reactor Vessel Arrangement	244
A-2	VBWR Vessel Cross Section	245
A-3	Typical Fuel Assembly	246
A-4	Core Arrangement for VBWR Tests	247
A-5	Core Orificing Configuration	248
A-6	Rod Oscillator System	249

LIST OF ILLUSTRATIONS (Cont'd)

FIGURE	TITLE	PAGE
A-7	Control Rod System Block Diagram	250
A-8	Control Rod System Schematic	251
A-9	Control Rod Oscillator Mechanism	252
A-10	Assembly Drawing for Instrumented Fuel Assemblies	253
A-11	Instrumented Assembly Showing Fuel Bundle and Instrument Probe Before Assembly	254
A-12	Lower Tie Plate Instrumented Assembly for Fuel Bundle	255
A-13	Lower Portion of Instrumented Probe for Instrumented Assembly	256
A-14	Upper Portion of Instrumented Probe for Instrumented Assembly	257
A-15	Instrumented Probe Showing Static Pressure Taps	258
A-16	Upper End of Instrumented Assembly Channel Showing Detail of Lock	259
A-17	Schematic Diagram, Instrumentation Fuel Cycle Stability Experiment	260
A-18	Placement of Instrumentation Components in VBWR Control Room	261
C-1	Calibration of Pace Reluctance Type Differential Pressure Transducers - Reactor Pressure Calibration	297
C-2	Calibration of Pace Reluctance Type Differential Pressure Transducers - Steam Flow Transducer	298
C-3	Calibration of Pace Reluctance Type Differential Pressure Transducers - Feedwater Flow Transducers	299
C-4	Calibration of Pace Reluctance Type Differential Pressure Transducers - Recirculation Pump No. 1	300
C-5	Calibration of Pace Reluctance Type Differential Pressure Transducers - Recirculation Pump No. 2	301
C-6	Pressure Drop Test Results - Instrumented Nosepiece Flowmeter ΔP Assemblies	302
C-7	Pressure Drop Across Fuel Bundles of Instrumented Assembly	303
C-8	Pressure Drop Across Fuel Bundle and Riser Instrumented Assemblies	304
C-9	Calibration of the Turbine Type Flowmeter	305
C-10	Calibration of High Power Density Research and Development Program In-Core Flowmeters	306

LIST OF ILLUSTRATIONS (Cont'd)

FIGURE	TITLE	PAGE
C-11a,b,c	Overall Channel Gain Calibration (11a through 11c)	307-309
C-12	Bias Voltage at Input Terminals of Ampex Recorder	310
C-13	Attenuation of 60-Cycle Filter	311
C-14	Estimate of Frequency Response of Brush Recorders	312
C-15	Responses of Potter Turbine Type Flowmeters	313
C-16	Responses of Recirculation Flow Transducers	314
C-17	Analog Band Pass Frequency Analyzer	315
C-18	Typical Band Pass Filter Recordings for Steady-State Analysis	316
C-19	Typical Band Pass Filter Recordings for Rod Oscillator Amplitude Analysis	317
C-20	Phase Shift Analysis Circuit	318
C-21	Band Pass Filter Calibration Circuit	319
C-22a,b	Band Pass Filter Calibration Curves	320-321
C-23	Band Pass Filter Bandwidth	322
C-24	Band Pass Filter Transient Response Circuit	294
E-1	Schematic - Fourier Spectrum Analyzer	346

LIST OF TABLES

TABLE	TITLE	PAGE
I-1	Synopsis of VBWR Stability Reports	4
III-1	Objectives of Present Report	22
III-2	Objectives of Fuel Cycle Stability Task	24
VII-1	Summary of Reactor Operating Conditions for 5 Runs	37
VII-2	Detailed Data as Shown in Figures VII-6 to VII-10	52
VII-3	Ion Chamber and Band Pass Output Spectra Locations	54
VII-4	Observations Obtained From Time Trace Analysis Runs 15-1, 15-18, 15-19	82
VII-5	Relative Flow Restraints for Calculated 20 MW, 7650 gpm Run	85
VII-6	Calculated System and Two-Phase Hydraulic Resonant Frequencies	89
VII-7	Analyzed Rod Oscillator Runs	101
VII-8	Rod Worth Determinations From The Rod Oscillator Data	120
VII-9	Feedback Gain Determinations	124
VII-10	Stability Gain Margin Determinations	131
VII-11	Comparison of Peak-to-Peak Flux Noise and System Gain Margins	132
VII-12	Quantitative Rod Oscillator Test Results	140
VII-13	Table of Transients	169
VII-14	Recirculation Flow Transient - Run 15-8-20, Forced Circulation, Baffles Closed	172
VIII-1	Properties of Delayed Neutrons	176
VIII-2	Pre-Test Analysis Results	207
A-1	Tabulation of Fuel Element Changes to Grid Plan for VBWR Stability Test	230
A-2	Characteristics of Fuel	231
A-3	Summary of Core Physics Data	232
A-4	Control Rod Worth for Control Rod #7	234
A-5	Operating Limits for Test Core	235

LIST OF TABLES (Cont'd)

TABLE	TITLE	PAGE
C-1	Calibration of Turbine Type Flowmeters	267
C-2	Summary of Transducer Calibrations	268
C-3	Manufacturer's Specifications for Kintel Amplifiers (Model 112-A)	275
C-4	Estimate of Uncertainty Intervals for Parameters	284
E-1	Methods - Developed and Methods - Under Study	329
E-2	Comparison of Properties of Various Data Handling Systems for Time Series	330

ACKNOWLEDGEMENT

Contributors to this report

J. M. CASE
W. H. COOK
M. R. HACKNEY
V. E. HAZEL
J. A. HODDE
C. L. HOWARD
R. O. NIEMI
J. R. RINDE
H. J. SCHNEIDER
C. L. SWAN
T. TILLINGHAST

SECTION I

INTRODUCTION

The present generation of boiling water reactors has exhibited operation with reasonably low noise levels, good transient response characteristics and no signs of undamped oscillatory operation. At this point, the BWR may be considered to have good stability characteristics. However, it is not obvious that future reactors operating with large amounts of reactivity invested in voids and with minimal coolant flows would perform as well. Stability analysis and the VBWR stability data indicate that less stable operation will be obtained under these conditions.

Improvement in economics of power generation from nuclear reactors consists, in part, of improving reactor performance. The improvement here is the result of increased power generation for a given size reactor vessel, pumps, piping, etc. Under these conditions, the reactor system stability can be shown to be reduced unless design changes are made.

The question of how reactor system stability and transient response is to be determined for the more complex cases which are mentioned above has become of a great deal of interest to designeer and theoretician. ANL-6561[1] states that prediction of stability from a wholly theoretical approach is difficult to attain because of the complexity of the system and the inability to describe the physical events taking place. This experiment and the accompanying analysis address themselves to the objective of determining the ability of the theory to first describe the events taking place in the VBWR stability tests. A second objective is to obtain by well-instrumented tests the physical events that are actually taking place, and to provide a basis for a more generally useful and improved analytical model. Other associated objectives are given in Section III.

The test program funding for preparation of this report and special reactor test instrumentation, including instrumented fuel assemblies and readout instruments, were supported by the AEC Fuel Cycle Development Program. Table I-1 shows a synopsis of the reporting of elements of the stability task of this program. Prior

to the testing, the reactor had undergone a modification program underwritten by APED. The modification included the addition of a number of features desirable to this test program.

The power stability tests in VBWR provide some unique developments to the development of power stability in boiling water reactors. Among these are:

1. The tests were oriented toward a wide span of parameters to obtain a good measure of analytical model performance. The BWR was especially suited to this type of investigation.
2. Forced and natural circulation modes of testing were provided.
3. Fuel tested was oxide fuel with geometry (and hence, thermal responses) typical of large power reactors.
4. The value of various test methods for stability were compared, including control rod oscillation, transient tests, and steady-state noise analysis.
5. In-core instrumentation was used extensively for the first time to obtain a comparison of average and local responses.

Results of these tests, as presented here, are based upon analytical methods which were available at the time the test was conducted, with a few exceptions. It is clear that an improved treatment could be made, and this is planned in the advanced analysis program discussed in Section IX.

Conclusions are made which show areas where experiment and analysis agree well. There are other areas where they do not agree, and additional work on the analytical model is indicated. The primary area for future work is shown to be of particular importance to the improvement of theory for high performance reactors.

BWR power improvement can be seen to be aided in several ways by this work. For example:

a. Power increases can be made in low flow rate forced circulation and in natural circulation reactors with assurance that the analytical model determines the stability and transient responses well.

b. Noise measurements based upon amplitude are shown to be unreliable as measures of stability and should not be used as a basis for operation of a reactor. Additionally, orificing is shown to reduce the noise level significantly.

c. The combination of control rod oscillation testing and magnetic tape recording provides a sound basis for examining the stability of an operating reactor, and for up-rating plants already in operation.

d. An area of concern in prediction of stability is shown to exist in high flow (say, above 4 fps inlet velocity) reactors, and further work is required. Analytical model work should be pursued in several areas to improve this.

TABLE I-1

SYNOPSIS OF VBWR STABILITY REPORTS

REPORT	CONTENT
GEAP-3709 - 3rd Quarterly Progress Report. March 1961	Preliminary tests in the VBWR are discussed, along with preliminary data analysis and stability and transient analysis ideas.
GEAP-3781 - 4th Quarterly Progress Report. June 1961	Instrumented assembly design is discussed.
GEAP-3794 - "Plan for the VBWR Stability Experiment", W. H. Cook, J. A. Hodde, C. L. Howard, R. O. Niemi. August, 1961.	Instrumentation, data analysis, and stability and transient response analysis for the experiment are described.
GEAP-3835 - 5th Quarterly Progress Report. September, 1961	Brief outline of proposed reactor stability tests is presented.
GEAP-3898 - 6th Quarterly Progress Report. December, 1961	Detailed calibration of the instrumented assemblies for VBWR test are described and the pre-test analysis of the test presented in detail.
GEAP-3935 - 7th Quarterly Progress Report. March, 1962	Several aspects of steady-state noise analysis are given from VBWR test results. An outline of hydraulic stability loop tests is presented.
GEAP-4048 - 8th Quarterly Progress Report. June, 1962	Steady-state flux noise results are presented, and a hypothesis concerning the possible effects of surface waves upon steady-state flux noise is stated. A mathematical theory is presented.
GEAP-4061 - "Water Surface Waves in Boiling Water Reactors". C.L. Howard, R. G. Hamilton. August, 1962	A demonstration test of the Cooper, Lonquet-Higgins(*) surface wave induced type pressure oscillations in a closed vessel is reported.

(*) "An Experimental Study in Standing Water Waves", R.I.B. Cooper and M.S. Lonquet-Higgins. Royal Society Proceedings. Ser. A, May 7, 1951.

TABLE I-1 (Cont'd)

SYNOPSIS OF VBWR STABILITY REPORTS

REPORT	CONTENT
GEAP-4094 - 9th Quarterly Progress Report. September, 1962	The possibility that the fine structure of AUTO code output is a manifestation of surface wave responses is discussed. The preliminary code for autocorrelation (AUTO) is presented along with tests of its accuracy. The steady-state noise characteristics of flow measurements are discussed in detail. Considerations of noise responses of flux and flow introduce a theory of the propagation of disturbances in channels. An approximation analysis of physical events is presented.
GEAP-4159 - 10th Quarterly Progress Report. December, 1962.	Initial hydraulic stability loop results are discussed and compared to analytical model predictions. Further work is reported on noise tests. These tests, conducted on a natural circulation reactor configuration, show no pressure oscillations of the type discussed in GEAP-4061 for the two-phase region.
GEAP-4215 - 11th Quarterly Progress Report. March, 1963.	A detailed presentation of transient tests of the hydraulic stability loop is presented.
GEAP-3971 - "VBWR Stability Test Report". June, 1963	Final summary report of reactor stability tests.
GEAP-4301 - 12th Quarterly Progress Report. June, 1963.	A preliminary discussion of power oscillation test results in the hydraulic stability test loop is presented. A discussion of the modified autocorrelation code, DART, is presented. An analysis of driving force spectrum for steady-state power is discussed, showing a "non-white" spectra with large amplitudes below 1 cps.

SECTION II

SUMMARY

An extensive series of power stability tests were conducted in the Vallecitos Boiling Water Reactor during November and December, 1961. Tests were conducted with both natural and forced circulation coolant flow over a wide range of flows and powers. Instrumentation, in addition to regular process instruments, included five (*) bundles with the provision for measuring inlet flow rate, neutron flux at three axial core locations, pressure drop, and temperature. Test data was recorded on oscillograph recorders and magnetic tape.

The VBWR was designed specifically for this type of experiment. A wide range of operating conditions is permitted with the same core. This range of conditions is possible in few, if any, other reactors. Tests were conducted as follows:

Forced Circulation	
Power MWt	1, 15, 20, 26
Flow gpm	2600 to 20,000
Pump Head Ft.	0 to 290
Core Bypass Leakage % of core flow	0 to 400
Natural Circulation	
Power MWt	9 to 20

Pre-test analysis of the dynamic responses were used to guide the experimental parametric study. Analysis was conducted by averaged parameter control system analysis techniques, and solutions were obtained on an analogue computer. The system representation includes reactor kinetics, fuel thermal responses, thermal-hydraulic responses, and void reactivity response. Thermal-hydraulic response analysis, which is unique to this investigation, consists of solutions of the equation of motion, continuity, energy and fluid transport time. These equations are evaluated representing the reactor as a single (point) node.

(*) Two belong to the Consumer High Power Density Research and Development Program.

The results discussed in Section VII of this report represent only a portion of the test data. Five runs which represent the best parametric comparison of theory and experiment that could be obtained from the data were chosen for analysis. The data analysis methods discussed represent the best analysis methods available at the beginning of the program. It is pointed out in Sections VII, VIII and IX that an advanced analysis program will produce much improved results, particularly in terms of exact representation of data and well-defined evaluation of the analytical model.

A. ROD OSCILLATOR TESTS

Rod oscillator tests were concluded to be the primary source of quantitative information from the VBWR tests. The pre-test analysis was conducted for two modes of thermal hydraulic oscillation, the oscillation of the entire loop, which will be designated as loop analysis, and the oscillation of thermal-hydraulically uncoupled parallel channels, or parallel channel analysis.

The shapes of the power transfer functions as measured by the in-core ion chambers and the external μμA flux monitor are essentially identical for a given test condition. The micro micro-ammeters were employed for the power response results discussed below.

1. Power Responses With Well-Damped Loop Hydrodynamics

Two reactor conditions were examined with well-damped forced circulation hydraulics, as shown below:

Power	Run No.	Flow	Comment
15 MWt	15-1	20,000 gpm	Maximum Forced Circulation
15 MWt	15-9	4,000 gpm	High Head, Valve Controlled Flow
15 MWt	15-19	4,000 gpm	Low Head, Speed Controlled Flow

The two 4,000 gpm runs produced almost identical transfer functions. This indicates that the system is well-damped even in the most frictionless condition that can be operationally produced with the forced circulation loop.

The experimental power transfer functions for the 4,000 gpm case were compared with loop analysis results. Analysis and test results agree well at this flow and indicate that the system responses are loop hydrodynamic responses for the low flow, closed circuit, forced circulation mode of operation. Increasing the flow rate from 4,000 gpm to 20,000 gpm, it was observed that the resonant frequency of the power transfer function increases with increasing flow. The flow dependence is, however, shown not to be large. The flow dependence predicted by pre-test analysis showed much larger changes in frequency. It is believed that a much refined evaluation of the differences between theory and experiment will come from the advanced data analysis program of Section IX. These differences are felt to be real and are thought to be accounted for by definite aspects of the theory.

The evaluation of the average channel responses, improvement of the void coefficient of reactivity determination, and the inclusion of a multi-node thermal-hydraulics representation in the analytical model are the primary factors which are believed to be an influence in aligning theory and experiment. The theory employed in the pre-test analysis does not provide a satisfying representation of the average channel, or average parameter to be employed in the analysis. An uncertainty remains as to the weighting of the different channels, and channel locations upon the measured power responses.

When power transfer functions for low flow rate, closed circuit, forced circulation runs and the corresponding high flow runs are compared, it is found that the low flow runs show resonance peaks which have large amplitudes compared to the high flow runs. This difference has been attributed to the difference in the void coefficient $\left(\frac{\Delta K}{\beta} \Big/ \frac{\Delta \bar{R}_g}{R_g}\right)$ at the two steam void levels resulting. The void coefficient of reactivity, it is concluded, is a major contribution to the stability and transient response characteristics.

No resonant hydraulics were observed in any of the closed flow circuit, forced circulation rod oscillator tests. The fluid dynamics for this

mode of operation was concluded to be exceedingly stable and damped for all cases investigated.

The amplitude of the recorded flow noise, compared to the amplitude of oscillation of flux during the rod oscillator runs, was always small. The ratio of the variation of flow to the variation of flux varied from 10 per cent during the low flow runs to 25 per cent at the 20,000 gpm test point. This points up the lack of response of the flow to rod oscillation.

The stability gain margin, the constant by which the experimental gain at 180° phase lag must be multiplied to equal one (condition for instability), is shown in Section VII to decrease with increasing core voids. Therefore, the stability of the VBWR system is seen to decrease with increasing voids. This is in accordance with the trend of the pre-test analysis.

The total power reactivity feedback gain and the void coefficient of reactivity both increase with increasing core voids. This is also in accordance with the trend of the theory.

2. Power and Flow Responses with Under-Damped Hydraulic Natural Circulation and Forced Circulation Bypass Flow.

Two reactor conditions were examined under these conditions:

a. Natural circulation within the reactor vessel at 15 MWt (Run 15-18).

b. Forced circulation at 4,000 gpm and 15 MWt with the baffle doors open (Run 15-16).

The natural circulation test (15-18) and the forced circulation with baffle doors open test (15-16) have power transfer functions of similar shape. It is reasoned that the baffle door passage is large enough so that bypass flows, either positive or negative, do not appreciably alter the effective single-phase gravity driving head which exists across the core in natural circulation.

Resonant hydraulics at 0.4 - 0.5 cps were exhibited within the reactor core for both the natural circulation test and forced circulation

test with baffles open. The flow resonance was demonstrated in two ways. First, by observation of the unorificed instrumented assemblies' turbine flow meter; and second, by the existence of a characteristic dip in the power transfer function. This dip is not seen in the closed loop, forced circulation tests, or by the pre-test analysis for loop-type mode of oscillation. It is shown, however, by the parallel channel analysis of the core channels. It is concluded that these two tests are examples of a reactor core with uncoupled parallel flow channels and strong nuclear coupling.

The effect of inlet orificing on fuel elements is to damp flow oscillations or response. This was observed from a comparison of the flow response of the unorificed and orificed instrumented assemblies during the natural circulation rod oscillator test.

B. TRANSIENT TESTS

Although the transient test techniques, in theory, should provide the same information that the rod oscillation tests provide, in the practical case this does not turn out to be true. Transient tests of the VBWR are considered to provide no essential information which is of value in quantitative determination of the power stability and transient responses of the VBWR. There are several reasons for this. The most basic one is due to the fact that one cannot practically retrieve much information from the response of a few seconds duration without introducing errors in data analysis and the mathematical description of events. More practically, two important limitations appeared from the fact that test conditions that demonstrated satisfactory stability and transient response characteristics emphatically could not be obtained, and that noise components served to obscure the results.

C. STEADY-STATE TESTS

1. It was observed that during steady-state operation, the amplitude of flux noise was relatively little effected by power level changes, but more effected by flow changes. Increasing the flow rate increased the amplitude of flow noise. This observation is of considerable

importance in that it points out that the largest amplitude noise occurs at the point adjudged to be most stable. Rod oscillation tests and theory both show that at low flows the reactor is nearer a point of instability than at the higher flow point. The amplitude of flow noise for forced circulation tests in the VBWR, therefore, shows an erroneous indication of stability. On this basis, the operational amplitude of oscillations is questionable as a source of stability information.

2. The peak frequencies obtained from the output of the band pass filter for flow and power do not show the same parametric change demonstrated by theory. Additionally, the responses are not well-defined functions of frequency. The frequency responses shown indicate that as the flow increases the peak frequency change of test observation is substantially less than expected from theory. A possible explanation of this deviation from theory, in terms of surface wave phenomena, was explored and reported separately (GEAP-4094 and GEAP-4061). Subsequent tests (GEAP-4159) have raised doubts about this possibility.

3. Steady-state flux oscillations at frequencies of one cycle per second and below were in-phase over the core. Oscillations at two cycles per second and above did not show a relationship between different core locations.

4. No inter-relationships can be seen in the fluxes and flows. This observation may be because of the spatial averaging of fluxes, or because of a combination of both spatial averaging of fluxes and the random responses of channels.

5. It was previously mentioned that flow oscillations in response to control rod oscillation were obtained near the resonant frequency of the system during natural circulation operation. At all other frequencies, the flow noise was far greater than the flow response to power. The flow response to power, even at the resonant frequency, was not to increase the amplitude of flow noise by adding a sympathetic flow component to power, but, rather, to cause the existing flow noise to become "ordered" with power variations. i.e., the

amplitude of the flow noise at this frequency was essentially the same during rod oscillations as it was just under the influence of steady-state noise. The foregoing observations lead to the following very important conclusion:

If the relatively large scale power disturbances induced by rod oscillation just barely caused a noticeable ordering of the flow noise, then the equivalent noise disturbances must be at least as large as, if not larger than, those power generated void disturbances which are caused by rod oscillation.

6. Steady-state flux noise recorded on in-core ion chambers varies in frequency content with position in the reactor. Ion chambers one-fourth of the way up from the bottom of the core and the external ion chambers both have very little high frequency noise (3 - 30 cps). In the high flow center region of the core, ion chambers located higher up in the core showed increasing high frequency content. In the outer, flow orificed regions of the core, very little high frequency flux noise was present. Core voids were very high and velocities very low in this region. Section VII discusses the consideration of propagation disturbances and shows that these responses could be explained by this concept.

7. Recirculation pump system noise was shown not to be a definite influence upon core responses.

D. CONCLUSIONS

The VBWR stability experiments have produced detailed information regarding in-core fluxes and flows as well as system operational parameters. These have been assembled from known measurement techniques and analytical methods into what appears at this point to be a comprehensible and understandable picture of the stability, transient response, and operational noise character of the reactor and system. The conclusions are based upon experimental points taken over a range which was indicated to best demonstrate the responses of the reactor.

1. Absolute Stability

Although the pre-test analysis parametric studies were not always

done at conditions as close as desired to test conditions to produce refined relationships, the following may be stated:

a. The reactor stability theory described in this report predicts the stability characteristics of the VBWR very well for natural circulation operation of the plant. Forced circulation operation conditions are predicted equally well for systems whose flow velocities in the two-phase region are not too far removed from natural circulation. It is believed that this theory is adequate for any boiling water reactor having similar characteristics to the VBWR.

b. High flow rate (say, above 4 - 5 fps inlet velocity) forced circulation plants will require additional work on the theory. A number of significant guides for this further work have been pointed out in Sections VII, VIII, and IX. It is concluded that a satisfactory theory for reactors similar to the VBWR in operating principles can be achieved by the steps outlined in Section IX.

c. The two most significant parameters effecting the absolute stability of this reactor were:

    1. The void coefficient of reactivity.
    2. The condition of system hydraulics.

    The VBWR, as it was operated during these tests, showed a greater sensitivity to the void coefficient of reactivity. It is concluded that these two parameters would be the first two which effect the VBWR stability. Other parameters, such as pressure and fuel time responses, can have sizeable effects in some reactor systems.

d. Determination of the average parameter or average channel responses needs further work to establish a close relationship between predicted and test performance. Spatial representation of thermal hydraulics and void reactivity coefficients are key investigations in this area.

e. Rules of thumb for predicting absolute stability are of little use in high flow forced circulation systems. A system analysis, as described in this report, is much more reliable than intuitive treatment.

f. It is concluded that operational noise cannot be used as a measure of absolute stability. This conclusion is discussed more fully in the operational noise conclusions.

g. Rod oscillation tests have provided significant and quantitative absolute stability data in these tests. Steady-state noise and transient response tests have not. Rod oscillator tests should be conducted on every boiling water reactor which has significant design differences from those for which there is absolute stability data.

h. Quantitative data, derived from hydraulic stability loop tests, are required for void transfer functions. These important data will provide a basis for model analysis improvement in the thermal hydraulic response area, and in the average parameter analysis area.

i. An advanced analysis program is required to obtain really significant gains from the work conducted thus far. Such a program is outlined in Section IX.

2. Operational Noise And Its Effect On BWR Stability

a. The VBWR experiments definitely show that steady-state oscillations in power or flow cannot be used as an indication of absolute stability. These tests, in fact, show flux and flow parameters which indicate the wrong direction in stability trends. A reactor operator, it is concluded, would need specific knowledge of:

1. Reactor system characteristics,
2. Sources of reactor excitation,
3. Frequency and magnitude distribution of noise excitations,

to make satisfactory conclusions.

b. For some fluid dynamic or other conditions reactor operation may be limited by steady-state noise before it is limited by being unstable in the absolute sense. This was encountered when operation of the reactor was attempted with the core bypass baffles open and full 20,000 gpm flow. The inoperability arose from the flux noise of about $\pm$ 25% which tripped the + 25% high flux scram instruments.

c. It is concluded that orificing of flow channels produces a considerable reduction in noise amplitude.

d. The VBWR test data and the accompanying hydraulic stability loop test program give promise of significantly improved understanding of noise phenomena in boiling water reactors. Two aspects are worthy of note:

1. The natural circulation rod oscillator tests are a source of in-core information on core and flow responses to specific excitation, namely, the rod oscillation.

2. A theory has been advanced for propagation of disturbances from excitation forces. The theory predicts the correct range of frequencies for the measured responses of VBWR.

No definite conclusions will be drawn at this time for these items except to say that they are plausible contributions to explain portions of the measured phenomena and provide a good basis for initial detailed work on noise.

SECTION III

OBJECTIVES OF VBWR STABILITY STUDIES

The primary objective of the VBWR stability studies is to make significant progress in developing a reactor stability and transient response analytical model for boiling water reactors. Such a model does not exist presently. It is imperative that a more detailed understanding upon which such a model is based be obtained before BWR's are exploited for their full capabilities in the production of economic nuclear power. In order to accomplish the above, a series of objectives must have been reached as tabulated below. These objectives, of necessity, encompass a great deal more than may be accomplished in the VBWR studies, although significant progress should be made in most areas.

1. Instrumentation, experimental techniques and analytical techniques which are capable of detecting incipient oscillations must be developed.
2. Reactor stability data describing the significant parameters must be obtained. This data would include that obtained from instrumentation internal to the reactor core.
3. The predictions of analytical reactor stability models should be compared to test data to determine the ability of the analytical model to predict the stability performance of the reactor system.
4. Analytical model improvements may then be introduced based upon the understanding obtained above.
5. Steady-state operational and transient behavior of the reactor are an integral part of the satisfactory stability performance and are to be considered concurrently.

A complete investigation of these objectives necessarily includes numerous items which could not be studied in conjunction with the VBWR reactor. Important examples of these are extensive spatial effect studies, variable lattices and significant changes in fluid dynamics of the two-phase flow system.

Specific objectives of the VBWR program are discussed in relation to the VBWR tests and the hydraulic stability loop studies under two headings in the following paragraphs. The first deals with the specific objectives of this report. The second deals with the objectives of the entire Fuel Cycle Stability Task.

1. VBWR Stability Data

To determine the effect of the following parameters on the stability performance of the VBWR Reactor System,

a. Power,
b. Flow,
c. Orificing of fuel channels,
d. Mode of operation (forced or natural circulation),
e. Core bypass flow area,
f. Water level,
g. External loop resistance,

three test types are included:

a. Steady-state,
b. Control rod oscillation,
c. Operational transients.

2. Test Data Analysis

a. Objectives of this Report

An objective of this test report is to relate the results obtained from preliminary analysis of test data. The effects of the above test parameters were obtained by visual analysis and preliminary forms of mathematical analysis of the experimental data. Visual analysis consisted predominantly of peak-to-peak magnitude readings, phase angle readings, and determination of the mean values of test parameters. Such an analysis provides less accurate data, but performs the vital function of establishing the validity of experimental parameters and provides a physical feel of the nature of the reactor system responses.

It is also an objective to report mathematical analysis of test data of a

specific set of runs screened by visual examination. The analysis of data reported here is obtained from the output of a band pass filter network. While the output of these analyses serve to evaluate the character of the VBWR responses, the contribution from the subsequent portions of the program are expected to produce the significant improvements in reactor stability model analysis.

A discussion of mathematical aspects of data analysis (Section IX) provides an introduction to the problems of the band pass filter analysis and introductory material on more advanced methods.

The above preliminary data analysis methods are then used to determine test results from:

a. Operational parameter and transient tests,
b. Steady-state test data involving the responses in neutron flux and flow to the excitations of the system. Such analysis is subsequently called noise analysis.
c. Determine the system transfer functions in response to neutron flux oscillation.

The rod oscillation tests will yield:

a. Neutron flux-reactivity transfer functions,
b. Flow-reactivity transfer functions,
c. Phase angle relationships.

The final objective of this report is to compare predicted values of transfer functions with the experimental data. This comparison provides a basis for understanding the results of the tests and also establishes a datum point from which future data analyses and model analyses may be compared.

The objectives are tabulated in Table III-1

b. Objectives of Fuel Cycle Stability Task

A clear-cut analysis method for the experimental data which had proven

reliability and good error analysis characteristics was not available at the initiation of this work. It is, therefore, the first objective to evaluate the best course to follow in the analysis of data. Mathematical analyses consist of the following:

1. Code calculation involving statistical auto-correlation and Fourier transform analyses to obtain frequency responses of flow and neutron fluxes. The reliability, accuracy and operating cost of this analysis method is then to be determined.

2. A similar analysis by digital filter methods is to be examined.

3. Evaluation of the analogue band pass filter as a means of providing reliable data is to be completed.

4. Analogue methods of Fourier spectrum analysis are to be investigated.

   This step is a key step in obtaining the final objective of the stability task; that of developing improved model analyses for reactor stability. Until limits of error, utility ranges, speed, and cost can be determined, no assurance may be had that real improvements in model analysis may be had, or if significant quantities of data may be analyzed.

The Fuel Cycle Stability Task objectives are best described with the above background from Table III-2. Reference to hydraulic stability loop objectives is given here for completeness, and is discussed in subsequent paragraphs, along with other specific items listed in the table.

The following four paragraphs define specific objectives in the above table.

1. Model Analysis - Reactor model evaluation by means of reactor experimental data.

   a. Models:

      The reactor analytical model is composed of the following component models:

1. Reactor kinetics,
2. Fuel,
3. Hydrodynamics,
4. Reactivity - voids,
5. Doppler coefficient,
6. Pressure - voids.

b. Method of Evaluation

The models which compose the reactor model have different characteristics in the low, intermediate, and high frequency regions. Intermediate frequency is considered to be in the neighborhood of the resonant or dominant frequency of the hydrodynamic model. By comparing the model predictions and the experimental data in the various frequency regions, the inadequacies of the various models are detected.

c. Rod Oscillator Tests

The rod oscillator tests yield flow reactivity and flux reactivity transfer function and phase angles over the frequency spectrum. Comparison of the predicted and actual transfer functions will yield model weaknesses.

d. Transient Tests

The various models composing the analytical reactor model are linearized about the operating point. The transient test data and the transient predictions will be compared to determine the range of applicability of the linearized model.

e. Hydrodynamic and Fuel Model Evaluation

Another check of the combination of hydrodynamic and fuel models can be made by using the experimentally measured heat generation as an input to the fuel model. From the output of the hydrodynamic model, the velocity is obtained. Comparison with the experimentally measured velocity yields the differences between model predictions and experiment. The experimental signal will contain the response to extraneous excitations as well as the velocity-heat

response. This procedure supplies additional information for evaluating the excitation forces and the fuel and hydrodynamic models.

2. Hydrodynamic Model Evaluation by Means of Stability Loop

The use of a stability loop has the advantages over a reactor experiment of reducing the number of parameters involved, or more specifically, eliminates the reactivity-power feedback. This permits a more detailed evaluation of the hydrodynamic model. The objective is to evaluate the accuracy of the model in predicting the effect of:

a. Heat input,
b. Flow,
c. Subcooling,
d. Loop inertia,
e. Void transport velocity,
f. Point heat input,
g. Steam-water shear forces.

3. Model Improvement

The objective of the model improvement phase is to recognize from the loop and reactor model analyses the strong points and weaknesses of the various component models and the composite reactor model, and to modify the models to improve their functioning.

4. Application to Other Reactors

The stability data from other reactors can be used for additional checks on the improved model (generated in (3) above). The model can then be used to predict the effects on stability of the following:

a. Fuel time constant (fuel diameter or thickness and thermal properties),
b. Void coefficient of reactivity,
c. Doppler coefficient.

TABLE III-1

OBJECTIVES OF PRESENT REPORT

1. Obtain reactor stability data with in-core instrumentation to determine the effects of the following parameters:

    a. Power,
    b. Flow,
    c. Mode of Operation,
    d. Bypass Flow Area,
    e. Water Level.

    The detailed effects of orificing and external loop resistance will not be reported in the present report. The scope of analysis will also be limited to visual analysis of the external neutron flux (micro-microammeter).

2. Determine the effectiveness and life of in-core instrumentation for obtaining stability data.

3. Develop experimental techniques and analytical techniques for the detection of incipient oscillations, and for establishing future stability test procedures.

4. Determine neutron flux-reactivity transfer functions, flow-reactivity transfer function and phase relationships for various parameters. The scope of the present report is limited to presentation of representative results of analyses.

5. From transient tests, determine overshoots, damped frequencies, and damping coefficients. The scope will be limited to the analysis of one run.

6. Determine low, intermediate and high frequency range prediction capabilities of reactor model. The scope will be limited visual analysis and some electric filter analysis of a number of traces to show representative responses.

TABLE III-1 (Cont'd)

7. Obtain limited number of analyses to demonstrate analytical techniques and representative results for:

    a. Visual analysis of peak-to-peak magnitudes and phase angles,

    b. Code calculation using auto-correlation, statistics, and Fourier transform methods,

    c. Electric filter (band pass type) analysis,

    d. Transient tests,

    e. Rod oscillator tests,

    f. Steady-state noise tests.

TABLE III-2

OBJECTIVES OF FUEL CYCLE STABILITY TASK

1. Obtain reactor stability data with in-core instrumentation to determine the effect of the following parameters:

    a. Power,
    b. Flow,
    c. Orificing,
    d. Mode of operation, natural or forced circulation
    e. Bypass flow area,
    f. Water level,
    g. External loop resistance.

2. Determine the effectiveness and life of in-core instrumentation for obtaining stability data.

3. Develop experimental techniques and analytical techniques for the detection of incipient oscillations and for establishing future stability test procedures.

4. Compare relative utility, speed, and cost of visual and mathematical analysis of data.

5. Compare utility, speed, and cost of:

    a. Autocorrelation, statistical and Fourier code analysis,
    b. Numerical filter analysis,
    c. Electric filter analysis.

6. Determine noise excitation characteristics from steady-state noise signals.

7. Determine neutron-flux-reactivity transfer function, flow-reactivity transfer function and phase angle relationships for parameters listed in (1-a) to (1-g).

TABLE III-2 (Cont'd)

8. From transient tests, determine overshoots, damped frequencies and damping coefficients.

9. From rod oscillator tests and model predictions, determine low, intermediate, and high frequency prediction capabilities of reactor model. Determine model capability of predicting effects of power and flow external loop resistance and orificing on neutron flux and velocity responses.

10. Determine whether loop-type or parallel channel-type oscillation predominates.

11. From transient tests and model analyses, determine prediction capabilities of linear model for large transients.

12. Evaluate hydrodynamic and fuel models by using experimental heat input into analog model to obtain velocity response and comparing with experimental velocity response.

13. Use hydraulic stability loop experimental data to evaluate hydrodynamic model with particular reference to:

    a. Power input,
    b. Flow,
    c. Subcooling,
    d. Loop inertia,
    e. Void transport time,
    f. Point heat input,
    g. Steam-water shear forces.

14. From the determination of the strengths and deficiencies of the model, as determined by reactor experiments, loop experiments, and analysis, devise model improvements and integrate improvements into an overall reactor model. Hydrodynamic and physics models are involved.

TABLE III-2 (Cont'd)

15. Re-evaluate improved model by use of reactor data from other sources. Revise model again if necessary. Using refined model, predict the effects on stability of:

    a. Fuel time constant (fuel diameter or thickness and thermal properties).

    b. Void coefficient of reactivity.

    c. Doppler coefficient.

SECTION IV

TEST FACILITY

The test facility, which is the VBWR reactor, was designed to provide wide flexibility in modes of operation and in core loading. Included in the facility was provision for a rod oscillator mechanism, extensive use of in-core instrumented fuel assemblies, and readout instrumentation. A detailed description of the test facility is given in Appendix A.

Coolant Circulation

Figure IV-1 shows a schematic diagram of the reactor circulation system. Coolant was circulated by either forced or natural circulation in these tests. The flow path for forced circulation passes coolant upward through the core, through vertical risers and out of the truncated conical baffle located above the core. The free surface of the system is about 5 feet above the core outlet. In this 5-foot space, the two-phase flow configuration of the reactor channels is changed, the steam passing upward and the recirculation flow passes over the top of the cone and into suction lines located at four points on the vessel periphery. Feedwater is introduced to the recirculation flow a few feet down the suction lines. The flow is then to the pumps and, hence, returning to the reactor vessel in two lines which enter the vessel 180° apart and deliver it through chutes to the plenum chamber below the core.

Natural circulation is accomplished by opening four baffle doors located at the level of the top of the riser channels shown in Figure IV-1. The flow path is upward through the core with the recirculation flow separated in the space between the riser top and the water level. The recirculation flow is then downward through the baffle doors and to the plenum chamber below the core.

Core Composition and Power Distribution

The core fuel load consisted of pelletized UO_2 clad with either zircaloy or stainless steel. Rod diameters are 1/4 to 1/2 inch, with enrichments varying from 2.7

to 4.5 per cent. Details of the loading are provided in Appendix A. An effort was made to make the core as consistent as possible in its makeup, although, because of the core makeup, this was not entirely possible.

The power distribution for the core was calculated prior to the test by two-dimensional diffusion theory methods using three neutron energy groups. The calculations were done in conjunction with thermal hydraulic calculations in an attempt to make the results as meaningful as possible. A detailed description of the core power distributions and thermal hydraulic calculations is provided in Appendix A.

Control Rods

Control of the reactor is accomplished by operation of seven control rod drives. Each drive has two control rod boxes attached to it. The control rods have fueled followers designed to approximate the characteristics of the fuel. Control rod worths were determined experimentally by a period and temperature coefficient technique. Appendix A gives these results.

The time variable inputs of reactivity required for the rod oscillation tests were applied to the core with the central VBWR control rod (No. 7) by a specially designed rod oscillator system. This system, described fully in Appendix A, provided, at any point of rod withdrawal, a sinusoidal position displacement of the rod over a frequency range of 0.03 cycles/second to 3 cycles/second at amplitudes up to $\pm$ 1.0 inch, and other motions. The rod displacement is obtained with a double acting hydraulic cylinder driving a lever arm in contact with the rod stop of the control rod drive line. Hydraulic fluid is supplied to the cylinder through an electronically controlled servo valve to generate the desired reactivity variation. The system operated functionally independent of, and compatible with, the rod drive motor train, allowing normal operation and scram of the rod at any time.

Instrumentation

A maximum of twenty of forty-two possible primary measurement outputs were recorded on a fast readout system located in the VBWR control room. Seven of these signals were reactor control rod and process instruments.

Valid measurements were obtained from each instrumented assembly for three ion chambers and of inlet water flow. Five instrumented assemblies were provided. The other parameters measured were signal outputs of:

a. A gamma compensated ion chamber fed to a micro-microammeter.

b. Flow through two recirculation pumps.

c. Reactor feedwater and main steam flows.

d. Pressure in the steam dome of the reactor pressure vessel.

e. Motion of the control rod oscillator.

A more detailed description of these measurements is provided in Appendix A.

Twenty channels of Brush, high-speed strip chart recording were provided. In parallel with this were twelve channels of Ampex FM magnetic tape recording. The strip chart records provided a permanent record and enabled study of operating characteristics and a physical understanding of the process to be obtained. The tape recording provided a permanent record which is used for the band pass filter and more advanced data analysis methods.

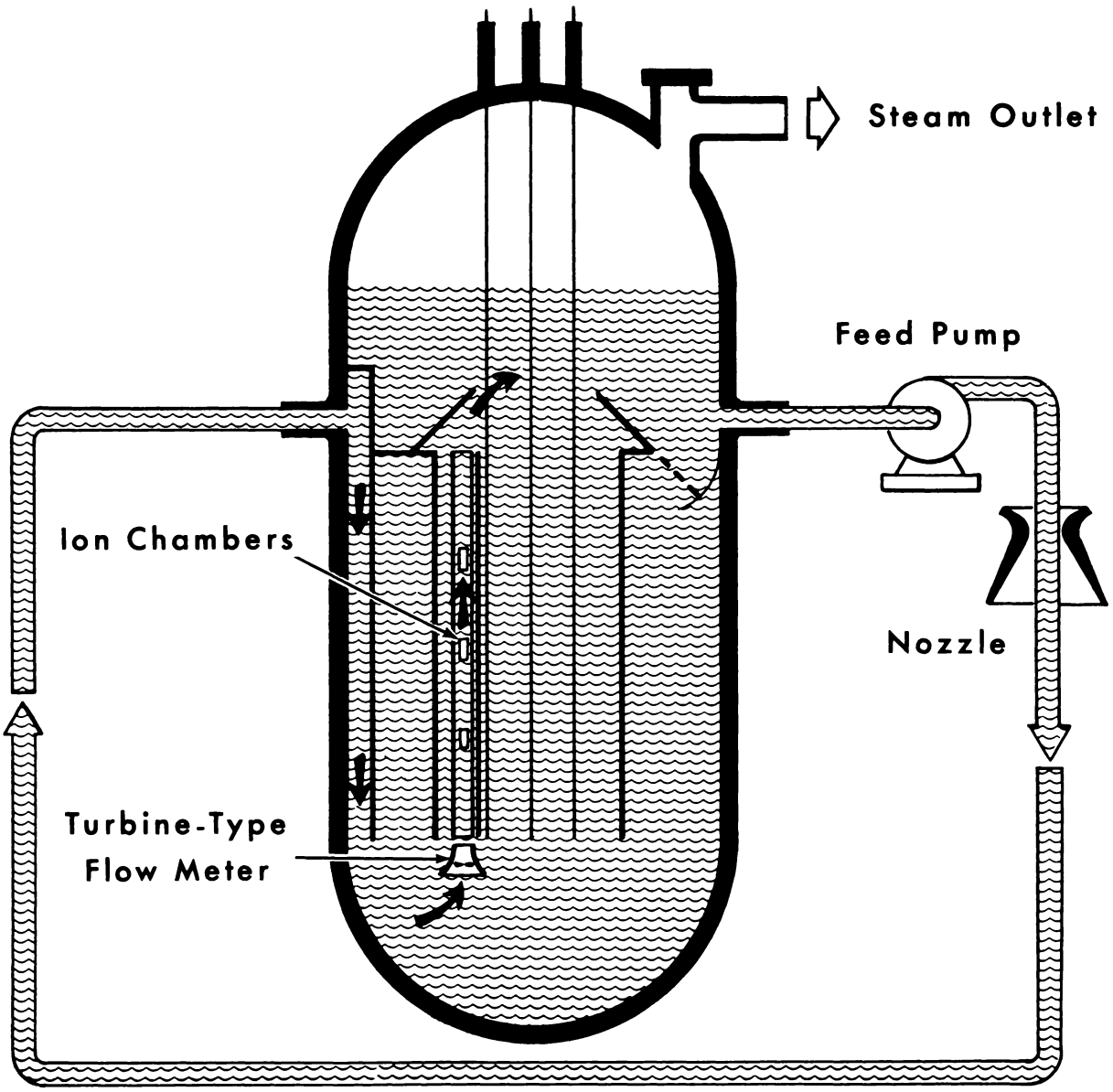

FIGURE IV-1 SCHEMATIC DIAGRAM - REACTOR CIRCULATION SYSTEM

SECTION V

TEST PROCEDURES

Written procedures for each type of test were prepared and approved prior to conducting the experiment.

Safety criteria used throughout contained the following basic limits:

1. The power-flow relationship combined with scram settings was such that a burnout margin of at least 1.5 was maintained at all times, including a loss of pump accident.

2. Power changes or oscillations, as indicated by the external ion chambers, were always maintained within the range of $\pm$ 25 per cent of the nominal test value.

3. Operation of any test equipment, particularly the rod oscillator, was only by persons specifically instructed in the operating requirements and authorized by the Reactor Test Program Engineer.

4. Operation of the rod oscillator was started only from a steady-state condition. The operator monitored at all times the recorder traces of rod position and reactor flux to insure that the amplitude-frequency limits and reactor power oscillation limits were not exceeded. At each new test condition, rod oscillation amplitude was started at zero and increased to the desired value. Rod oscillation amplitude was limited to a $\pm$ 10¢ reactivity as determined by a control rod worth calibration on November 3, 1961.

More details of steady-state and transient operation and specific safety considerations are provided in Appendix B.

SECTION VI

DATA REDUCTION

This section describes the following steps in data handling:

a. Instrument calibrations
b. Frequency response of instrumentation
c. Measurement errors
d. Data analysis use of a band pass filter network.

More advanced methods of data analysis, using digital techniques and analogue Fourier spectrum analyzer techniques, are described in Appendix E. Detailed treatment of the data reduction is carried out in Appendix C.

A. Instrument Calibration

Primary instruments for process system pressure measurements consisted of Pace variable reluctance-type differential pressure transducers. In-core instruments consisted of five instrumented assemblies, 3 belonging to the Fuel Cycle Development Program and 2 belonging to the High Power Density Research and Development Program.

These instruments were calibrated prior to operation in VBWR, and checks of the calibration were made at several points during the instrument operation. The Pace transducers were bench-calibrated according to the detailed description of Appendix C, and showed an accuracy of calibration of better than 0.1% of full scale. The instrumented assemblies of the Fuel Cycle Program were calibrated in the General Electric Heat Transfer Facility in San Jose. The procedures and equipment used were described in GEAP-3898, "Fuel Cycle Development Program, Sixth Quarterly Progress Report", October - December, 1961. Those assemblies from the High Power Density Research and Development Program were also calibrated in the Heat Transfer Facility. The completed results are being issued as GEAP-3896, "Calibration of Two Instrumented Fuel Assemblies for High Power Density

Development Project", by E. Janssen and J. A. Kervinen.

Characteristics of the in-core flow meters appeared satisfactory prior to insertion in the reactor, as did pressure differential and thermocouple calibrations. These results are given in Appendix C, along with the methods of maintaining calibration. During the test program in the VBWR, the ion chambers were checked against heat balance and power distribution measurements; however, no assured calibration during operation was obtained because of an uncertain leakage current created by moisture in leads.

The flow meters suffered from deterioration of the permanent magnets during VBWR operation. The meters were gradually dropped from service with only flow meter "C" still useable at the end of the two months of stability testing. Flow signals from Assembly "D" (in the highest flux) became unuseable after 4 - 5 weeks, and from Assembly "E" after 8 weeks.

Successful measurements of the time dependent temperatures and pressure drops were not obtained during reactor operation. A detailed discussion of this is given in Appendix C.

B. Frequency Response of Instrumentation

The frequency response of the Brush oscillograph recorders was obtained after the Brush recorders were installed in the readout system. Gain and phase shift were also obtained for the electrical noise suppression filters and the amplitude attenuation of the signal due to input grid voltage feedback from the Ampex recorder. Kintel D.C. amplifiers and the Ampex tape recorder were assumed to have flat frequency responses from D.C. to approximately 2K cps. Further details of readout instrumentation are provided in Appendix C.

The in-core flow meters response rate was estimated and compared with its readout instrumentation. Figure C-16, Appendix C, gives the response rate including all components of the readout system except the Brush oscillographs. Readout instrumentation contributes most of the response limitation.

Frequency responses of recirculation flow transducers and their pressure lines is indicated to be flat up to 100 cps. In-core ion chambers are estimated to have flat frequency response from D.C. to greater than 2 K cps.

C. Experimental Accuracy

Studies have been conducted of the accuracy of experimental-data recovered from the test program. The study, which is reported in Appendix C, accounts for the errors in a conventional error analysis approach, and includes scale factor errors and reading errors.

After the scale factors were computed, they needed to be applied to the data by reading oscillograph pen deflections, or by performing some operation on the tape recorded data. In the case of the oscillograph data, an additional uncertainty occurred due to accuracy of reading the oscillograph traces. Assuming a representative amplitude (peak-to-peak) on the trace of 10 chart lines, and an uncertainty in reading the trace of 1/2 chart line, the total uncertainty of the data derived from the oscillograph-recorded traces was computed to be $\pm$ 10% (20 to 1 odds).

The data recorded on the tape recorder was frequency analyzed as described in Appendix C. The following general statements can be made about the uncertainties:

1. The relative amplitudes have an error of 6% within a two-mean deviation spread about either side of the mean (95% confidence limit). The gain versus frequency curve for the band pass filter showed the greatest spread in repeatability at the lower frequencies (about 0.03 to 1.0 cps). The repeatability was 5.7% for a two-mean deviation spread was calculated for Run 15-1-2 at a frequency of 0.2 cps. The data spread was calculated for Run 15-1-2 at a frequency of 0.1 cps and was 6.0% (95% confidence). The spread in the data is approximately equal to the uncertainty in the band pass gain. A discussion of the band pass filter network used for analysis of the data is given in Appendix C.

2. The uncertainty in the absolute values of the tape recorded data is $\pm$ 10%, within two-mean deviations, or 95% confidence limits. This deviation is composed of contributions from the band pass analyzer (repeatability) and from the scale factor for the mean value in the zero suppressed case. The potential gain in accuracy from improving the calculation of the scale factor for the mean value is 4 per cent.

D. Data Analysis Use of a Band Pass Filter Network

A band pass filter network was used as the major technique of data reduction. The tape recorded signals were analyzed for frequency content, the output of the filter network being amplitude of oscillation times frequency as a function of frequency. The technique was used for analysis of steady-state and rod oscillator data. The results, based on these measurements, are presented in Section VII.

Appendix C describes in detail the equipment, its calibration and use in data reduction. Appendix E discusses qualitatively the problems introduced by the mathematical characteristics of the band pass filter and compares it to improved methods of data analysis. A great deal of effort was made to obtain consistency of results in data analysis. This is due primarily to (a) meticulous care in calibration and in experimental technique, and (b) the use of a tape recorded input signal. The latter permits measurement of all frequencies from exactly the same signal input.

SECTION VII

TEST RESULTS

Data are presented in this section for

1. Operational characteristics and transients,
2. Steady-state noise, and
3. Rod oscillator tests

of the VBWR reactor. The first intention of this section is to characterize the results of the test. Second, a physical understanding of the results has been sought and outlined based upon a limited number of tests and the analytical methods available at the time the work was done. Comparison of the data with pre-test analyses is largely contained in Section VIII.

Section VII-A discusses the analysis of steady-state strip chart traces of the data to determine qualitative and limited quantitative information from the steady-state runs. The objective of both the rod oscillator tests and the transient tests is to define the reactor system characteristic. Both tests contain two fundamental and common qualities:

1. A known reactor disturbance, and
2. A recording of the reactor system's response.

The rod oscillator test was the most direct, accurate, and easy to analyze method available for obtaining the system characteristic, and provided detailed experimental information about the reactor system's dynamic response. Although the transient tests, in theory, will provide the same information as the rod oscillator tests, the combined effects of

a. The short time interval of the system response,
b. The noise level, and
c. The presently inadequate data analysis techniques,

make this method limited in its value for system analysis.

The essential features of the results are obtained by analysis of five equal power test runs as follows:

TABLE VII-1

SUMMARY OF REACTOR OPERATING CONDITIONS FOR 5 RUNS

ANALYZED FROM VBWR TESTS - FIGURES VII-6 - 10

DATE	RUN NO.	MODE OF CIRCU-LATION	POWER MWt	FLOW 1000 gpm	INLET VEL. fps HOTTEST ELEMENT	PUMP	PUMP HEAD FEET
12/5/61	15 - 1	Forced	15	20	8.2	Both	200
11/22/61	15 - 9	"	15	4		#1	290
12/28/61	15 - 19	"	15	4.4		#2	7 1/2
12/4/61	15 - 16	"	15	4		#1	290 Baffles Open
12/11/61	15 - 18	Natural	15	4.3		None	None

The primary independent parameters of the experiment are the parameters in the circulation system. Adjacent runs in the above table differ by change of one parameter.

Some brief ideas determined from the test results are as follows:

1. The steady-state noise in operation is only slightly dependent upon the flow for normal forced circulation operation. There appears a somewhat sharper dependence upon power. Opening the baffle doors to produce a large bypass leakage path to the core, however, creates a much sharper dependence upon flow.

2. Steady-state flux traces show a surprising insensitiveness to flow rate which would not have been predicted from theory. Further, and very important to the consideration of the operation of reactors, is the fact that the percentage amplitude of noisy oscillations in flux increases as flow moves in a direction which produces more stable responses. This is not predicted by theory.

3. Steady-state flow traces in distinction to flux traces show a frequency relationship with flow rate which goes in the same direction as theory, although, it does not agree at high flow rates. The percentage amplitude of noisy oscillations in flow moves, as does flux, in a direction which is opposite to that predicted by theory.

4. Rod oscillation tests produced results which show good agreement of experimentally determined fluxes with theory for the natural circulation case. Experiment and theory are progressively less in agreement at higher flow rates for forced circulation. Forced circulation operation is shown to be devoid of oscillatory hydraulic characteristics. Flow responses as a result of rod motion were always small compared to flux responses. The only observed case where rod motion drove the flow occurred in natural circulation near the resonant frequency of the system.

5. The steady-state noisy oscillation information, by itself, is seen to contain more information than can be understood with just the steady-state traces alone. These traces are the result of at least the following influences:

    a. A reactor system characteristic,
    b. The source(s) of reactor noise excitation(s),
    c. The frequency and magnitude distribution of noise excitation(s).

    Only the noise spectrum provides a known relationship which measures the combined effect. Specific information about any one of the above is not obtained. The effects of all three unknowns must be obtained before an accurate generalized analytical description of stability and operating noise can be determined for this reactor, and of more importance, for the representation of reliable design criteria for future reactors. It appears erroneous conclusions could be drawn from the consideration of steady-state noisy oscillation information.

SECTION VII-A

STEADY-STATE NOISE

Analysis of steady-state noise traces has been conducted on neutron flux traces and flow traces for the above tabulated runs. These analyses have been done to:

1. Describe as well as possible the most significant portion of the data and obtain from it a physical understanding of the processes of the reactor.
2. Obtain frequency and amplitude correlations visually to show the interrelation of the parameters. This involves the phase relationship, the character of the traces, and the frequency spectrum as obtained by the band pass filter.
3. Study the effect of parameters of operation to determine the characteristics of the variables with parameter changes.
4. Compare these with pre-test analysis to determine the ability of the model to predict observed response.

The tests are discussed in the following order:

1. Operational parameters
2. Neutron flux traces
3. Flow traces.

SECTION VII-A-1

OPERATIONAL PARAMETERS

The reactor test program was oriented to demonstrate the effects of the following operational parameters on the steady-state noise:

a. Power
b. Flow
c. Water level
d. Mode of operation - natural and forced
e. Core bypass flow
f. Orificing
g. External loop resistance.

The results of orificing and external loop resistance will be reported in a subsequent report. Some reference is made to these results in the discussion of rod oscillator results. Some of these data are from tests other than the five major tests itemized in Table VII-1. They are presented here to introduce the operational character of the reactor.

The analysis of the effects of the operational parameters was limited to peak-to-peak visual measurements. The reading accuracy of the traces is estimated to be $\pm$ 0.2 mm. For small variations of the order of 1 mm, this amounts to a significant error. The variations were usually greater, of the order of 3 to 5 mm, and the reading error proportionally smaller. The length of time in which a search for the peak-to-peak value was made has an effect on the value found. Longer traces increased the probability of finding a larger peak-to-peak value. It is expected that later mathematical analyses will reduce substantially the spread of the data. The effects of the visual analysis are presented in Figures VII-1 through VII-4.

The steady-state noise is a function of the sources of excitation forces which exist in the reactor system under "steady-state" conditions, the dynamic characteristics of the reactor system (transfer function), and the frequency and magnitude distribution of noise excitation. The steady-state noise, therefore, is not directly a measure of the reactor system stability.

High steady-state noise is, as a first consideration, indicative of either or both of the following:

a. High excitation forces or additive combinations of excitations.
b. Low damped oscillatory system.

Trends indicated by the steady-state noise are the combined effect of trends of the excitation forces and of the system characteristic.

Figure VII-1 shows the external flux peak-to-peak percentage variation (peak-to-peak relative to the average) as a function of power level for two flow levels. The flux noise appears to be only slightly dependent on flow for the higher flow levels (10,000 - 20,000 gpm, which corresponds to 4.3 to 8.2 feet per second inlet velocity in the hottest elements), the noise being higher for the higher

flow rate. The noise increases as the power increases from 15 to 26 MW (average power density equals 37 to 64 KW/liter in hottest fuel cycle elements). The vertical lines in Figure VII-1 indicate the magnitude of error due to a reading error of $\pm$ 0.3 mm in determining the peak-to-peak magnitude. In Figure VII-2, the peak-to-peak variation of external flux is presented as a function of flow for various powers. The insensitivity of flux to flow variation in the flow range of 10,000 to 20,000 gpm, as shown in Figure VII-1, is confirmed. In addition, the effect of flow is found to be small in the low flow range down to 2,500 gpm; the sensitivity of flux to flow increased slightly in the low flow range. The effect of power is again found to be greater than that of flow.

In Figure VII-2, the effect of opening the bypass flow baffles is shown. Opening the bypass baffles offers a low resistance return path for flow variations in the core fuel elements. The flow variations have three alternate return paths:

1. Through the recirculation loop
2. Through other fuel elements
3. Through the bypass flow path.

When the baffles are closed, all three return paths represent high flow resistance paths and are not conducive to flow oscillations. With the bypass flow baffles open, the external path resistance is low, which is expected to give rise to parallel channel-type flow oscillations. The flux oscillation was found to be very sensitive to the recirculation flow rate when the bypass baffles were open.

The flow through instrumented elements "E" and "C" (high and medium power density fuel cycle elements) changed only about 10 per cent when the recirculation flow was increased from 4,000 to 10,000 gpm with the baffles open (150 per cent increase). Subsequent analysis must show whether the excitation forces were changed or the effects were caused by the uncoupling of the elements from the high resistance return path.

Another operating mode in which the flow return path resistance is low is natural circulation. In Figure VII-3, the peak-to-peak flux variation is shown as a function of power. In natural circulation, the effect on oscillation of a power change can be considered to be constituted of a power level effect and a flow

effect, since feedback causes an adjustment of flow with power. The flow effect can be considered to be approximated by the flux oscillation sensitivity shown by forced circulation, baffles open, data. The power (flux) contribution would then be the variation with the power change minus the flow effect. The total change in μμA peak-to-peak oscillation is 7.3% (17.3 - 10) going from 10 to 20 MW.(Figure VII-3). The flow contribution from 4,300 gpm to 5,200 gpm is 2.4% (9.8 - 7.4). (Figure VII-2). The contribution of increasing the power is then 7.3 - 2.4, or 4.9%. Power is shown to be somewhat more significant than flow in increasing amplitude of flux oscillations.

In Figure VII-4, the mean values of instrumented assembly flows (C and E elements) are presented as a function of power level for natural circulation operation. The instrumented assembly flow is a function of the reactor power to the 0.278 power. The instrumented assembly flow increases 21 per cent for a 100 per cent increase in power.

In Figure VII-5, the instrumented assembly flows for forced circulation operation are shown. For the case with baffles open, the instrumented assembly flow changes very little with the recirculation rate. This is as expected. The flows through the elements are established roughly by the condition that the pressure drop across the core is equal to the gravity head of the liquid column in the core bypass path. The core flow distribution at this condition establishes the recirculation flow rate (reference flow). At recirculation rates greater than reference flow rate, flow is down through the open baffle area and adds to the recirculation flow rate to maintain the core at roughly a constant flow rate. Since the flow through instrumented assemblies "C" and "E" are so independent of the recirculation flow rate, the instrumented assemblies cannot be used to determine the core flow rate response under natural circulation conditions with any accuracy.

The flow through the instrumented assemblies with forced circulation, baffles closed, is alsc shown in Figure VII-5. The non-linearity of the flow through instrumented assembly "E" is very significant at low flows. The flow appears to become asymptotic to a constant flow rate at low flows. It is surmised that there is downflow through the restricted bypass flow area and, also, possibly through some of the low power elements.

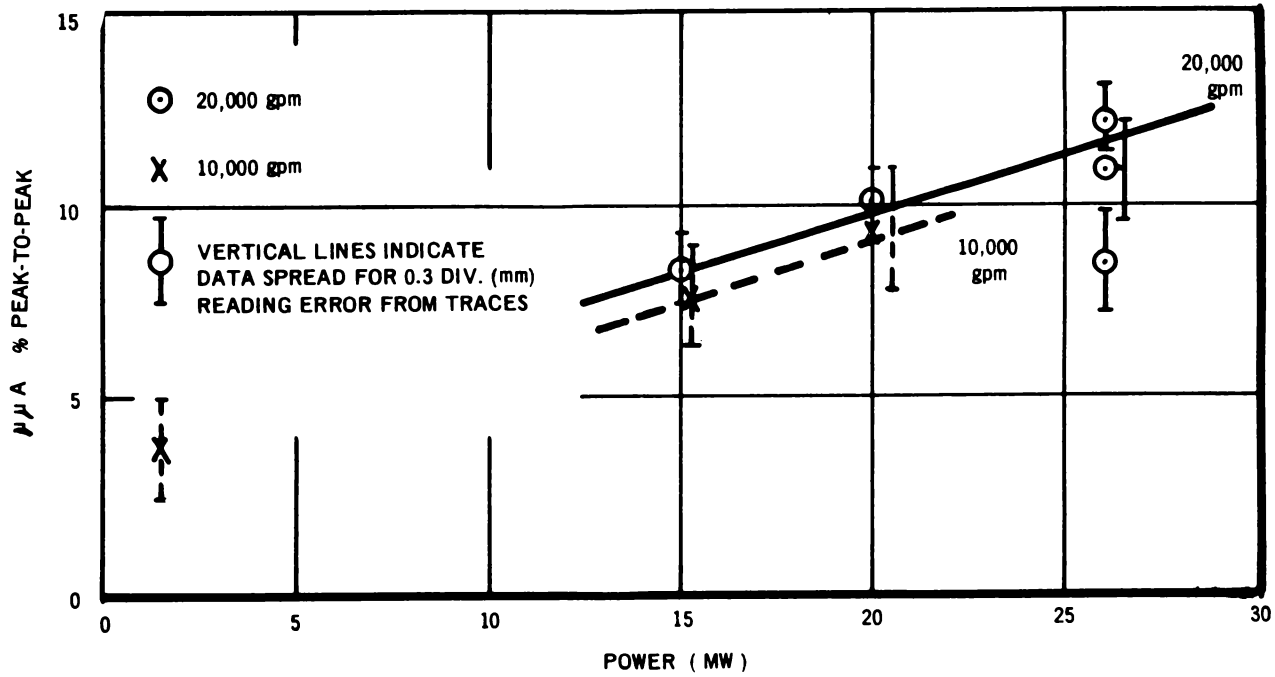

FIGURE VII–1 EXTERNAL FLUX PEAK-TO-PEAK PERCENTAGE VARIATION
vs POWER (MW) (FORCED CIRCULATION)

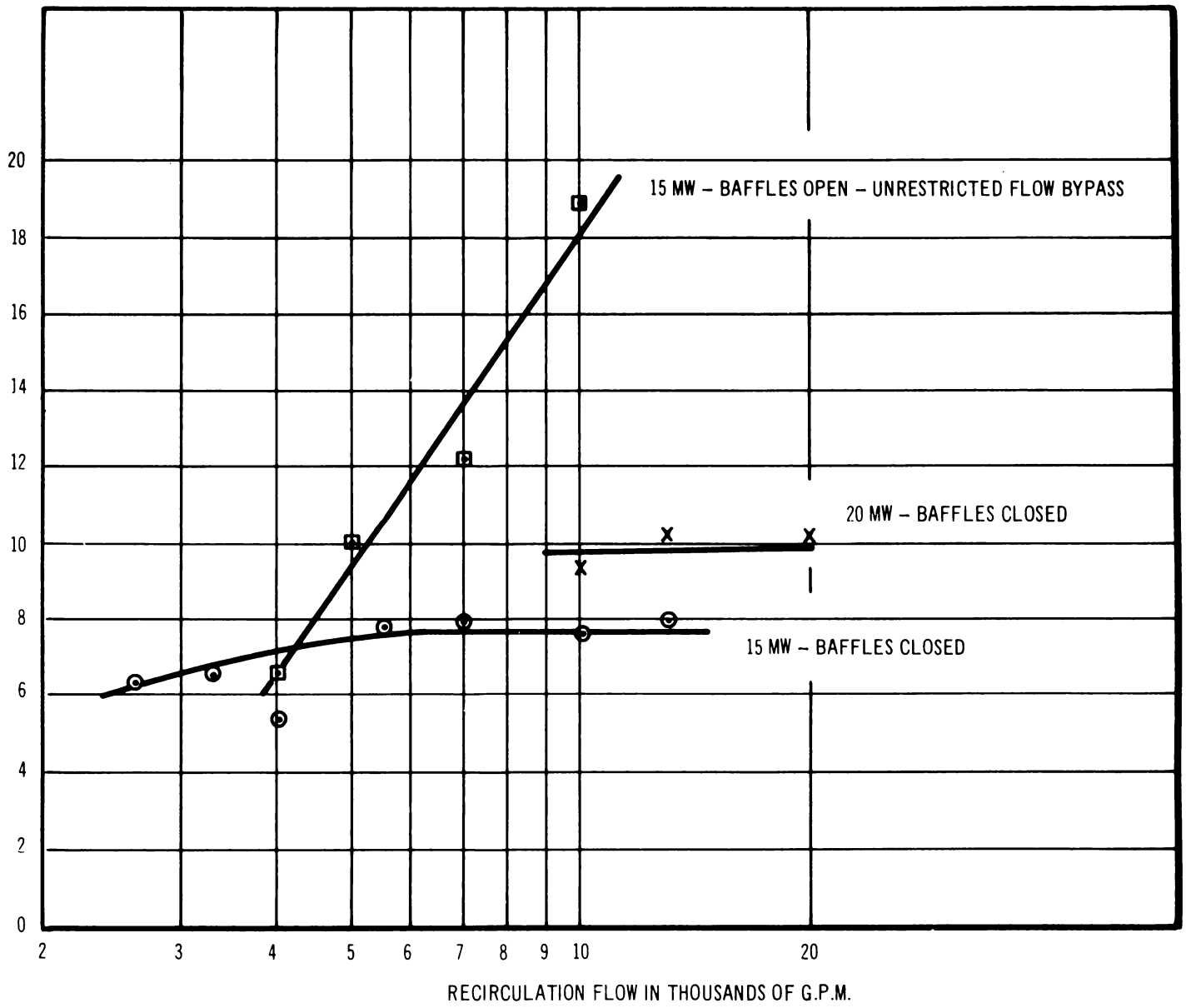

FIGURE VII–2 EXTERNAL ($\mu\mu$A) FLUX PEAK-TO-PEAK vs FLOW FOR FORCED CIRCULATION

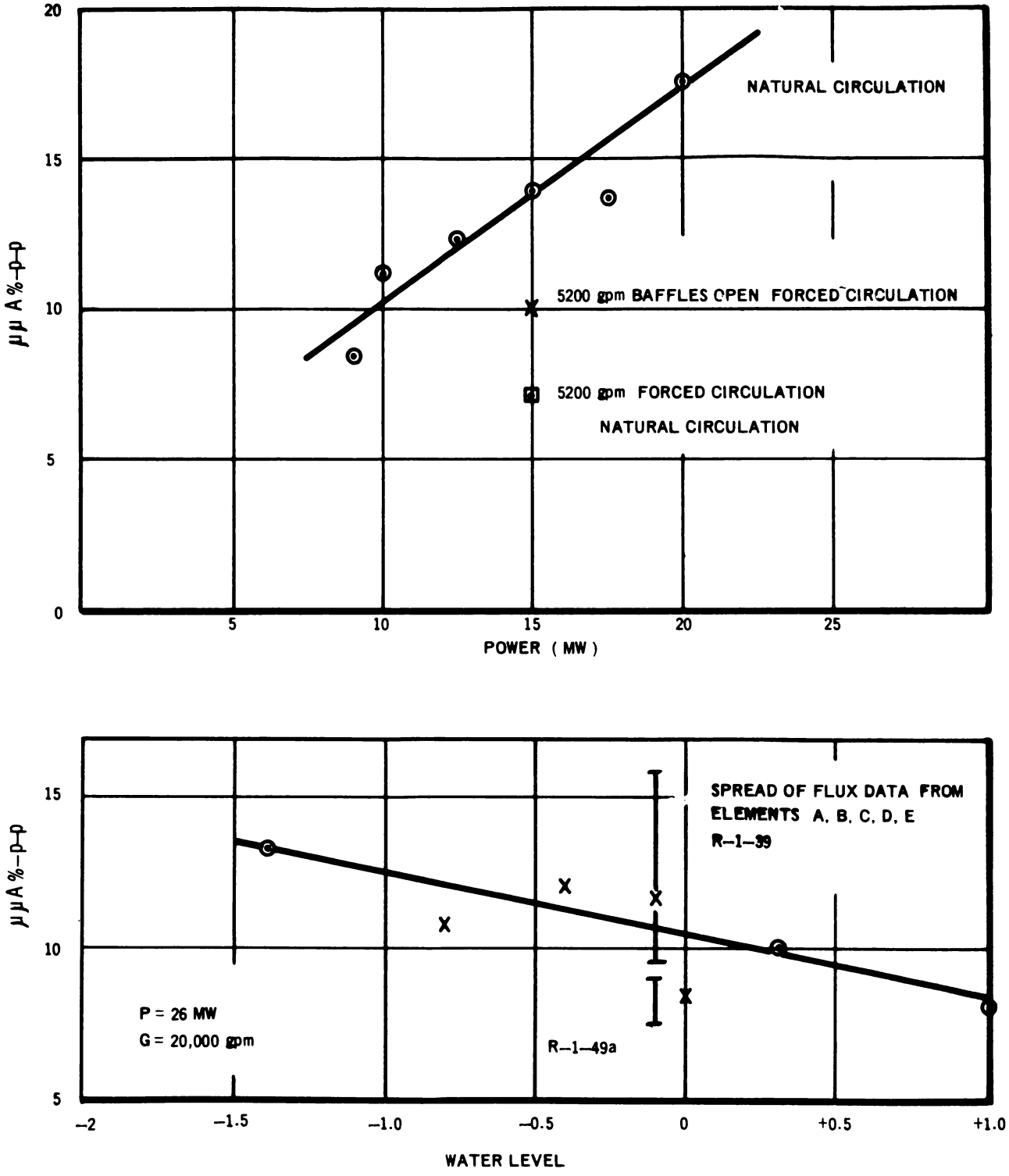

FIGURE VII-3 EXTERNAL FLUX PEAK-TO-PEAK PERCENTAGE VARIATION vs POWER – NATURAL CIRCULATION CASE

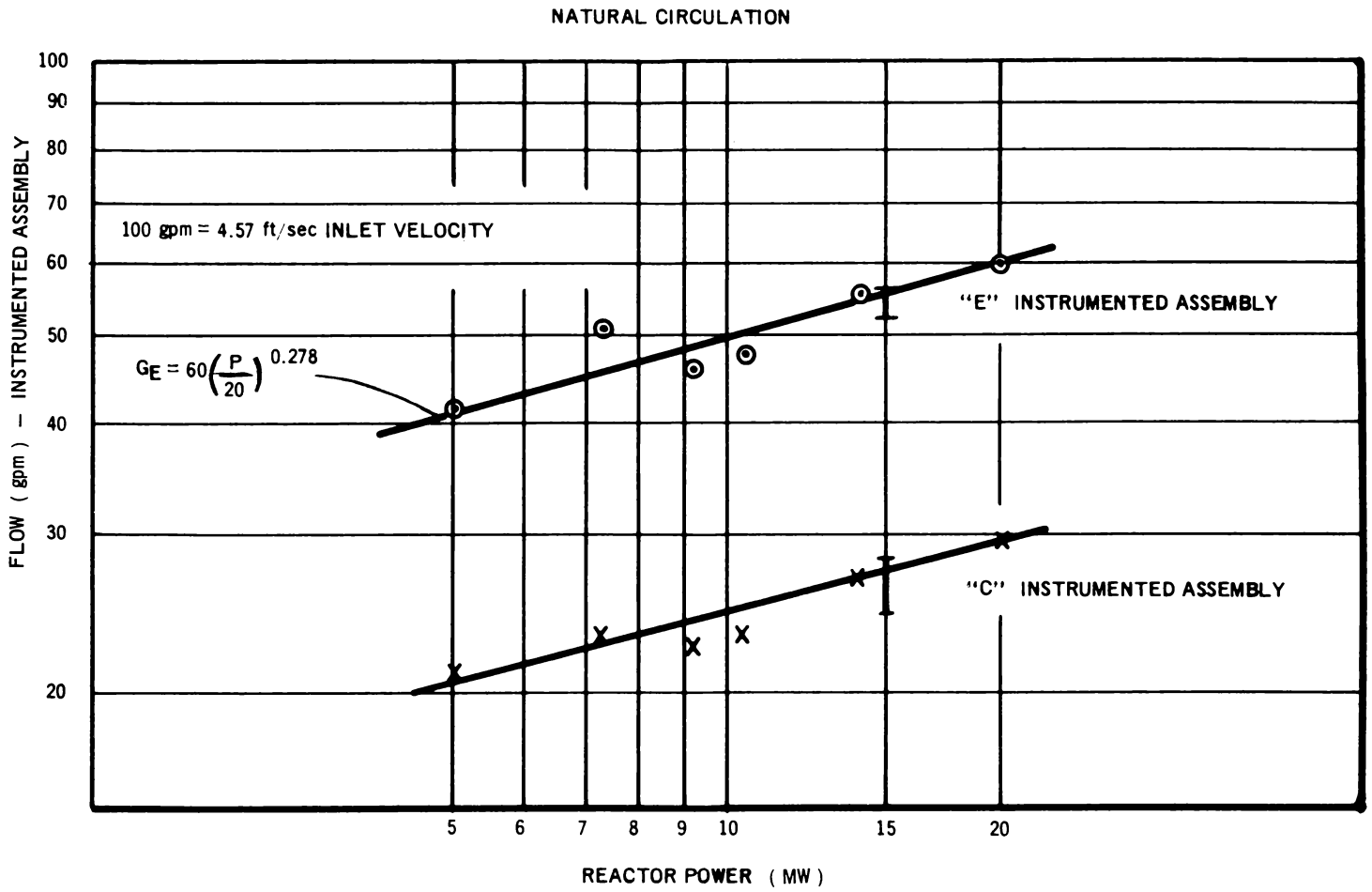

FIGURE VII–4 INSTRUMENTED ASSEMBLY FLOWS vs POWER MW

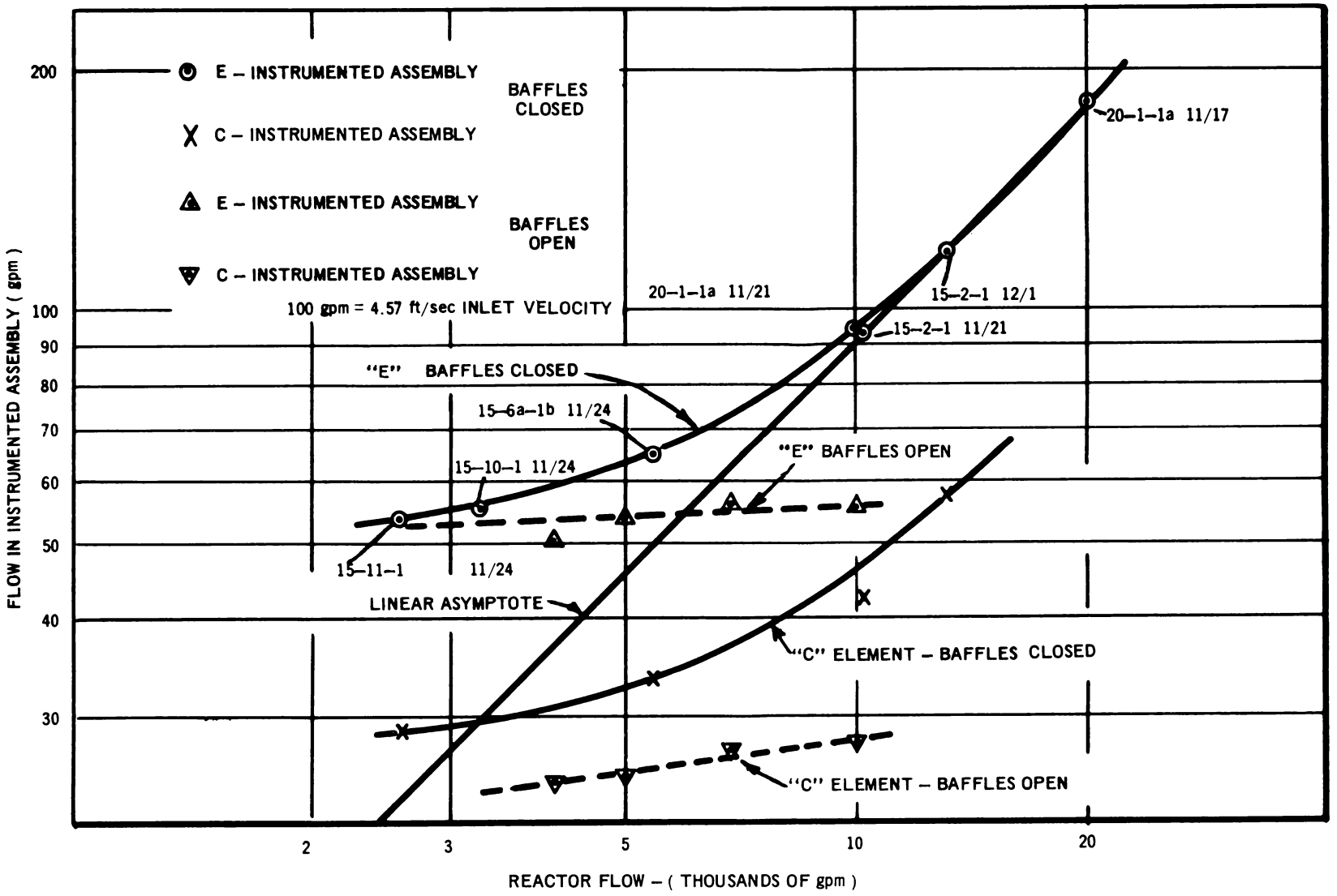

FIGURE VII–5 INSTRUMENTED ASSEMBLY FLOW vs REACTOR FLOW

SECTION VII-A-2

NEUTRON FLUX TRACES

Flux traces have been studied for the series of runs given in Table VII-1. The measurements have been made in two Consumers and three Fuel Cycle instrumented assemblies of the design discussed in Section IV and Appendix A. The in-core flux chambers are at the one-quarter, center, and three-quarter points of the core. The counter outside the core is located halfway up the vertical height and outside the vessel. Frequency response of the instrumentation and primary instruments is given in Section VI and Appendix C. Heat balances for power determination were made by a net of measurements isolating the reactor. Main contributors are recirculation, steam, feedwater, and clean-up flows. Environmental heat losses for the reactor were calculated.

Traces for the steady-state operation of the reactor are shown in Figures VII-6 to VII-10 for the reactor operating conditions in Table VII-1. Flux parameters which are shown on the traces are the micro microammeter and A, B, C, or D in-core ion chambers. Three different chart speeds are shown as labeled on the Figures. The discussions that follow refer to the high speed traces where from 10 to 30 seconds of the trace are chosen as representative after visual examination of the entire trace.

PHASE RELATIONSHIPS

Figure VII-6 shows traces of Run 15-1 for 15 MW, 20,000 gpm operation. Channels 6, 7, 8 show the mico microammeter and in-core chambers C-501 and C-502 respectively. Examination shows that these three power measurements are in phase everywhere on the trace. Amplitudes and the character of the traces also appear the same for this case.

Comparing Figure VII-6 with the other power traces in Figures VII-7 to VII-10, the traces appear, in some cases, to have a different character. The low frequency components, say, up to 1 cps, are in phase as described above. There is a high frequency component which may be seen in Figure VII-8 for chamber A-503 compared to A-502 and A-501. This high frequency component shows no apparent

phase relationship with the other fluxes. The frequency of this flux is 5 - 20 cps. The high frequency component is thought to be a function of bubble dynamics of the two-phase mixture. A further discussion of this is given under spatial variations below. The traces of neutron flux generally show no obvious correlation to the in-core or loop flows. More detailed analysis may show a weak correlation.

The significance of this observation is that a strong coupling evidently exists throughout all parts of the core. Perturbations in power at any local point are apparently averaged with the other signals, and every instrument sees substantially the same responses. Comparing the results of coupling, as obtained here, with results obtained in the Dresden Nuclear Power Plant Reactor, the flux responses of the Dresden reactor best reacted as random or uncorrelated oscillations. This indicates the Dresden reactor size is sufficient for nuclear uncoupling of areas of the core. The VBWR reactor has a 3-foot diameter and 3-foot high core; whereas, the Dresden core is 10 feet in diameter and 8 feet, 8 inches high. This will be discussed further with the spatial dependence discussion.

AMPLITUDE

Amplitudes of oscillation are shown by examination of traces to be relatively insensitive to flow. This is shown by examination of Figure VII-2. It should be mentioned that, in the course of the tests, the amplitude of the signals from ion chambers were effected adversely by the fact that leakage currents were found to be present. The leakage currents were variable with time and, in effect, caused an error in the absolute voltage measured in readout. The amplitudes of cscillation on this bases are subject to question in their intepretation. There does not appear to be a question about the character of the traces themselves, however, since in most flux traces the character is reproduced in very good detail.

SPATIAL FLUX STUDY

Examination of the flux traces in Figure VII-6 or the traces from the lowest ion chamber of Figures VII-7 to VII-10 show no spatial effects. A fundamental frequency of up to one cps is shown by these traces. A strong spatial effect may be

seen, however, in the examination of traces which show a higher frequency (5 to 20 cps) content. Figures VII-8 and VII-9 show a strong spatial effect in the vertical direction for Chambers A-503, 502, and 501. Channel A is located in position F-7 near the core center. The high frequency content, however, does not appear in the measurements taken in Channel C located in position J-4 at the outside of the core. The trace of Chamber C-502 shows this in Figures VII-6 and VII-10. The channel location, and the fact that the channel was orificed, represent the ostensible changes other than local channel power level. The exit quality of this channel is, however, higher than that of the channels at the core center which are not orificed. A parallel observation may be made that high frequency oscillations do not appear in the signals of the micro microammeter located external to the core. The μμA receives an average reading of the flux leaking from the side of the core at the midpoint in elevation. The current of neutrons must first pass through a considerable thickness of water, aluminum, and steel. At this point, the higher frequency component could either be average out, or, it quite plausibly could be assumed that the oscillations are local void-produced phenomena for which the effect could not be measured by the μμA. High frequency oscillation from Channel A, as shown in Figure VII-9, is consistent with previous measurements made in the Dresden Nuclear Power Station tests when the reactor was operated at high voids. Not only were the high frequencies present at points above the boiling boundary, but when the boiling boundary location was moved upward, a chamber which was then re-located below the new boundary would lose its high frequency component.

The question arises - what causes the high frequency oscillation, and how is it related to the operation of the reactor? In particular, does it have any effect on operating changes or ultimate stability of the boiling water reactor? It was concluded from a study of the Dresden Nuclear Power Station test data alone that the high frequency was a result of random density variations of the two-phase media. Subsequent studies of several neutron physics problems have indicated that there are no unexpected phenomena to be encountered, and the conclusion is still valid. It was also concluded during the above studies that since the frequencies of these oscillations were of the order of a decade above the time responses of the fuel there can be only a small feedback to the moderator coolant.

The fuel must then see essentially a steady flux.

Another consideration which might be advanced as a contributor to this spatial disturbance is discussed in Section VII-C. This consideration describes the possibility of transient responses propagated up the channel by inlet flow disturbances as a possible means of obtaining some of the observed spatial flux characteristics.

CHARACTER OF TRACES

Figures VII-6 through VII-9 show the incore and μμA traces for runs where the system was operated in forced circulation. The general character of these traces can only be described as random oscillatory. If one compares these traces with Figure VII-10, however, it is immediately apparent that there is a difference in the character of the traces. The oscillations have more of the appearance of sinusoidal traces and they take on the character of a system with harmonics or more than one frequency.

Since the pre-test analysis shows the forced circulation to be well-damped, one would expect the character to be well-damped. The natural circulation system, by the pre-test analysis, is less damped than the forced circulation system. Roots of the characteristic equations of hydraulic response are significantly reduced for the natural circulation runs (from about 1.0 to about 0.30, and the damping coefficients are reduced from about 0.4 to 0.1). This would indicate probably oscillatory character without divergent oscillations. Propagation of disturbances, discussed in Section VII-D, is presumably less impeded by channel restraint in the natural circulation case so that the effect of flow perturbations should be more prominent in this case.

Figure VII-2, previously discussed, shows that the amplitude of peak-to-peak oscillations increases with increasing flow in forced circulation. This may be determined from examination of traces of Figures VII-6 through VII-9. This is a significant observation in that pre-test analysis theory would indicate that the system is going in the direction of greater stability; hence, at least presumably, less noisy operation. Since the general characteristics of reactor responses are shown to be predicted by dynamic analysis theory as outlined in Section VII-B

and Section VIII, it appears that a much improved mathematical and physical understanding of the noisy oscillating system must be obtained before steady-state data are useful in predicting power stability.

Frequency characteristics, discussed in the following paragraphs, are also visible in the general character of the traces of Figures VII-6 to VII-10.

FREQUENCY ANALYSIS OF STEADY-STATE RECORDINGS

A band pass filter was used to perform frequency analyses of the steady-state recordings as described in Section IV and Appendix A. These results provide insight into several aspects of the dynamic performance of the reactor system. The following Table lists the steady-state frequency data which forms the basis for this section of the report.

TABLE VII-2

DETAILED DATA AS SHOWN IN FIGURES VII-6 to 10

Type of Instrument	Run 15 - 1	Run 15 - 9	Run 15-19	Run 15-16	Run 15-18
External Flux	μμA	μμA	μμA	μμA	μμA
Internal Flux Top	C-503	D-503	A-503	A-503	C-503, A-503
Middle	C-501		C-502, A-502	A-502	
Bottom	C-501			A-501	C-501
Internal Flow	E-201		E-201	E-201	E-201
External Flow	Loop 1 Loop 2		Loop 2	Loop 1	

The data from the natural circulation operation indicates that the system composed of the core and natural circulation fluid flow path has two natural frequencies; i.e., there are two peaks, one at 0.1 and one at 0.7 cycles/second. This suggests that the core transit time for controlling fuel channels is in the order of 1/0.7 or 1.4 seconds (2.1 ft/sec) and that the loop transit time is in the order of 1/0.1 or .10 seconds. These transit times are compatible with the understanding of the system as discussed in Section VII-C. Every frequency spectrum shown in Figures VII-11 to VII-25 has a peak in the range of 0.4 to 1.0 for steady-state noise spectra. This includes in-core fluxes, flows, and recirculation loop. Resonant frequencies of the system, as given by the predictions of Section VIII, do not always agree with these experimental results.

Examination of the high frequency side (2 - 20 cps) of the spectra provide several observations.

1. Incore Flux. Figure VII-26 shows normalized spectra for Run 15-16, forced circulation, with baffles open. This plot shows the μμA, external power measurement along with ion chambers A-501, 502, 503. A-501 is at the bottom, A-503 is at the top of the channel. Examination shows there is a progressively increasing amplitude in the 2 - 20 cps range from the bottom to the top of the core. This corresponds to the increasing void content. Several ideas may be advanced for this high frequency oscillation. The basic idea is that it is the result of variation in local void content. Pressure oscillations could conceivably create such an effect. Another method by which they could be created is the thermal hydraulic transient effects produced by perturbations in flow or other parameters lower in the channel and propagated up the channel. Section VII-C discusses these ideas. Further work is required to establish the importance of these and other possible phenomena, and evaluate the detailed nature of their effect. It has previously been pointed out that the high frequency signal disappears in instrumented Assembly C which is on the edge of the core and is orificed.

2. External Flux. It might be expected that the frequency content of the external ion chambers would be similar to the midpoint (502) ion chamber signals. It is not, however, and is similar to the lower ion chambers. There is very little amplitude above 5 cps. Several explanations have been advanced in the discussion of spatial character of flux traces. These included:

   a. Geometric attenuation of high frequencies by the transmitting medium, due primarily to proximity to a local disturbance.

   b. Averaging of neutron current from a large core volume by the external chamber results in a smoothing of perturbations which are local in nature. No depreciation of accurate sensing of perturbations which effect a large fraction of core volume would be encountered from this source.

Spatial characteristics of flux have been discussed previously. The spectra show no significantly different results than were advanced in the spatial characteristic discussion. Tabulated below are the runs which are significant in showing the spatial effect along with the figure numbers which show spectra from band pass filter output.

TABLE VII-3

ION CHAMBER AND BAND PASS OUTPUT SPECTRA LOCATIONS

RUN NUMBER	CHAMBER	BAND PASS OUTPUT SPECTRA FIGURE NUMBER
15-16	A	VII - 17
15-9	D	VII - 19
15-18	A, C	VII - 13
15-19	A, C	VII - 15
15-1	C	VII - 11

Figure VII-27 shows μμA spectra with amplitudes normalized at .7 cps. There is somewhat of an indication that the high frequency side of the spectrum is moved upward with increasing flow. This is not a strong effect. The low frequency side shows an increasing amplitude with decreasing flow. A particularly large low frequency amplitude is shown for the case of reactor operation in forced circulation with baffle doors open. The basis for this particular response is considered to be uncoupled responses of the fluid dynamic paths with nuclear coupling. In general, the characteristics observed here seem in agreement with the predictions of pre-test analysis theory in that a more responsive system to low frequencies would be expected for the low flow system as compared to the high flow system. Noise excitations also enter into this picture.

The effect is still further amplified for natural circulation operation of the reactor as shown in Figure VII-13(a) to (d). Previous discussion in this section discusses the possible transit time effects and proposes ideas which relate the noise excitation to this as outlined in Section VII-C.

NOTE: THERE IS A PROBLEM IN THE USE OF THIS RUN IN THAT ROD #7 WAS NOT PLACED CORRECTLY. 15-1-3 WAS A BETTER RUN.

FIGURE VII-6

RUN:	15-1-1,2
DATE:	DEC. 5, 1961
MODE OF CIRCULATION:	FORCED
POWER	15 MW(t)
NOMINAL FLOW:	20,000 gpm
PUMP NO:	BOTH
PUMP HEAD:	200 FEET

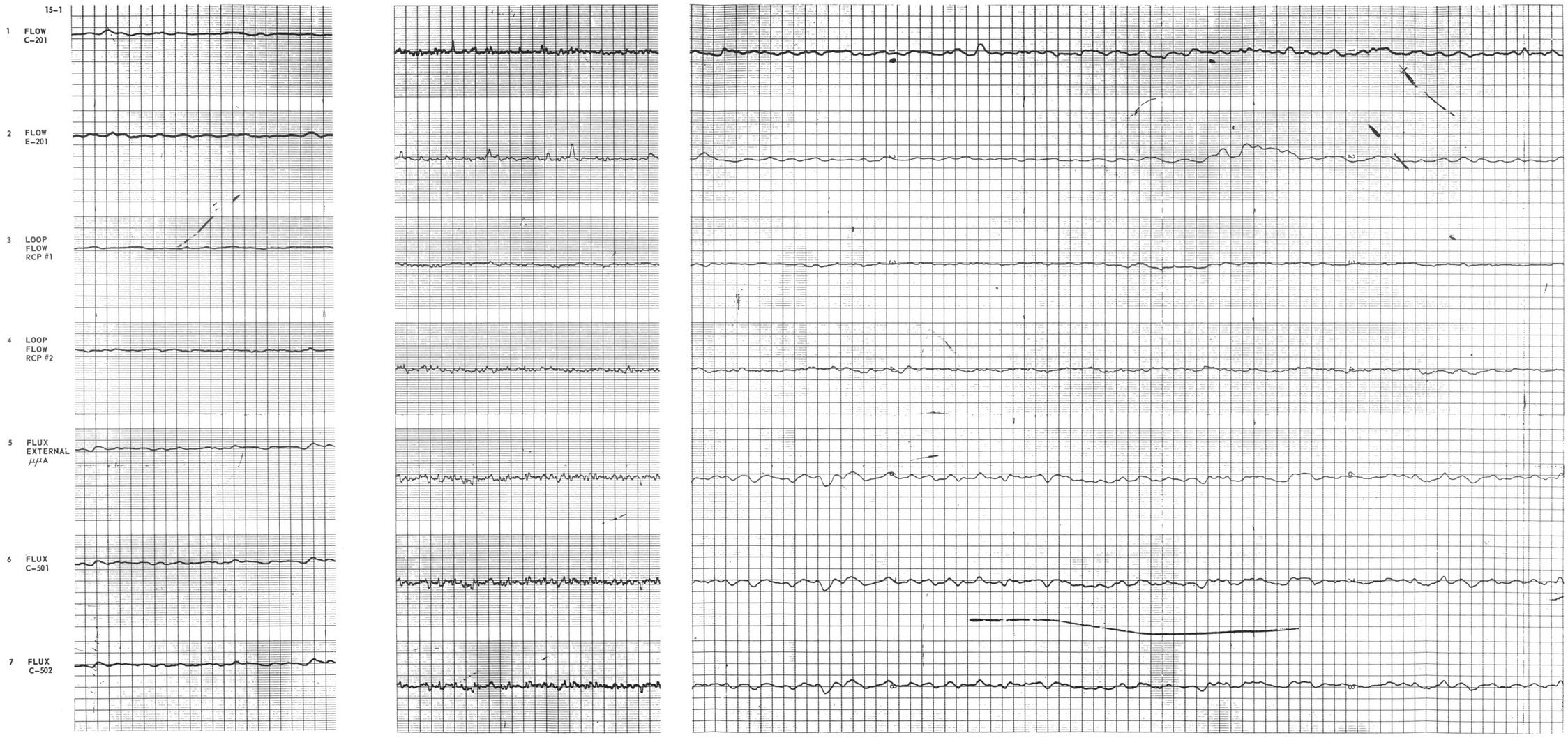

NON ZERO SUPPRESSIONS
TIME: 10 mm/second

ZERO SUPPRESSED
TIME: 2 mm/second

ZERO SUPPRESED
TIME: 10 mm/second

FIGURE VII–7

RUN:	15–9–1a,1b
DATE:	NOV. 22, 1961
MODE OF CIRCULATION:	FORCED
POWER:	15 MW(t)
NOMINAL FLOW:	4,000 gpm
PUMP NO:	1
PUMP HEAD:	290 FEET

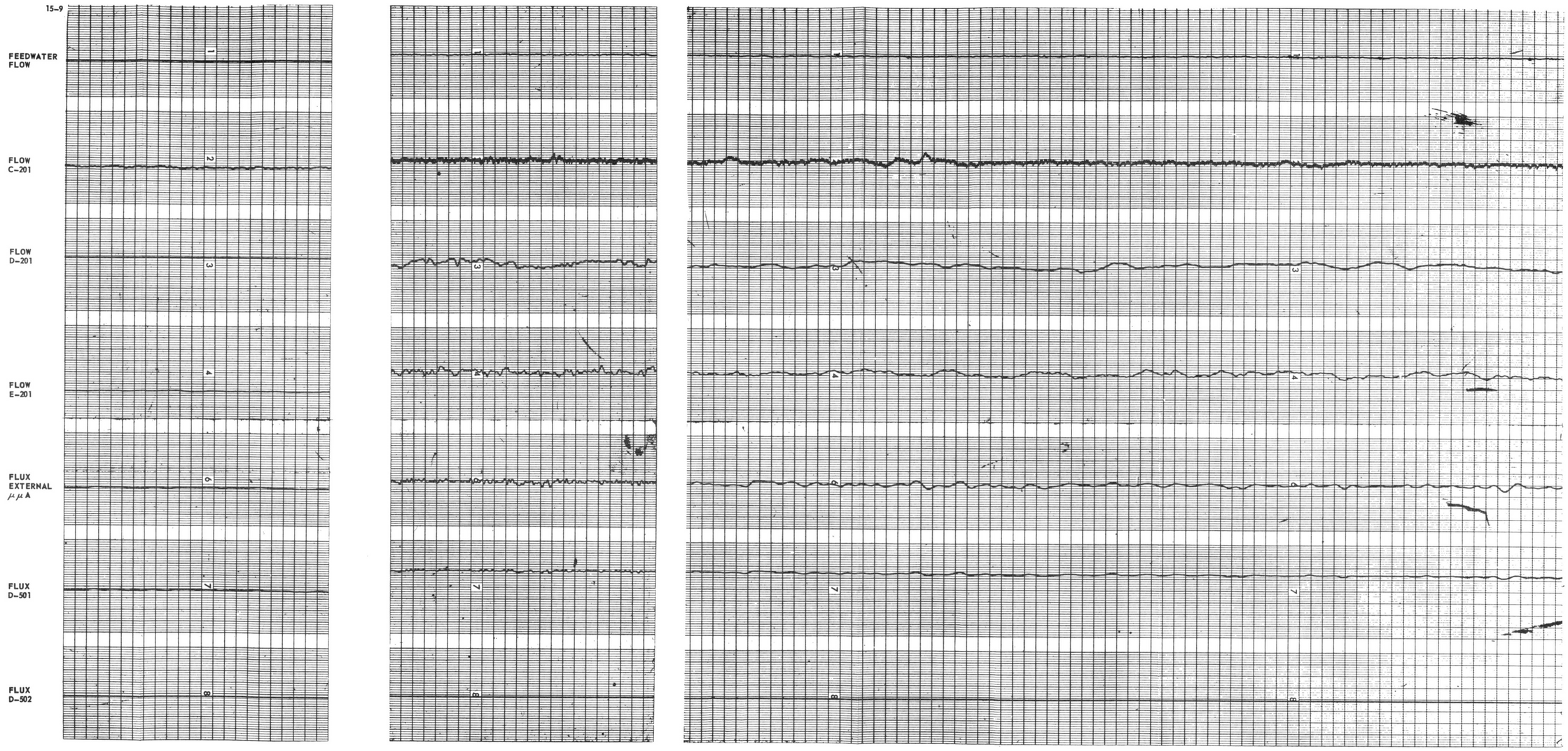

NON ZERO SUPPRESSIONS
TIME: 10 mm/second

ZERO SUPPRESSED
TIME: 2 mm/seconds

ZERO SUPPRESSED
TIME: 10 mm/seconds

FIGURE VII–8

RUN:	15–19–2,3
DATE:	DEC. 28, 1961
MODE OF CIRCULATION:	FORCED
POWER:	15 MW(t)
NOMINAL FLOW:	4,400 gpm
PUMP NO:	2
PUMP HEAD:	7½ FEET

NOTE: PULSES IN CHANNEL ONE ARE FALSE INDICATIONS CAUSED BY ELECTRICAL NOISE.

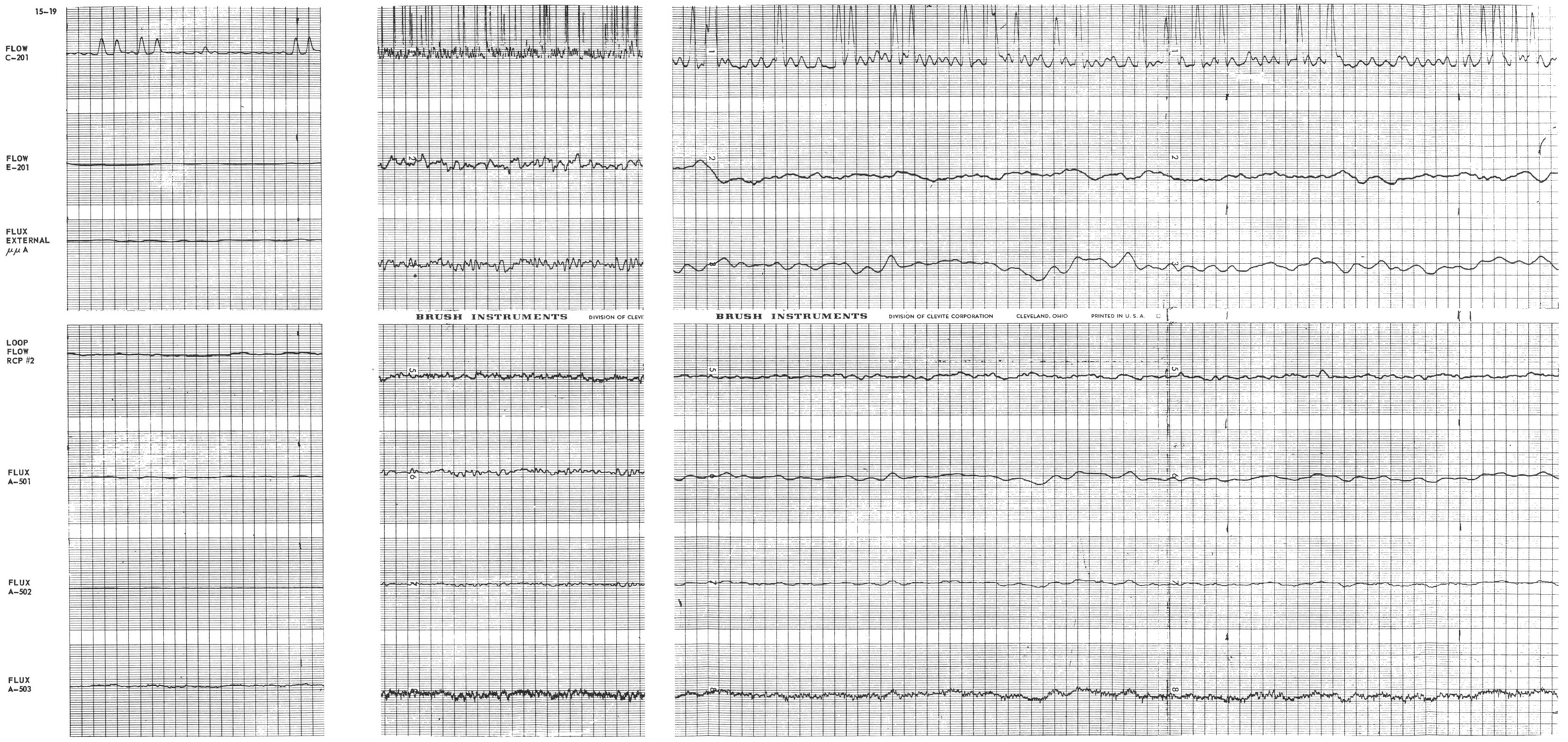

NON ZERO SUPPRESSIONS
TIME: 10 mm/second

ZERO SUPPRESSED
TIME: 2 mm/second

ZERO SUPPRESSED
TIME: 10 mm/second

FIGURE VII–9

RUN:	15–16–1,2
DATE:	DEC. 4, 1961
MODE OF CIRCULATION:	FORCED
POWER:	15 MW(t)
NOMINAL FLOW:	4,000 gpm
PUMP NO:	1
PUMP HEAD:	290 FEET, BAFFLES OPEN

NOTE: PULSES IN CHANNEL ONE ARE FALSE INDICATIONS CAUSED BY ELECTRICAL NOISE.

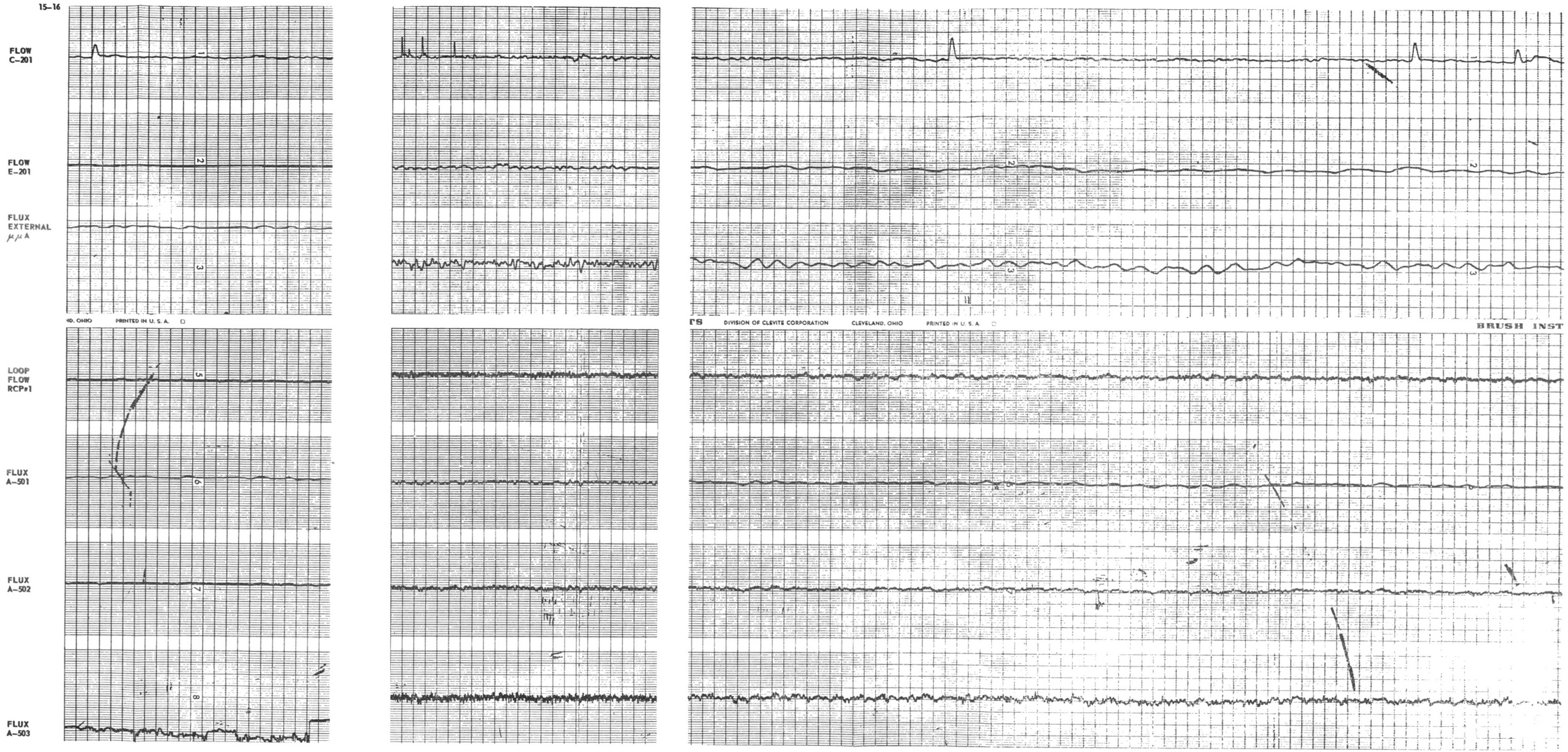

NON ZERO SUPPRESSIONS
TIME: 10 mm/second

ZERO SUPPRESSED
TIME: 2 mm/second

ZERO SUPPRESSED
TIME: 10 mm/second

DRIFT IN ION CHAMBER SIGNAL CAUSED BY MOISTURE IN CONNECTORS.

FIGURE VII–10

RUN:	15–18–1,2
DATE:	DEC. 11, 1961
MODE OF CIRCULATION:	NATURAL
POWER:	15 MW(t)
NOMINAL FLOW:	4,3000 gpm
PUMP NO:	NONE

NON ZERO SUPPRESSIONS
TIME 10 mm/second

ZERO SUPPRESSED
TIME 2 mm/second

ZERO SUPPRESSED
TIME 10 mm/second

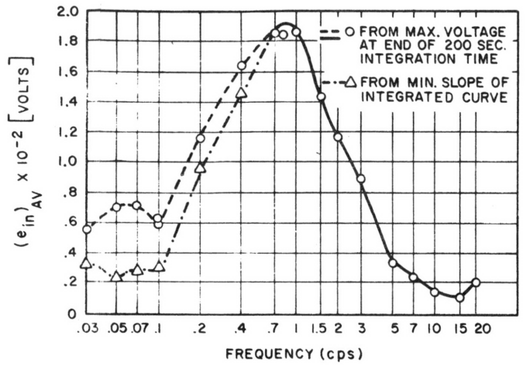

(a) BAND PASS ANALYSIS MICRO MICRO AMMETER ($\mu\mu$A)

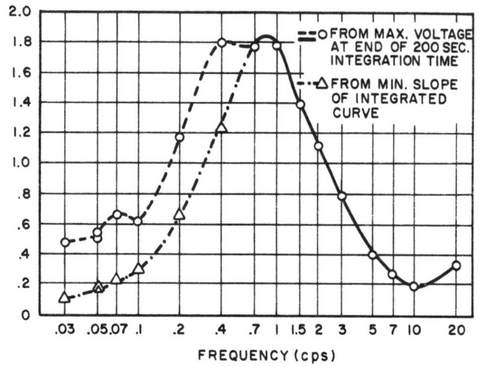

(b) BAND PASS ANALYSIS C-501 IN CORE FLUX

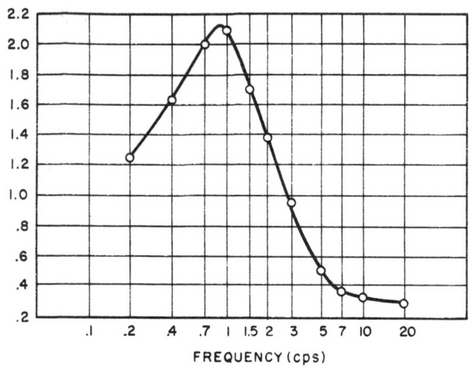

(c) BAND PASS ANALYSIS C502 IN CORE FLUX

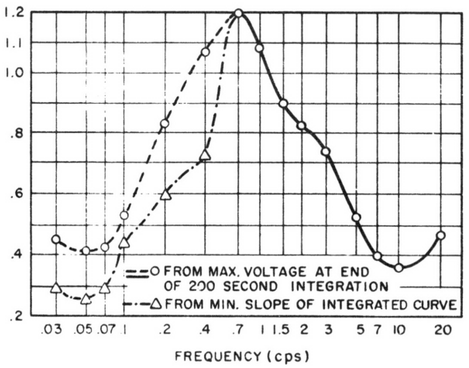

(g) BAND PASS ANALYSIS RCP-2

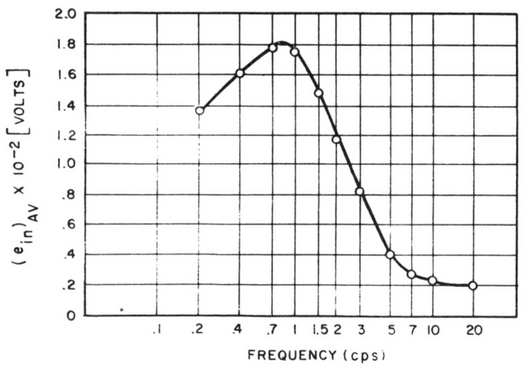

(d) BAND PASS ANALYSIS C503 IN CORE

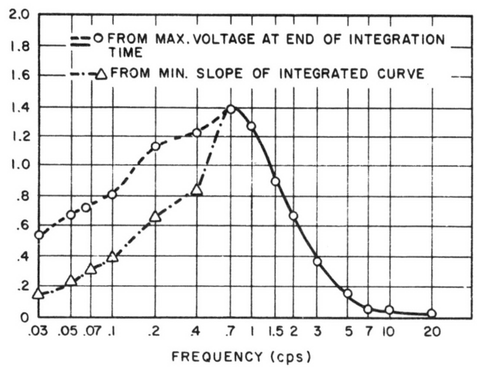

(e) BAND PASS ANALYSIS E 201 CORE FLOW

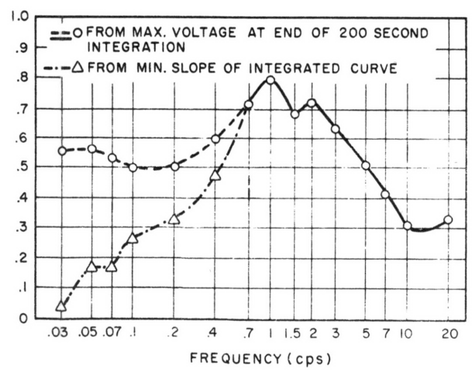

(f) BAND PASS ANALYSIS RCP-1

FIG. VII-11. FORCED CIRC. RUN 15-1-2 $G_1 = G_2 = 10{,}000$ gpm STEADY STATE NOISE

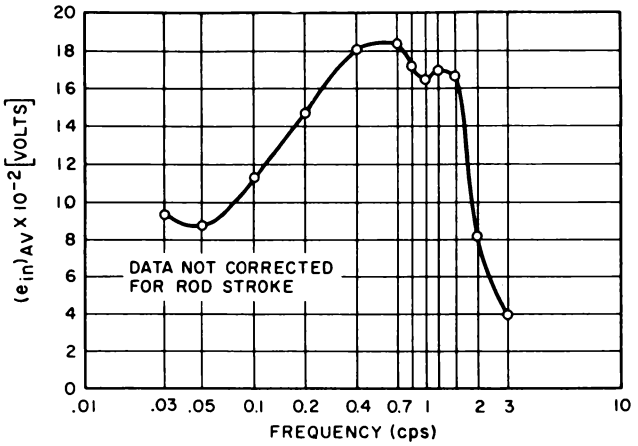

(a) BAND PASS ANALYSIS MICRO MICRO AMMETER ($\mu\mu$A)

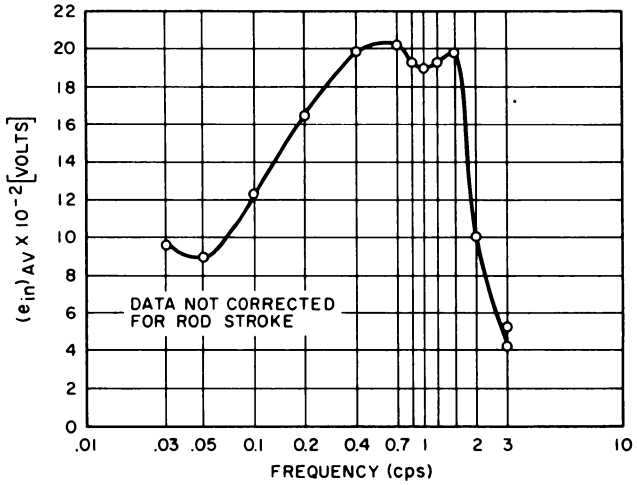

(b) BAND PASS ANALYSIS C501 IN CORE FLUX

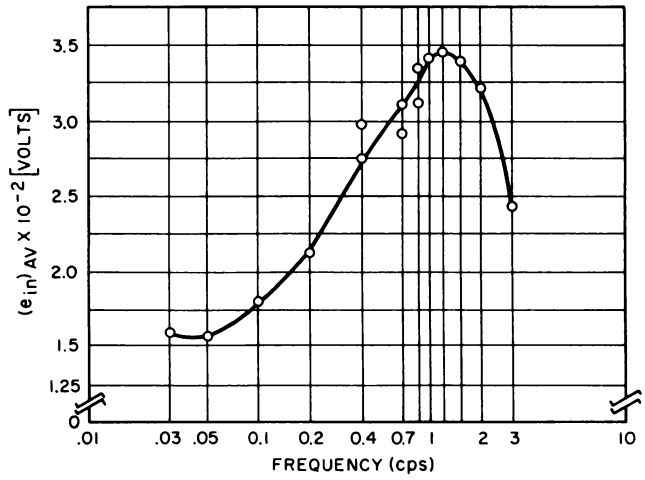

(c) BAND PASS ANALYSIS E201 IN CORE FLOW

FIG. VII-12. FORCED CIRC. RUN 15-1-(4-15) $G_1 = G_2 = 10{,}000$ gpm (Flow, 20,000 gpm) ROD OSCILLATOR

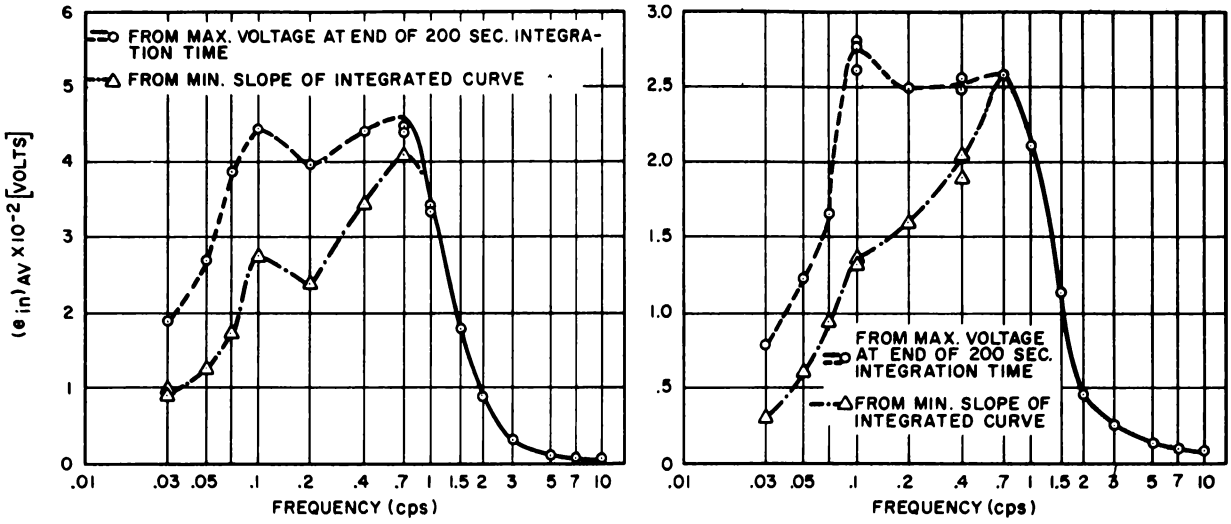

(a) BAND PASS ANALYSIS MICRO MICRO AMMETER ($\mu\mu$A)

(b) BAND PASS ANALYSIS C501 IN CORE FLUX

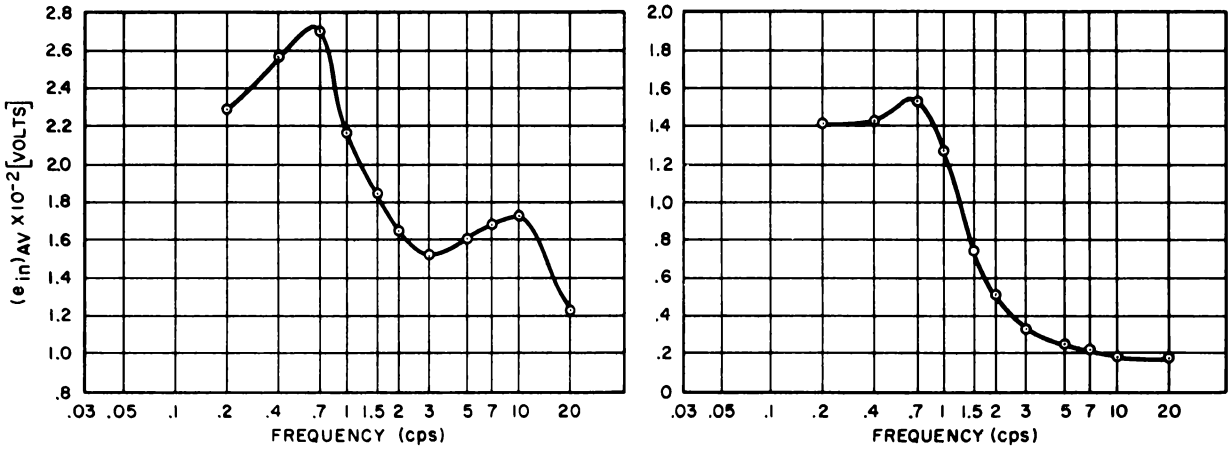

(c) BAND PASS ANALYSIS A503 IN CORE FLUX

(d) BAND PASS ANALYSIS C503 IN CORE FLUX

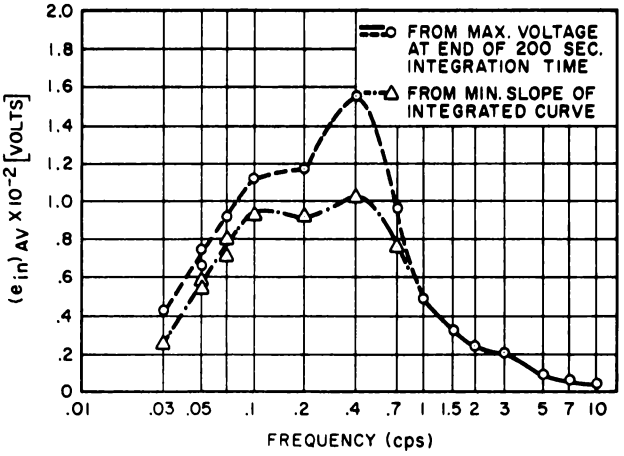

(e) BAND PASS ANALYSIS E201 IN CORE FLOW

FIG. VII-13. NATURAL CIRC. RUN 15-18-2 STEADY STATE NOISE

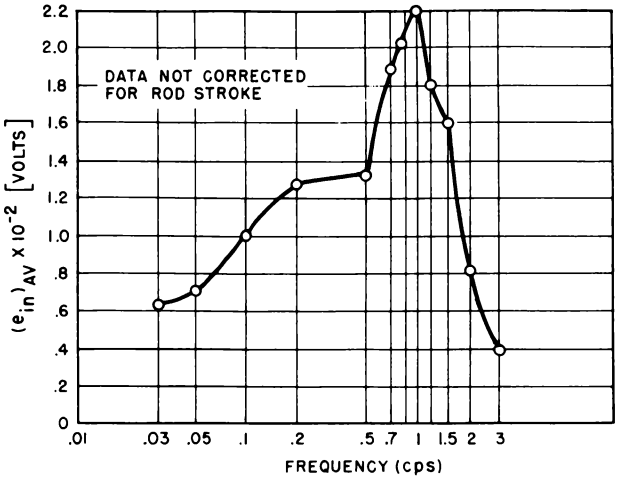

(a) BAND PASS ANALYSIS MICRO MICRO AMMETER ($\mu\mu$A)

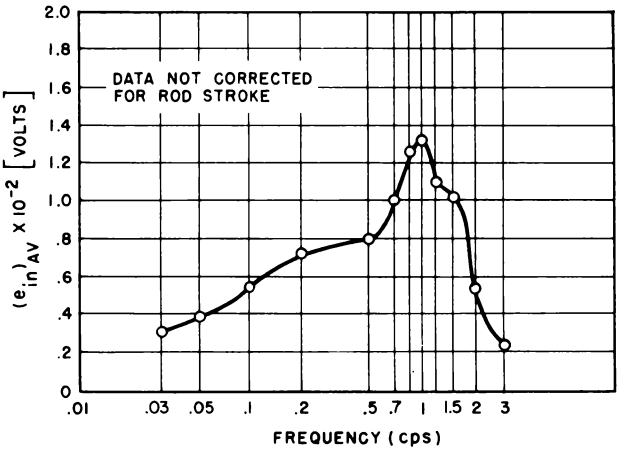

(b) BAND PASS ANALYSIS C501 IN CORE FLUX

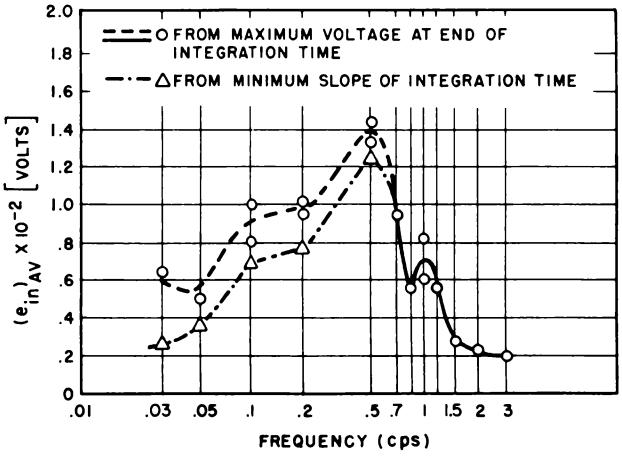

(c) BAND PASS ANALYSIS E201 IN CORE FLUX

FIG. VII-14. NATURAL CIRC. RUN 15-18-2
ROD OSCILLATOR

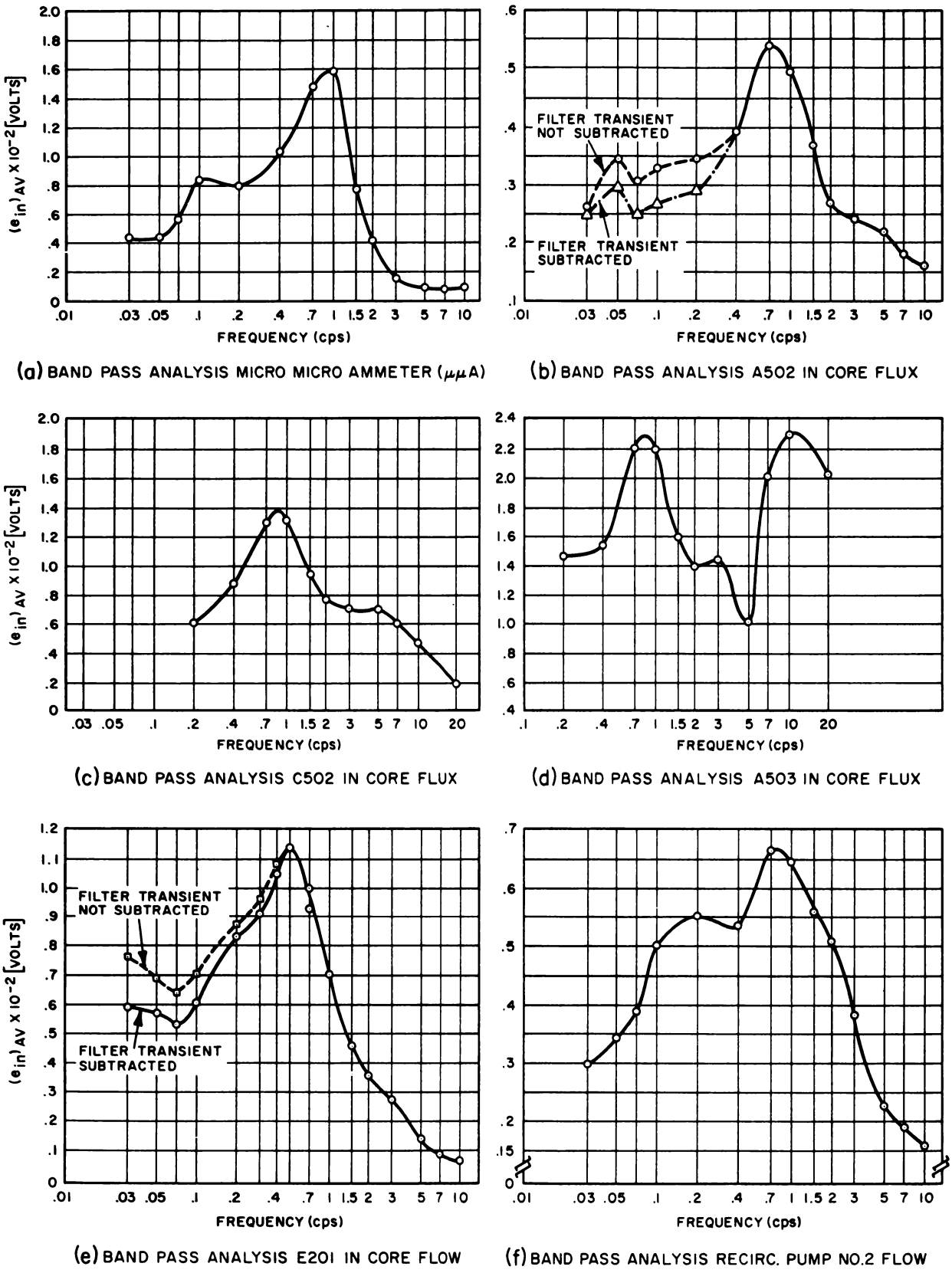

(a) BAND PASS ANALYSIS MICRO MICRO AMMETER ($\mu\mu$A)

(b) BAND PASS ANALYSIS A502 IN CORE FLUX

(c) BAND PASS ANALYSIS C502 IN CORE FLUX

(d) BAND PASS ANALYSIS A503 IN CORE FLUX

(e) BAND PASS ANALYSIS E201 IN CORE FLOW

(f) BAND PASS ANALYSIS RECIRC. PUMP NO.2 FLOW

FIG. VII-15. FORCED CIRC. RUN 15-19-3 STEADY STATE NOISE

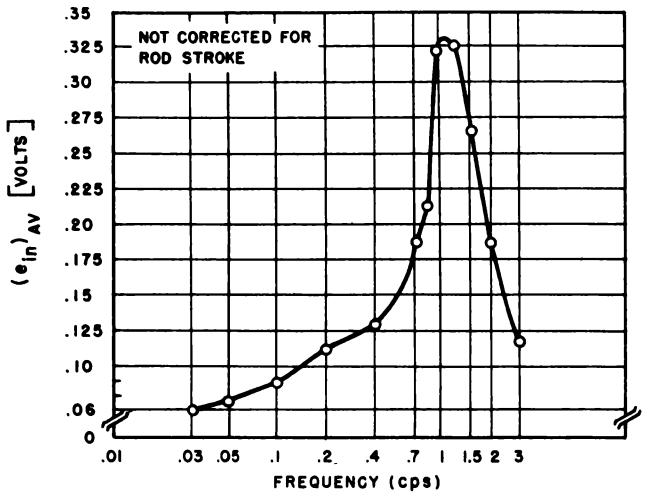

(a) BAND PASS ANALYSIS MICRO MICRO AMMETER ($\mu\mu$A)

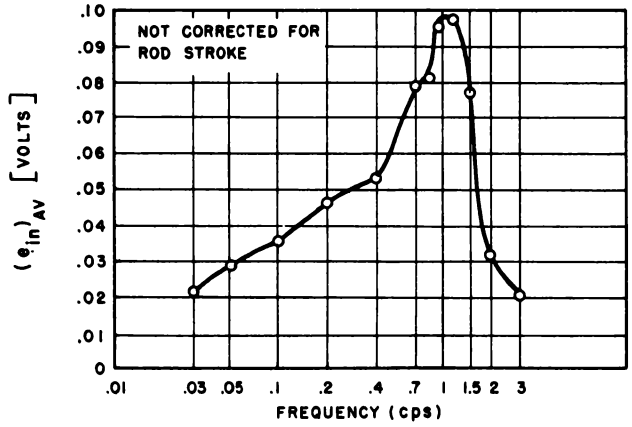

(b) BAND PASS ANALYSIS A502 IN CORE FLUX

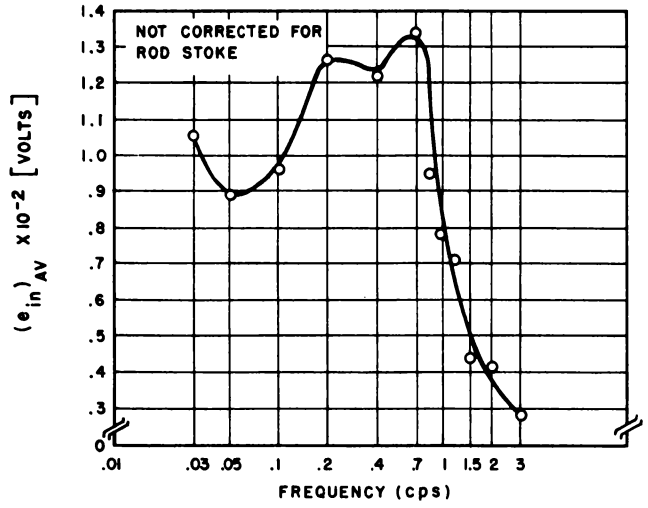

(c) BAND PASS ANALYSIS E201 IN CORE FLOW

FIG. VII - 16. FORCED CIRC. RUN 15-19-(4→15)
ROD OSCILLATOR

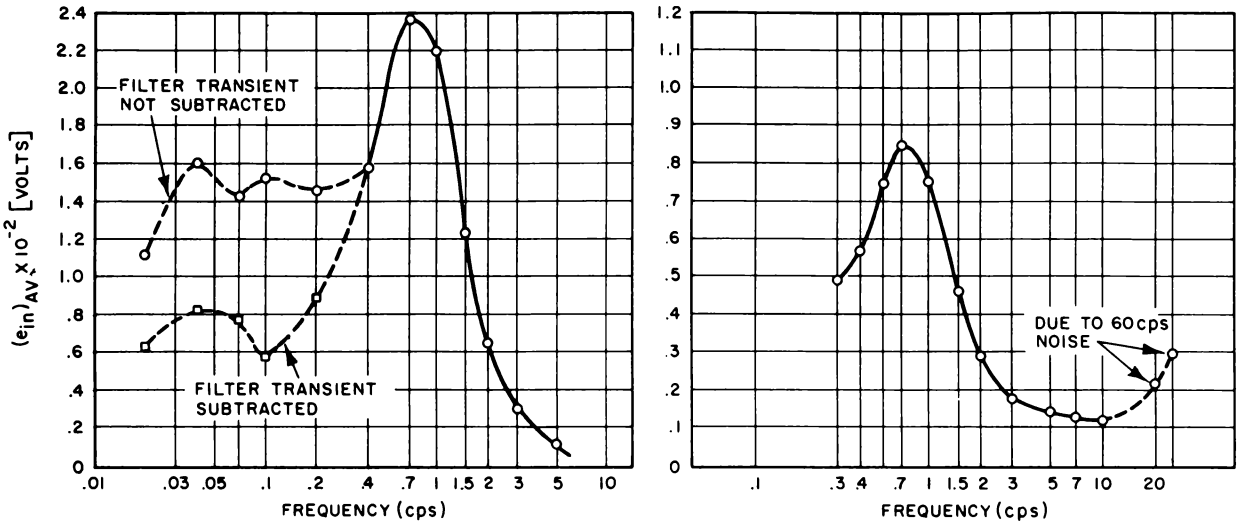

(a) BAND PASS ANALYSIS MICRO MICRO AMMETER ($\mu\mu$A)

(b) BAND PASS ANALYSIS A501 IN CORE FLUX

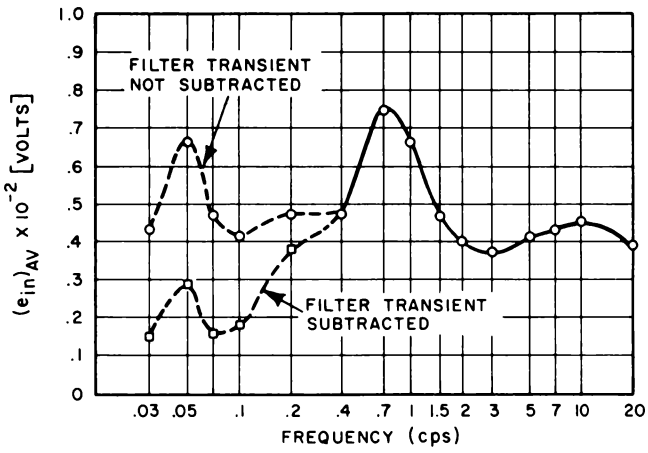

(c) BAND PASS ANALYSIS A502 IN CORE FLUX

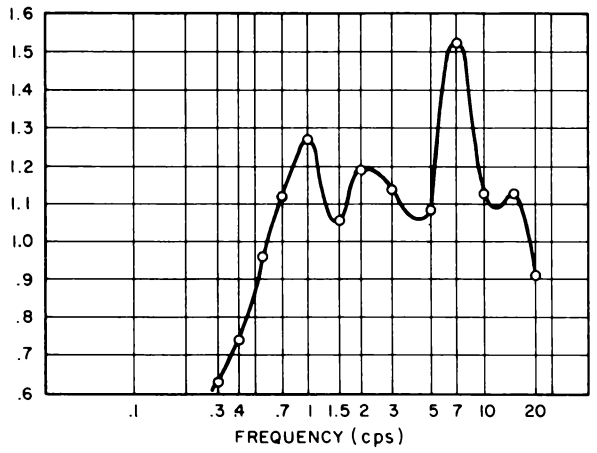

(d) BAND PASS ANALYSIS A503 IN CORE FLUX

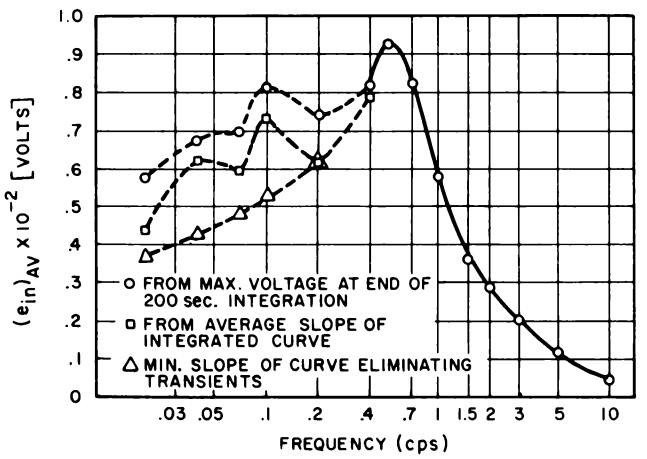

(e) BAND PASS ANALYSIS E201 IN CORE FLUX

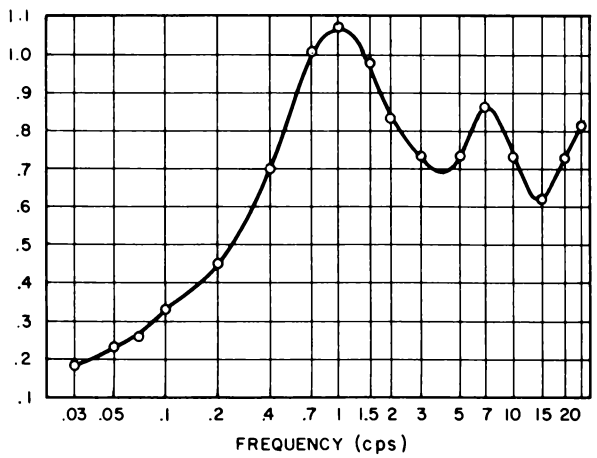

(f) BAND PASS ANALYSIS RCP-1, FLOW

FIG. VII-17. FORCED CIRC. BAFFLES OPEN RUN 15-16-2 STEADY STATE NOISE

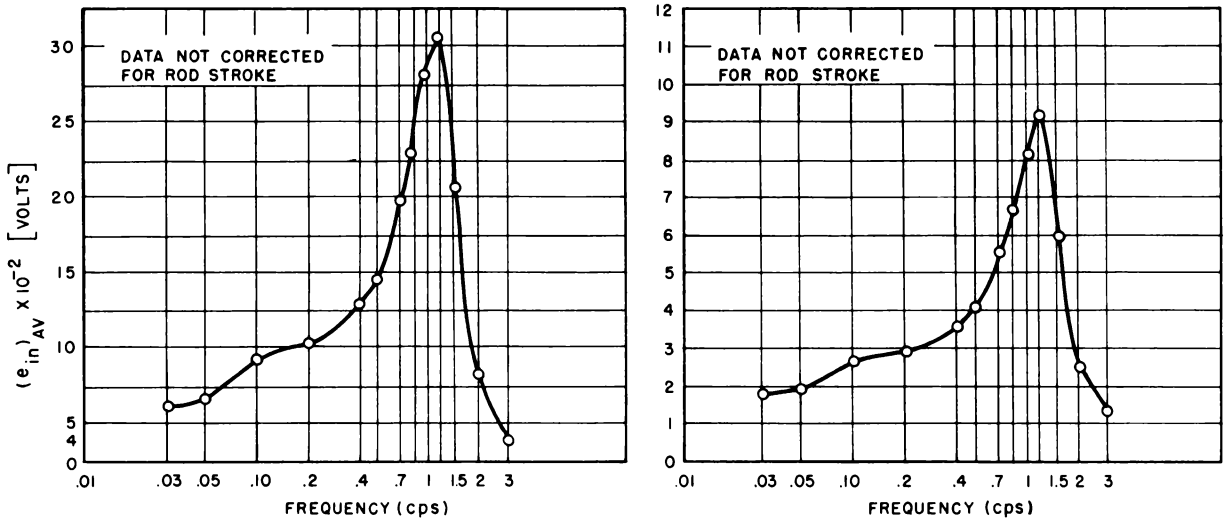

(a) BAND PASS ANALYSIS MICRO MICRO AMMETER ($\mu\mu$A) OPEN RUN 15-16-2

(b) BAND PASS ANALYSIS A502 IN CORE FLUX OPEN RUN 15-16-2

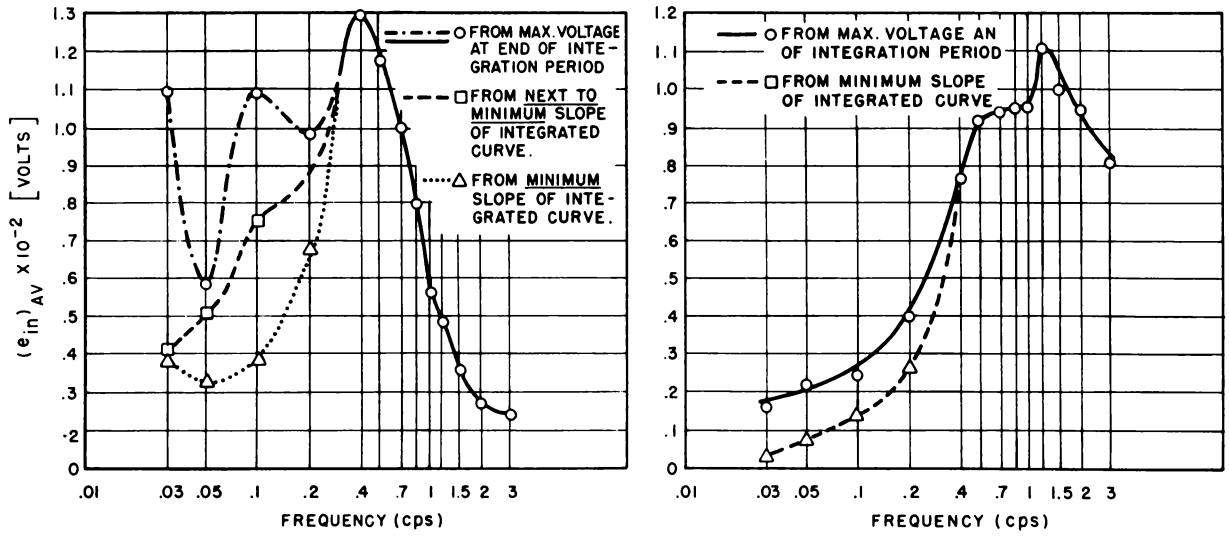

(c) BAND PASS ANALYSIS E201 IN CORE FLOW OPEN RUN 15-16-(4→15)

(d) BAND PASS ANALYSIS RCP-1 FLOW OPEN RUN 15-16-(4→15)

FIG. VII-18. FORCED CIRC. BAFFLES OPEN ROD OSCILLATOR

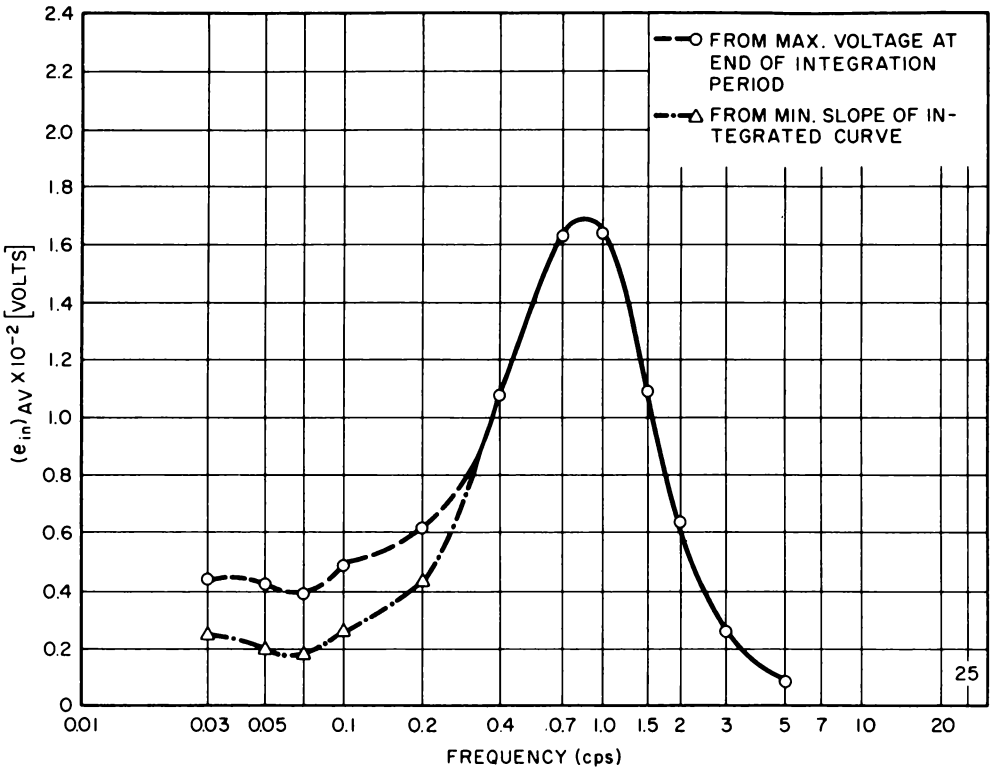

(a) BAND PASS ANALYSIS MICRO MICRO AMMETER ($\mu\mu$A)

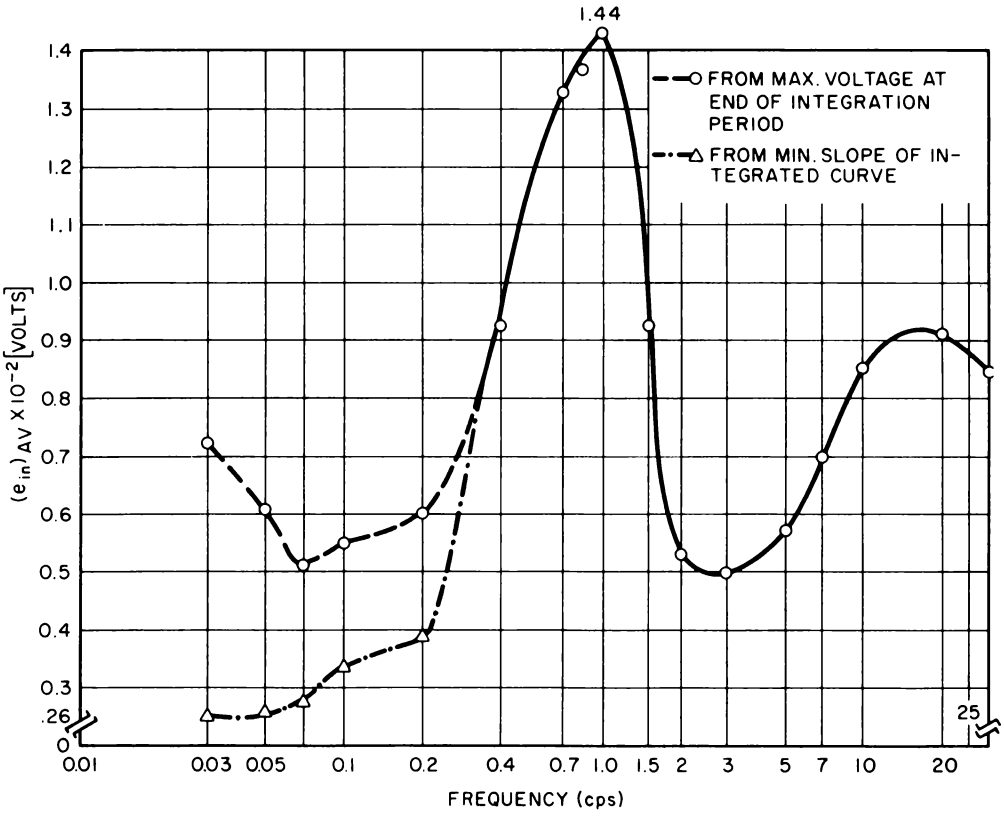

(b) BAND PASS ANALYSIS D503 IN CORE FLUX

IG. VII-19. FORCED CIRC. RUN 15-9-16 G_1 = 4,000 gpm STEADY-STATE NOISE

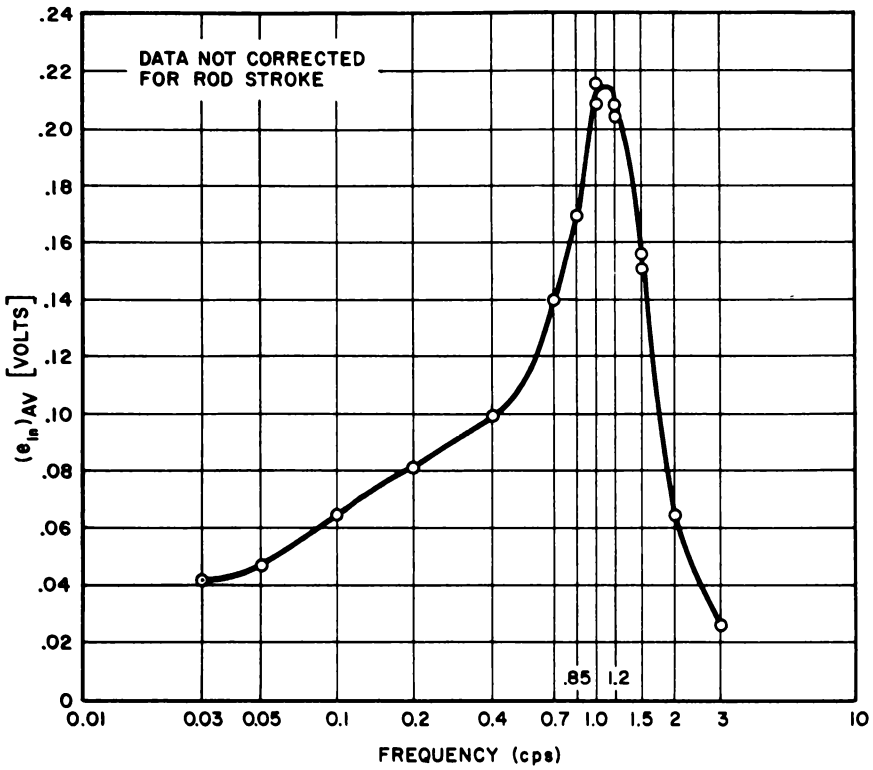

(a) BAND PASS ANALYSIS MICRO MICRO AMMETER ($\mu\mu$A)

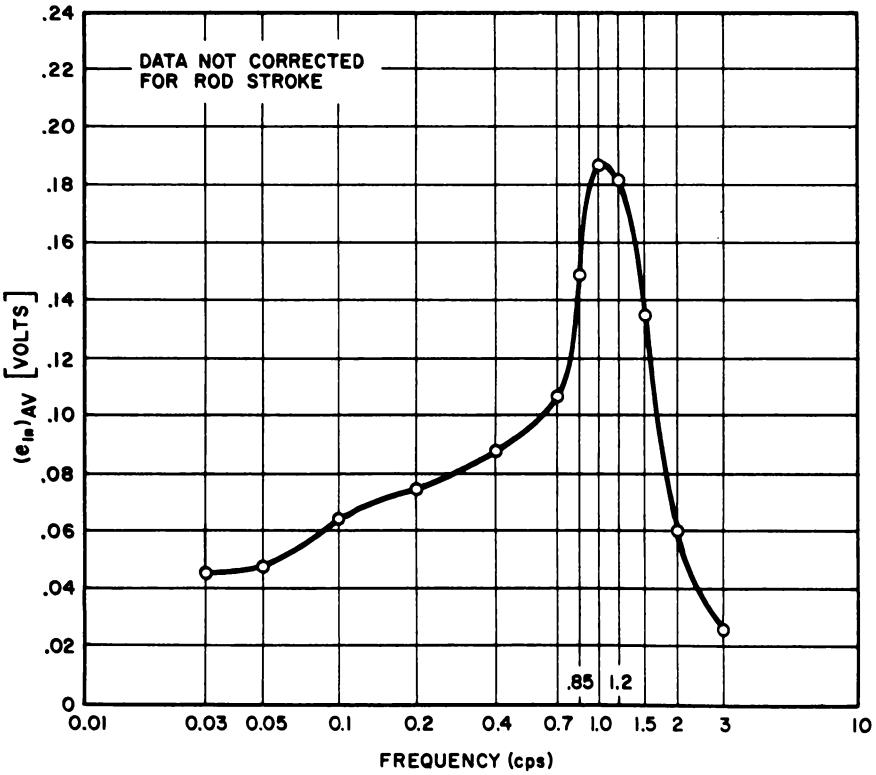

(b) BAND PASS ANALYSIS D503 IN CORE FLUX

FIG. VII-20. FORCED CIRC. RUN 15-9, G_l = 4000 gpm
ROD OSCILLATOR

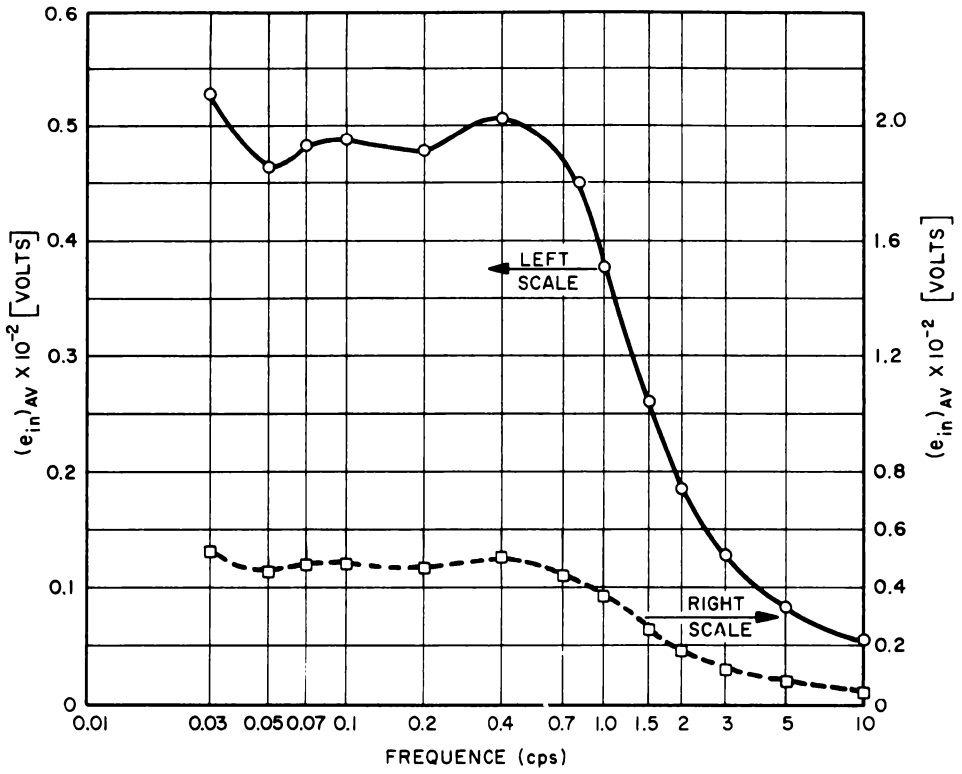

(a) BAND PASS ANALYSIS MICRO MICRO AMMETER ($\mu\mu$A)

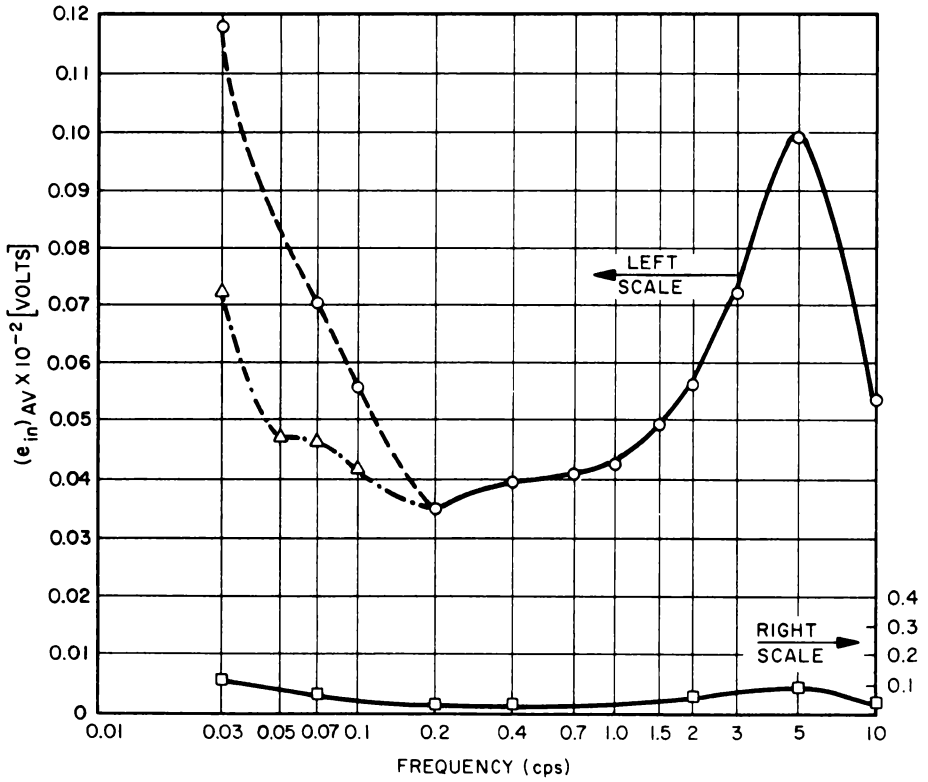

(b) BAND PASS ANALYSIS A502 IN CORE FLUX

FIG. VII-21. FORCED CIRC. RUN 0-2-2, RCP-1=10,000 gpm STEADY STATE NOISE

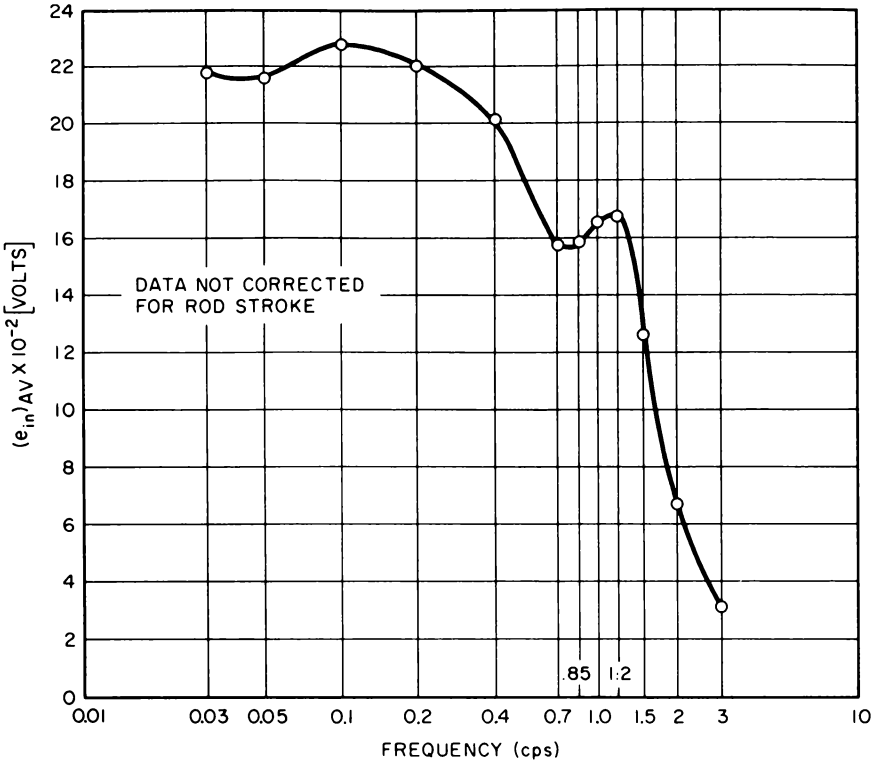

(a) BAND PASS ANALYSIS MICRO MICRO AMMETER ($\mu\mu$A)

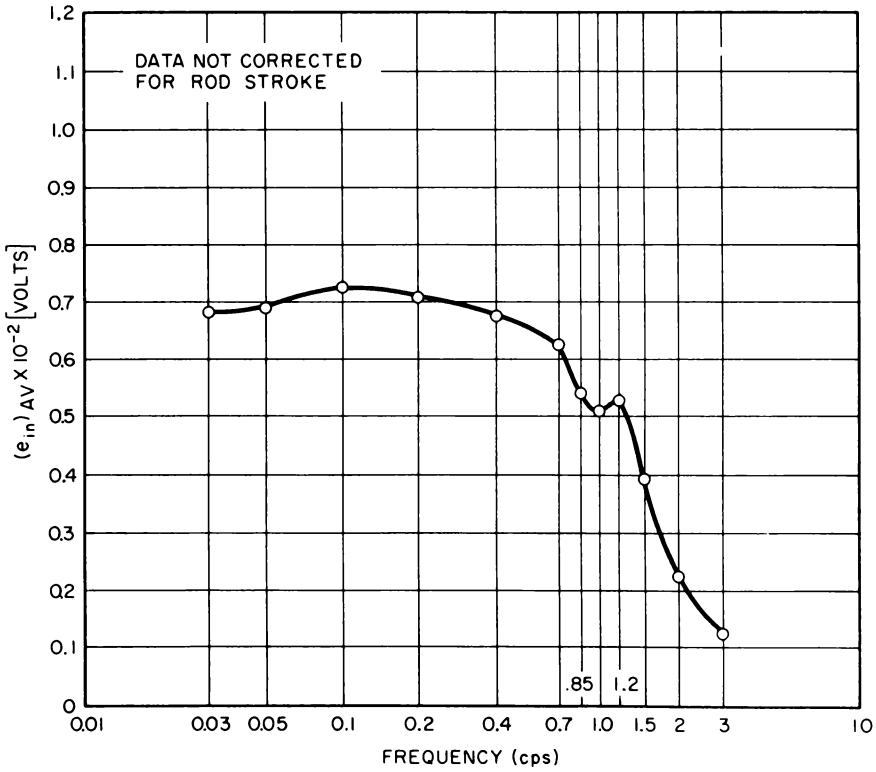

(b) BAND PASS ANALYSIS A502 IN CORE FLUX

FIG. VII-22. FORCED CIRC. RUN O-2 RCP-1 = 10,000 gpm ROD OSCILLATOR

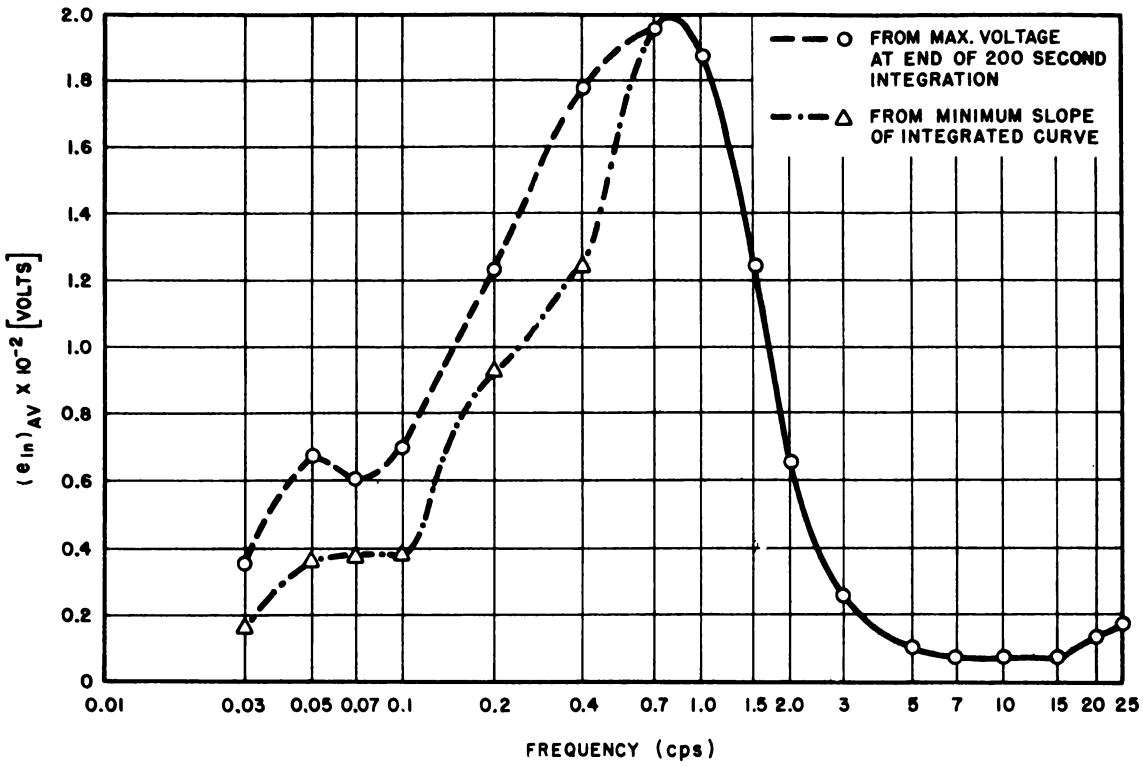

(a) BAND PASS ANALYSIS MICRO MICRO AMMETER ($\mu\mu$A)

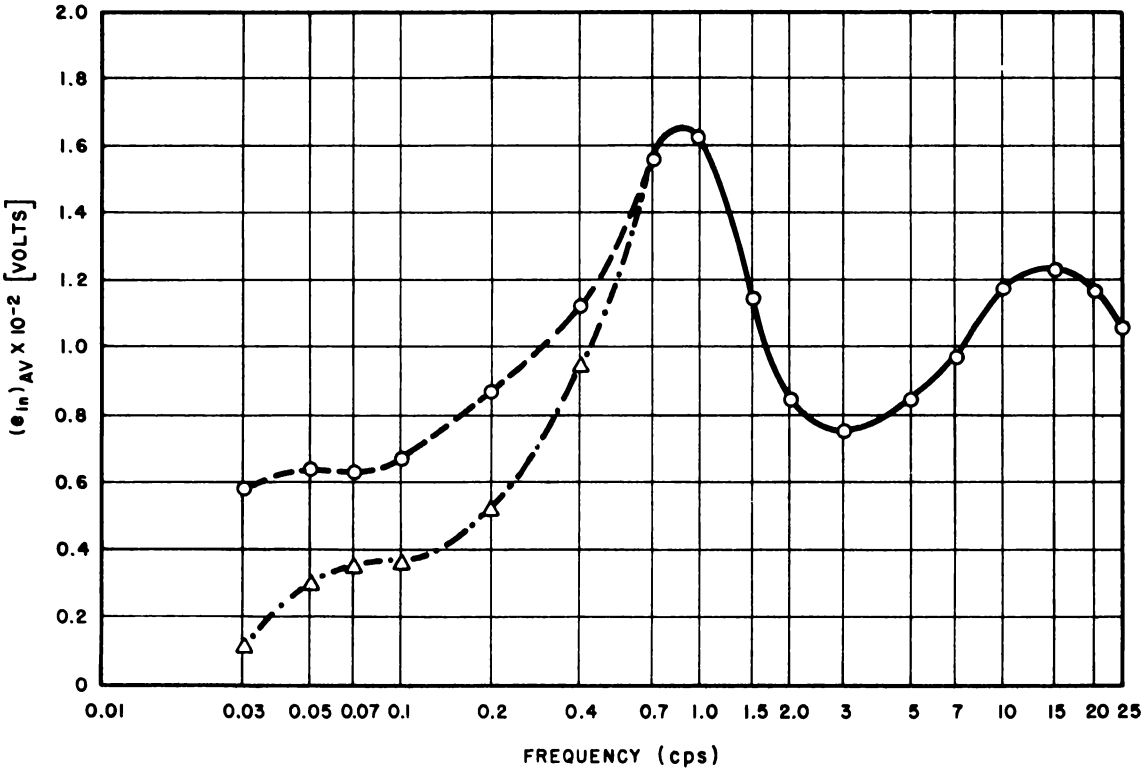

(b) BAND PASS ANALYSIS D503 IN CORE FLUX

FIG. VII-23. FORCED CIRC. RUN 15-11-36, RCP-1=2600 gpm STEADY STATE NOISE

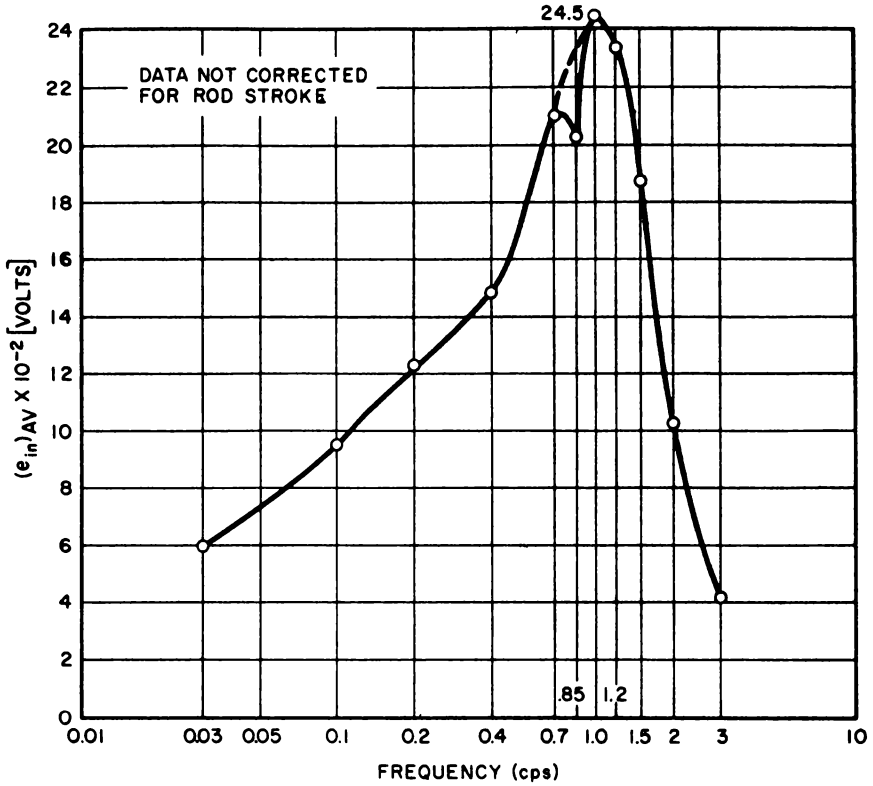

(a) BAND PASS ANALYSIS MICRO MICRO AMMETER ($\mu\mu$A)

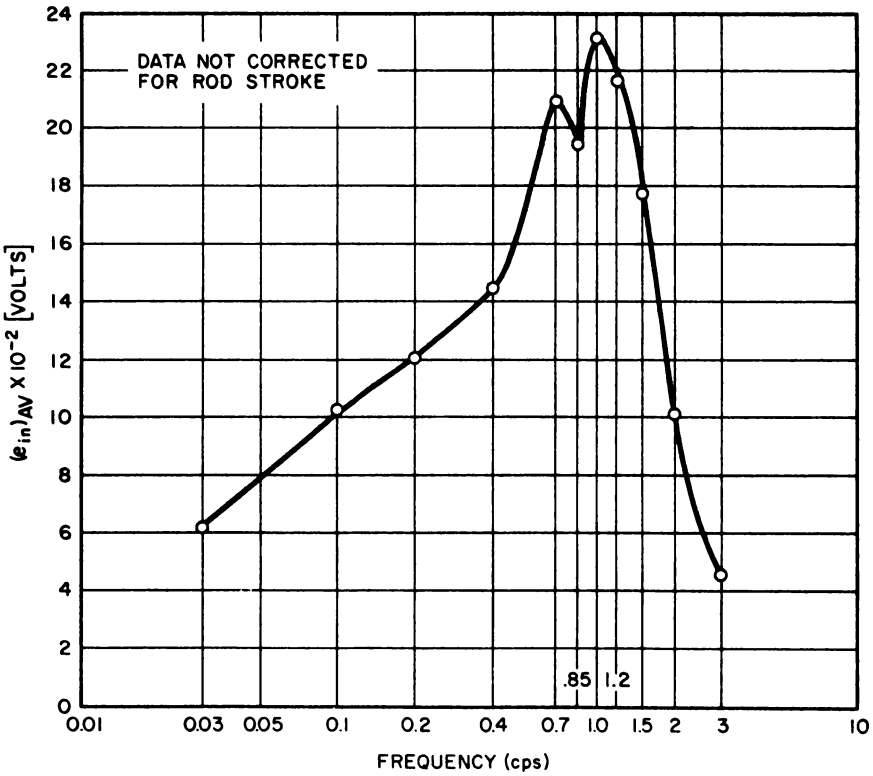

(b) BAND PASS ANALYSIS D503 IN CORE FLUX

FIG. VII-24. FORCED CIRC. RUN 15-11, RCP-1 = 2600 gpm
ROD OSCILLATOR

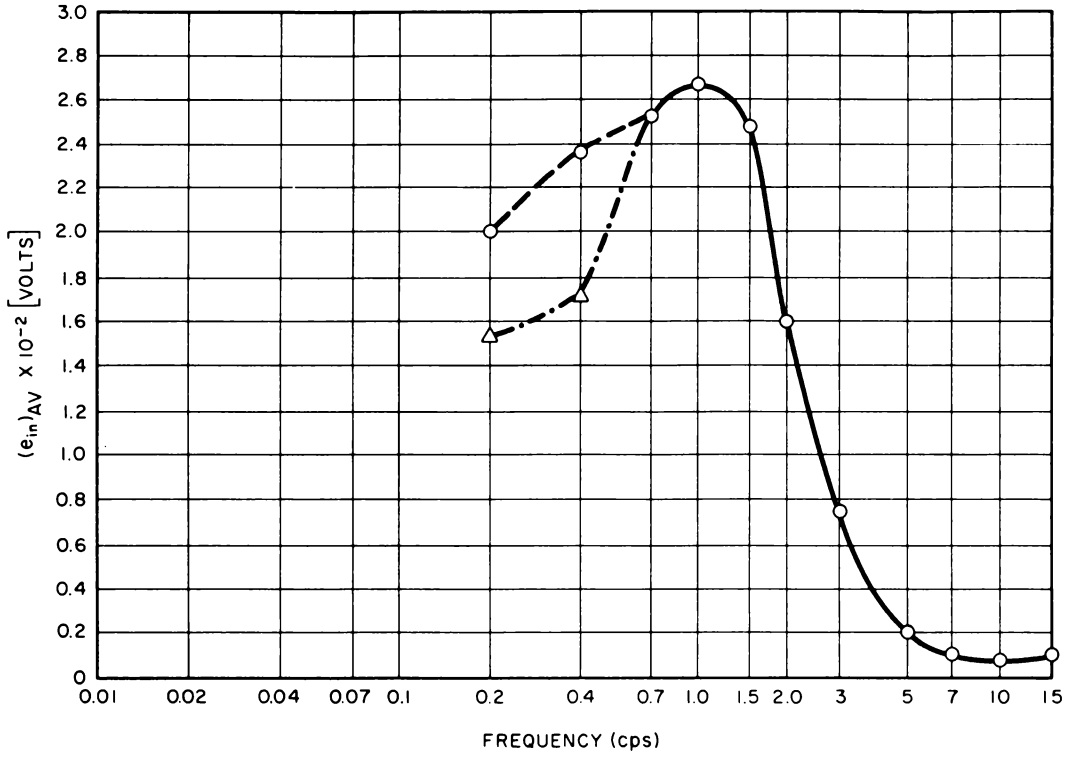

(a) BAND PASS ANALYSIS MICRO MICRO AMMETER ($\mu\mu$A)

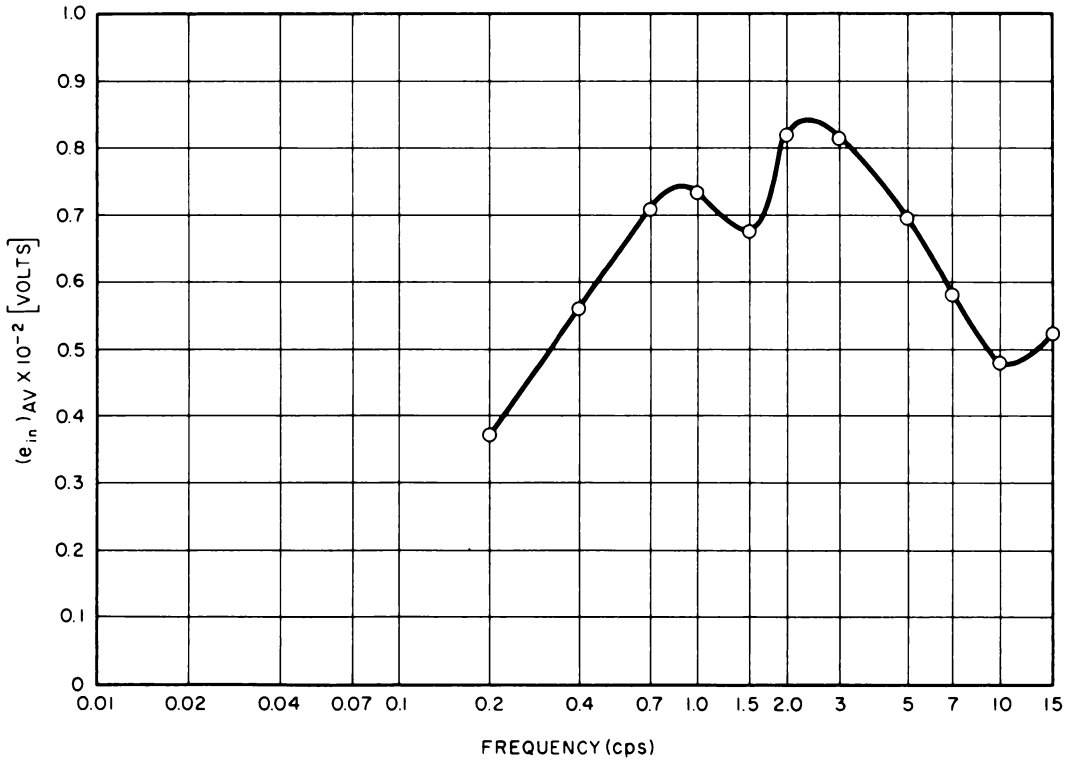

(b) BAND PASS ANALYSIS RCP-1

FIG. VII-25. FORCED CIRC. RUN 15-3-14b RCP-1 = 10,000 gpm STEADY-STATE NOISE

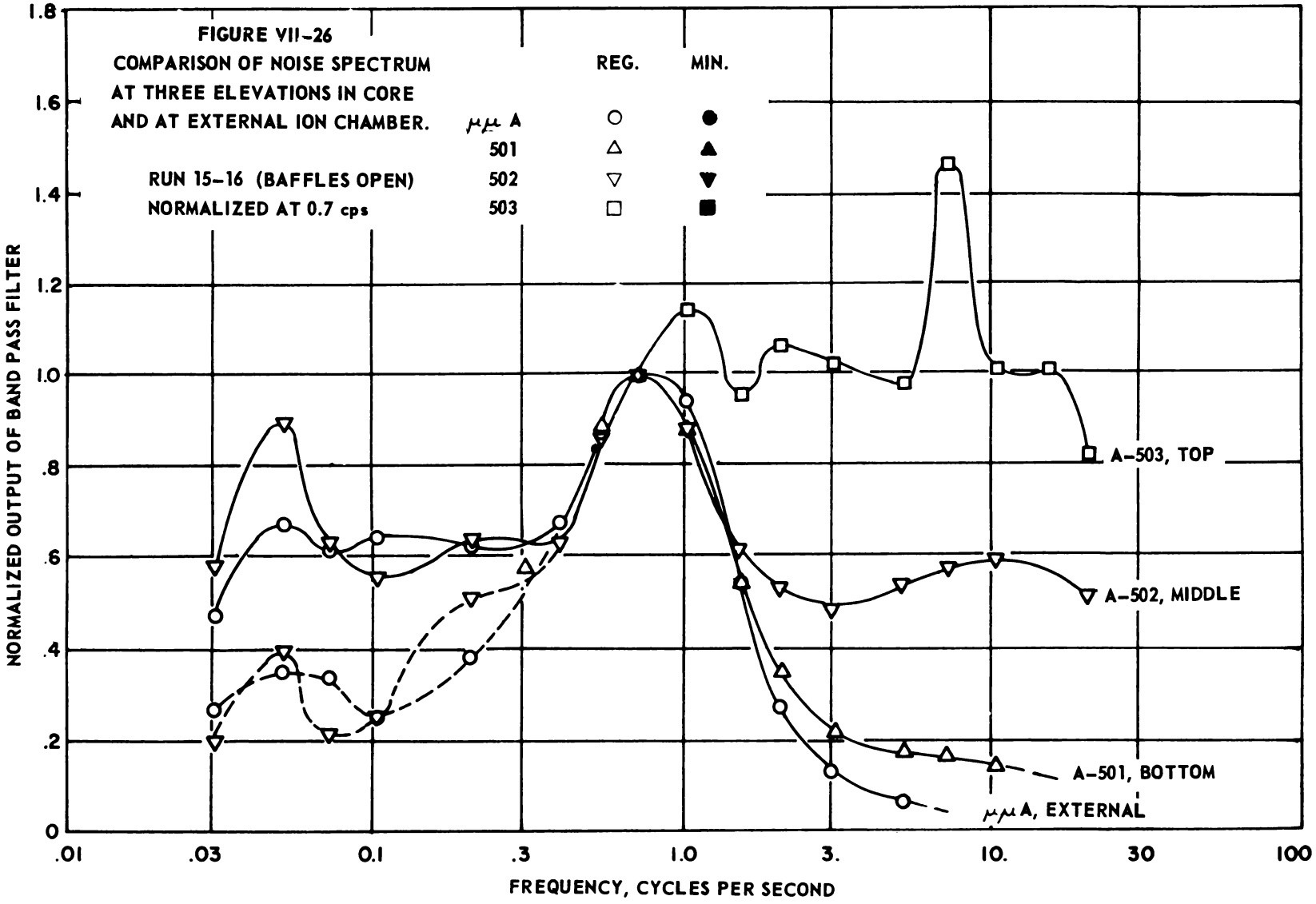
FIGURE VII-26
COMPARISON OF NOISE SPECTRUM AT THREE ELEVATIONS IN CORE AND AT EXTERNAL ION CHAMBER.
RUN 15-16 (BAFFLES OPEN)
NORMALIZED AT 0.7 cps
REG.
MIN.
μμ A
501
502
503
NORMALIZED OUTPUT OF BAND PASS FILTER
FREQUENCY, CYCLES PER SECOND
A-503, TOP
A-502, MIDDLE
A-501, BOTTOM
μμA, EXTERNAL
1.8
1.6
1.4
1.2
1.0
.8
.6
.4
.2
0
.01
.03
0.1
.3
1.0
3.
10.
30
100

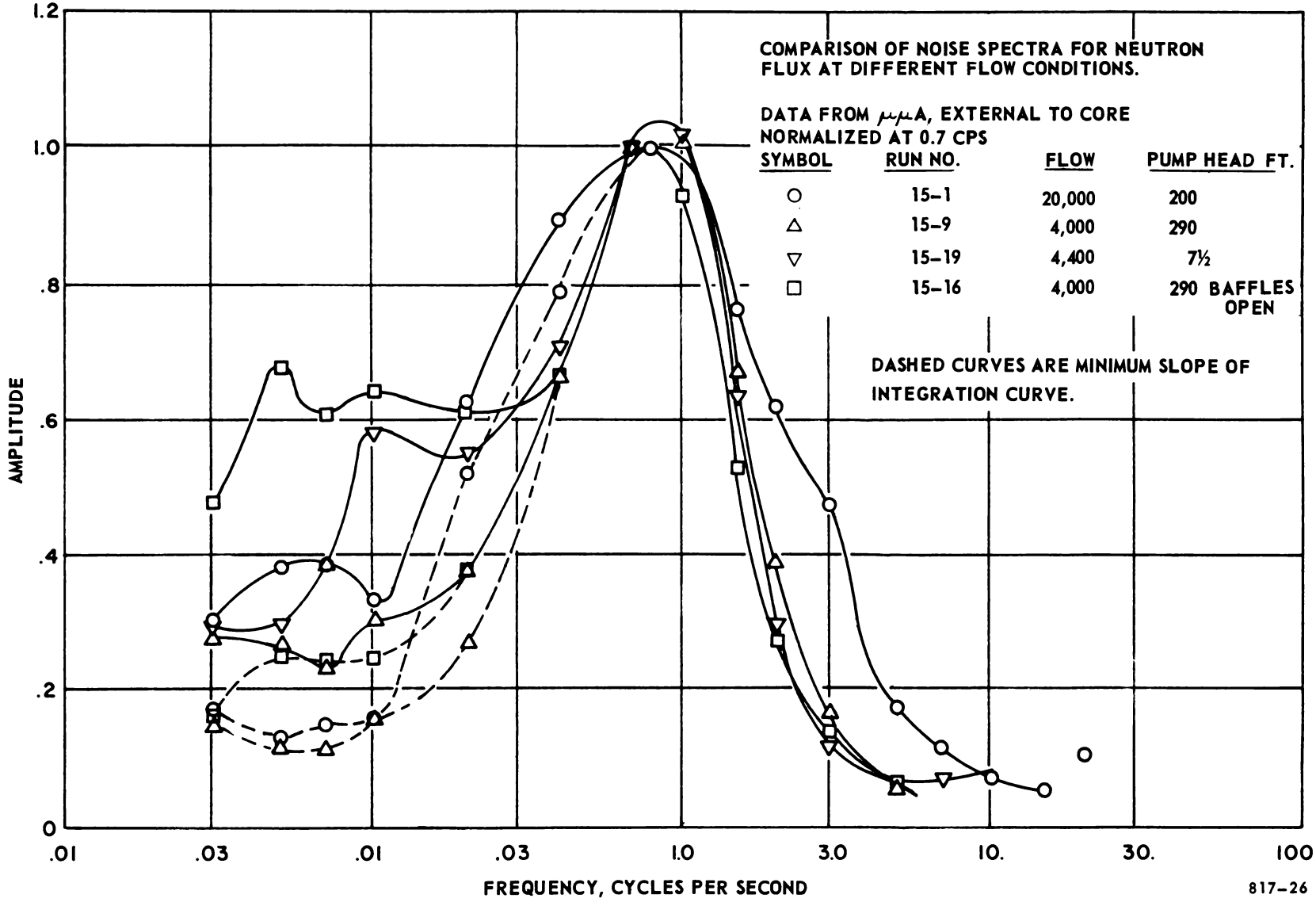
COMPARISON OF NOISE SPECTRA FOR NEUTRON FLUX AT DIFFERENT FLOW CONDITIONS.
DATA FROM μμA, EXTERNAL TO CORE NORMALIZED AT 0.7 CPS
SYMBOL RUN NO. FLOW PUMP HEAD FT.
○ 15-1 20,000 200
△ 15-9 4,000 290
▽ 15-19 4,400 7½
□ 15-16 4,000 290 BAFFLES OPEN
DASHED CURVES ARE MINIMUM SLOPE OF INTEGRATION CURVE.
AMPLITUDE
1.2
1.0
.8
.6
.4
.2
0
.01
.03
.01
.03
1.0
3.0
10.
30.
100
FREQUENCY, CYCLES PER SECOND
817-26

FIG. VII-27

SECTION VII-A-3

FLOW TRACE ANALYSIS

In-core flow measurements were made in two Consumers and three Fuel Cycle instrumented assemblies during this series of tests. The measurement equipment is described in detail in Section IV-D and Appendix A. The primary instrument is a Potter Aeronautical Company turbine-type flow meter attached to the inlet of the channel. The responses and calibrations are reported in Appendix C. The frequency response characteristics of the Potter flow meter and the results of the steady-state calibration test are also found in Appendix C.

Measurements of recirculation pump flow are made using ASME standard throat tap nozzles. Pressure measurements were made for this test using Pace reluctance type pressure transducers have a 0 to 6 psi range. These transducers are described in detail in Section VI and Appendix C. Reproducibility of the transducers was shown to be within 2%.

Traces for steady-state operation of the reactor are shown in Figures VII-6 to VII-10. The operating conditions for these five test runs are tabulated in Table VII-1. The flow path for runs 15-1, 15-9, 15-19 are (referring to Figure IV-1) from the core inlet, through the core and risers to the top of the core baffle. Above this is the separation free surface. The pump suction in this scheme is drawn from the vessel at a point opposite the cone baffle. Feedwater is injected at approximately this point and the mixed, subcooled stream passes through the pump (delivery head-flow curve Figure VII-28). For operation of both pumps, the discharges mix the order of 20 feet before re-entry to the vessel. Introduction into the vessel is by two chutes; one on either side of the vessel.

The flow path for Run 15-16 is the same as the forced circulation path except (refer to Fig. IV-1) the baffle doors located on either side of the core at a level of the riser discharge are opened. This provides a bypass to the core which has relatively low resistance to flow. Run 15-18 was accomplished securing the pumps and operating a core internal natural circulation loop through the above described baffle doors. This is the normal flow path for natural circulation operation of the reactor.

The visual analyses of data from trace and spectra were done to accomplish the objectives cited at the beginning of Section VII-A. Table VII-4 tabulates the observations obtained from time trace analysis of the measured test variable for Runs 15-1, 15-18, and 15-19. Column (1) tabulates observations which have been made for steady-state results. Rod oscillator results are discussed in Section VII-B.

PHASE RELATIONSHIPS

There appear to be no evidences of phase relationships between individual channel flows themselves in any of the runs. Pump flow records do not show phase relationships with in-core flows. There do not appear any defined phase relationships with power for any of these test runs, either forced or natural circulation. This is not unexpected since the pre-test dynamic analysis of the loop indicated desirable negative roots to the characteristic equations and desireable damping coefficients. Natural circulation operation for the test runs of Table VII-1 were estimated by pre-test analysis to have lower numerical root values and damping coefficients. The values are in a range where one might expect to see oscillatory behavior in the flow.

FUNDAMENTAL FREQUENCIES

E-201 flow meter traces for Run 15-1-3 (Figure VII-6)(20,000 gpm) show a low frequency oscillation not evidenced in Recirculation Pumps (RCP) 1 and 2 flows for this run. When the flow is reduced to 4,000 gpm (Figure VII-8) using RCP-2, an oscillation of about 2 cps appears in all flow trances, including the pump. RCP-2, E-201, and C-201 appear to have no correlation between them which is discernible. The corresponding natural circulation run 15-18-2 (Figure VII-10) shows frequencies greater than 1 cps for C-201, with still higher frequencies for E-201. In addition, these traces contain an evident harmonic content. A comparison will be made of those observations in the paragraphs discussing band pass filter analysis.

AMPLITUDES

Amplitudes of oscillation are tabulated in Table VII-4 for each of the variables. For Run 15-1-3 (Figure VII-6) it may be observed that E-201 flow meter shows a larger peak-to-peak flow oscillation than either RCP-1 or RCP-2. Also, there is

a significantly greater amplitude for RCP-2 than for RCP-1. When the forced circulation flow is reduced to 4,400 gpm in Run 15-19-3, (Figure VII-8), there is a significant reduction in peak-to-peak oscillation. Figure VII-29 shows data for a series of forced circulation runs from 20,000 gpm, two-pump operation to the 4,400 gpm Run 15-19-3.

CHARACTER OF TRACES

Figure VII-6 shows the trace for Run 15-1-2 for 15 MWt operation with two pumps. The trace shows flow meter C-201 and E-201 (this particular trace was taken at a time when control rod 7 was in the wrong location compared to the other tests). Comparing these traces to flows recorded for RCP-1 and RCP-2, both traces show small low frequency oscillations of a random nature. It is evident that these traces contain high frequencies compared to C-201 and E-201. This is also shown by the spectra of these runs in Figure VII-30. When the flow is reduced in the reactor to 4,000 gpmp by stopping Pump 2 and throttling the discharge valve (Run 15-9) (Figure VII-7), there is some reduction in amplitude of noise and frequencies above 1 cps disappear from the traces. There is no strong verification of this from band pass analysis of traces.

A similar low flow run was made using recirculation pump 2 which is a variable speed pump. This run was made by reducing pump speed and delivery head to approximately 4,000 gpm and 7.5 feet, respectively. The character of in-core flow traces for these two runs is very similar. The recirculation flow trace for RCP-2 cannot be compared since one was not obtained for Run 15-9. However, if one compares the traces for 15-1 and 15-19, there is little difference in the traces or in the peak frequencies of the spectrums obtained (Figure VII-11 and Figure VII-15). The indication here is that, although there is some reduction in noise level, there is little that can be inferred about a change in the flow system by examining this low flow, low head run trace.

Natural circulation runs (Run 15-18) are shown in Figure VII-13. These data were made with the internal natural circulation flow scheme discussed in Section IV. Examination of the steady-state flow traces shows amplitudes of oscillation slightly higher than obtained for the 4,000 gpm forced circulation runs (15-19).

TABLE VII-4

OBSERVATIONS OBTAINED FROM TIME TRACE ANALYSIS

RUNS 15-1, 15-18, 15-19

RUN	INST.	15-1-2, 3 ZERO SUP. STEADY-STATE	15-1-4 .03 cps	15-1-9 .7 cps	15-1-10 .85 cps	15-1-11 1.0 cps	15-1-12 1.2 cps	15-1-13 1.5 cps
15-1	C-201	SIGNAL OUT	SIGNAL OUT	- - - -	- - - -	- - - -	- - - -	- - - -
	E-201	15.5% PTP Oscillation. No phase relation to μμA. There is a definite low frequency not evident in RCP-1, 2.	Flow oscillations larger and more sinusoidal than in 15-1-3 (steady-state)	No response to rod motion. Appearance is that of steady-state.	NO SIGNIFICANT	CHANGE FROM	15-1-9 →	
	μμA	16.0% PTP Oscillation. All fluxes in phase.	All traces have different characteristics than steady-state. μμA leads rod oscillation.	μμA leads rod motion, shows presence of harmonics.				μμA phase lead on rod motion reduced to zero.
	RCP-1	4 - 6% PTP	No evidence of response to rod motion	No response to rod motion.	NO SIGNIFICANT	CHANGE FROM	15-1-9 →	
	RCP-2	9 - 12% PTP	No evidence of response to rod motion. More high frequency oscillations than RCP-1.	No response.	NO SIGNIFICANT	CHANGE FROM	15-1-9 →	

TABLE VII-4 (Continued)

RUN	INST.	15-18-2 ZERO SUP. STEADY-STATE	15-18-3 .03 cps	15-18-5 .1 cps	15-18-6 .2 cps	15-18-7 .5 cps	15-18-8 .7 cps	15-18-9 .85 cps	15-18-10 1.0 cps	15-18-11 1.2 cps	15-18-12 1.5 cps
15-18	C-201	6.5% PTP Sinusoidal oscillation. f > 1 cps No phase relationship.	7.5% PTP No phase relationship. f approx. 1 cps.	10.6% PTP Phase relationship flow down strong.	6.5% PTP High frequency find. No phase relationship.	8.1% PTP No phase relationship between C-201 and E-201.	6.5% PTP C-201 and E-201 have weak phase sympathetic but not resonant.	8.1% PTR No phase relationship, C-201 and E-201.	8.1% PTP $f_{C-201} > f_{E-201}$. No phase rel. C-201 and E-201.	PHASE RELATIONSHIP WASHED	OUT
	E-201	10.3% PTP Harmonic sawtooth. No phase relationship. $f > f_{C-201}$.	10.3% PTP Weak phase to rod position. f approx. 3 cps leads rod 20° to 30°.	8.5% PTP f approx. .7 cps. E lags μμA 30° to 40°.	10.3% PTP No phase to C-201. Phase lag to μμA 1 - 1.7 sec.	9.2% PTP Phase lag to μμA 1.5 sec.	13.8% PTP Well defined relationship between μμA and E-201 over entire trace. Phase lag μμA and E approx. 1 sec.	9.8% PTP Some response to μμA in phase, but not quantitative.	12.7% PTP No apparent phase μμA and E-201. (perhaps phase approx. 18)	SOME EVIDENCE OF FLUX RESPONSE	
	μμA	10.7% PTP In phase work with fluxes weak. Fundamental f approx. .2 cps.	13.3% PTP	12.0% PTP	24.0% PTP Phase relationship to E-201.	22.6% PTP	26.7% PTP Harmonic sinusoidal sawtooth.	24.0% PTP f approx. .1 cps.	28.0% PTP f approx. .15 cps.	PHASE RELATIONSHIP WASHED	OUT

TABLE VII-4 (Continued)

RUN	INST.	15-19-3	15-19-4	15-19-5	15-19-10	15-19-11	15-19-12	15-19-13
		ZERO SUP. STEADY-STATE	.03 cps	.05 cps	.85 cps	1.0 cps	1.2 cps	2.0 cps
15-19	C-201	8.8% PTP			Electrical disturbance in trace.		Sinusoidal characteristic to trace.	
	E-201	5.4% PTP There appears to be an approx. 2 x pa oscillation in all flow measurements including pump.			6.8% PTP Variable phase lag with μμA indicated by correspondence of flow and power peaks. More harmonic trace appearance than 15-19-3, indicating effect of flow power.	3.2% PTP Relationship to μμA is evident. There is a decreasing response compared to 15-19-10.	3.2% PTP Traces have approx. 2 cps content as well as considerable low frequency large amplitude oscillation. Phase relationship to μμA less evident than run 15-19-10.	Decreased influence of power. Traces have characteristics of 15-19-3, the steady-state runs.
	μμA	5.0% PTP Power responds to flow changes.	Power responds to flow changes Oscillations roughly in phase					Power oscillation amplitude considerably diminished.
	RCP-2	4.4% PTP Weak indication of μμA following RCP in-flow c changes. No evidence of pump and channel flow phase relationship from traces.		Considerable high frequency component approx. 5 cps.	Phase relationship to power less defined at low frequency power.		1.5% PTP Contains a high frequency signal about 5 cps. It also contains a low frequency component at approx. 8 cps.	

The traces also show frequencies greater than 1 cps. It may also be said that low frequency oscillations are larger for the natural circulation system than for the corresponding forced circulation runs. Although there is no phase relationship in evidence between power and in-core flow measurements, the μμA traces also show a larger low frequency oscillation characteristic than in the preceding forced circulation runs.

Run 15-16 was conducted with forced circulation (RCP-1) but with the baffle doors open to provide a bypass path to the core. Traces for the steady-state run are shown in Figure VII-17. In-core flow measurements show a decidedly different characteristic for this run. The flow, as indicated by those measurements, is very quiet. RCP-1 measurements, on the other hand, show a high frequency oscillation. The source of this oscillation is not known.

EFFECT OF FLOW CHANGES AND ORIFICING

Figure VII-29 shows the peak-to-peak amplitude of oscillation of flows from E-201, C-201, and RCP-1 as a function of reactor flow. Reactor power is 15 MWt. Channel E is a Fuel Cycle element with no restraint in the inlet. Channel C has an orifice at the inlet of the channel. Relative restraints in the two channels are shown by COFFI code calculation in Table VII-5. This is a pretest calculation, and is not intended to represent an exact test condition.

TABLE VII-5

RELATIVE FLOW RESTRAINTS FOR CALCULATED

20 MW 7650 GPM RUN

		Orificed	Unorificed
Inlet velocity	- fps	3.04	4.50
Exit quality	- %	2.93	1.84
Exit void	- %	33	23
Friction 0 P	- psi	.09	.13
Elevation head	- psi	1.33	1.46
Acceleration	- psi	.03	.04
Inlet loss	- psi	1.09	.76
Contraction-Enlargement	- psi	.11	.26

Total loss for the two channels is 2.66 psi. It should be noted that a change of .33 psi at the inlet loss created by orificing may be considered as the cause of the change in the amplitudes of noise reported in Figure VII-29. This is not proven to be the case since one would have to interchange the functions of the two channels to be sure that there is not a different noise level response for the two channels as the result of some as yet unexplained phenomena. RCP-2 oscillation amplitude is shown in the lower trace. Its amplitude appears to be constant for any flow level for the data reported. The curves of Figure VII-29 verify an observation made in the course of analysis of a rod oscillator test which is very significant to the understanding of the stability relationship to operating noise level. In Figure VII-29, the noise amplitude of a 20,000 gpm flow is shown to be considerably higher than at 4,000 gpm for both the E-201 (unorificed) channel and the C-201 (orificed) channel. Model analysis shows, however, that proceeding from the high flow to the low flow point, the gain margins are reduced. On this basis, the amplitude of oscillation should logically be expected to be greater. A more complete discussion of the model aspects of this is given in the discussion of rod oscillator test analysis. The implication of this result to the operation of a reactor plant is that flow noise in normal operation is not a criteria for stability by itself, and that, as the system approaches an undamped oscillatory operational point, the oscillations will then appear from a relatively quiescent noise trace compared to higher flow conditions.

Two natural circulation data points are shown in Figure VII-29. These points are for E-201 and C-201. They are represented at 4,000 gpm, the anticipated natural circulation flow level for the reactor. Amplitudes of oscillation are shown to correspond with the corresponding forced circulation flows. There does not appear to be any substantiation for expecting the amplitudes of oscillation to be the same for forced and natural circulation of corresponding flows. This is because the flow mechanisms are entirely different for the two cases, as are driving force and induced flow oscillation spectrums from the single phase portion of the loop of each. A detailed discussion of this will be given in the following section.

BAND PASS FILTER OUTPUT SPECTRA FOR STEADY-STATE RUNS

Figures VII-30 through VII-33 are normalized spectra outputs from the band pass filter. These are normalized based upon peak point observations. Analysis of the responses of the flow system based upon the output spectrum and the assumption that the input spectrum is white noise is the usual approach to the responses of linear devices. There is no assurance, however, in this case, that the input spectrum is, in fact, white. The complexity of the system and the characteristics of possible contributors to input excitation may, in fact, point to other phenomena for input excitation. Because of this, the data are discussed and referred only to the spectrum characteristics. Well-founded extensions of this will come only after a more detailed analytical program has been carried out. Section VII-C, however, discusses noise excitation and proposes two possible bases for explaining some of the observations. The filter output spectrum for Run 15-1 is shown in Figure VII-30. μμA, E-201, RCP-1, and RCP-2 spectra are shown. All peak values are between .7 and 1 cps. There are too few data at this time to define the data in an exacting manner. Parametric variations are valid only to the extent that the experimental results are defined. On the low frequency side of the peak, all flow measurements agree closely. No measure of agreement is seen on the high frequency side, where band pass errors are smaller than on the low frequency side. Pre-test analysis data for in-core flows shows a broad band between .75 and about 3 or 4 cps. However, the pre-test analysis readout accuracy was low for these runs so it would be better to refer the hydraulic resonances to the output (purely hydraulic) of the SATR code. This frequency is shown to be 1.66 cps.

Run 15-18, the natural circulation operation run, shows the following: First, the μμA peak compares well with that of Run 15-1 (.7 cps to .85 cps, respectively). There does appear to be a difference at the low frequency end where a low level peak appears for the natural circulation run at about .1 cps. Looking at E-201, the peak value has moved to .4 cps from a .75 cps peak for the 15-1 run. This is a very broad peak extending down to .1 cps. Indications are that the .1 cps peak influences the low level peak shown in the μμA spectrum. It is interesting to point out that the μμA always peaks at a higher frequency than does the flow in-core for all the runs discussed here. One can reason that this is due to the fact that the μμA responses are a function of flow responses and reactor kinetics

rather than flow responses as above, thus increasing the frequency observed. Section VII-C discusses noise excitation phenomena and specifically deals with this point.

Run 15-19 is a forced circulation run with Recirculation Pump 2 operating. Peak frequencies are indicated for this run between .5 and 1 cps.

E-201	-	.5 cps
RCP-2	-	.8 cps
μμA	-	1.0 cps

It is interesting to note that RCP-2 has a higher frequency here than in 15-1, though a lower amplitude. RCP-2 also contains considerably more high frequency than does E-201 or μμA, as well as considerably more low frequency. It would be difficult to identify RCP-2 as a major contributor to the frequency characteristics of the in-core quantities as a result of this. Detailed comparison of all the traces confirm this for the three runs discussed in detail. μμA and E-201 spectra are not greatly different from those obtained in 15-1. A lower frequency is shown for E-201 as a result of the reduced flow (.5 cps compared to .7 cps).

STEADY-STATE FLOW ANALYSIS DISCUSSION AND CONCLUSIONS

The following items are the indicated results of the VBWR experiments. The first group represent observed responses to the recirculation flow system.

1. No clear indication is given that the recirculation pump spectra changes with flow rate effect the power (μμA) measurements on the high frequency side of the μμA spectra peak (as parametric changes).

2. The high frequency responses of E-201 internal flow measurements are definitely effected by the flow rate to the reactor. Runs 15-1 and 15-19 show this effect. This appears to be reflection of the shift of frequency peak as a function of flow rate, and, in this respect, is consistent with model analyses. The method of normalizing the data (Figures VII-30 through VII-34) was based upon amplitude normalization of peak values.

3. Sources of the high frequency components in RCP-1 are not known. These could be real or instrument, or pipeline vibration induced. A conclusive analysis of the primary instruments has not as yet been made. Comprehensive understanding of measurements for the frequency range of the test data may make marked changes on the results.

4. RCP-1 and RCP-2 show considerable differences in amplitude of oscillation. These probably are the result of known piping flow path differences for the two pumps. Interpretation of flows in two-pump operation is difficult under these circumstances.

5. The high frequency side of the peak for spectra of RCP-2 look the same for the two runs, 15-1 and 15-19. The low frequency side indicates 15-19 to have a large amplitude low frequency component and is indicative of a low frequency loop-type flow oscillation. The source of such an oscillation is not known. The logical pattern of responses for a flow system where the amount of damping and the velocity are decreased is followed by the low frequency response.

The second group represents conclusions regarding the model analysis based on the current status of trace analysis.

1. Model analysis, as described in Section VIII, shows a linear response of computed frequencies with flow rate. This is shown in Table VII-6, and plotted in Figure VII-34.

TABLE VII-6

CALCULATED SYSTEM AND TWO-PHASE HYDRAULIC RESONANT FREQUENCIES

TEST RUN	FLOW	FREQUENCY (Test)	FREQUENCY (With Nuclear Feedback)	FREQUENCY (SATR)
15-1	20,000	.85	.7 - 3.0*	1.66
15-19	4,000	.5	.8	.54
15-16	4,000 (Baffles Open)	.5		
15-11	2,600	.4	.75	.39
15-18	Natural	.5		

*Lack of sensitivity in pre-test analogue output. This is discussed in Section VIII.

The output of the pre-test analysis analogue runs is subject to a lack of sensitivity which made it difficult to determine the peak frequencies. Because of this, the SATR run resonant frequencies (digital) were used for comparison. This is a purely hydraulic frequency without nuclear feedback. In this sense, the comparison is not valid, and the apparent differences will be smaller than indicated. The results show a departure from the predicted resonant frequency as computed from the SATR code. This difference is over-emphasized, since kinetics and fuel thermal model would tend to lower the 1.66 cps value. Noting the frequencies of the peaks obtained from the power spectrum, it is interesting to see that the frequencies are much lower than predicted by the dynamic analysis model at high flows. At low flow, the results are closely in agreement. It is not immediately apparent at this time how large differences actually exist. Several reasons, such as non-linearity in pressure drop response or inability of the theory to account for the modes of oscillation, might be advanced to account for the differences. The primary effect which is expected to come into play is a multi-node representation of the two-phase equation. Considerable work on the model analysis and investigation of forthcoming loop tests for this phenomena should shed light on the matter. It is interesting to note that a similar observation was made with regard to measured frequency responses of water level in a natural circulation loop in the early work done at Argonne National Laboratory.[2] Recently, the work of H. Christensen shows similar results for void transfer functions when the experimental data are compared to the theory of Zivi and Wright,[3] and Akcazu.[4] Recent work done in Sweden shows that multi-node model analysis has reconciled the results of Christensen.[5] Since the VBWR channel flow measurements are the first of this type, it seems likely that the above observations are the result of flow oscillations.

An additional observation which should be further considered is the fact that the departure from theory occurs in the most highly damped cases which also have the highest amplitude oscillations. In contrast, the low flows with correspondingly lower damping demonstrate no radical departure from theory and have lower amplitudes of oscillations. A fundamental

question about the physical nature of the contributions to the frequency spectrum is also to be raised as a result of this. A discussion of this is given in Section VII-C.

2. Tests confirm pre-test dynamic analysis which indicated the recirculation flow loop to be well-damped. No phase relationships with the flows were observed.

The next conclusion has to do with the significance of the amplitudes of flow oscillations as a measure of flow stability. It is believed, based on present understanding of the amplitudes of oscillation, that amplitude alone obtained from tests such as these do not provide a measure of flow stability. Test results, as discussed in connection with Figure VII-29, show that amplitudes of oscillation may be reduced when going in the direction of less stable flow. A much improved mathematical and physical understanding of noise must be obtained before steady-state noise information is useful to predict the stability characteristics of flow. As mentioned above, Section VII-C discusses this in detail. This does not change the theoretically expected trancition from random to an oscillatory system prior to unstable oscillations in flow, but it may indicate that the amplitudes of noise from other sources, either extraneous or contributing, could mask the effect until an advanced state of unstable flow existed. Analytical instruments are presently being considered to handle the study of periodic components in noise traces for which the signal to noise ratio is low. These are expected to increase understanding of the make-up of steady-state noise traces.

A second observation concerning noise measurements has to do with orificing of flow channels. The effect of orificing as shown in Figure VII-29 is apparently to reduce the amplitude of noise for Channel C or Channel E. It is interesting to note that the exit void fraction for Channel C is larger than that of Channel E. Qualitatively, the responses of the orificed channel are in keeping with expected dynamic analysis results. Further analysis will be required before detailed comparison can be made.

The next series of observations are general observations added for completeness.

1. No conclusion on spatial flow effects in the core are possible with the existing data.

2. Band pass filter characteristics place limitations on the conclusions, especially if trace characteristics are different for two cases.

3. The frequency response of in-core flowmeters is adequate for the range of frequencies covered experimentally. No correction is required.

The foregoing analysis of steady-state data for fluxes and flows has been conducted based directly upon the output of the band pass filter network described in Appendix C. The output of this device actually is equivalent to:

$$(\text{Signal Amplitude})^{\frac{1}{2}} \times \text{Center Frequency}$$

Therefore, the output, as plotted, has a weighting factor of frequency included. Some frequency shifts may be introduced by this means; however, relative comparisons of data are not effected.

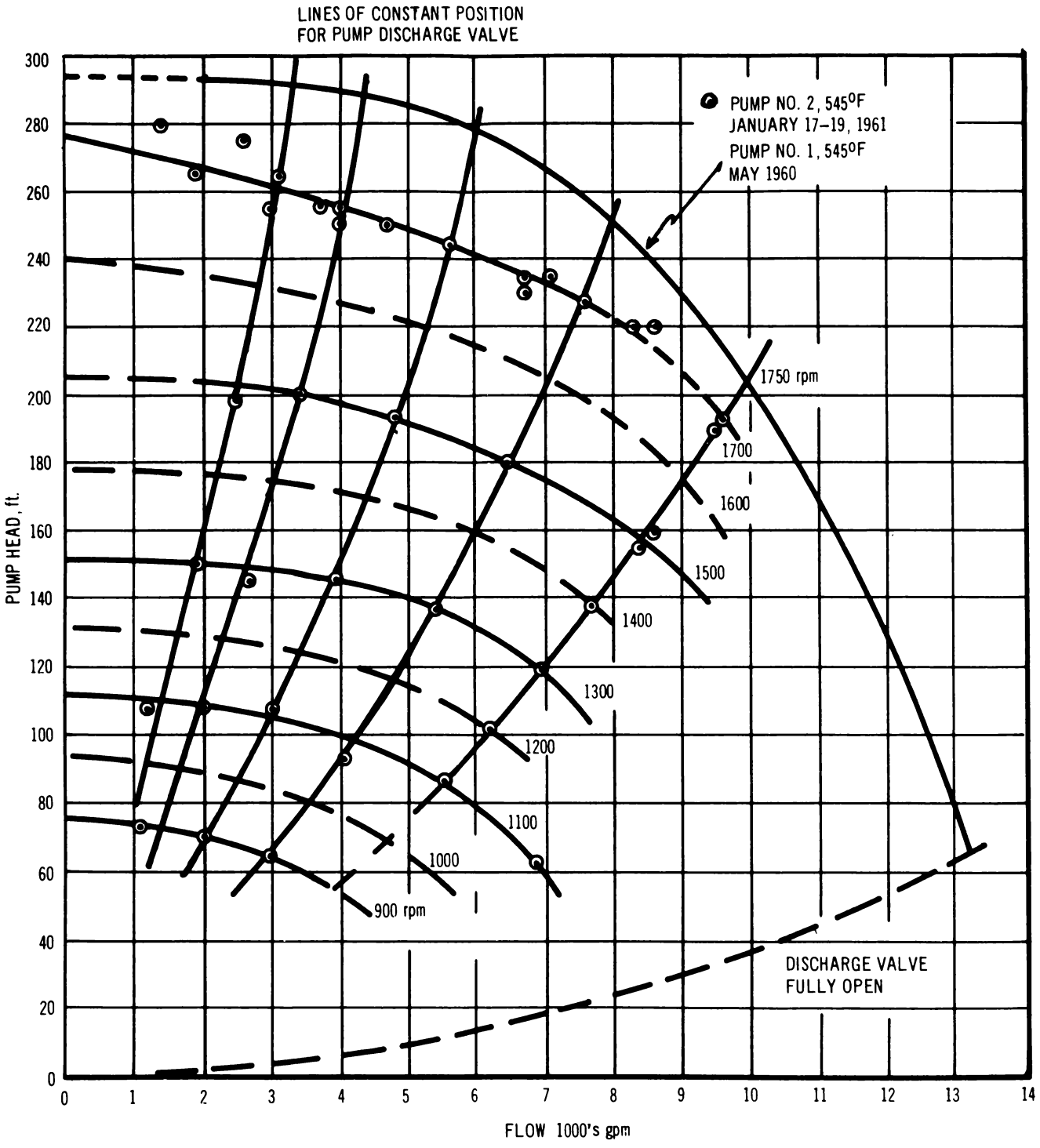

FIGURE VII–28 FLOW – PUMP HEAD RELATIONSHIP FOR VBWR RECIRCULATION PUMPS 1 & 2

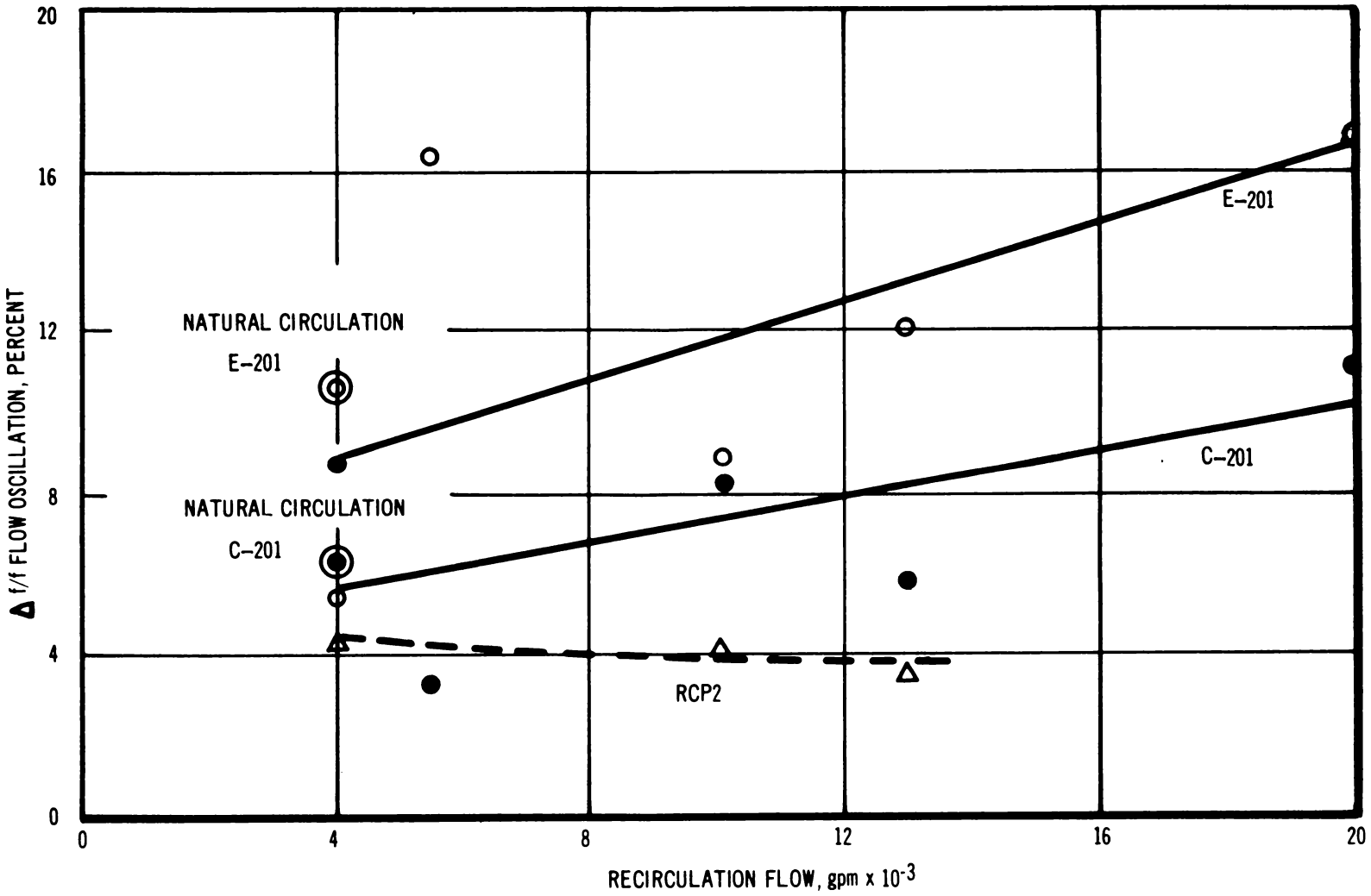

FIGURE VII-29 STEADY STATE FLOW NOISE EFFECT OF FLOW, ORIFICING ON NOISE

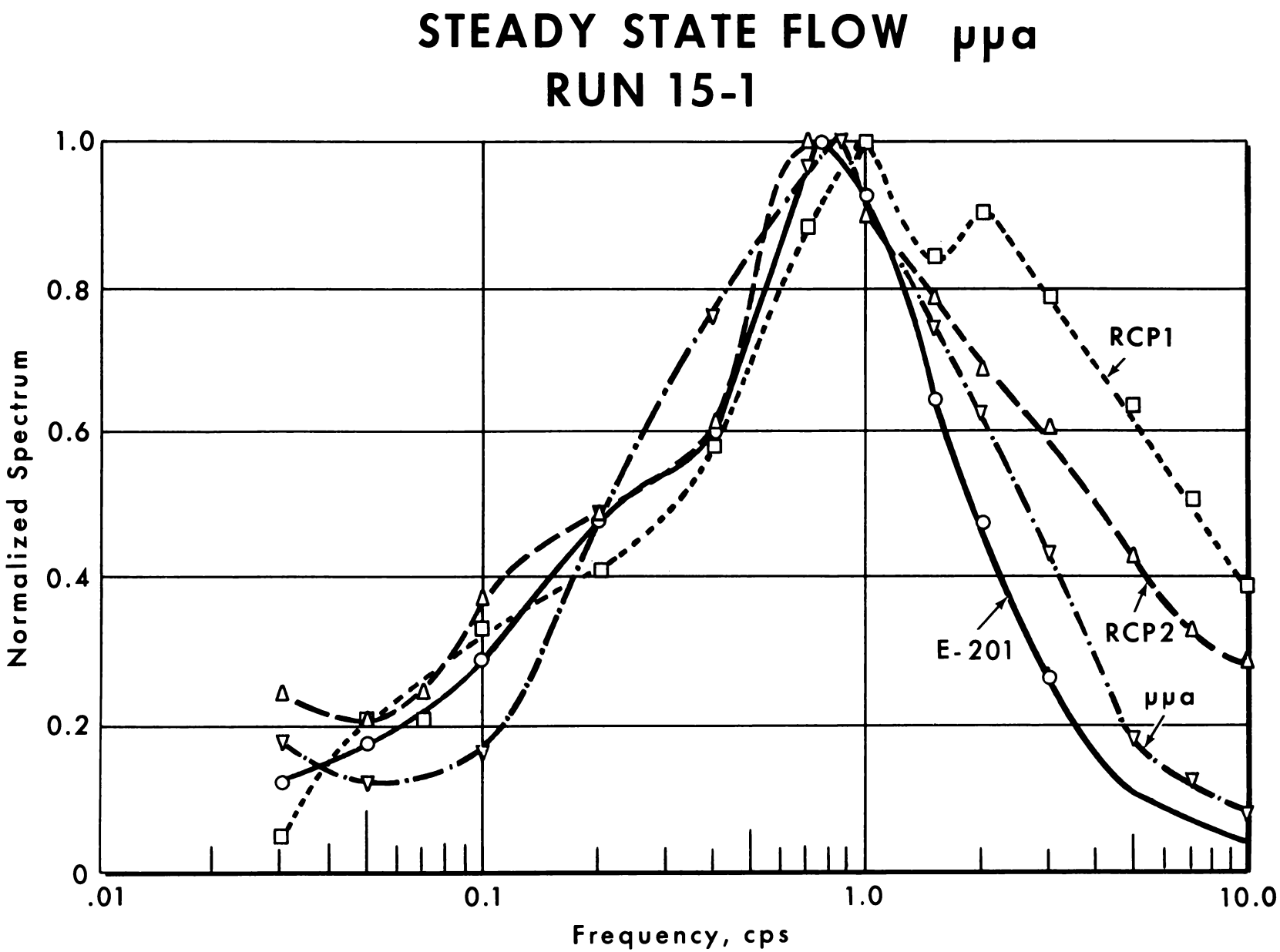
STEADY STATE FLOW μμa
RUN 15-1
Normalized Spectrum
1.0
0.8
0.6
0.4
0.2
0
.01
0.1
1.0
10.0
Frequency, cps
RCP1
RCP2
E-201
μμa

FIG. VII-30

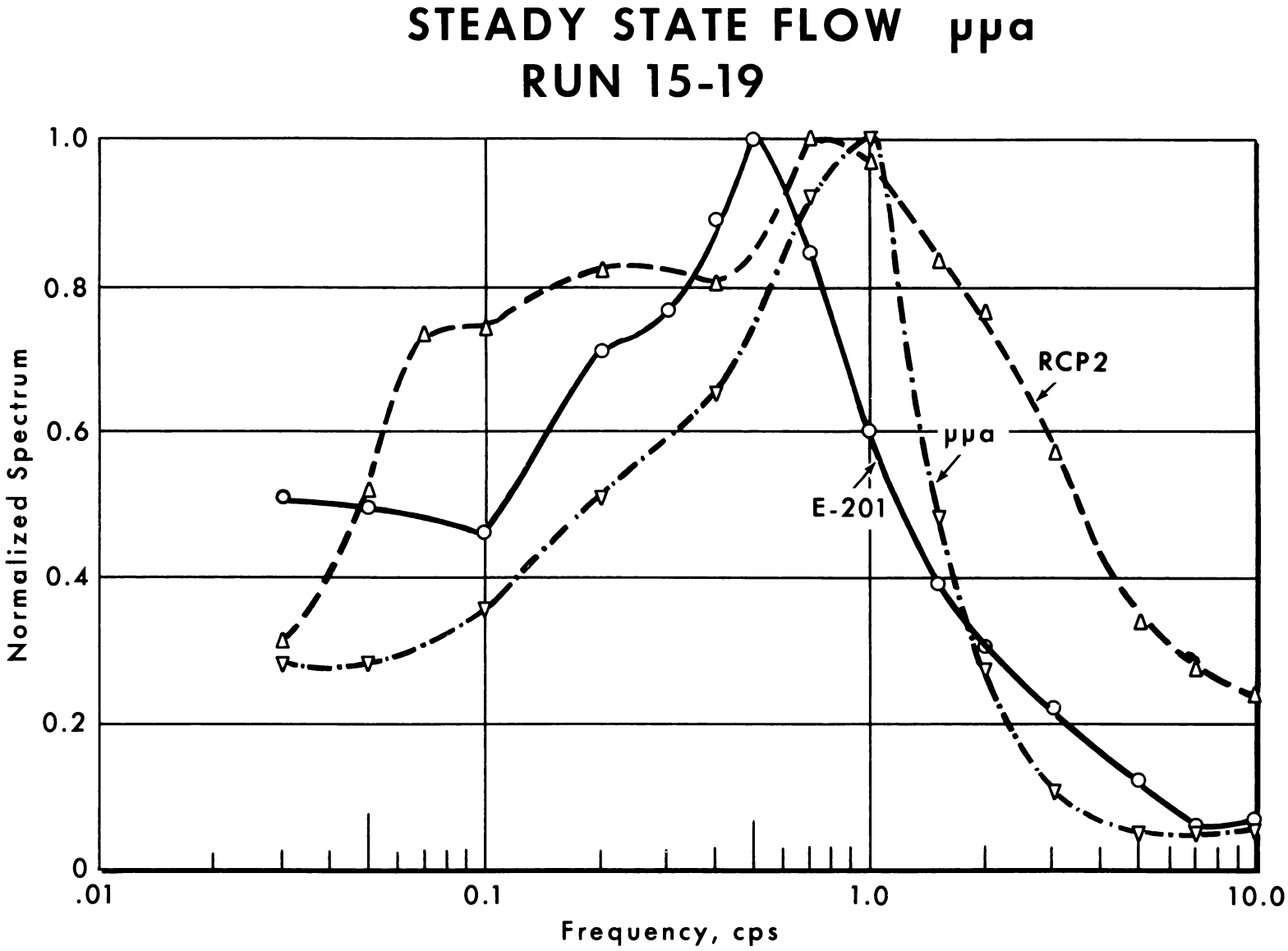
STEADY STATE FLOW μμa
RUN 15-19
Normalized Spectrum
1.0
0.8
0.6
0.4
0.2
0
.01
0.1
1.0
10.0
Frequency, cps
RCP2
μμa
E-201

FIG. VII-31

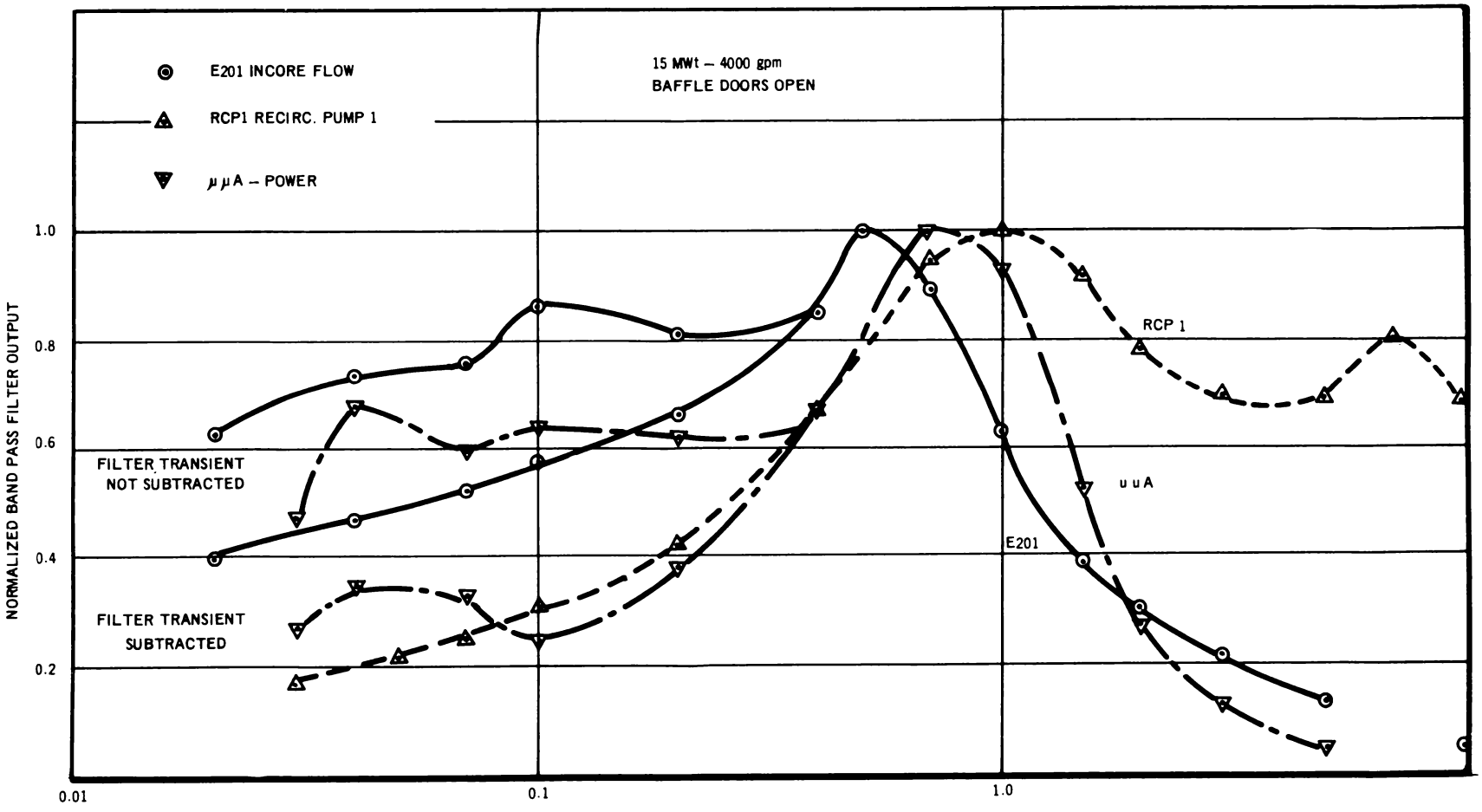

FIGURE VII–32 FLOW SPECTRA RUN 15–16

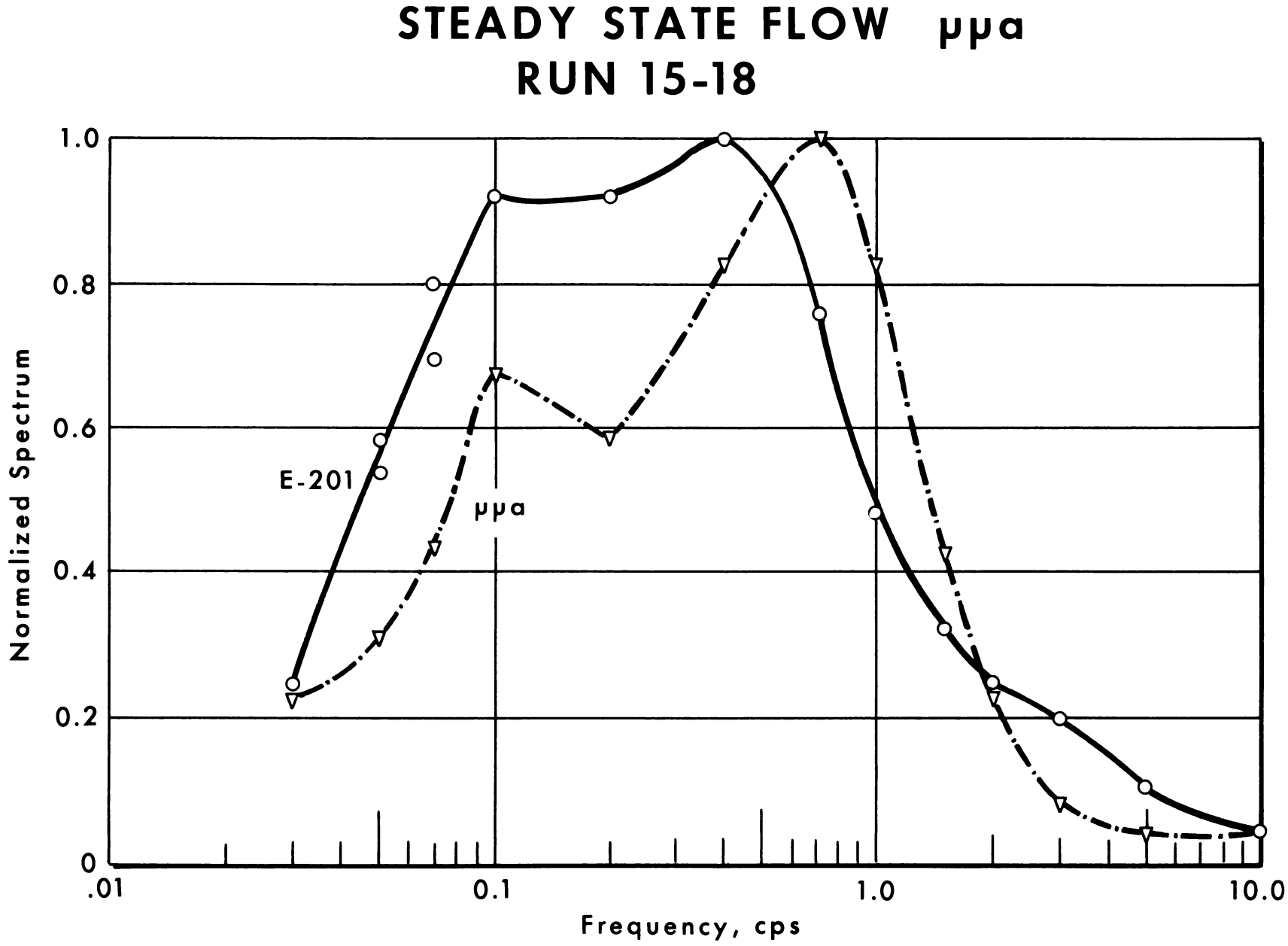
STEADY STATE FLOW μμa
RUN 15-18
1.0
0.8
0.6
0.4
0.2
0
Normalized Spectrum
E-201
μμa
.01
0.1
1.0
10.0
Frequency, cps

FIG. VII-33

FREQUENCY COMPARISON

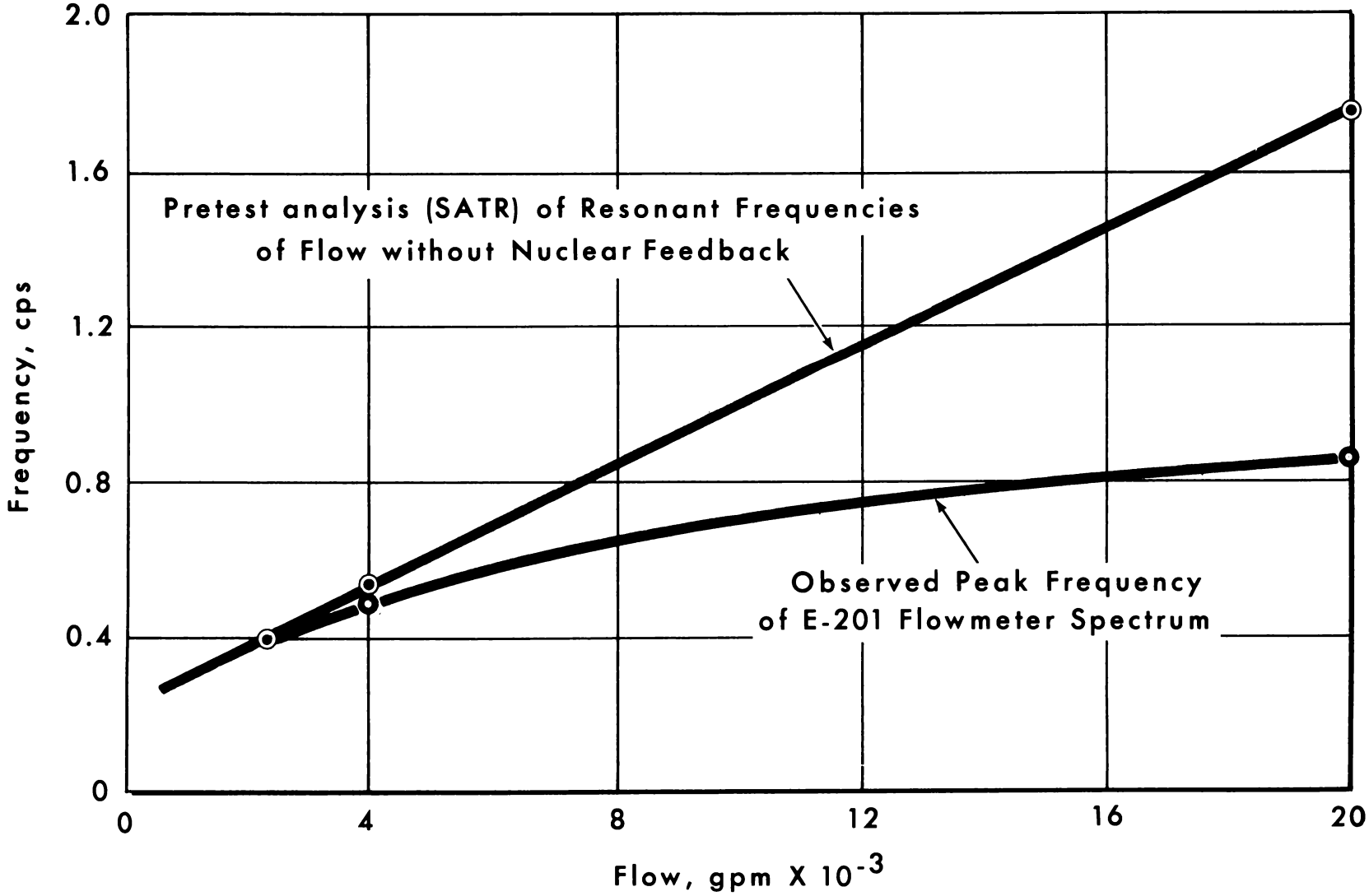

FIG. VII-34

SECTION VII-B

ROD OSCILLATOR TEST ANALYSES

The purpose of the rod oscillator test, as was mentioned before, was to measure the response of the reactor system (output) as a result of a known disturbance (input). The measured response of the reactor system can be considered to be one of the parameters, out-of-core power, in-core flux, or fuel element flow. The known disturbance was, of course, the rod motion. Each rod oscillation test sequence, therefore, has a capability of defining these three classes of output as transfer functions for rod motion.

By defining the relationship between rod motion and reactivity, the above transfer functions can be expressed as:

1. Out-of-core power from reactivity $\left(N^* / \Delta K\right)$ μμA
2. In-core flux from reactivity $\left(N^* / \Delta K\right)$ In-core
3. Fuel element flow from reactivity $\left(V^* / \Delta K\right)$

These are the general categories of transfer functions which were extracted from the rod oscillator data and selected for analysis in this report. Although they do not exhaust the complete data potential, they do tell a reasonably comprehensive story about reactor system stability and dynamic response. This section is not intended to be a complete presentation of all of the rod osccilation data taken during the stability tests. Rather, it is a partial presentation of selected test runs. Selected runs show representative trends in system response with respect to changes in reactor operation conditions. The balance of the test runs will be the subject of a continuing analysis which will complement the work presented here.

Table VII-7 is a listing of five (5) test runs which were the subject of this analysis. Each test run was examined for either the transfer function for out-of-core power or in-core flux. The fuel element flow transfer function was examined for only one test condition. The selection of the number of runs, and the number of transfer functions of each run was a compromise to gain the widest understanding

of VBWR dynamics with a limited data reduction effort.

TABLE VII-7

ANALYZED ROD OSCILLATOR RUNS

Run Number	Reactor Power MWt	Pump 1 Flow gpm	Pump 2 Flow gpm	Total Flow gpm	Comments
15-1	15	10,000	10,000	20,000	
15-9	15	4,000	-0-	4,000	High Pump Head, Valve controlled flow.
15-19	15	-0-	4,000	4,000	Low Pump Head, Pump speed controlled flow
15-18	15	-0-	-0-	-0-	Natural Circulation.
15-16	15	4,000	-0-	4,000	Forced Circulation. Baffle doors open.

CONTROL ROD RESPONSES FROM PEN RECORDER TRACES

Time varying experimental data were recorded two ways during the stability tests:

1. By pen recorder yielding a permanent fast response time-dependent trace of the measured parameter.

2. By magnetic tape recorder yielding a permanent record of the time-dependent electrical output of the measuring transducers. Playback of the magnetic tape will produce exactly the signals in the exact form in which they were produced during the tests.

The tape recordings of the test data were invaluable for analysis purposes. They facilitated data reduction techniques which could not have been economically feasible with only pen recording traces. Section VI and Appendix C describe the methods employed in this work. The application of these data reduction techniques will be discussed in some detail later in this section.

The pen recorder traces, however, provide an excellent visual record of the raw data as it was taken off the reactor. Some representative pen traces are presented here for the purposes of discussion. These representative traces were taken from the natural circulation test at 15 MWt. The natural circulation run was selected because:

1. It demonstrates most vividly the problems of reducing data in the presence of both noise and rod responses.
2. It demonstrates definite in-core hydrodynamic oscillations occurring in sympathy with the core power oscillations.

Two types of pen recordings were made:

1. Record Data: These traces were simultaneously made with the tape recordings and taken specifically for a permanent record of the test. The pen recorders used for this purpose were hooked-up in parallel with the tape recorder. These traces record exactly the same voltage signal that is recorded on the magnetic tape. The voltage level and zero suppression of the signal at this point was controlled and regulated by the master instrument patch panel. Reactor parameters measured for this purpose were recorded on a bank of twenty (20) pen recorder channels. These 20 channels of recording equipment consisted of one eight-channel and two six-channel pen recorders.
2. Control Data: These traces were made primarily for the purpose of providing control information for the rod oscillator operator. These traces were made on a two-channel pen recorder and always traced a record of the same two reactor parameters; Rod #7 position, and out-of-core neutron power. The signal level and zero suppression of these two parameters were controlled and regulated by conventional pen recorder pre-amplifiers.

A record data trace of the natural circulation, 0.5 cps, rod oscillator run is presented in Figure VII-35. Shown on this trace are two in-core flow measurements, four in-core ion chamber measurements, an out-of-core flux measurement, and a recording of Rod #7 position. Several observations can be made from this trace:

1. The position of Control Rod #7 is being varied in almost a perfect sinusoid. The control rod servo-mechanism performance was uniformly good throughout the tests.

2. Even though the reactor input disturbance (Rod #7 insertion) is a single frequency sinusoid, the output reactor responses are not single frequency sinusoids. They appear to contain harmonics and strong components of the steady-state noise in addition to the fundamental frequency.

3. The power as measured out-of-core by the μμA leads in phase the control rod motion. This effect should not be unexpected. The analytical model of the reactor is analogous to a reactive network and predicts this same phase behavior (see Section VIII).

4. The in-core ion chambers appear to follow very closely the out-of-core power measurement made by the μμA. This behavior was observed also in the steady-state analysis. (See Section VII-A).

5. The unorificed instrumented assembly's flow (E-201) does not have any apparent phase relationships with the orificed assembly's flow (C-201). A discussion of the above two phenomena is presented in Section VII-A.

A control data trace of three rod oscillator frequencies for the 15 MWt natural circulation test series is presented in Figure VII-36. Shown in this figure for each of the three frequencies are the control rod position and the power response of the μμA. Worthy of mention is the rod motion for the low frequency run of this test series. It is observed that the rod stroke at the top of its withdrawal for 0.03 cps contains some comparatively high frequency noise. This was found during the test to be caused by steam condensation on the rod position potentiometer and was rectified for subsequent test runs. The effect of this noise on the 0.03 cps rod oscillator run, however, will be negligible, negligible because the noise is of small amplitude and short period compared to the fundamental rod oscillator frequency.

Two other observations can be made from Figure VII-36.

1. Two of the three limits for rod oscillator amplitude are demonstrated here.

   a. In the case of the 0.03 cps and the 0.5 cps runs, the rod amplitude was limited by the maximum permissible linear displacement ($\pm$ 0.7 in).

   b. The rod oscillator amplitude for the 3.0 cps run was limited by the dynamic loading of the rod mechanism at that frequency ($\pm$ 0.125 in.). The amplitude limit imposed by maximum power swings is not demonstrated here.

2. The flux noise which is superimposed on the fundamental power response appears to hold to its same general frequency character regardless of the rod oscillation frequency. The noise is observed to have a consistent frequency dominance in the 0.5 cps range. In the case of the 0.03 cps rod oscillator run, the noise frequency is high compared to the fundamental power response. Therefore, the noise appears to be riding on top of the power response. In the case of the 0.5 cps rod oscillator run, the noise frequency is the same order of magnitude as the fundamental power response. Therefore, the noise appears to be manifested as an irregular wave shape in the power response. In the case of the 3.0 cps rod oscillator run, the noise frequency is low compared to the fundamental power response. Therefore, the power response appears to be riding on top of the noise. The characteristics and influence of noise are discussed in detail in the data reduction section which follows.

Figure VII-37 is a control data trace of the 0.2 cps rod oscillator run of the 15 MWt, natural circulation test series. Recorded in this trace are the Control Rod #7 position and the out-of-core power measured by the $\mu\mu$A. This figure displays the nature of the reactor behavior during rod oscillator start-up. At the beginning of the trace (left side of the figure), the rod motion has not yet begun, and the flux response is composed of only steady-state noise. At the end of the trace (right side of the figure), the amplitude of the rod oscillation has come to equilibrium and the flux measurement is composed of both noise and flux response to rod motion. Between the beginning and the end of the trace, rod oscillation is begun and its amplitude is gradually increased up to the equilibrium

stroke. Noteworthy is the response of the neutron flux as the amplitude of rod oscillation is increased. It is observed from Figure VII-37 that there appears to be a rather well-defined band in time (t) and/or an amplitude of rod oscillation (A) where the flux response begins to respond with noticeable regularity to rod motion. i.e., When the time was less than (t), and the rod amplitude was less than (A), the flux response displayed no consistent periodicity of time (t). On the other hand, an apparent consistent periodicity developed for time greater than (t) and rod amplitude greater than (A).

The above mentioned phenomena can be explained, in part, by recognizing that the response of neutron flux to small amplitude rod motion was not large compared to the total or integrated spectrums of steady-state flux noise. Therefore, it follows that the rod-induced response was not discernible from the noise spectrum until a large rod oscillation amplitude was reached. This argument, however, does not explain the almost abrupt change or non-linearity in flux response from an irregular behavior to a a noticeable regularity of Period T. This "locking in" of flux response can perhaps be explained by remembering that the reactor, in the natural circulation condition, recirculated its coolant flow within the reactor vessel. This flow configuration serves to uncouple the core flow channels from the high pressure drop, external recirculation loop, thereby reducing the hydrodynamic damping of the flow system. Moreover, this uncoupling of the external recirculation loop allows the individual fuel element flow channels to operate hydrodynamically independent of one another. This occurs because the recirculation flow path within the reactor vessel is almost devoid of frictional pressure drop. Therefore, the core, ΔP, remains essentially constant (influenced by single phase gravity head) regardless of flow variation through the fuel elements. And, finally, that the individual fuel elements cannot hydrodynamically influence one another without a pressure drop communication.

The VBWR natural circulation flow system, is therefore, a complex combination of many oscillators that are almost completely uncoupled hydrodynamically. These oscillators, however, are coupled to one another by the resulting thermodynamics of the neutron coupling across the reactor core. This is discussed in Reference (6).

Each element within the reactor core acts as an oscillator, the characteristics of which depend upon the thermodynamic and geometric properties of each fuel element. Some oscillators have low natural frequencies, while others have high natural frequencies. It is not surprising then that the flux response of Figure VII-37 should seem to "lock-in" with rod motion after a somewhat irregular start-up. The rod oscillator is attempting to order a group of non-uniformly damped flow channels with unlike natural frequencies by the rather loose control of thermodynamic coupling. This explanation is further verified by observation of the forced circulation test data. In forced circulation, the flow channels were tightly coupled and well-damped by the external recirculation loop. It was found in these cases that the flux response to rod motion was not "spongy" or irregular for even the smallest of rod strokes. Contrary to the loosely coupled natural circulation core, the flux responded with immediate regularity to the start-up of rod oscillation. In summary, it can be concluded that the natural circulation rod oscillator test provides an example of the response of uncoupled parallel flow channels with neutron coupling.

METHOD OF DATA REDUCTION

The object of the rod oscillator test was to measure the frequency response of the reactor system to a sinusoidally varying control rod disturbance. The result of these measurements, after data reduction, becomes the determination of one or more of the reactor transfer functions. It is necessary, in order to determine a given transfer function, to measure the relative amplitude and phase between the selected input and output parameters. But, a review of the flux and rod position data in Figures VII-35 through VII-37 show that the relative amplitude and phase of two parameters is not easily ascertained. The sinusoidal disturbance of the rod position is easily read visually from the data traces. The flux response, on the other hand, is a complex combination of noise and rod motion response, and cannot be read by visual means. Rather, it must be analyzed by mathematical techniques. The mathematical technique used to analyze the rod oscillator data was an application of the same analogue band pass filter equipment as was used for the steady-state analysis. (See Appendix C).

The following is a discussion of the flux response data reduction. The analytical techniques outline herein were used for both in-core and out-of-core rod oscillator data reduction. As was the case in the previous section, the natural circulation test sequence is used as an example.

a. Rod Oscillator Flux Response Description

The neutron flux variation measured while the rod is being oscillated at a given frequency (ω) may be described:

$$N^* = N^* \text{ rod} + N^* \text{ noise} \qquad \text{(VII-1)}$$

Where N* denotes the normalized neutron density variation in per cent of the steady-state level.

Equation VII-1 states that the percentage variation in measured flux level during rod oscillation is composed of the variation due to rod motion plus flux noise. The flux noise is postulated to be composed of the steady-state component (see Section VII-A), and non-linear components dependent upon power level and rod oscillator frequency.

$$N^* \text{ noise} = N^* \text{ noise(steady-state)} + N^* \text{ noise } f(N) + N^* \text{ noise } f(\text{rod frequency}) \qquad \text{(VII-2)}$$

Where f(N) denotes a function of power level.

Several observations may be made from test data which show properties of this equation:

1. It was observed from Figure VII-37 that during the period of small amplitude rod oscillation, the steady-state noise (N*noise (steady-state)) appeared to be of the same order of magnitude as did the total flux variation (N*). The steady state noise, as it appears in Figure VII-37, is, however, the integrated noise level. When the steady-state noise is separated into its frequency spectrum (see Section VII-A), the resulting individual frequency components of noise are quite small compared to the composite rod oscillator responses (N* noise f (rod frequency)) at those frequencies. In other words, the amplitude contribution of the steady-state noise at any frequency is almost negligible compared to the total flux variation (N*)

measured while the rod is being oscillated at the same frequency. These amplitude contributions were less than 10% of the total in each case, except the natural circulation tests where it approached 25%.

2. Referring again to Figure VII-37, it is interesting to observe the noise as the rod oscillation amplitude is increased. It is observed from this trace that the amplitude of the total flux variation (N*) after the rod oscillation has come to equilibrium is not appreciably larger than the steady-state flux noise, (N* noise (steady-state)). Since the variation (N*) has a very noticeable sympathetic oscillation with the rod movement which is not evident in the steady-state, it is concluded that the total noise present during rod oscillation is less than, or equal to, the steady-state noise:

$$\text{N* noise} \leq \text{N* noise (steady-state)} \qquad \text{(VII-3)}$$

This observation, of course, is based upon the entire mixed noise level, and does not preclude the possibility that specific frequency components of N* noise can be larger than their N* noise (steady-state) counterparts. However, the likelihood that such a condition exists is probably remote.

Based upon the above logic and reasoning, it is assumed, for data reduction purposes, that equation VII-3 is valid for the individual frequency spectrum components as well as for the entire mixed spectrum. This assumption enables us to describe the maximum possible contribution of noise to total flux variation (N*) as the steady-state noise spectrum (N* noise (steady-state)). Substituting equation VII-3 into equation VII-1, and expressing the noise as its maximum possible:

$$\text{N*} = \text{N* rod} + \text{N* noise (steady-state)} \qquad \text{(VII-4)}$$

When filtered at a frequency (ω) corresponding to rod motion frequency:

$$\text{N*}(\omega) = \text{N* rod}(\omega) + \text{N* noise (steady-state)}(\omega)$$

One further assumption is made. It is assumed that the value of steady-state noise at any frequency is not a vector quantity. i.e., although the noise contains definite periodic components of some statistical magnitude, it does not contain a corresponding phase relationship for these components. In orther words, the periodic components remain periodic for only a small number of cycles. Therefore, when the magnitude is integrated and averaged over a large number of cycles, it is done with the band pass device, the phases cancel and nullify one another. This assumption simplifies the data reduction problem considerably. Applying this assumption to equation VII-4, it is possible to obtain the rod flux response at a given frequency (N^* rod (ω)) from the filtered total flux variation ($N^*(\omega)$) merely by algebraic subtraction of the steady-state noise frequency component at the rod oscillation frequency (N^* noise (steady-state)(ω)). This technique is discussed in greater detail in the next section.

It is important that one point be made clear - - it is not necessary that either of the above two assumptions be valid in order for this rod oscillator analysis to be accurate. As long as the noise portion of the total flux variation is small compared to the rod response, any assumption can be made about the noise frequency spectrum and/or phase without affecting appreciably the rod response determination. The only way in which the above scheme for rod response determination could yield inaccurate results is if there were large non-linear components of flux noise. This possibility seems very unlikely, even in the loosely coupled, natural circulation condition. The possibility is even more remote in forced circulation where no evidence of significant non-linearities were recorded.

b. Band Pass Filter Techniques

Equation VII-4 is the defining equation used for rod oscillation data reduction. It states that the total flux variation measured during rod oscillation (N^*) is equal to the flux responses due to rod motion (N^*) rod + the steady-state noise (N^* noise (steady-state)). The use of

the band pass filter equipment for the analysis of steady-state noise has already been introduced in Section VII-A. The steady-state noise in equation VII-4 corresponds to the results of that analysis.

Each rod oscillator test sequency consisted of oscillating sinusoidally the center control rod at distinct frequency increments from 0.03 cps to 3.0 cps, and simultaneously recording reactor parameters. In the case of the natural circulation sequence, for example, twelve frequency increments were selected: 0.03; 0.05; 0.1; 0.2; 0.5; 0.7; 0.85; 1.0; 1.2; 1.5; 2.0; and 3.0 cps. Each of these points in frequency represent a data point in the frequency analyses of the reactor transfer functions.

Data for each of the frequency increments, or runs, were recorded on both pen traces and magnetic tape. Figures VII-35, 36, and 37 are pen recorder traces made for the natural circulation test sequence. One can appreciate, by inspection of these traces, the utter futility of attempting a visual transfer function analysis on these recordings. These traces, however, can be analyzed mathematically. One such mathematical technique is the band pass filter device which very conveniently accepts as input the voltage parameter analogue recorded on magnetic tape.

A detailed description of the band pass analyzer is presented in Appendix C. Included in this description is a schematic diagram of the band pass hook-up. Figure VII-38 is a pen recording of an example rod oscillator band pass analysis. The test which is shown being analyzed is the 0.05 cps, natural circulation run. The output parameter being evaluated is the $\mu\mu$A. Each pen channel in Figure VII-38 is a recording of a definite sequential step in the band pass analysis of the data. Each of the steps in the analysis correspond to specific points in the wire hook-up of the band pass device.

The bottom channel of Figure VII-38 is a recording of the raw $\mu\mu$A total flux variation (N*). The top channel of this figure is a recording of the $\mu\mu$A signal after band pass filtering. The pass band of the filter is set for the frequency corresponding to the rod motion oscillation.

The top center channel is the rectified and filtered μμA signal. The bottom center channel is the integral of the rectified and filtered μμA signal. It is this integrated signal which is adjusted by the circuit scale factors to yield the average voltage value of the parameter oscillation at the pass band frequency. The peak voltage value of the total flux variation is determined by multiplying this result by $\pi/2$. Conversion from a voltage oscillation to a per cent of steady-state oscillation in the parameter is accomplished by application of the instrument circuit readout scale factors to these band pass results, and subsequently dividing by the measured steady-state reactor conditions.

The total flux variation for a given rod oscillator run (N*) contains a single fundamental frequency due to rod motion plus the noise component. This noise component is identical to the steady-state noise (see equation VII-4). Therefore, when the band pass device, with a finite band width, is used for analysis, it measures the "spike" frequency due to the rod disturbance, plus the same integral of the noise appearing under the band width that was obtained for the steady-state analysis. This integral of noise, it should be remembered, is not a vector quantity. i.e., it has a definite frequency spectrum but no consistent phase relationship. Thus, if the value of the steady-state noise at the frequency corresponding to rod motion is subtracted from the band pass analysis of the total flux variation (N*), then the end result is the single frequency "spike" which is, by definition, the response to rod oscillator (N* rod).

It should be pointed out that the filter bandwidth which caused a problem in the steady-state analysis does not affect the results of the rod oscillator analysis. i.e., the filter band width obviously will not affect the integral of a "spike" frequency response which occurs near the midpoint in its filter window. Therefore, the filter bandwidth will not affect the evaluation of the N* rod component of the total flux variation. It is true, of course, that the band width does have an effect upon the resolution of the noise spectrum component of the total flux variation (N*). However, if the observation is made that the noise spectrum is

the same during rod oscillation as it was during steady-state, then whatever error is introduced by bandwidth or overlap in the total flux variation (N*) is subtracted back out when the rod response (N* rod) is calculated. Even if this assumption is invalid, the results are still accurate because of the high signal to noise ratio described earlier.

c. Experimental Amplitude and Phase Relationships

It is necessary, in order to determine a given transfer function, to measure the relative amplitude and phase between the selected input and output parameters. The rod motion during the rod oscillator tests is, of course, the selected input parameter. It has already been observed that the rod amplitude can be easily read from the pen recorder traces. It has also been observed that the various output reactor parameters are complex in response and cannot be read accurately by visual means. The band pass technique described in the previous section, however, provides a method for determining the amplitude of these complex responses. One further step in calculation is necessary before these input and output amplitudes can be related to one another with some meaning. This step is the determination of the relationship between ΔK and rod amplitude. This step has two parts: First, it must be known what this general relationship is (linear or non-linear and by what degree); and second, the absolute reactivity worth ($\Delta K/\beta$) of rod displacement must be determined.

The first determination listed above was satisfied by physics calculations. These calculations show that the reactivity from rod displacement relationship is linear over the range of test amplitudes. The determination of the absolute rod worth was determined from the experimental data. This was accomplished by normalizing the power transfer functions to the zero power transfer function. This procedure is discussed in greater detail in the next section.

The determination of the phase relationship between the input and output parameters is a separate problem. It is next to impossible to extract this phase relationship directly from the experimental data. This diffi-

culty in data analysis arises from the following restrictions:

1. Control Rod #7 and its mechanical linkages constitute a spring-mass system which uncouples the rod position indicator from the control rod proper. This spring-mass system has been appraised by calculation to produce a possible 5 - 10° phase error in the rod position indicator. The largest error occurs at the high frequency rod movements. It should be pointed out that the effect of this spring-mass system was shown by calculation to be insignificant in the rod amplitude determination.

2. The extremely complex wave forms of the flux and flow responses make an accurate phase determination very difficult. And, high accuracy in phase resolution is an absolute necessity for gain and phase margin interpretation of the rod oscillator data (less than 3° error). This range of accuracy cannot be afforded by the analogue band pass filter equipment.

For the above two reasons, no attempt was made to measure directly the input/output phase relationship from the experimental data. Rather, the phase relationship was determined from the magnitude relationship by the use of Bode's first theorem.(7)

$$B(\omega d) = \frac{\pi}{2}\left|\frac{dA}{du}\right|_0 + \frac{1}{\pi}\int_{-\infty}^{+\infty}\left[\left|\frac{dA}{du}\right| - \left|\frac{dA}{du}\right|_0\right] \ln \coth\left|\frac{u}{2}\right| du \qquad \text{(VII-5)}$$

Where:

$B(\omega d)$ is the phase shift of the network in radians at the desired frequency (ωd)

A is the attenuation in nepers where 1 neper = ln e

u is a numeric that is the logarithn of the ratio of the actual frequency (ω) to the frequency (ωd) at which the phase shift is sought. Thus:

$$u = \ln \frac{\omega}{\omega d}$$

DATA ANALYSIS AND RESULTS

The results of the rod oscillator tests fall into two general categories of transfer functions:

a. The neutron flux response to cyclic ΔK insertion (includes both in-core and out-of-core flux measurements).

b. The in-core fuel channel flow response to cyclic ΔK insertion.

These two categories are discussed separately in the following sections.

A. Neutron Flux from ΔK Transfer Functions

1. Reactor System Relationships

The dynamics of a boiling water reactor can be represented schematically by the logic block diagram of Figure VII-39.

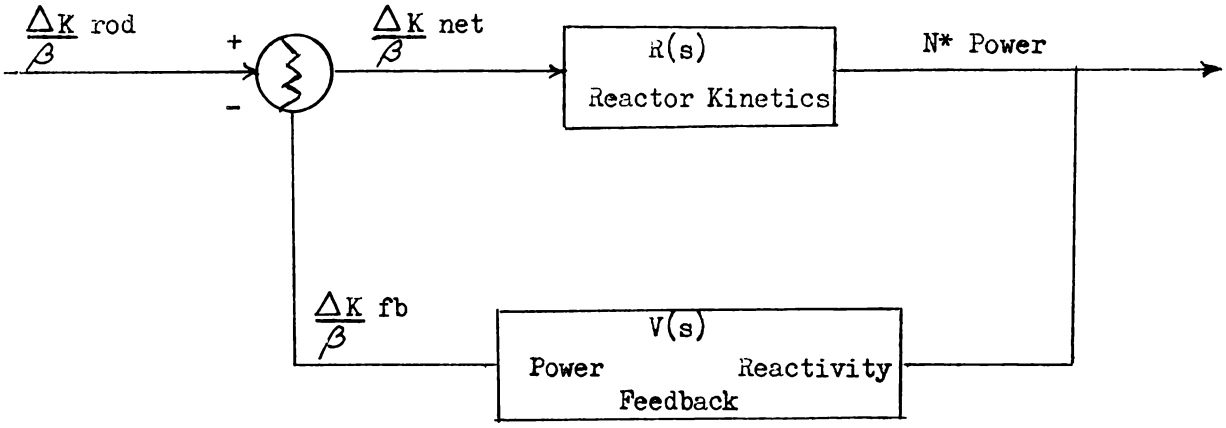

LOGIC BLOCK DIAGRAM FOR RESPONSE OF THE VBWR

FIGURE VII-39

The reactor transfer function corresponding to this system is derived in Reference (8).

$$\frac{\text{N* Power}}{\Delta K \text{ rod}} = \frac{R(s)}{1 + R(s)\ V(s)} \qquad \text{(VII-6)}$$

Where:

(s)	complex frequency (radians/sec)
N*	is the power variation in per cent of steady-state value
R(s)	is the zero power reactor kinetic function
V(s)	is the power reactivity feedback function
$\frac{\Delta K}{\beta}$ rod	is the rod displacement reactivity in delayed neutron fractions
$\frac{\Delta K}{\beta}$ fb	is the feedback reactivity
$\frac{\Delta K}{\beta}$ net	is the net reactivity

The zero power reactor kinetics function (R(s)) is a reasonably well known relationship. A plot of this relationship, R(s), is presented in Figure VII-40 (Reference (9)). It is observed from Figure VII-40 that the gain of the R(s) relationship is approximately equal to one (0 db) between the frequencies of 0.1 and 3.0 cps.

The power reactivity feedback function (V(s)), however, is not as well defined. It is a complex relationship which includes the combined feedback effects of pressure-voids, heat-voids, etc. It is not necessary for the purpose of data analysis, however, that this feedback function be completely defined. All that is necessary is that we recognize the feedback function to be analogous to a high frequency filter. i.e., The magnitude of the feedback function begins in the steady-state or low frequency end of the spectrum with a gain greater than one (0 db) and remains constant with increasing frequency until a "cut-off" point is reached, above which the gain attenuates with increasing frequency. The magnitude of this feedback function attenuates through a gain of one (0 db crossover point) somewhere between 0.1 and 1.0 cps. A plot of an example feedback function is presented in Figure VII-41.

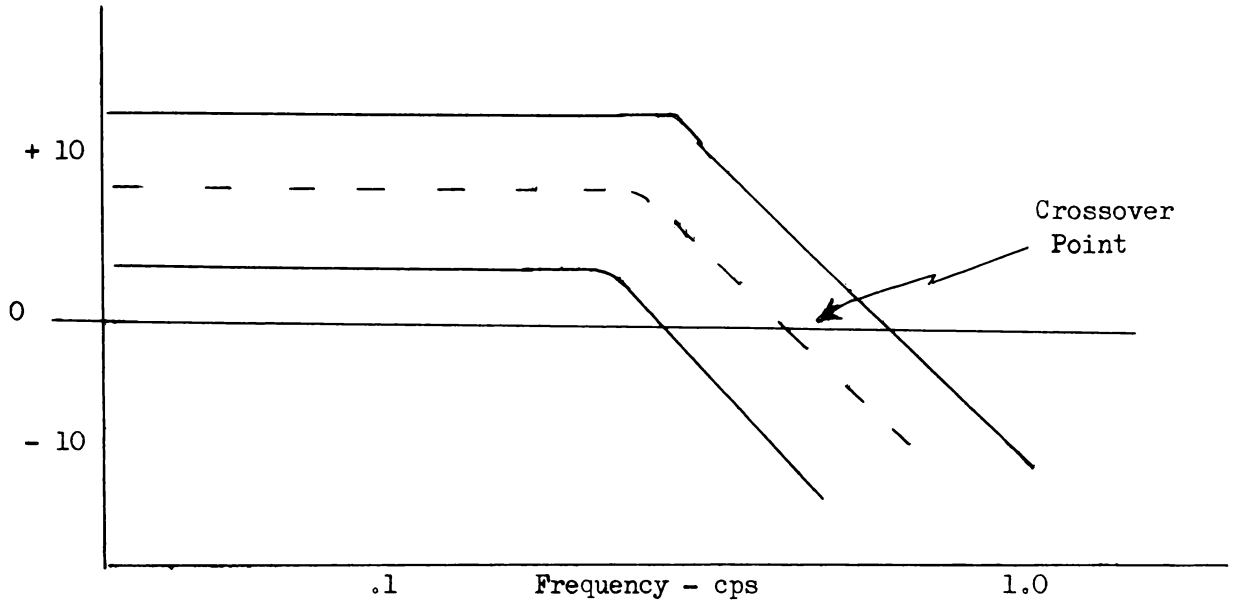

FIGURE VII-41

EXAMPLE FEEDBACK FUNCTION FOR REACTOR KINETICS

Referring to the zero power reactor kinetics function of Figure VII-40, the foregoing description of the power-reactivity feedback function, Figure VII-41, and the relation of equation VII-6, the following statements can be made:

a. As complex frequency, s, decreases below the crossover point, the magnitude of the feedback function, V, becomes greater than one, and the magnitude of the zero power kinetic function, R, is one or greater. Hence, the term $1 + RV$ approaches RV and thus the reactor power transfer function $R/(1 + RV)$ approaches $1/V$.

b. As the complex frequency, s, increases above the crossover point, the magnitude of the feedback function, V, becomes less than one, and the magnitude of the zero power kinetic function, R, is one or less. Hence, the term $1 + RV$ approaches 1 and thus the reactor power transfer function approaches R.

Figure VII-42 is a sketch showing a possible boiling water reactor power transfer function plotted against dimensionless frequency. This sketch illustrates the relationships between the zero power kinetics function, R(s), the power reactivity feedback function, V(s), and the reactor power transfer function, R/(1 + RV).

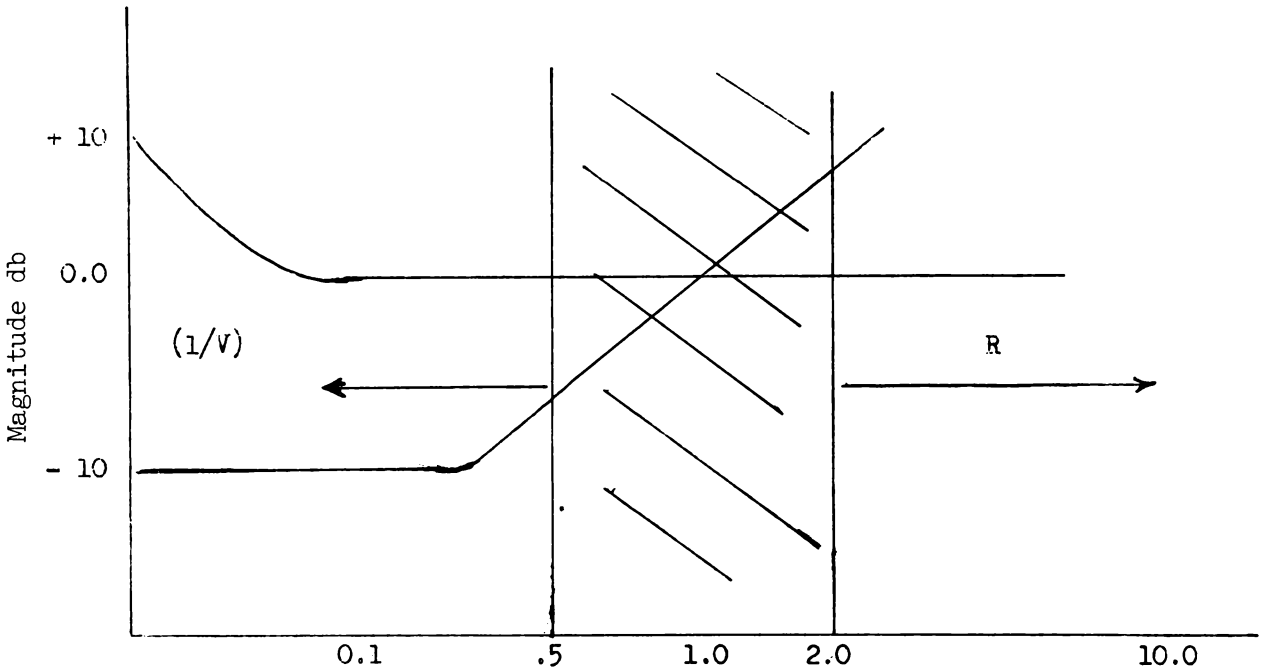

DIMENSIONLESS FREQUENCY CHARACTERISTIC

BWR POWER TRANSFER FUNCTION

FIGURE VII-42

The band in the center of the sketch defines the region of V(s) crossover. This band is the transition region where the R/(1 + RV) transfer function does not look like 1/V or R, but, rather, is determined by the combined phase and gain characteristics of both. The width of this band is taken to be 2 octaves in frequency. It is estimated that beyond this band of crossover, the 1/V and R approximation for the R/(1 + RV) transfer function is accurate within 10%.

Fortunately, in the case of the rod oscillator data, the above mentioned band of crossover is bracketed on both sides by experimental test points. This band, however, occurs somewhat closer to the high frequency end of the rod oscillator spectrum than at the low end. This means that the R(s) approximation for the transfer function at high rod oscillator frequencies is less than the 1/V(s) approximation of the transfer function at low rod oscillator frequencies. Nevertheless, the reactor transfer function R/(1 + RV) has the magnitude of R(s) within 5 per cent at the 3.0 cps frequency. The low frequency end of rod oscillator (0.03 cps), then, has the magnitude of 1/V within less than 5 per cent.

2. Rod Worth Normalization

It has been demonstrated by the explanation presented in the preceding section that the rod oscillator test data and the zero power reactor kinetics function should coincide at 3.0 cps. The constant by which the experimental curves must be divided to make them coincide is the reactivity worth of the rod displacement for the test case. Figure VII-43 is the rod oscillator μμA flux response curve obtained for the natural circulation test series. The flux amplitude in this curve has been normalized to a $\pm$ 0.7 inch rod displacement. Using this natural circulation test series as an example, the rod worth determination was obtained as follows:

> The experimental curve of Figure VII-43 was normalized so that its 3 cps point coincided with the zero power reactor kinetics function of Figure VII-40. The 3 cps point on the zero power

kinetics curve is $-\frac{1}{2}$ db, or essentially, 0 db, (a gain of one). This means that the percentage oscillation in flux at 3 cps, shown in Figure VII-43, is equal to the ΔK disturbance in cents for the given rod displacement. The worth of the rod displacement obtained from this normalization was 6.95¢ ($\Delta K/\beta$) for 0.7 inch. The flux response curve can now be presented in terms of a $\pm$ 10¢ reactivity oscillation. This relationship is convenient for comparison to the pre-test analysis (see Section VIII). Figure VII-44 shows the μμA flux response curve for a $\pm$ 10¢ reactivity oscillation. Also shown in this figure is the 10.0¢ ($\Delta K/\beta$) normalized flux amplitude curve for the C-501 in-core ion chamber measurement.

The foregoing procedure was used to obtain the rod displacement worth in each of the five test sequences analyzed. This normalization was performed on both the out-of-core flux recording (μμA) and a representative in-core flux measurement. The normalized flux amplitude curves for rod oscillator tests 15-16, 15-9, 15-19, and 15-1, are presented in Figures VII-45 through VII-48, and the values of Table VII-8. It is observed that the in-core and μμA flux amplitude curves after normalization are remarkably similar. The shapes of the two types of flux curves have some minor differences. It is believed, however, that attaching any physical significance to these differences is not justified at this time because of the unknown instrument and readout errors of the in-core ion chambers. These errors are yet to be determined.

Most instruments, as a general rule, are more capable of accurately measuring relative differences in a variable than they are in establishing an accurate measurement of absolute level. It is possible that the curves of Figures VII-44 to VII-48 and the values in Table VII-8 provide data indicating that this is the case for the in-core ion chambers. i.e., each of the normalized in-core flux amplitude

TABLE VII-8

ROD WORTH DETERMINATIONS FROM THE ROD OSCILLATOR DATA

CONTROL ROD #7 POSITION - VARYING ROD BANK POSITION

TEST NUMBER	REACTOR POWER MWt	TOTAL FLOW gpm	COMMENTS	MEASUREMENT	SPECIFIC INSTRUMENT	ROD WORTH $\Delta K/\beta$ /in. cents/inch	
15-18	15	- - -	Natural Circulation	External Flux Monitor	μμA #2	9.95	
				In-core Ion Chamber	C-501		7.75
15-16	15	4,000	Forced Circulation Baffle Doors Open	External Flux Monitor	μμA #2	9.13	
				In-core Ion Chamber	A-502		5.16
15-9	15	4,000	Forced Circulation High Pump Head Valve Controlled Flow (high voids)	External Flux Monitor	μμA #2	11.1	
				In-core Ion Chamber	D-503		12.6
15-19	15	4,000	Forced Circulation Low Pump Head Speed Controlled Flow (high voids)	External Flux Monitor	μμA #1	10.9	
				In-core Ion Chamber	A-502		7.9
15-1	15	20,000	Forced Circulation Maximum Flow (low voids)	External Flux Monitor	μμA #2	14.7	
				In-core Ion Chamber	C-501		31.8

traces of Figures VII-44 through VII-48 represent a relative measurement of a single in-core ion chamber as the rod oscillator test is stepped through its frequency spectrum. Only small deviations are observed between these relative measurements and their corresponding measurements of the μμA. On the other hand, the rod displacement worths of Table VII-8 represent the in-core ion chambers interpretation of absolute flux level. Very large deviations are observed between these in-core measurements and their corresponding μμA recordings.

It is possible, of course, that the small and/or large variations between the in-core and μμA measurements of flux have some physical significance. Again, however, the reader is cautioned that no firm interpretation of the in-core data is justified at this time. The worth of this in-core flux data and its significance should, and will, be the subject of a continuing analytical program. Until such time as the characteristics of these in-core ion chambers are clearly defined, their data significance should be limited, and the use of their measurements as a foundation for physics postulation (rod worths and void coefficients) should be avoided. For the present, and for the purpose of this report, we shall confine the flux interpretation and discussion to the out-of-core μμA recordings.

One final, and very significant, observation can be made from μμA data presented in Table VII-8. This observation concerns the relationship between rod worth and core-steam volume. First, it is important to recognize that, insofar as core voids are concerned, test 15-9 should be identical to test 15-19, and test 15-18 should be essentially the same as 15-16. This is true because in the case of Runs 15-9 and 15-19, the core power, inlet subcooling, and recirculation flow are identical. Furthermore, no conditions are known to exist which would change the core flow distribution, power distribution, etc. The same sort of a parameter identity exists between tests 15-18 and 15-16. Here, it is assumed that the bypass path around the core afforded by the open baffle doors shunts any effect that the forced circulation of 15-16 may have in addition to natural circulation. This assumption

is particularly good in the low recirculation flow range. There are, then, essentially three core-steam volume conditions expressed by the five runs analyzed:

a. A high core steam volume condition represented by tests 15-9 and 15-19.

b. A low core steam volume condition represented by test 15-1.

c. An indeterminate core steam volume condition represented by the natural circulation run 15-18 and test 15-16. This flow condition, although inaccurately estimated, is, without a doubt, closer to the 4,000 gpm flow, high void condition than it is to the 20,000 gpm flow, low void condition.

It is observed from the μμA data of Table VII-8 that the worth of the rod per inch of displacement decreases with increasing voids. No attempt is made at this time to attach much physical signficance to the rod worth normalization factors for runs 15-18 and 15-16. It should be remembered that the data for these runs was exceedingly difficult to analyze because of the "loose" hydraulic coupling. Therefore, it is known that these curves contain more error than the others. As was the case with the in-core flux measurements, the measurement of absolute level (rod worth) is eyed with considerable skepticism. The measurement of relative values (curve shape), however, is considered significant, and is discussed in detail in a later section.

3. Power Reactivity Feedback Determination

It was shown earlier that the reactor power transfer function becomes the reciprocal of the power reactivity feedback function (1/V) in the low frequency end of the spectrum. The reactivity feedback function is, of course, a frequency dependent relationship. It is reasoned, however, that the low frequency end of the rod oscillator spectrum (0.03 cps) approaches the steady-state or equilibrium condition. i.e., A frequency of 0.03 cps is low enough that the flux measurements are

essentially in the steady-state equilibrium with the control rod-induced reactivity change. It appears from an observation of the curves of Figures VII-44 through VII-48 that this assumption is good. Notice that the μμA flux responses appear to be either already flat at 0.03 cps, or, at least nearing a flat or horizontal shape.

The value of the reactor power transfer function at 0.03 cps is taken to be equivalent to the reciprocal of the steady-state power reactivity feedback gain. This gain is expressed as the cents in reactivity feedback per per cent change in reactor power $(\frac{\Delta K}{\beta}/N^*)$. If one reasons that virtually all of this reactivity feedback is due to the combined effect of Doppler and power-generated steam void changes, then the void coefficient of reactivity can be obtained by calculation. The calculated Doppler coefficient (0.75 cents/%) is subtracted from the total reactivity feedback gain, and this result is then divided by the calculated power to void relationship. The accuracy of the void coefficients of reactivity which are thus obtained from the rod oscillator data are therefore dependent upon calculations in two ways:

a. The determination of the Doppler coefficient $(\Delta K_D / N^*)$

b. The determination of the power to void relationship (R_g^*/N^*).

The results of both the total power reactivity feedback gain and the void coefficients of reactivity are presented in Table VII-9. Column 2 of the table lists the total feedback reactivity gain in cents of reactivity per per cent change ir power level. Column 5 lists the void coefficient of reactivity gains in cents of reactivity per per cent change in core average void fraction. It is observed from these columns that both the total reactivity feedback gain and the void coefficient of reactivity gain increase with increasing average core void fraction. Two things should be made clear at this point: First, the units of both types of gains cited above are cents per per cent. These gains reported in other units may display an altogether different relationship with average core voids. This point should be remembered when these results are compared to the results of other

TABLE VII-9

FEEDBACK GAIN DETERMINATIONS

REACTOR POWER IS 15 MWt FOR ALL CASES REPORTED

TEST NUMBER	TOTAL RECIRCULATION FLOW gpm	COMMENTS	AVERAGE CORE STEAM VOIDS $\overline{R}_g$ %	1/V	POWER REACTIVITY FEEDBACK GAIN ΔK fb/N* (V) cents/%	POWER REACTIVITY FEEDBACK EXCLUSIVE OF DOPPLER cents/%	POWER TO VOID GAIN $\overline{R}^*_g/N^*$ %/%	VOID COEFFICIENT OF REACTIVITY $\frac{\Delta K}{\beta}$ Voids $\overline{R}^*_g$ cents/%
			(1)	(2)	(3)	(4)	(5)	(6)
					1/(2)	(3) - 0.75		(4)/(5)
15-18	- - -	Natural Circulation	- - -	0.23	4.35	- - -	- - -	- - -
15-16	4,000	Forced Circulation Baffle Door Open	- - -	0.30	3.33	- - -	- - -	- - -
15-9	4,000	Forced Circulation High Pump Head Valve Controlled Flow	0.20	0.275	3.64	2.89	.638	4.53
15-19	4,000	Forced Circulation Low Pump Head Speed Controlled Flow	0.20	0.25	4.00	3.25	.638	5.09
15-1	20,000	Forced Circulation Maximum Flow	0.08	0.46	2.17	1.42	.80	1.78

tests in order than erroneous comparisons will not develop. Second, the two types of gains are presented arbitrarily as a relation with average core voids. The results should not be misconstrued to indicate that these gains for all reactors, or even for the VBWR, are solely dependent upon the average core void condition. Rather, the results indicate that the reported relationship was observed specifically for the VBWR at the conditions analyzed, and that extrapolation of the test data to other reactors or reactor conditions should be done by the use of analytical models which have been verified by the reported data, not by apparent experimental correlations.

4. Power Transfer Function Curve Interpretation

The power transfer functions for the five rod oscillator tests analyzed are presented in Figures VII-44 through VII-48. Each figure contains both the in-core ion chamber and μμA measurement of the power transfer function. As was mentioned before, the shapes of the two types of flux curves are closely similar, and what minor differences do occur, are considered, at this time, to be within the unknown limits of the in-core ion chamber measurements. Therefore, these differences are not considered significant and the μμA curve is used as the reference representation of the power transfer function.

A great deal of information can be obtained about a system by visually studying the shape of its transfer function. One thing, for example, which can be observed from the shape of the transfer function is the existence or lack of existence of oscillating characteristics. i.e., The existence of oscillatory properties in a system is characterized by relatively sharp peaks and/or valleys in the system's transfer function. On the other hand, a very stable system will display no such peaks or valleys in its transfer function. A measure of a system's stability, then, is the degree of sharpness displayed in its transfer functions' peaks and valleys. Another system characteristic which can be observed from the transfer function is the natural frequencies, if any exist. The undamped natural frequencies of existing

oscillatory characteristics are found by locating the frequencies at which the peaks and/or valleys in the transfer function occur.

The following conclusions are made from a visual examination of Figures VII-44 through VII-48.

a. The natural circulation test (15-18) of Figure VII-44 and the forced circulation with baffle door open test (15-16) of Figure VII-45 are similar in shape. This might well be expected since the core hydrodynamics of the two conditions are essentially the same. The baffle door passage is large enough that bypass flow, either positive or negative, does not appreciably alter the effective single-phase elevation head which exists across the core in natural circulation. Therefore, 4,000 gpm forced circulation with a core hydraulic parallel bypass or shunt closely resembles natural circulation core flow conditions.

b. The high head, valve-controlled, 4,000 gpm forced circulation test (15-9) of Figure VII-46 and the low head, speed-controlled 4,000 gpm forced circulation test (15-19) of Figure VII-47 are essentially identical in shape. Since the core hydraulics for these two tests are the same, it can be concluded that the differences which exist in the recirculation loop have no effect. This phenomenon can be interpreted to indicate that the recirculation flow system is well damped even in the most frictionless condition which can be operationally produced (15-19), and that additional recirculation flow loop friction, although large (15-9), has no effect because the hydraulic damping is already essentially saturated.

c. The 20,000 gpm, forced circulation test (15-1) of Figure VII-48 is unique compared to the other four test results.

d. It is observed by comparing the 4,000 gpm tests of (b) above to the 20,000 gpm test of (c) above, that the reactor system increases in stability as recirculation flow is increased. i.e., The power transfer functions for both of these tests are essentially devoid of valleys in their amplitude spectrums, but do contain amplitude peaks near the high frequency end of the spectrums. This peak is very noticeably higher for the low flow tests than for the high flow test.

e. It is observed by comparing the 4,000 gpm runs of (b) above to the 20,000 gpm run of (c) above, that the resonant frequency of the power transfer function increases with increasing flow. This flow dependence of frequency is not large. The resonant frequency of the 4,000 gpm runs are about 1.0 cps, while the resonant frequency of the 20,000 gpm run is about 1.2 cps.

f. It is observed from the natural circulation test and the forced circulation with baffle doors open test((a) above) that their transfer functions contain a characteristic valley in the frequency spectrum. This amplitude valley exists in addition to, and at a lower frequency than, the high frequency peaks already described above.

The occurrence of these low frequency troughs is very significant. Just as the high frequency peaks are indicative of a resonance in the entire reactor system, these troughs indicate a resonance in the core hydrodynamics. The low frequency portion of the power transfer functions was explained earlier to appear as the reciprocal of the feedback function (1/V). Therefore, a dip or trough in 1/V indicates a peak or resonance in V. This resonance is in the hydraulic portion of the feedback function, and occurs at a frequency of 0.4 to 0.5 cps. It is important to note that this indication of hydraulic resonance in the natural circulation transfer function agrees well with the observations made earlier in the discussion of the pen recorder traces. A core inlet flow sympathetic variation

with power was also observed from the pen recorder trace of 0.5 cps (see Figure VII-35).

Since the existence of a trough in the low frequency portion of the power transfer function denotes a resonant hydraulic system, the absence of such a dip must indicate stable hydraulics. Therefore, it can be concluded that both the 4,000 gpm forced circulation tests and the 20,000 gpm forced circulation test have stable hydraulic systems. This conclusion is further verified by the observations of (b) above.

5. Gain Margin Determination

It was mentioned above that the system stability of the 4,000 gpm forced circulation tests was less than the 20,000 gpm test. This conclusion was obtained by comparing the relative peak sharpness of the two transfer functions. This interpretation of relative stability, although very useful, is coarse and does not provide a precise relative measurement of system stability.

The purpose of the gain margin determination is not only to establish an accurate relative stability comparison of these two tests, but also to ascertain an absolute measure of stability at each test condition. This measure of stability, the gain margin, is the factor by which the entire reactor system gain can be increased before divergent oscillations of instability will occur. The predominant factor which influences system loop gain is the void coefficient of reactivity. Therefore, one can reason, for the convenience of data interpretation, that the gain margins listed in this section are for the amount by which the void coefficient of reactivity for the VBWR test conditions could have been increased before divergent power oscillations occurred. The reader is strongly cautioned not to think in terms of operating the VBWR, or any other system for that matter, up to the limit of instability. It must be remembered that instability, as it is defined here, is the point where divergent oscillations occur. Undesirable operating

conditions occur long before the gain margin of a system becomes zero. A good rule of thum for a safe operating gain margin is a factor of 2 or more. The following are justification for this rule:

a. The design considerations for a dynamic system generally demand that the gain margin not be less than a factor of two in order that its control will not be over-responsive.

b. The gain margin is extracted from the data by considering the reactor system to be of linear response. The error thus introduced, although not considered large, is, nevertheless, present and could put the system nearer divergent oscillations than predicted.

c. Although the gain margin is specifically defined as a factor, it would be difficult indeed to physically alter, by design modifications, the gain of a reactor system without changing the dynamic response upon which the gain margin is based. i.e., To alter the void coefficient of reactivity of a reactor would almost certainly mean a change in the core hydraulic passages. Therefore, the alteration means not only a change in the void reactivity gain, but also a change in the hydrodynamics of the system.

A gain margin determination was conducted for the 4,000 gpm forced circulation test condition and the 20,000 gpm forced circulation test condition. Test 15-9 was selected as representative of the 4,000 gpm condition.

Figures VII-49 and VII-50 are power transfer function plots of tests 15-9 and 15-1, respectively. The magnitude of the transfer function in these figures are given in db. The phase angles are plotted for frequencies between 1.0 and 3.0 cps. These phase relationships were obtained by the use of Bode's first theorem which was previously introduced in the method of data reduction. The gain margins for the high and low forced circulation test conditions were resolved as follows:

The denominator of the experimental transfer function was analytically resolved and set equal to zero. i.e., from equation VII-6, the denominator of the power transfer function is $(1 + R(s)\ V(s))$. Setting this quantity equal to zero:

$$R(s)\ V(s) = -1 \qquad \text{(VII-7)}$$

The condition where the product of the zero power reactor kinetic function (R(s)) and the power reactivity feedback function (V(s)) is equal to minus 1 occurs where the total system gain is equal to plus 1, and the phase lag is equal to 180°. The constant by which the experimental gain, at 180° phase lag, must be multiplied in order to equal one is the gain margin of the system.

The product R(s) V(s) was analytically resolved from the experimental transfer function by the application of complex algebra. From equation VII-6, the experimental transfer function $N^*/\Delta K$ is defined:

$$N^*/\Delta K = \frac{R(s)}{1 + R(s)\ V(s)} \qquad \text{(VII-8)}$$

dividing by the zero power reactor kinetics function of Figure VII-40, and taking the reciprocal:

$$\frac{\frac{1}{R(s)}}{1 + R(s)\ V(s)} \cdot \frac{1}{R(s)} = 1 + R(s)\ V(s) \qquad \text{(VII-9)}$$

The product of R(s) V(s) was then obtained by the use of a "Nichols" chart.[8] The experimental frequency response of R(s) V(s), thus obtained, was then substituted in equation VII-7, and the gain margin established.

Table VII-10 summarizes the results of the gain margin determination. Several observations can be made concerning the results of the gain margins:

a. The stability of the reactor system increases with increasing flow. The high flow test is a factor of 9.44/4.12, or 2.29 more stabile than the low flow test. This same stability trend was established in the preceding section.

b. It is observed from Table VII-10 that the power reactivity feedback gain for the high flow test is a factor of 3.82/2.17, or 1.76 less than for the low flow test. Since it has already been shown that the hydraulics for both of these tests are stable, it can be concluded that the major contribution to the trend of decreasing stability with decreasing flow is the flow dependence of the feedback gain. NOTE: As gain margin decreases, the feedback gain increases.

c. The significance of geedback gain to stability is dramatized by the test conditions of 15-9 and 15-1. These conditions represent a reactor system with stable hydraulics which is being driven nearer instability by primarily an increase in feedback gain.

TABLE VII-10

STABILITY GAIN MARGIN DETERMINATIONS

TEST NO.	COMMENTS	AVERAGE CORE VOIDS	GAIN	MARGIN
			db	Factor
15-9	4,000 gpm Forced Circulation	0.2	12.3	4.12
15-1	20,000 gpm Forced Circulation	0.08	19.5	9.44

6. Steady-State Peak-To-Peak Flux Noise and System Stability

Figure VII-51 is a control data pen recording of the steady-state flux noise for the 20,000 gpm forced circulation test, a 4,000 gpm forced circulation test, and the natural circulation test. It is observed from this figure that the 20,000 gpm test condition has the largest peak-to-peak flux noise (about 15%), the 4,000 gpm test has the smallest with about 6%, and the natural circulation test is in-between with about 13% peak-to-peak noise.

It is very important that the significance of the peak-to-peak flux noise not be misinterpreted. Table VII-11 summarizes the gain margins and the peak-to-peak flux noises of tests 15-1 and 15-9.

TABLE VII-11

COMPARISON OF PEAK-TO-PEAK FLUX NOISE AND SYSTEM GAIN MARGINS

TEST NO.	COMMENTS	AVERAGE CORE VOIDS	GAIN MARGIN	PEAK-TO-PEAK FLUX NOISE
		%	Factor	%
15-9	4,000 gpm Forced Circulation	0.2	4.12	6.0
15-1	20,000 gpm Forced Circulation	0.08	9.44	15.0

Table VII-11 shows that the amplitude of the steady-state flux noise increases with increasing flow. The reactor gain margin, however, is seen to increase with increasing flow. Thus, it is demonstrated that the consideration of peak-to-peak steady-state flux noise measurement as a prime indication of reactor stability is entirely inadequate. It was found in the VBWR that not only did the steady-state noise peaks fail to indicate a trend toward unstable operation, but, even worse, indicated the reverse trend.

B. CORE COOLANT FLOW FROM ΔK TRANSFER FUNCTIONS

The core coolant flow from reactivity transfer functions can be defined as the in-core fuel channels flow response to a reactivity disturbance. It should be pointed out that this transfer function may not exist for a given reactor condition. A primary requisite for the existence of this transfer function is that the core flow must be a function of reactor power. i.e., The relationship sought is the reactivity to core flow response. The chain of reactivity influence begins first as an effect upon core power and completes its circuit as a power effect upon core flow. The foregoing requisite may be re-stated to say that if the hydraulics of the reactor recirculation loop is exceedingly stable, then the transfer function ($V^*/\Delta K$) will not exist. It may be concluded then that extracting the $V^*/\Delta K$ transfer function from the rod oscillator data is not as straight-forward as in the case of the power transfer function. A three-step procedure was used for the analysis of the in-core flow rod oscillator data.

First: The pen recorder traces of the given reactor condition were examined to determine if a sympathetic variation of flow with power and rod motion was displayed during the rod oscillator test.

Second: Measurements of the transfer functions' output (V^*) and input (rod motion) were obtained from the data in the same general fashion as was used for the power transfer function.

Third: The question was asked, "Does the relationship thus obtained represent the $V^*/\Delta K$ transfer function, or is it a maze of unidentifiable causes and effect?"

Having recognized that the extraction of the $V^*/\Delta K$ transfer function from the rod oscillator data would, at best, be difficult, the obvious selection for a first attempt at flow analysis was the natural circulation test, 15-18. i.e., It is recalled that hydraulic resonance and flow dependence upon power was displayed in both the pen recorder trace (Figure VII-35), and the power transfer function (Figure VII-44) of the natural

circulation test. Thus, the first step of the above three-step data analysis procedure was already accomplished - the existence of a power-related flow variation was undeniable. Next, the in-core flow (E-201) variation which was recorded on magnetic tape during rod oscillation was filtered and reduced by the band pass filter device. Finally, this reduced rod oscillator flow data was examined to see if it was reasonable. Unfortunately, these results, although not unreasonable, were difficult to assess. It was found that the rod oscillator frequency spectrum for E-201 was essentially the same in magnitude and frequency as its steady-state noise spectrum. One conclusion which could be drawn from such results is that the cyclic rod motion had not effect upon in-core flow. i.e., The flow transfer function did not exist for the natural circulation test condition. This conclusion, of course, cannot be valid because flow was observed to be influenced by power in both the steady-state pen recorder traces and the power transfer function. A second conclusion which can be drawn from these results is that the flow response to rod motion was identical to the steady-state noise spectrum. This conclusion, like the previous one, cannot be valid because the pen recorder traces show the flow responses to be different during rod oscillation than during steady-state. The most likely conclusion which can be drawn from these results is that the flow noise was a manifestation of an excitation which was large compared to the power oscillation influences. Therefore, any differences in the steady-state noise spectrum brought about by rod oscillation are small and difficult to separate from the "mask" of noise. Moreover, the overlap error in the band pass filter technique of data analysis is inadequate to detect these small differences. The end result of these two difficulties was to cause the effect of rod motion to appear as though it ordered the existing flow noise oscillations without changing the amplitude of the variations. This conclusion explains both 1) the fact that the evidence of a flow dependence upon power was observed; and at the same time, 2) the fact that no discernible difference was observed in the rod oscillator flow spectrum and the steady-state flow noise spectrum.

In any event, it can be concluded from the example analysis that, in natural circulation, the flow noise (frequency spectrum components) is at least equal in magnitude to whatever flow response may result from rod motion. The response of flow to rod motion was larger in the natural circulation test with baffle doors open. Moreover, no sympathetic variation of flow with rod motion was discernible in the other forced circulation tests. Therefore, these series of tests, at best, only provide data with small differences between the rod oscillator response and the steady-state noise spectrum. The natural circulation example analysis, therefore, dramatized the absolute necessity for improved analytical techniques before flow transfer functions can be resolved from the VBWR data.

One general observation can be made concerning the flow responses observed for all of the tests analyzed:

The flow noise and the flow response to rod motion (when displayed) were always small compared to the flux response to rod motion. In all test series but 15-1, the flow noise was about 10% of the rod oscillation flux response. The flow noise in test 15-1 (high flow) was approximately 25% of the flux response.

CONCLUSIONS AND SUMMARY OF RESULTS

Table VII-12 summarizes the quantatative information obtained from the rod oscillator tests. All data reported is for tests conducted at 15 MWt. The average core void fractions listed in the table are calculated values. Average core void fractions are not given for the natural circulation test or the forced circulation test with baffle doors open because it was felt that the core flow rates were not sufficiently well known.

It is observed from this table:

a. The worth of the oscillation rod (Column 2) appears to increase with decreasing average core voids.

b. The total power reactivity feedback gain (Column 3) increases with increasing average core voids.

c. The void coefficient of reactivity (Column 4) increases with increasing average core voids.

d. The stability gain margin (Column 5) is seen to decrease for increasing voids. Zero gain margin indicates an unstable reactor. Therefore, the stability of the VBWR system is seen to decrease with increasing voids.

It should be pointed out that the above observations are presented somewhat arbitrarily as a relation with average core voids. These observations should not be misconstrued to indicate that these reactor system parameters for all reactors, or even for the VBWR, are solely and uniquely related to the average void conditions.

e. The amplitude of the steady-state flux noise (Column 6) is seen to increase with increasing recirculation flow. The stability of the reactor system (Column 5), however, is seen to increase with increasing flow. Thus, it is demonstrated that the consideration of peak-to-peak steady-state flux noise measurements as a prime indicator of stability is entirely inadequate. It was found in the VBWR that not only did the steady-state noise peaks fail to indicate a trend toward unstable operation, but, even worse, indicated the reverse trend.

The following observations were made from an analysis of the rod oscillator data and the power transfer functions:

f. The shapes of the power transfer functions as measured by both the in-core ion chambers and the external μμA flux monitor are essentially identical for a given test condition. However, the absolute flux levels and/or the percentage variations measured by any two given chambers or monitors may or may not be identical. The data are inconclusive about this.

g. It was observed that the flux response actually led the rod motion in phase during the low frequency portion of the rod oscillator tests. This phenomena should not be unexpected. This condition merely serves to dramatize the electrical reactive network analogy of a reactor system.

h. The natural circulation test (15-18) and the forced circulation with

baffle doors open test (15-16) have power transfer functions of similar shape. This might well be expected since the core hydrodynamics of these two conditions are essentially the same. i.e., The baffle door passage is large enough that bypass flows, either negative or positive, do not appreciably alter the effective single-phase elevation head which exists across the core in natural circulation.

i. Resonant hydrodynamics at 0.4 ~ 0.5 cps were exhibited within the reactor core for both the natural circulation test and the forced circulation with baffle doors open test. This flow resonance was displayed two ways: First, by observation of the unorificed instrumented fuel assembly's turbine flow meter; and second, by the existence of a characteristic dip in the power transfer functions of these two tests.

j. The effect of inlet orificing on fuel elements is to damp flow oscillations or resonance. This was observed from a comparison of the flow response of the unorificed and orificed instrumented assemblies during the natural circulation rod oscillator test.

k. The natural circulation test and the forced circulation with baffle doors open test are very demonstrative examples of a reactor core with uncoupled parallel flow channels and strong neutron coupling.

l. The high-head, valve-controlled, 4,000 gpm forced circulation test (15-9) and the low-head, speed-controlled, 4,000 gpm forced circulation test (15-19) have power transfer functions which are almost identical. This identity can be interpreted to indicate that the recirculation flow system is well damped even in the most frictionless condition which can be operationally produced (15-19), and that additional recirculation flow loop friction, although large, (15-9), has no discernible effect because the hydraulic damping is already essentially saturated.

m. No resonant hydraulics were observed in any of the closed flow circuit, forced circulation rod oscillator tests.

n. It was observed that the resonant frequency of the power transfer function increases with increasing flow. This flow dependence is not large. The system resonant frequency of the 4,000 gpm runs are about 1.4 cps, while

the resonant frequency of the 20,000 gpm run is about 1.5 cps.

o. The in-core flow noise and the flow response to rod motion (when displayed) were always small compared to the flux response to rod motion. In all tests but 15-1, the flow noise was about 10% of the rod oscillation flux response. The flow noise in Test 15-1 (high flow) was approximately 25% of the flux responses.

p. Both of these reactor conditions are devoid of oscillatory hydraulic characteristics, yet, we definitely observe the reactor become less stable with decreasing recirculation flow. We observe, at the same time, an increase in the void coefficient of reactivity gain with decreasing flow. These two trends go hand-in-hand toward the direction of reactor instability. These data, therefore, show conclusively the detrimental effect of increasing void reactivity coefficients upon reactor stability. It can be definitely concluded that there are real design upper limits on the void reactivity coefficients established by stability limitations.

One very important conclusion about noise excitation can be drawn from the natural circulation rod oscillator test data:

q. The natural circulation test condition was shown to have a responsive or resonant hydraulic system. Thus, the effect of power or flux driving flow is displayed. Oscillation of the control rod caused a variation in power. This variation in power caused a corresponding change in core void content. And, finally, these changes in core void content caused the underdamped hydraulic system to respond with a fluctuation in the coolant flow.

It should be pointed out, however, that the effect of power oscillation upon flow were only discernible near the resonant frequency of the hydraulic system. At all other frequencies, the flow noise was far greater than the flow response to power. The flow response to power, even at the hydraulic resonant frequency, was not to increase the amplitude of the flow noise by adding a sympathetic flow component to power, but rather, to cause the existing flow noise to become "ordered" with the power variations. i.e., The amplitude of the flow noise at this frequency was essentially the same during rod oscillation as it was just under the influence of steady-state noise.

The foregoing observations lead to the following very important conclusion:

> If the relatively large scale power disturbances induced by rod oscillation just barely caused a noticeable ordering of the flow noise, then the equivalent noise disturbances must be at least as large, if not larger, than those power-generated void disturbances which are caused by rod oscillation.

Two final conclusions can be made concerning the conduction of stability tests and the interpretation of data:

r. Meaningful results could not have been obtained from the steady-state noise and the rod oscillator data had they not been:

   1. Recorded on magnetic tape,
      and
   2. Subsequently subjected to effective filtering techniques.

   Moreover, it was found that, due to the non-stationarity of the noise components, it was necessary that the data be filtered and averaged over reasonably long time durations in order to become accurate results.

s. The inadequacy of transient tests for reactor stability measurements is dramatized in the VBWR experiment by the combination of the presence of high noise components and the non-stationary character of that noise. In theory, the transient test will yield the same reactor information as will the rod oscillator test. Unfortunately, however, the reactor information in a transient test is squeezed into the comparatively short time duration of the reactor transient. This short time interval is not sufficiently long to accurately obtain the reactor characteristics from the test data. Therefore, in reality, the transient test does not provide the same stability information as does the rod oscillator test. In the case of the VBWR, the worth of the transient tests fell pitifully short of the comprehensive stability measurement provided by the rod oscillator tests.

TABLE VII-12

QUANTATATIVE ROD OSCILLATOR TEST RESULTS
ALL TESTS ANALYZED WERE CONDUCTED AT 15 MWt

TEST NUMBER	RECIRCULATION FLOW	COMMENTS	① CALCULATED AVERAGE CORE VOIDS	② ROD WORTH	③ POWER REACTIVITY FEEDBACK GAIN	④ VOID COEFFICIENT OF REACTIVITY	⑤ GAIN MARGIN	⑥ PEAK-TO-PEAK FLUX NOISE
			$\overline{R}_g$	———	$\frac{\Delta K}{\beta}$ fb/N*	$\frac{\Delta K}{\beta} / \frac{\overline{R}^*}{g}$	———	———
	gpm		%	cents/inch	cents/ %	cents/ %	Factor	%
15-18	- - -	Natural Circulation	- - -	9.95	4.35	- - -	- - -	- - -
15-16	4,000	Forced Circulation, Baffle Doors Open,	- - -	9.13	3.33	- - -	- - -	- - -
15-9	4,000	Forced Circulation, High Pump Head, Valve-Controlled Flow	0.2	11.1	3.64	4.35	4.12	6.0
15-19	4,000	Forced Circulation, Low Pump Head, Speed-Controlled Flow	0.2	10.9	4.0	5.09	- - -	- - -
15-1	20,000	Forced Circulation Maximum Flow	0.08	14.7	2.17	1.78	9.44	15.0

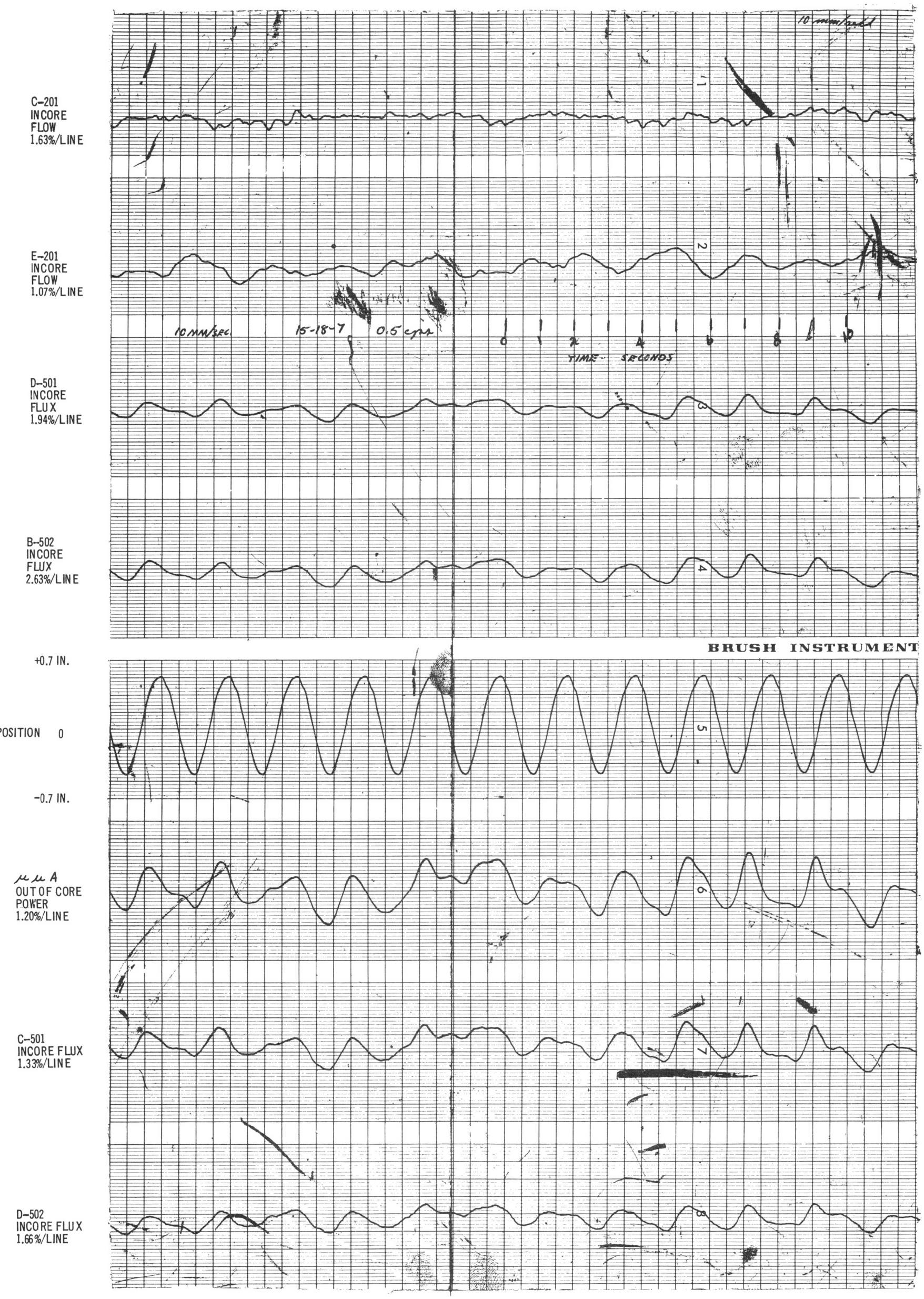

141

NATURAL CIRCULATION ROD OSCILLATOR TEST
RUN 15–18–7 0.5 cps RECORD DATA TRACE

FIG. VII-35

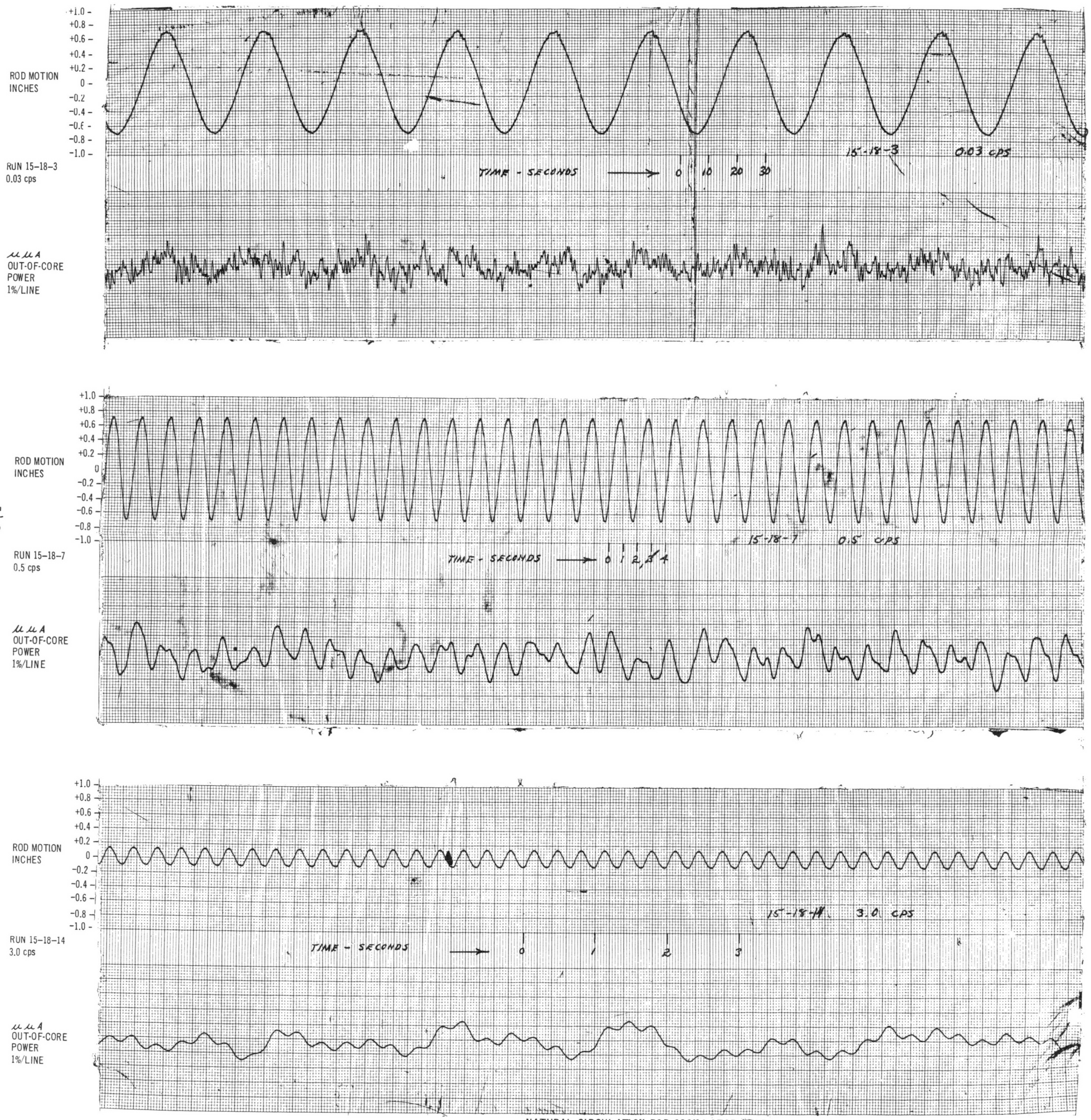

FIG. VII-36 NATURAL CIRCULATION ROD OSCILLATOR TEST
15 MWt CONTROL DATA TRACE

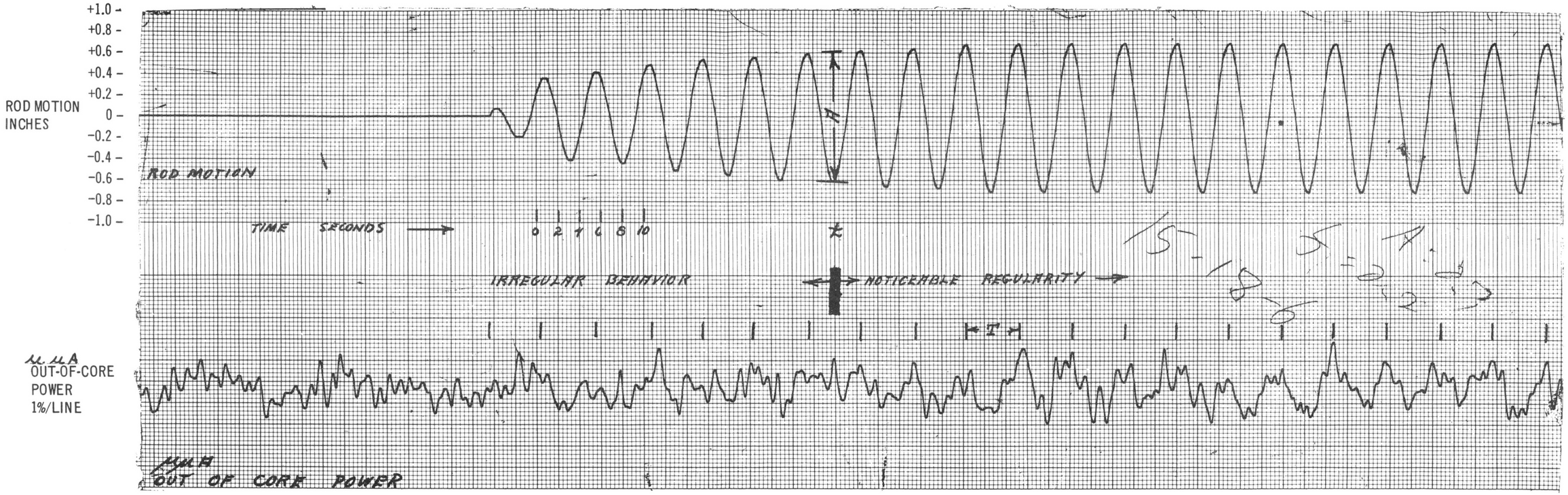

FIG. VII-37 NATURAL CIRCULATION ROD OSCILLATOR TEST
RUN 15–18–6 0.2 cps CONTROL DATA TRACE

FIG. VII-38 BAND PASS ANALYSIS OF NATURAL CIRCULATION ROD OSCILLATOR
TEST RUN 15–18–4 0.05 cps

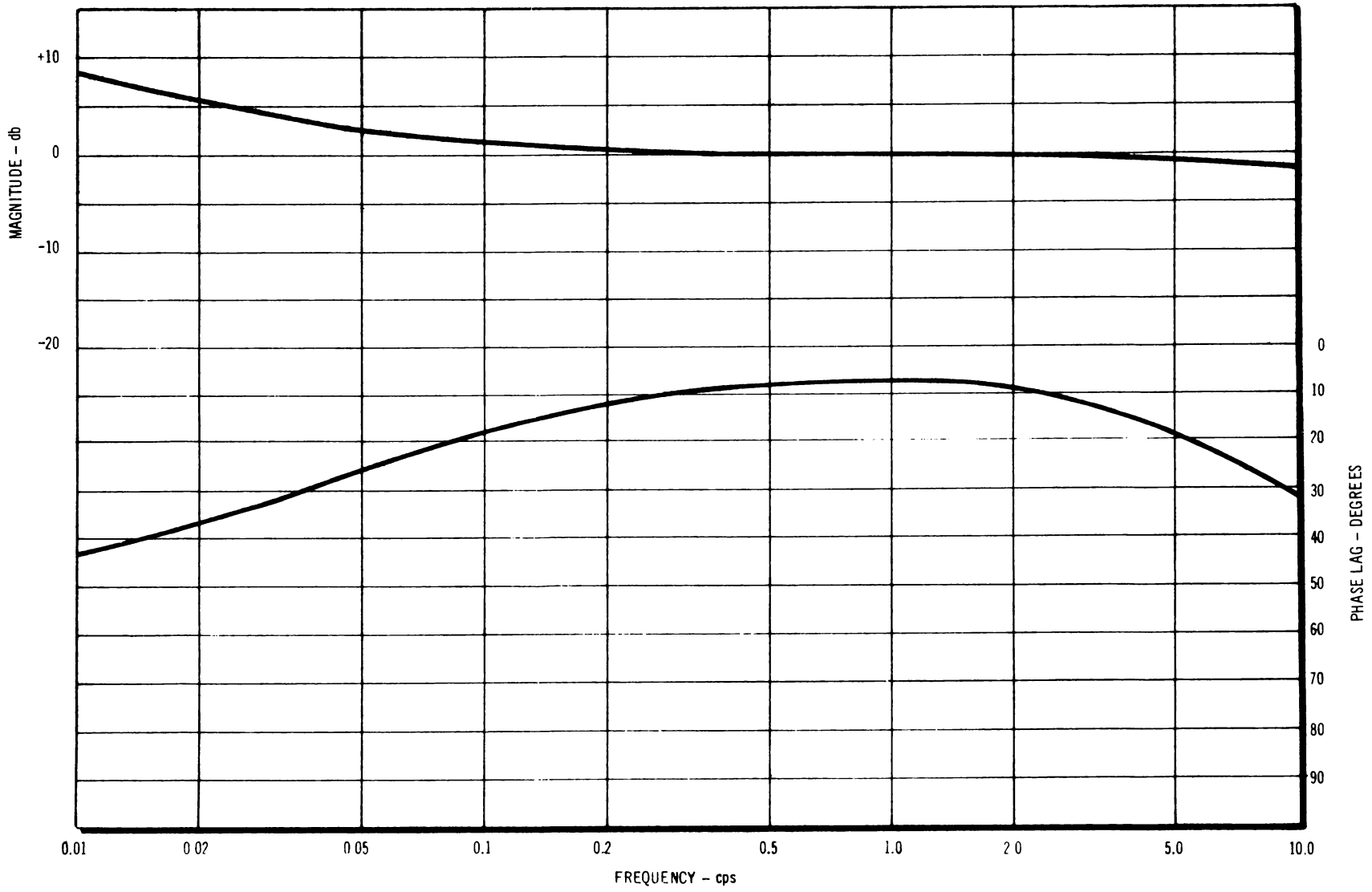

FIG. VII-40 ZERO POWER REACTOR KINETICS FUNCTION - R(S)

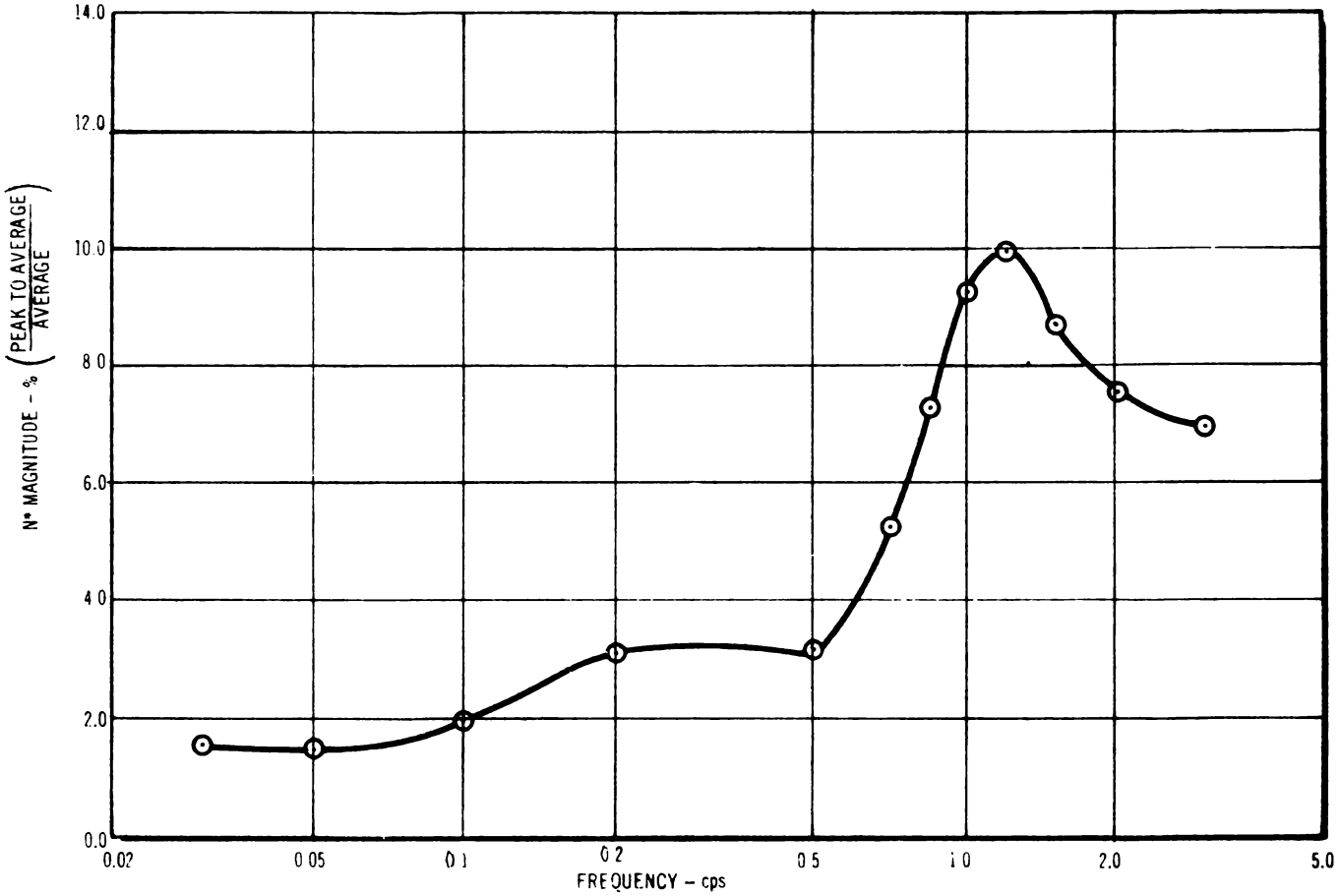

ROD STROKE ± 0.7 INCH

FIG. VII-43 ROD OSCILLATOR RESPONSE FOR NATURAL CIRCULATION TEST SERIES (15-18)

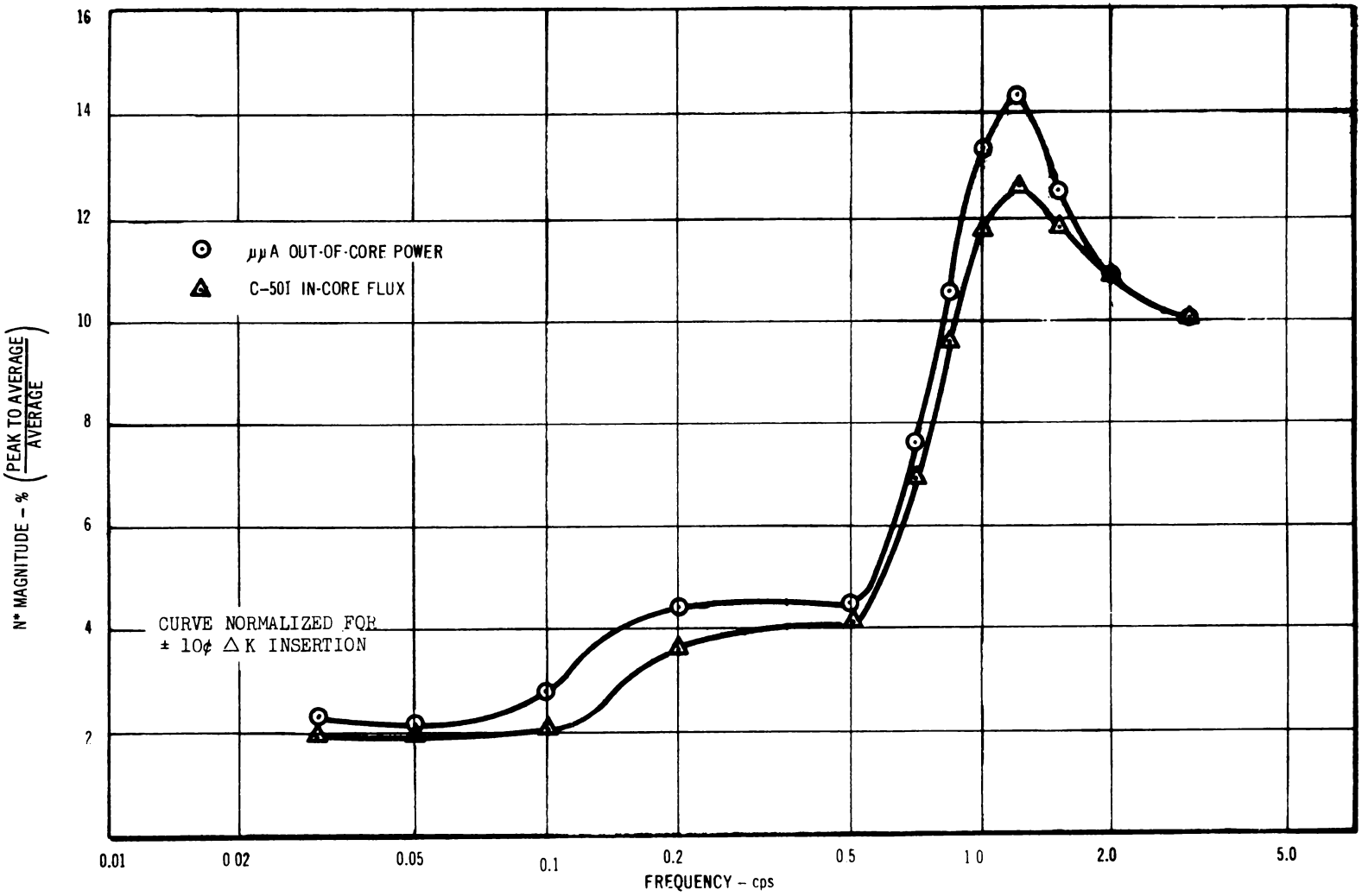

FIG. VII-44 NORMALIZED ROD OSCILLATOR RESPONSE CURVE FOR NATURAL CIRCULATION TEST SERIES (15–18) 15 MWt

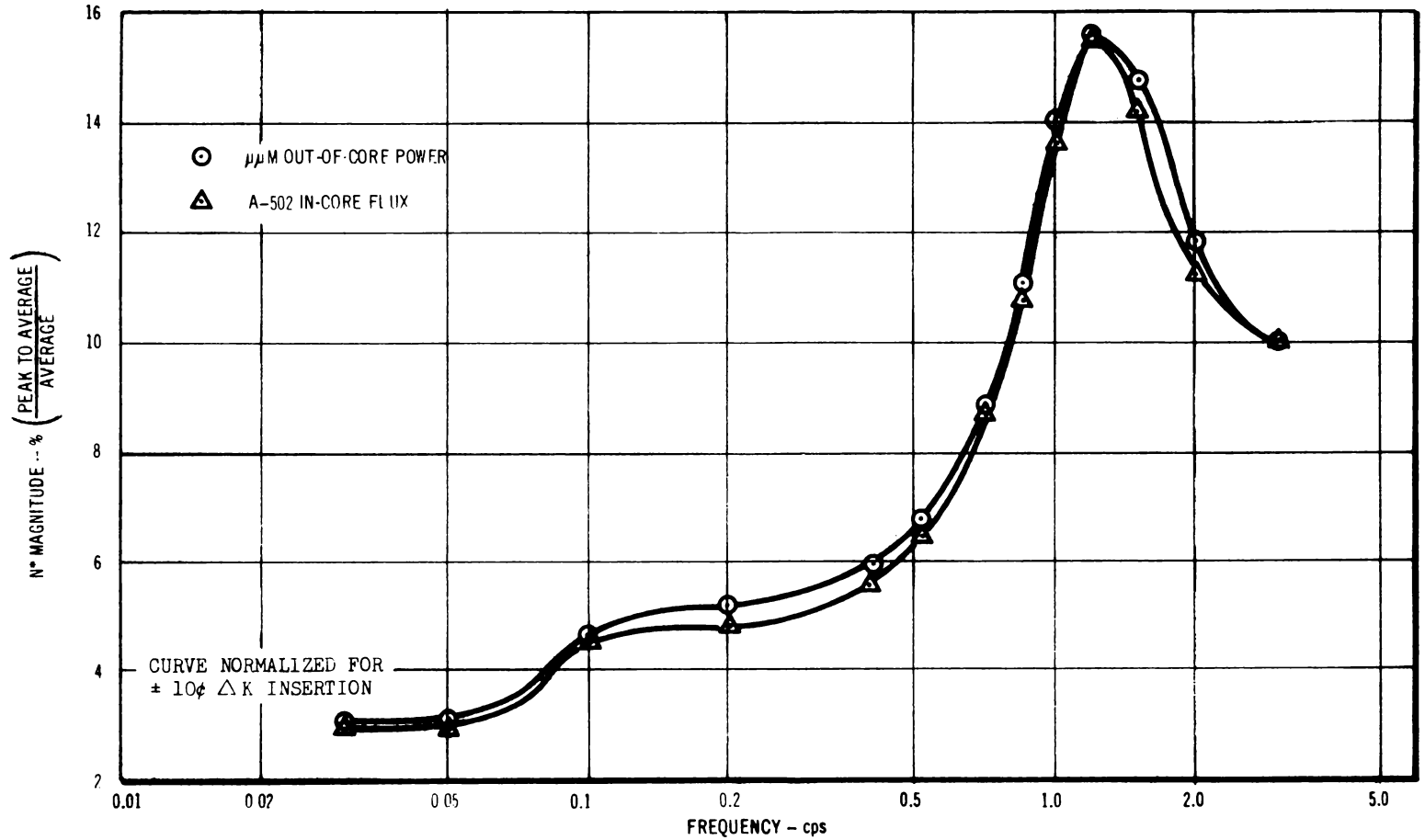

FIG. VII-45 NORMALIZED ROD OSCILLATOR RESPONSE CURVE FOR FORCED CIRCULATION BAFFLE DOORS OPEN TEST SERIES (15–16) 15 MWt

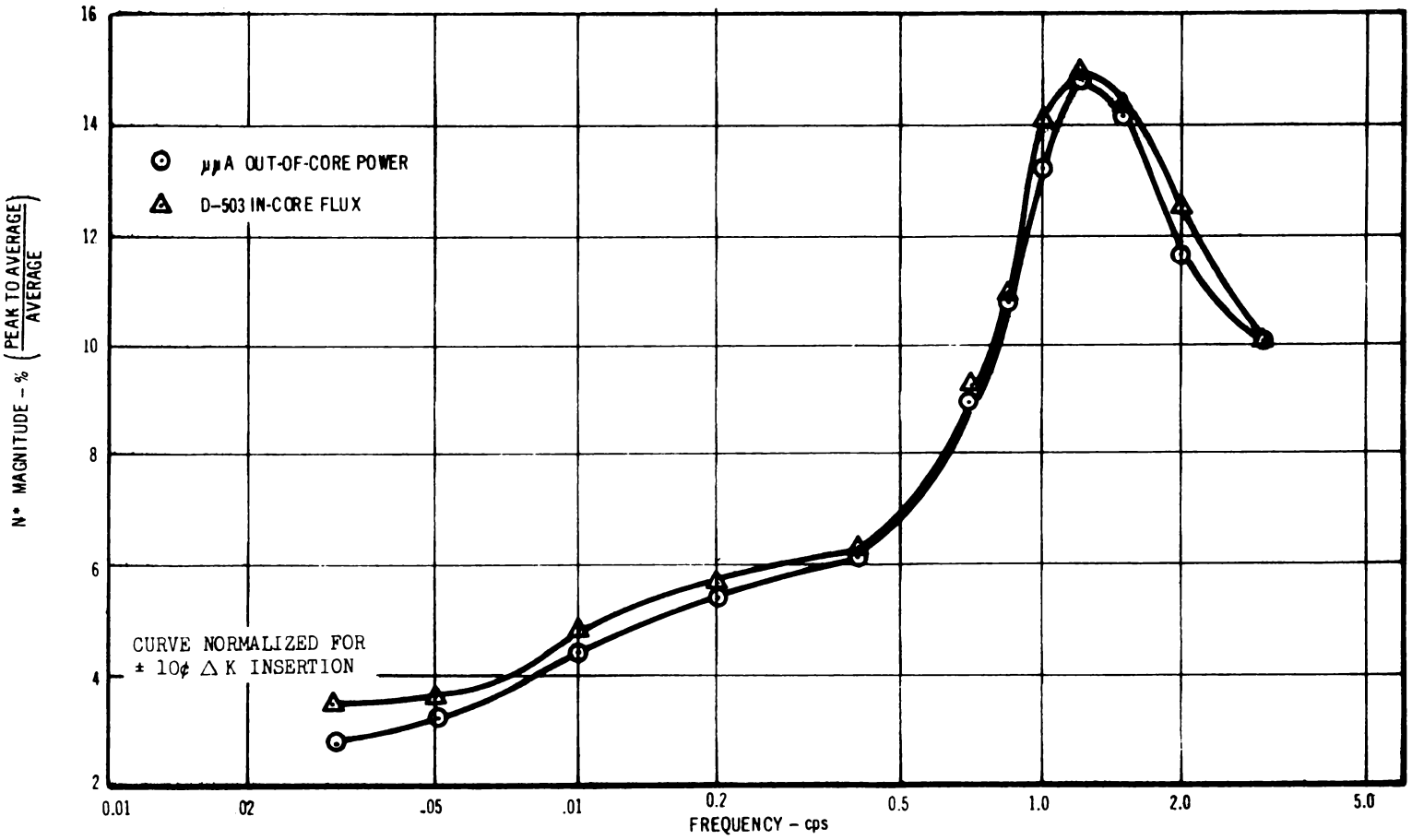

FIG. VII-46 NORMALIZED ROD OSCILLATOR RESPONSE CURVE FOR VALVE-CONTROLLED FORCED CIRCULATION 4,000 gpm TEST SERIES (15-9) 15 MWt

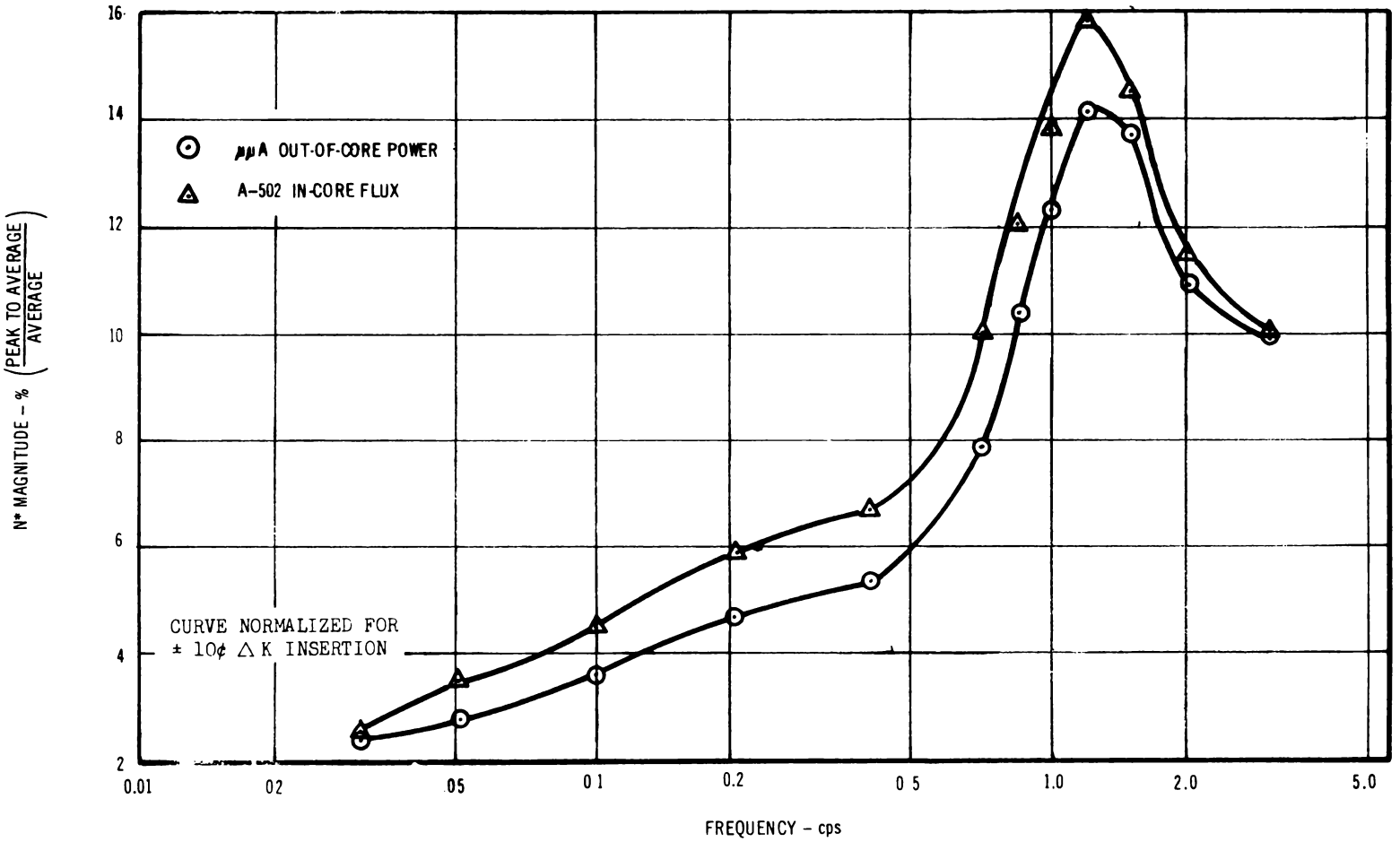

FIG. VII-47 NORMALIZED ROD OSCILLATOR RESPONSE CURVE FOR THE SPEED CONTROLLED 4,000 gpm TEST SERIES (15–19) 15 MWt

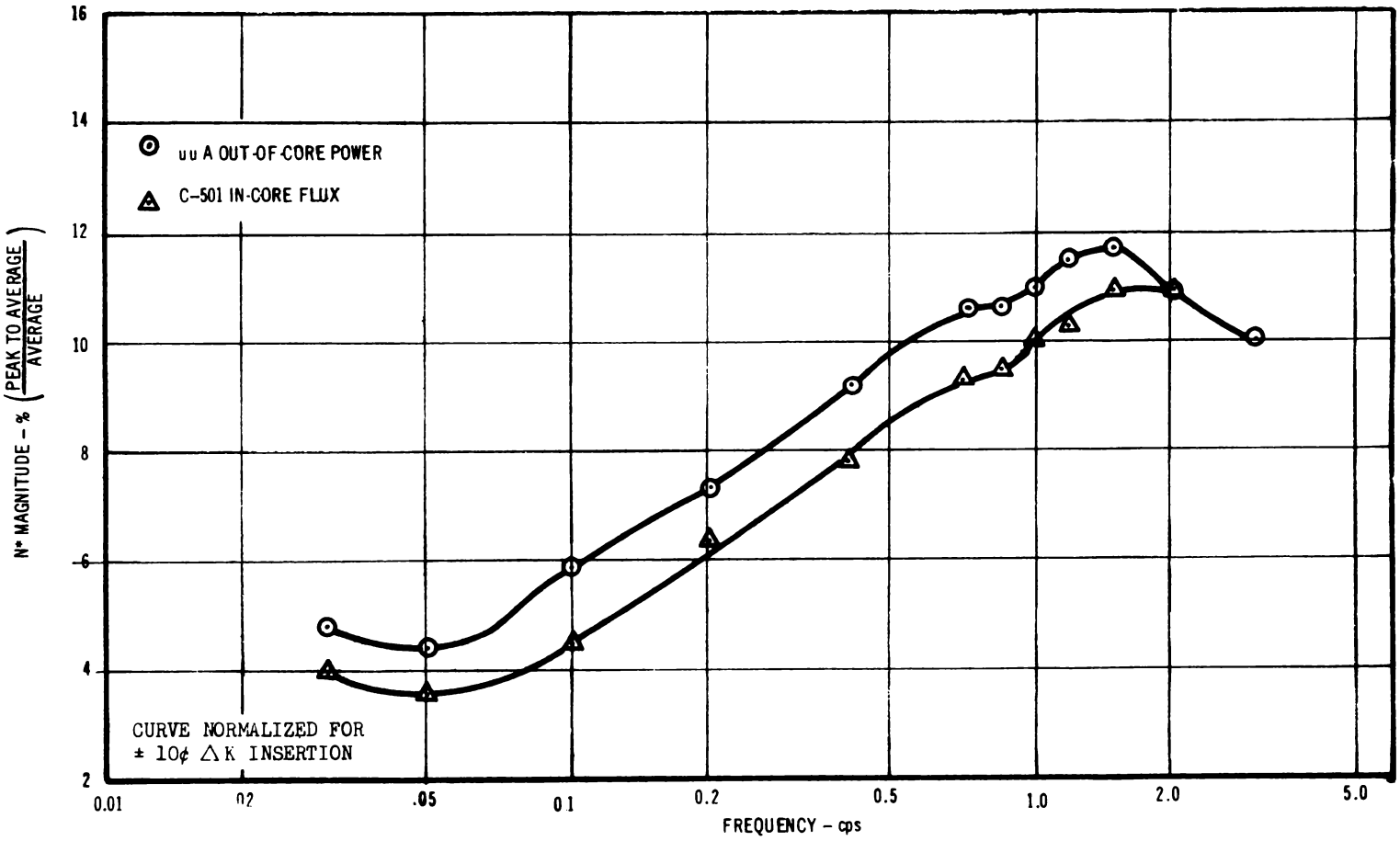

FIG. VII-48 NORMALIZED ROD OSCILLATOR RESPONSE CURVE FOR THE 20,000 gpm FORCED CIRCULATION TEST SERIES (15-1) 15 MWt

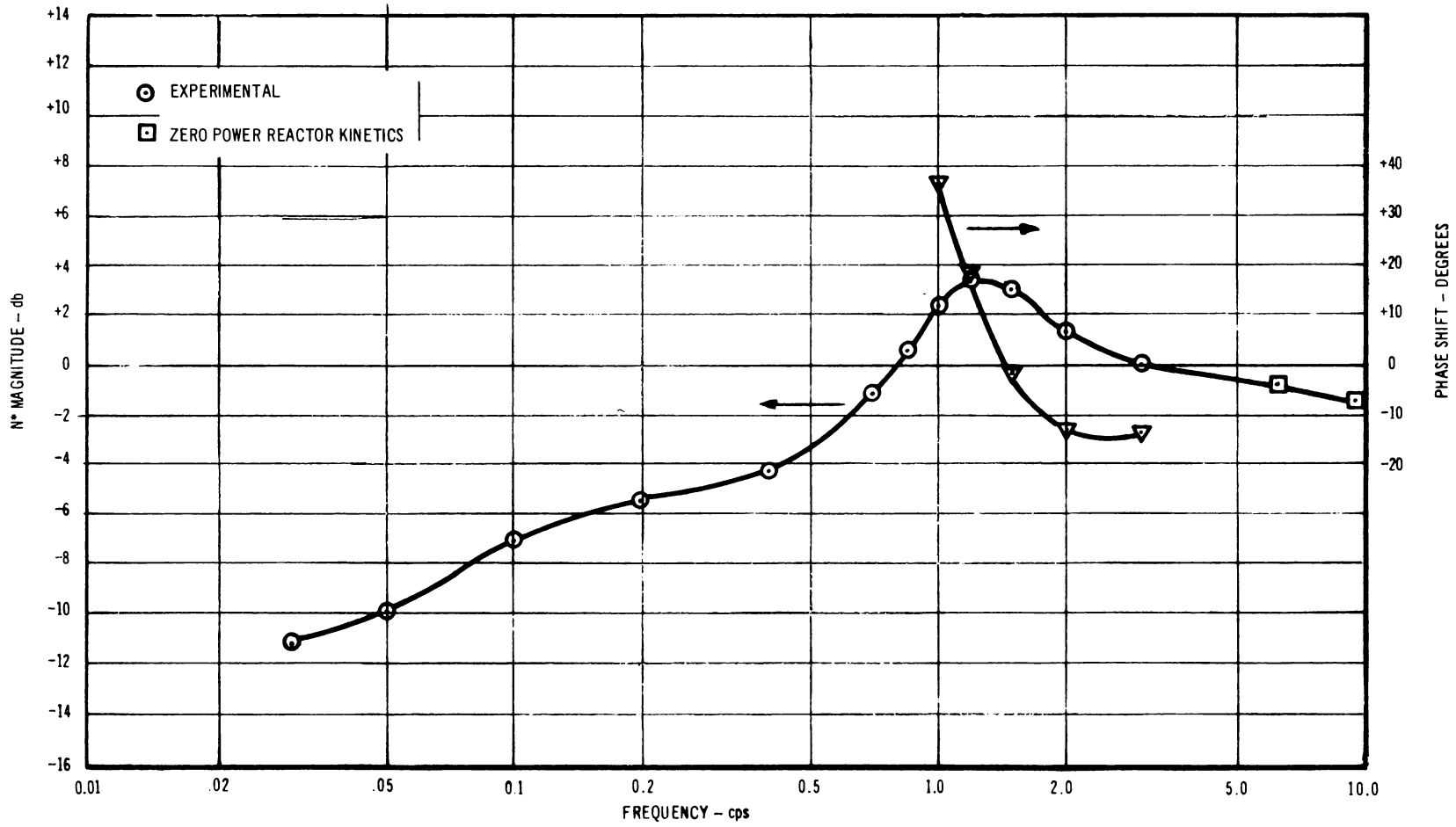

FIG. VII-49 POWER TRANSFER FUNCTION OF TEST SERIES (15-9)

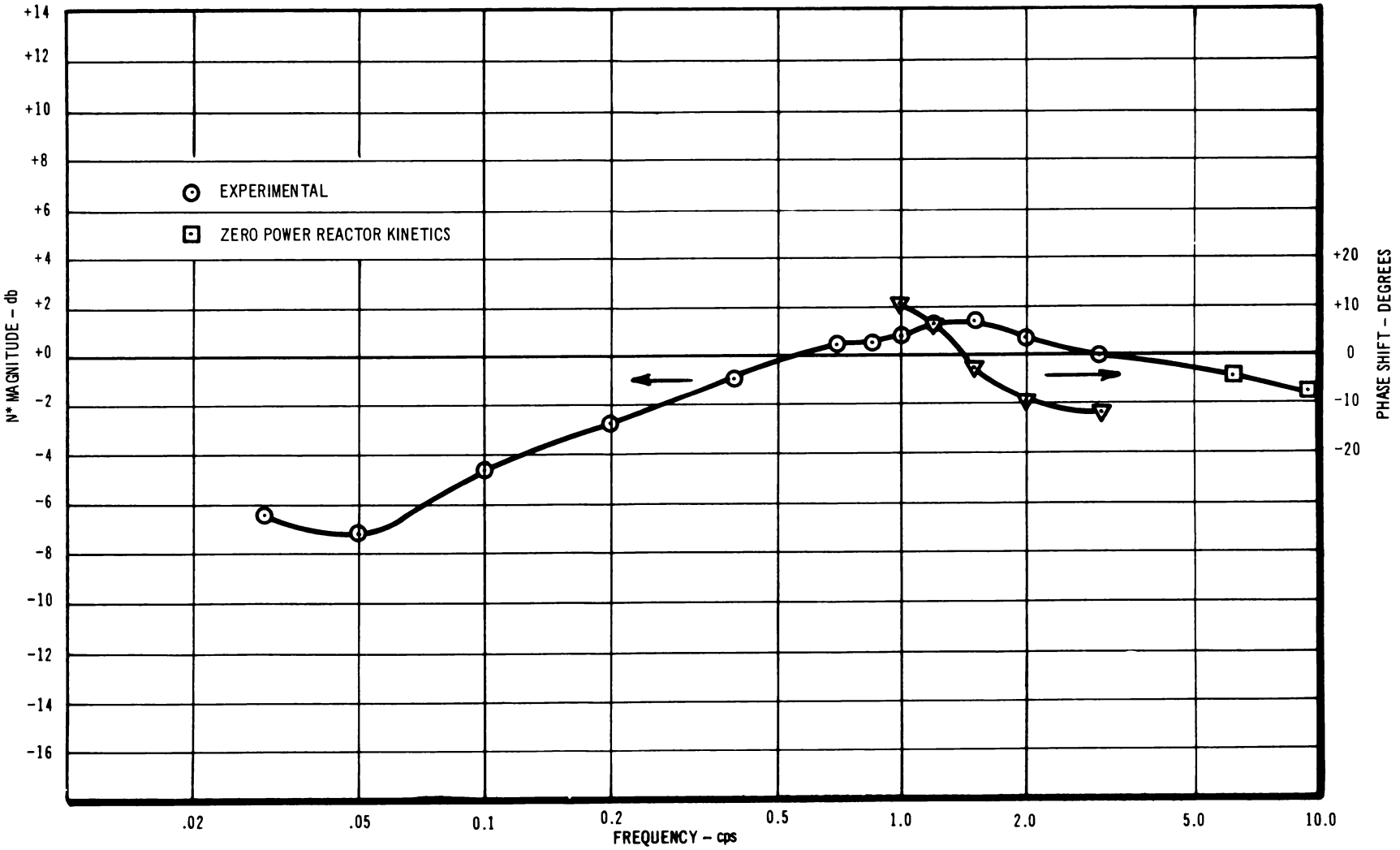

FIGURE VII–50 POWER TRANSFER FUNCTIONS OF TEST SERIES (15–1)

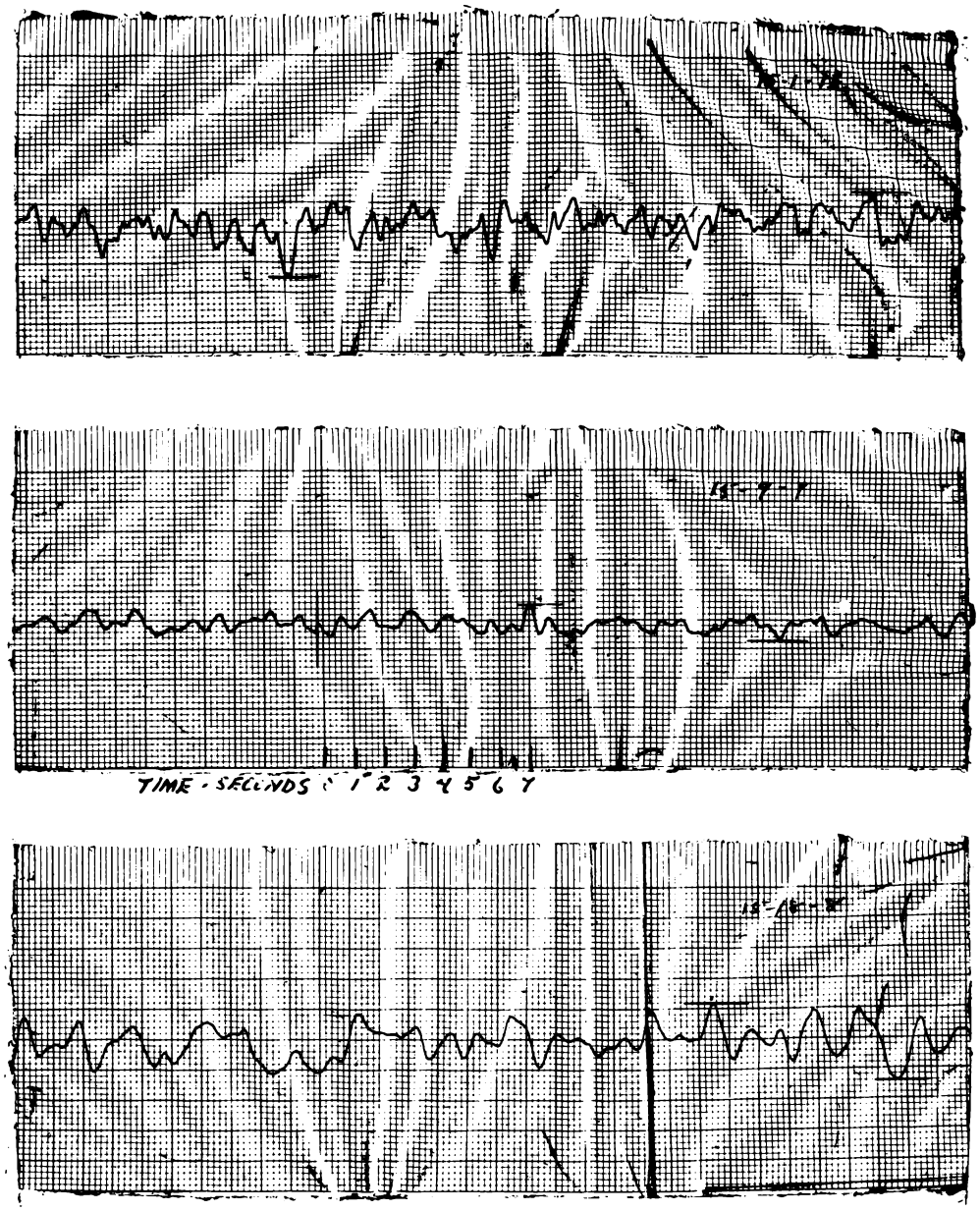

NOISE COMPARISON
20,000 gpm, 4,000 gpm AND NATURAL
CIRCULATION CONDITION CONTROL DATA TRACE

FIG. VII-51

SECTION VII-C

CONSIDERATION OF NOISE PHENOMENA

The presence of noise in fluxes and flows consistently had to be considered in the test results, both for steady-state and rod oscillation responses. It is not clear what their influence is upon the steady-state results obtained; however, methods of getting around the noise problems have been demonstrated in the consideration of rod oscillation test results, so far as flux responses are concerned. Any understanding of the way in which noise phenomena occur will be of value because:

a. Test result interpretation may be able to be improved for steady-state and rod oscillation.

b. Its use as a design, too, in reducing the effects of noise and improving operational stability characteristics.

c. Some improvements in system absolute stability may be realized.

VBWR test observations are interpreted here in terms of known response characteristics common to system analysis. The ideas are, in fact, common to the basic analysis of the system. The ideas presented are only of value as ideas which require further investigation. This is true, even though they do demonstrate in a unified model most of the characteristics observed and recognized from the tests. The reason is that in-pile tests are not well enough understood to confirm the ideas in a definite manner. Further work in out-of-pile tests and in reactors are required.

The following discussion will present basically an extension of the pre-test analysis theory. The extension is accomplished by recognizing the time variation characteristics of the model, whereas, previously, the results had been looked at only from its frequency response character.

ITEMIZED OBSERVATIONS OF NOISE PROPERTIES FROM 15 MWt RUNS

The following observations are conclusions reached from study of time traces and band pass filter output data:

a. The flux noise amplitude, as measured by both the μμA and in-core ion chambers, increases as flow rate increases. In-core flow noise increases in amplitude with increasing flow rate. Both the flux noise and the flow noise amplitude are attenuated sharply by the inlet channel orificing. Recirculation pump noise measurements do not increase with increasing flow.

b. Measured in-core flow noise frequencies increase with increase in flow rate. This is compared with the frequency increase predicted by theory employed in the pre-test analysis of Figure VII-34.

c. Peaks of the steady-state power oscillations do not continue to increase with flow rate increase in correspondence with resonant frequency. Dominant frequencies of test data lie in the interval .7 to 1.0 cps.

d. When spectra obtained from band pass filtering of time traces are examined, a high frequency noise appears above the boiling boundary on all in-core ion chamber measurements but the well-orificed channel. The amplitude of the high frequency component is greater in magnitude at the upper ion chambers than in the lower chambers. This is demonstrated by Figure VII-26.

e. The μμA measurements do not record the high frequency noise.

f. No phase relationships are seen in steady-state traces between inlet flow and in-core ion chambers. The 0.7 to 1.0 cps component of the μμA and ion chambers described in (c) above are always in phase.

g. Spectrum analysis shows a low frequency (.1 to .2 cps) peak in both in-core flow and flux for the natural circulation run. In addition, there is a peak in the .5 to .7 cps range. There is a definite difference in the character of this natural circulation trace from the forced circulation runs of similar flow.

RELATIONSHIP OF STEADY-STATE FLUX NOISE TO ROD OSCILLATOR MEASUREMENTS

a. The reactor response to rod oscillation is closely approximated by the theoretical predictions of the pre-test analysis. The correlation shows progressively larger disparity at higher flows with regard to frequency.

This correlation provides confidence in the ability of the present analytical model to describe the response of the VBWR system to a known disturbance; i.e., the theory and principles of system response which are employed in the analytical model used in the pre-test analysis appear to be applicable.

b. The apparent difference between the steady-state flux noise spectrum and the rod oscillator spectrum is attributable to the type of system disturbances. In the case of the steady-state spectrum, the reactor is disturbed by internal system perturbation(s). In the case of the rod oscillator spectrum, the reactor is disturbed by a known externally driven perturbation, in addition to internal perterbation(s).

c. Although the steady-state flux noise spectra do not bear any obvious similarities with the measured rod oscillator spectra, the same physical principles must be present in both situations to determine the system response. Therefore, any attempt to realistically predict the steady-state noise must include the basic theoretical principles which have already been verified by the rod oscillator tests.

d. There remains, then, the question of identifying the source(s) of flux noise excitations.

MEASUREMENTS OF POSSIBLE FLUX NOISE EXCITATIONS

a. Three possible broad categories of flux noise excitations are:
   1. Control rod vibrations
   2. Delayed neutron statistical behavior
   3. Changes in the moderator density.

b. It is believed that the absence of sharp "spikes" in the flux noise measurements indicate that control rod-excited noise does not exist.

c. Since the dominant frequencies of the flux noise are out of the range of delayed neutron statistics, this source of noise is also discounted.

d. Changes in the moderator density are considered to be the most likely source of flux noise. Moderator density changes can be effected in the following ways:

1. Temperature fluctuations in the inlet coolant flow

2. Core ΔP fluctuations affecting flow

3. Channel inlet flow fluctuations.

Of the three above possible sources of moderator perturbation, the only measurements made, which are entirely an excitation in nature, are the inlet flow oscillation.

A PROPAGATION OF DISTURBANCE THEORY FOR NOISE RESPONSES OF A BOILING WATER REACTOR

The nature of the propagation of disturbance theory is described in items (a) through (d) below.

a. When an electronic filter receives a constant amplitude periodic signal suddenly, there are two responses to the signal. First, a transient response which is a function of the characteristics of the filter and the input signal. Given sufficient time, the transient signal dies out and gives place to a steady-state response. Transient indicates a non-sinusoidal time varying response. Here, the expression steady-state denotes the response to a pure sinusoidal oscillation. Responses which are not varying in time are considered to be equilibrium. The transient, or first, type of response is the type characterized by this theory. The second, or steady-state type, is the response characterized by the pre-test frequency response method of solution.

b. In the BWR, perturbations with time dependent character, such as flow, temperature, etc., may be added to the system. A specific example is the inlet flow oscillations measured in the VBWR. These disturbances are propagated up the channel, changing conditions locally as they traverse. The nature of this response has been observed by Wallis and Heasley.[10] They found that the response of a heater section to disturbances in flow rate was rapid compared to the period of loop oscillation. This period is the resonant frequency as defined by steady-state analysis above.

Storrer[11] and Wallis and Heasley have advanced theories for this type of response.

c. The disturbance produces two characteristic time responses in a BWR.

1. Propagation through the core channel produces a disturbance or transient which immediately effects the core. The characteristic time for these disturbances is related to the residence, or transit time, in the core.

2. Subsequent propagation of the disturbance through the two-phase system produces two effects:

a. A transient time response of the two-phase system which is characterized by the entire two-phase system transit time.

b. A steady-state response (as defined above) which also is characterized by the entire two-phase transit time. The resonant frequency of this response is the one calculated from the model by frequency response techniques.

Additionally, two feedback loops, one in the fluid dynamics, and one including reactivity, may be set up using the responses above. These are discussed in the summary which follows.

d. The response can now be related to the reactor performance. If a disturbance occurs in the reactor core, there will be a transient or local effect dominated by the core characteristics, and there will be another effect dominated by the reactor two-phase system dynamics. Solution of system equations in the frequency domain yields the steady-state or systematic response. The local transient response is not included in these solutions. The nature of the transient response is determined by the character of the disturbances or excitation forces together with the system dynamics. A solution for the response of the system to a known non-periodic excitation would require a solution of the model equations as a function of time. It should be emphasized that the transient response will be different in frequency and amplitude for each type of excitation.

The solution obtained by the frequency analysis method would be a valid

solution under the following restrictive conditions. If the excitation forces can be considered as the summation of periodic forces, and the model equations are linear so that solution by superposition is possible, then the reactor response can be resolves as the sum of "steady-state" solutions of various frequencies. The accuracy of the solution will depend on the degree of fulfillment of the assumptions regarding the periodicity of the exciting forces and the linearity of the model equations. In general, these conditions are not satisfied and the response would have to consist of transient and "steady-state" components.

VBWR DATA COMPARED TO THEORY

The observed characteristics of VBWR steady-state noise data are described rather completely in items (a) through (e) in terms of the band widths of the observed data, the amplitude characteristics of noise and its spatial and phase relationships. The observed data points and the output of the band pass filter are the basis for this comparison.

a. Variation of Frequencies with Flow

Figure VII-52 shows the comparison of all available observed data and theoretically derived frequencies as a function of flow rate. Curves A through F as noted are the theoretical curves determined from pre-test analysis. The points are all the available peak frequency points obtained from spectral analysis. In several instances, there are multiple high frequency peaks which are also plotted.

Consider first the data between .4 and 2.0 cps, and curves A - D. Curves A, B are the theoretical resonant frequency curves, and C, D are the theoretical two-phase transit time. Peak frequencies of flow oscillation are seen to lie in the lower range (.4 to .8 cps) with forced circulation and natural circulation having an indicated different frequency response, based on the points available. External ion chamber data lie in the frequency range .75 to 1.0 cps, and show again, a difference in response between forced and natural circulation (as well as for forced circulation, baffles open, which is theoretically like natural circulation). It is worth noting that the high flow frequencies for both flow and ion chamber

are nearly the same. As was previously discussed in the flow dynamics section above, Curves A to D will not show as high frequencies at the high flow end when nuclear feedback and multi-node representation of the two-phase region are included in the theory. The above results constitute the "steady-state" comparison of data to the disturbance propagation theory, plus any transient responses which are characterized by the two-phase transit time.

Curves E and F are the frequencies derived from the theoretical core transit times for an unorificed channel (orificed approximately half this frequency). These curves have a relationship to the transient response for disturbances which effect the system response in transit across the entire core length. Disturbances which are effective over only part of the core would have a shorter transit time and the frequency would be higher. Data points for high frequency ion chamber signals are indicated by the superscripts in Figure VII-52. High frequencies occur above the boiling boundary. Frequency peaks occur from 2 to 20 cps for runs in the 2,600 to 4,400 gpm range. C channel data are discussed in (d) below. These data show a spread of responses which indicate a spectrum of possible effects from whole core, partial core length, and other effects, including the possibility of harmonics and 60-cycle response for this data. Further study and hydraulic loop tests will be required for further understanding.

b. Noise Amplitude Variation with Flow

VBWR noise amplitudes (e.g., Figure VII-29 for flow) increase with increasing flow rate. This characteristic can be shown by an approximation theory developed by Wallis and Heasley for the derivation of responses to flow disturbances. The model used is similar to the pre-test analysis, except that they have solves the equations in time. The pre-test analysis theory can do the same if solved in time and for multiple spatial nodes. This approximation theory, however, deals only with inlet flow perturbations. These relations are based on describing the boiling boundary, equations of motion, energy and continuity, and solving these in time. A perturbation in flow is then introduced and relations derived for the response in flow ΔV, density $\Delta \rho$, and pressure drop ΔF at any local

point as a result of inlet flow perturbations. These relations, derived in Appendix D, are as follows:

1. Flow $$\Delta V = \left[-\frac{\alpha}{s}\left(1 - e^{-st_b}\right) + 1 \right] \epsilon e^{st}$$

2. Density $$\Delta P = \frac{\alpha P}{V_o e^{\alpha t_{tr}}} \left[\frac{1 - e^{-st_b}}{s} + \frac{e^{-st_b}\left(1 - e^{(\alpha - s)t_{tr}}\right)}{s - \alpha} \right] \epsilon e^{st}$$

3. Pressure Loss $$\Delta F = \frac{F}{V_o e^{\alpha t_{tr}}} \left[\frac{\alpha e^{-st_b}\left(1 - e^{(\alpha - s)t_{tr}}\right)}{s - \alpha} - \frac{\alpha}{s}\left(1 - e^{-st_b}\right) + 2 \right] \epsilon e^{st}$$

A relation is also derived to give the dynamics of the boiling boundary (note that these are derived for the heated channel only).

Where:

ΔV = Flow perturbation anywhere in the channel as a result of the inlet flow perturbation

ΔP = The corresponding density perturbation at any local point in the channel.

ΔF = The corresponding local pressure loss computed for the exit of the channel.

α = $\dfrac{P_h \oint V_{fg}}{A_h \, h_{fg}}$

P_h = Heated perimeter channel

$\oint$ = Heat flux

V_{fg} = Specific volume of vaporization

A_h = Flow area of channel

h_{fg} = Heat of vaporation

s = Perturbation exponent

ϵe^{st} = Velocity perturbation

V_o = Initial velocity

t_b = Time to remove subcooling from liquid

t_{tr} = Transit time of evaporating liquid

T_{tr} = Transit time across heated channel.

The transient flux response of the reactor must be a function of the changes in velocity, density and pressure drop. Each of these is seen, from the equations, to be proportional to the amplitude of oscillation of flow, ϵe^{st}.

c. Increases in Amplitude of High Frequency Flux Noise with Elevation in Core

The above equations have been examined for amplitude of disturbances for 15 MW, 20,000 gpm conditions. Since the power response is proportional to the density perturbation in the channel, the theory predicts the increasing amplitude of flux oscillation with height in the core. Figure VII-53 shows a plot of versus distance above boiling boundary. Again, it should be pointed out that this is for the case of inlet flow perturbation, and not the more general case.

d. Effect of Orificing on High Frequency Noise

Data of VBWR shows that when a channel at the outside was orificed, the high frequency oscillations disappeared. It is logical to consider orificing as the cause of the disappearance of the high frequency content. By examining equations for ΔV, $\Delta \rho$, + ΔF, above, it can be seen that the response is proportional to the initial flow perturbations. Data shows (Figure VII-29) that orificing of the channels in question reduced the flow perturbations by a factor of 2. This substantially reduces the amplitude of the propagated disturbance. In addition, frequencies derived from core transit time are below 3.5 cps so that any signal from this source would be masked in the high frequency side of the single peak that is shown by measurement. Points C-2 and C-3 of Figure VII-52 show this.

Point C-2 at 4,000 gpm is a small amplitude peak which may indicate the presence of a perturbation occurring in a very slightly damped condition of the orificed channel.

e. No Phase Relationships are Seen Between Flows and Fluxes

The in-core fluxes average the neutron flux of a core region and not of an individual channel. Therefore, only under the conditions that all channels in a region are disturbed in flow simultaneously, and the disturbance propagation velocities are the same, will the flows and fluxes have any definite phase relationship derived from propagation of disturbances. In general, both of these conditions will not simultaneously exist. If all the channels in a region were perturbed in velocity, the flux response could be an average of the channels in one region and some relationship might be observable. Perturbation of individual channel velocities would lead to flux responses which are statistically related. The disturbance propagation theory does not deal with the statistical response effects, but it appears that the combination of effects would agree with what has been observed.

SUMMARY OF INTERPRETATION OF NOISE BY THE PROPAGATION OF DISTURBANCES

The disturbance propagation, as described in the theory presented here, demonstrates the type of characteristic observed in VBWR noise data. The degree to which it is demonstrated has not been conclusively shown. It is significant that similar phenomena to that observed in the VBWR are observed in the Dresden Reactor and in the Consumers Power Company Reactor. One may conclude that the observed phenomena are real and, apparently, consistent in character.

The specific comparison of VBWR data with the approximation theory shows:

a. A similar type of variation of frequencies with flow.

b. A similar noise amplitude variation with flow.

c. An increase in amplitude of high frequency flux noise with elevation in the core is shown by both.

d. The character of high frequency noise responses when orificing is applied can be explained.

e. The fact that no phase relationships are seen between flows and fluxes can be explained.

Subsequent work in the hydraulic stability loop facility at APED[12] has shown that a higher frequency (10 - 20 cps) oscillation in pressure drop across the channel occurs. This is believed to be due to the two-phase flow mechanism inducing a variable exit pressure loss due to the change in pressure drop with changes in flow composition (steam and water). This pressure drop oscillation, in turn, causes the necessary feedback to excite a flow oscillation in the channel. In the case of the loop, this would induce transient void responses and transient two-phase pressure drop responses. The system characteristics would determine equilibrium and frequencies of response.

A similar situation should exist in the reactor channels, and with the additional feedback of the reactivity disturbance induced by the void disturbance, the noise produced in the reactor channel could be explained, based upon the feedback loops discussed here.

On the basis of the above, the methods of reducing the noisy oscillatory character of a reactor such as VBWR can be shown by phenomena observed to be:

a. Increasing the inertia of the loop

b. Minimizing the exit losses of the heated channels, and riser of the system

c. Orificing of the channel inlets for the reactor channel.

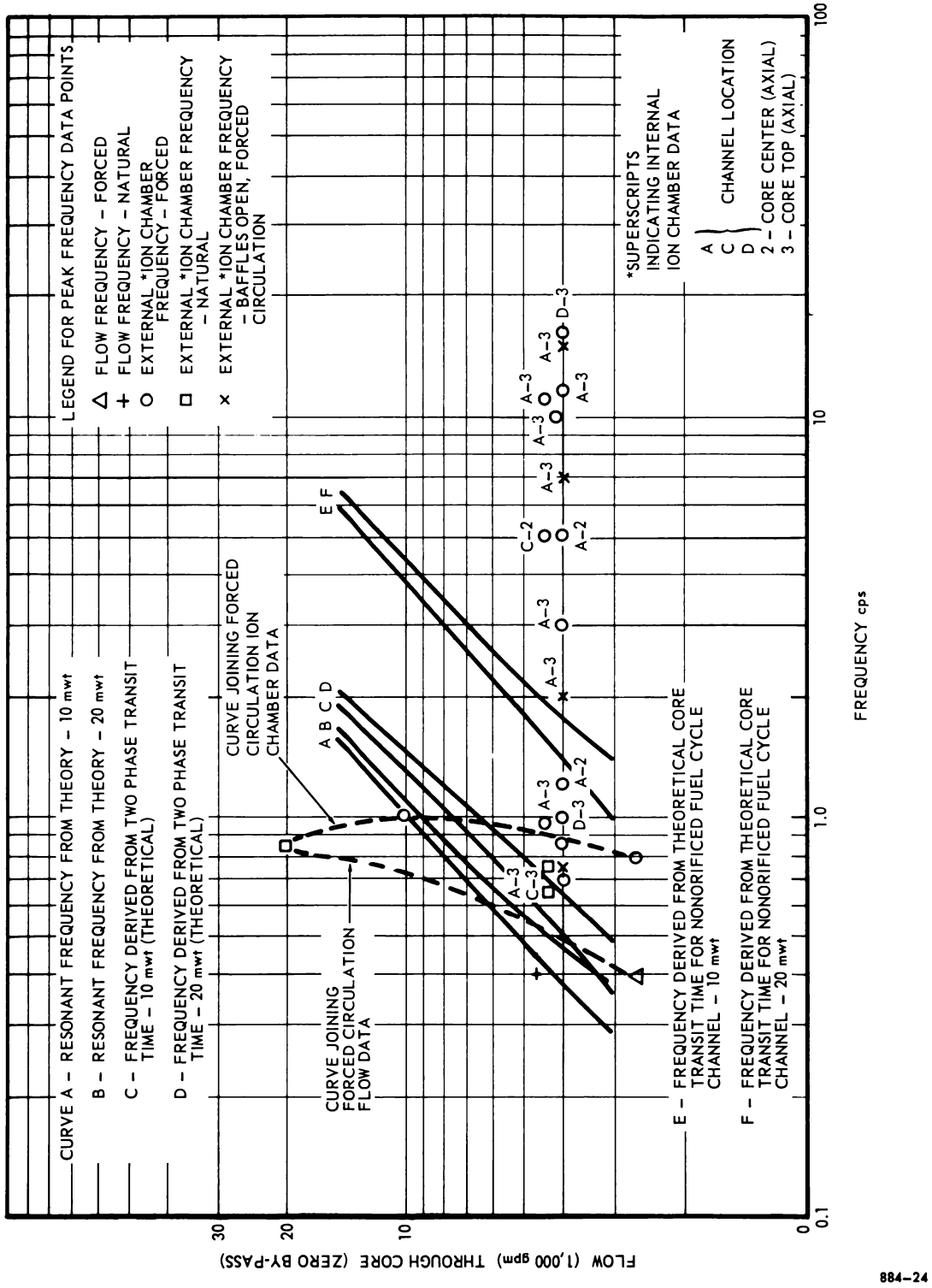

FIG. VII-52 COMPARISON OF THEORETICAL TRANSIT TIMES WITH EXPERIMENTAL POINTS FOR VBWR AT 15 MWt

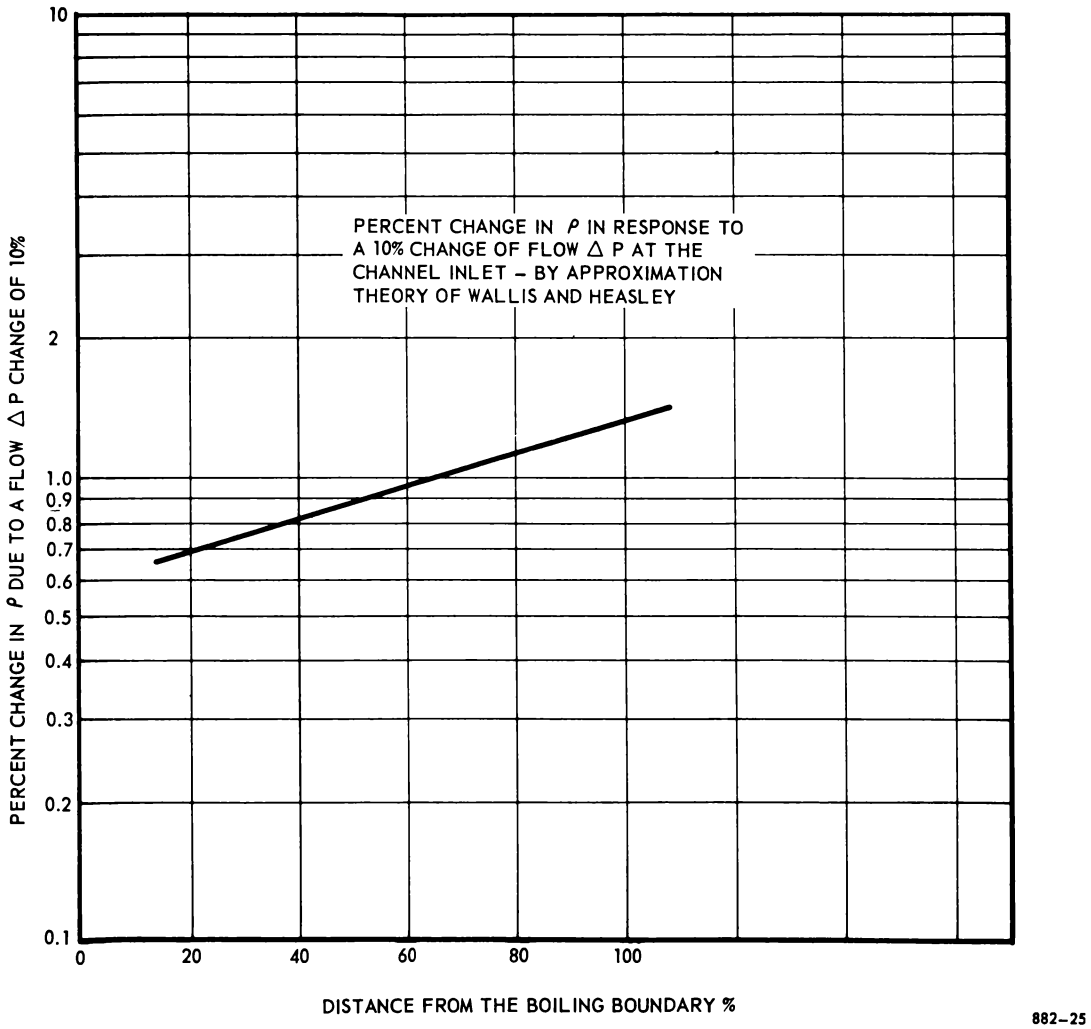

FIG. VII-53 DENSITY CHANGE RESPONSE TO CHANNEL ΔP CHANGE

SECTION VII-D

TRANSIENT TESTS

Test Description and Test Parameters

There were four types of transient tests conducted:

a. Recirculation flow

b. Feedwater flow

c. Steam flow

d. Control rod position

A summary of transient tests of type (a), (b), (c) are given in Table VII-13. The control rod transient tests are not listed separately, but are part of every rod oscillator test. These oscillator tests are summarized in Table VII-13.

The transient tests were conducted within the limitations of the safeguards restrictions. These restrictions are derived from pre-operational analyses which are usually conservative. The actual degree of conservation is manifested by the extreme stability of the recorded experimental responses to transients which pretest safeguards analyses indicated would yield appreciable, but safe, responses.

The weak response of the reactor system is very significant with respect to obtaining reactor information from transient tests. A transient test attemps to achieve with one test what a control rod oscillator arrangement achieves with a great many runs at many frequencies. In order to define the frequency response, a transient recording is required of such precision that the contribution of all frequencies can be extracted from the shape of the trace. In the neighborhood of a resonant frequency, the trace shape of the overshoot, damped oscillation frequency, and rate of decay is sensitive to various frequency responses and some information can be obtained. But, when the system is highly damped, the transient trace is insensitive to changes and little information can be obtained. For further discussion on the usefullness of rod oscillator tests and transient tests, see Reference (13).

TABLE VII-13

TABLE OF TRANSIENTS

TRANSIENT	RUN NO.	DATE	POWER	FLOW TOTAL	FLOW PUMP 1	FLOW PUMP 2
Recirculation Flow	15-3-16	11/25/61	15	10.0	10.0	0
	15-6a-24	12/1/61	15	5.5	0	5.5
	15-6b-18	12/1/61	15	4.2	0	4.2
	15-7-29	12/1/61	15	6.9	0	6.9
	15-8-20	12/3/61	15	5.4	5.4	0
	20-3-19	11/25/61	20	10.0	10.0	0
Feedwater Flow	15-3-14c	11/25/61	15	10.0	10.0	0
	20-3-17c	11/25/61	20	10.0	10.0	0
Steam Flow	15-3-15	11/25/61	15	10.0	10.0	0
	20-3-18	11/25/61	20	10.0	10.0	0
	R-1-59	11/16/61	26	20.0	10.0	10.0

The reactor system was relatively well-damped. This, combined with the safeguards restrictions on the allowable transients, limited the experimental responses to a region where it is doubtful if any significant information could be obtained.

In addition, the experimental steady-state noise was found to be very significant. Thus further confuses the transient analysis to the point where only a rough order of magnitude of the response can be obtained, and, then, only in the vicinity of the resonant frequency.

RESULTS

The responses to feedwater flow rate changes, steam flow changes, and control rod "step" changes (which actually amounted to a medium ramp change) were very small and insensitive. Only changes in recirculation rate provided any appreciable transients. The most "violent" response was to a fast recirculation flow change in which the flow changed about 25% in one second. The trace is shown in Figure VII-54, and the data are given in Table VII-14. See Figure VII-55 for explanation of terms used in Table VII-14. The power jump for the 25% increase in recirculation flow was about 20%.

The table shows the weakness of visual analysis of the data. Observe the variation in peak-to-peak fluctuation from the non-zero-suppressed and zero-suppressed traces. Code calculation of the variation should yield more consistent data. The flow data is partially consistent, but the flux is consistently lower for the zero-suppressed case. This indicates that in the length of trace examined (non-zero-suppressed) no large flux peaks occurred.

Percentage-wise, the changes in the mean values of flow and flux for the transient "step" were only about 1/3 of the recirculation flow change, for both the flow step increase and decrease.

The dominant resonant frequency and the damping coefficient were to be obtained from the transient tests. Both the flow and flux data were to be used. The channel flows did not oscillate enough to clearly define either the resonant frequency or the damping coefficient. The flux traces, however, yielded the resonant frequency and, very indefinitely, the damping coefficient. The damped

resonant frequency was found to range between 1.20 and 1.28 cps. From the pre-test analysis, the damped resonant frequency was calculated to be 1.11 cps. The stability model has, therefore, predicted the resonant frequency to be lower than shown by the experimental data.

The noise distortion of the traces made determination of the damping coefficient difficult and uncertain. Three measurements of the damping coefficient ranged from 0.34 to 0.60. The pre-test analysis gave the damping coefficient as 0.22.

TABLE VII-14

RECIRCULATION FLOW TRANSIENT - RUN 15-8-20

RUN NUMBER 15-8-20 FORCED CIRCULATION, BAFFLES CLOSED

Date: 12/3/61

Power: 15 MW

Total Flow: 5,400 gpm Pump 1 = 5,400 gpm Pump 2 = 0

CHANNEL NUMBER			4	3	1	7	8	6	2
TRANSIENT	IDENTIFICATION		FLOW PUMP 1 RCP-1	FLOW E HIGH POWER E-201	FLOW C ORIFICED MED. POWER C-201	FLUX LOWER C CHAMBER C-501	FLUX MIDDLE C CHAMBER C-502	FLUX EXTERNAL CHAMBER μμA	FLUX UPPER CHAMBER D-503
Flow decrease 5400 to 4530 gpm Step = - 870 gpm	Before Transient	Mean %	100	100	100	100	100	100	100
		Noise (p-p) (NZS)	4.4	6.9	6.7	7.6	10.7	8.1	12.3
		% (ZS)	4.5	9.4	6.8	4.8	7.1	5.1	7.6
	After Transient	Mean %	84.0	94.9	95.2	96.9	95.3	94.7	94.5
		Change in Mean %	- 16.0	- 5.1	- 4.8	- 3.1	- 4.7	5.3	- 5.5
		Noise (p-p) (NZS)	- - -	- -	- -	- -	- -	- -	- -
		% (ZS)	4.5	5.1	7.8	5.3	8.3	7.1	10.4
	Step	Step %	- 15.3	- 7.8	- 3.9	- 9.6	- 13.2	- 12.7	- 13.5
		Overshoot %	9.1	13.0	31.0	75.0	68.0	63.0	62.0
		Damped Frequency (cps)	- -	- -	- -	12.8	12.8	12.4	1.22
Flow Increase 4500 to 5700 gpm Step = + 1170 gpm	Before Transient	Mean %	100	100	100	100	100	100	100
		Noise (p-p) (NZS)							
		% (ZS)							
	After Transient	Mean %	125.7	108.5	108.5	107.2	110.6	110.3	112.1
		Change in Mean %	+ 25.7	+ 8.5	+ 8.5	+ 7.2	+ 10.6	+ 10.3	+ 12.1
		Noise (p-p) (NZS)							
		% (ZS)							
	Step	Step %	+ 26.6	+ 6.0	+ 6.0	+ 13.2	+ 20.8	+ 18.0	+ 16.2
		Overshoot %	0	0	20.0	45.0	43.0	48.0	47.0
		Damped Frequency (cps)	- -	- -	- -	1.20	1.24	1.22	1.22

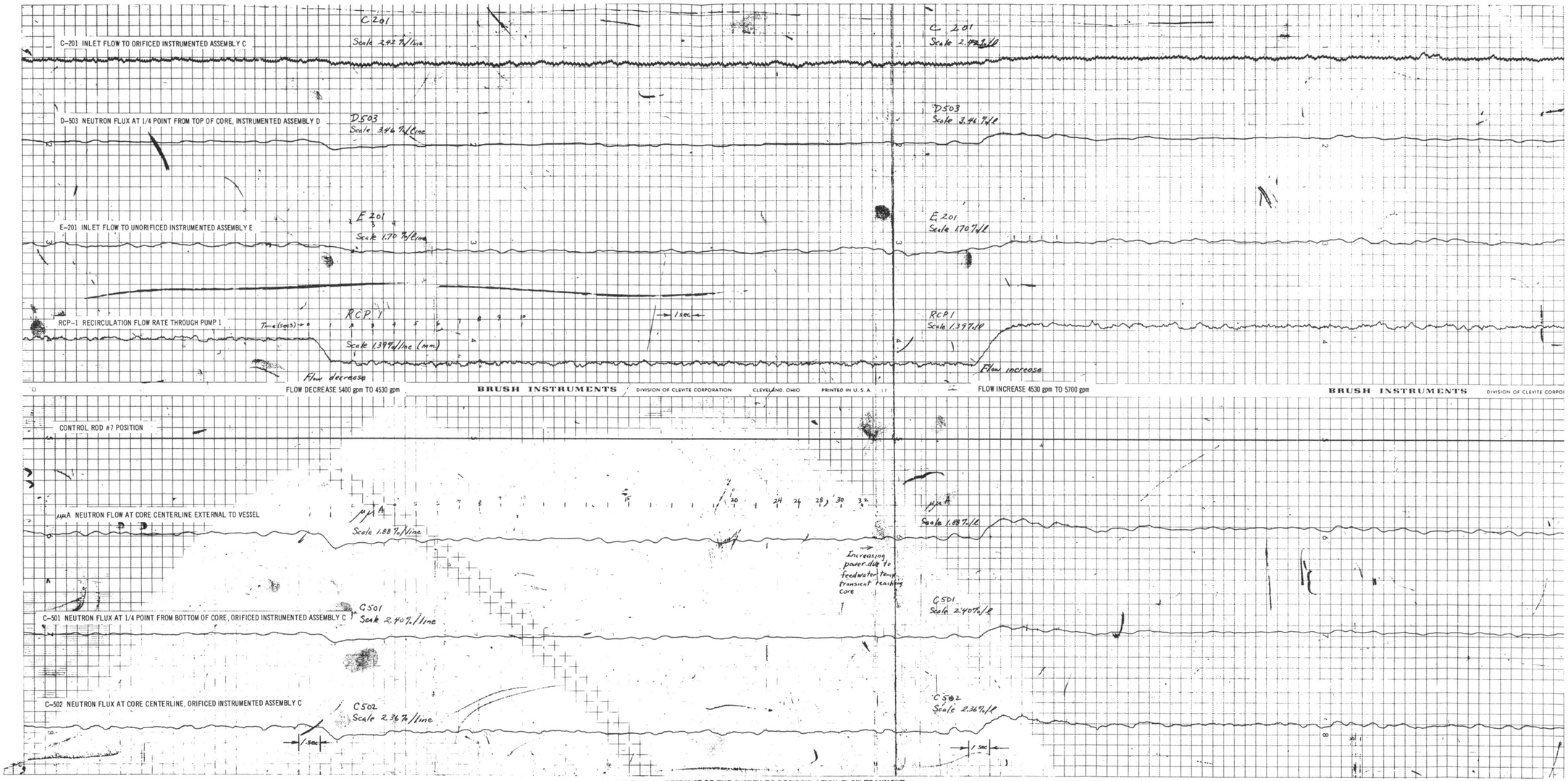

FIGURE VII-54 RESPONSE OF THE SYSTEM TO RECIRCULATION FLOW TRANSIENT

RUN 15-8-20 REACTOR POWER 15 MWt
CHART SPEED 10 mm/sec SUBCOOLING 9.72 BTU/lb

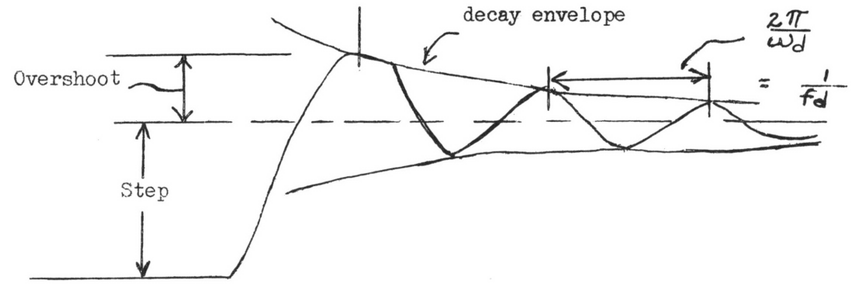

Conventional Step Transient of Simple Damped Harmonic System

(Characteristic Equation: $S^2 + 2\zeta\omega_o S + \omega_o^2 = 0$)

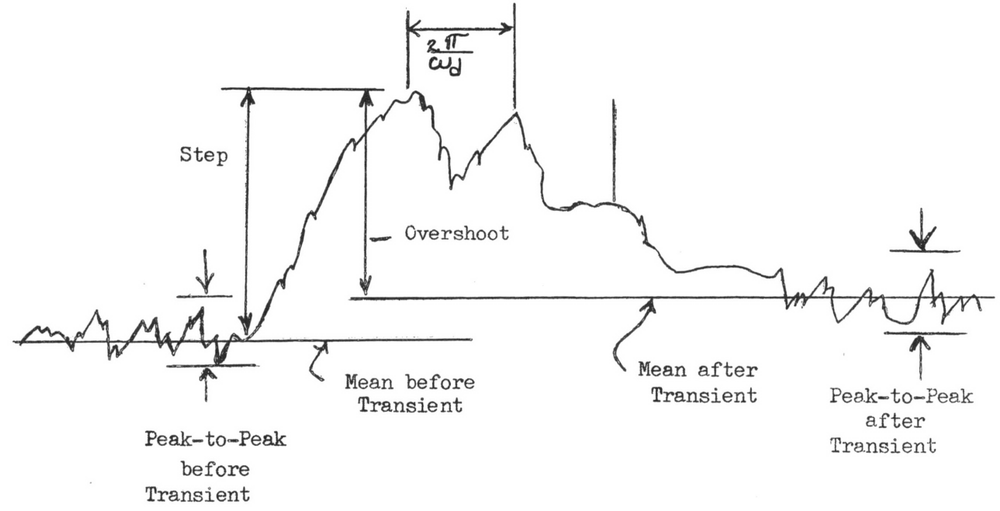

FIGURE VII-55 NOMENCLATURE OF TRANSIENT

SECTION VIII

COMPARISON TO PREDICTED RESULTS

A pre-test analysis was conducted prior to running the stability tests in the VBWR. The first object of the pre-test analysis was to help establish the test conditions which would yield the most valuable data. To this end, predictions were made of the reactor characteristics based upon the results of this pre-test study. A tabulation of these predictions, together with the results of the pre-test analysis, is presented in Section VIII-A. A second purpose of the pre-test analysis was to provide unbiased and unadjusted solutions of the analytical model which could be evaluated in the light of experimental results obtained during the tests. A comparison of the experimental results, thusfar obtained, to the pre-test analysis predictions is presented in Section VIII-B.

A. PRE-TEST ANALYSIS OF THE VBWR STABILITY TESTS

The dynamic analysis model employed for the pre-test analysis of the VBWR stability tests may be represented schematically by the logic block diagram presented below. This analytical model was applied to the VBWR plant and associated stability core in order to provide predictions of the effects upon stability of: core power, core flow, core bypass leakage, fuel element inlet orificing and external recirculation loop flow resistance.

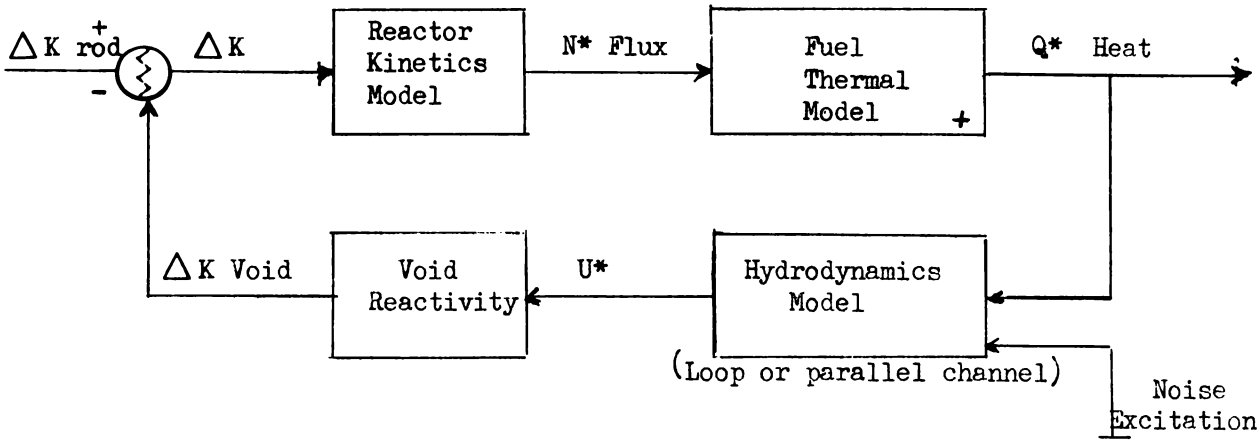

FIG. VIII-1 LOGIC MODEL FOR VBWR STABILITY ANALYSIS

The effects upon stability of both parallel flow channel hydrodynamics (uncoupled flow paths) and loop hydrodynamics (lumped core coupled to external recirculation path) were studied in this analysis.

1. The Analytical Model

The analytical model used for this study employs essentially the same considerations as have been applied to the stability analysis of GEAP-3795[14]. It contains as a ΔK feedback contribution only the regenerative effect due to heat-generated voids. The relative effect of Doppler and pressure compared to heat-generated voids were assessed and were found to be negligible for this test. The following sections are descriptions of the individual elements of the analytical model.

Reactor Kinetics Simulation: The reactor kinetics transfer function was a non-linear representation of the conventional six delay group thermal fission model with properties tabulated in Table VIII-1. The equation representing this simulation is:

$$\frac{N^*}{\Delta K} = \frac{1}{s\left[\tau_o + \sum_{i=1}^{6} \frac{\beta_i/\beta}{(s + 1/t_i)}\right]} \qquad \text{(VIII-1)}$$

* indicates normalized form (per unit values)

TABLE VIII-1

PROPERTIES OF DELAYED NEUTRONS

Delay Group	Mean Life t_i (sec)	Decay Constant $1/t_i$ (sec^{-1})	Fraction β_i/β
1	80.39	0.0124	0.033
2	32.78	0.0306	0.219
3	8.97	0.112	0.196
4	3.32	0.302	0.395
5	0.880	1.14	0.115
6	0.332	3.02	0.042

$\beta = 0.0065 \pm 0.0002$

$\ell^* = 5 \times 10^{-5}$ sec.

$\tau_o = \ell^*/\beta^* = 0.0078$ sec.

Fuel Element Thermal Time Constant Simulation: The fuel model simulation was a linear transformation of the thermal diffusion equation which relates to heat imparted to the fluid at the surface of the fuel element (Q^* in per unit values) to neutron density (N^*). This relationship is based upon a transient analysis of the temperature and heat transfer characteristics of a cylindrical rod with internal heat generation, given in GEAP-0805.[15] This analysis has been incorporated into a digital computer code (FTC) which provides, among other things, a transient expression for surface heat flux as a function of neutron power level. The form of this transient expression is a four-node series approximation of varying heat flux path length to the clad surface.

$$\frac{Q^*}{N^*} = \frac{0.826}{1 + 6.38(s)} + \frac{0.104}{1 + 1.16(s)} + \frac{0.038}{1 + 0.296(s)} + 0.032 \qquad \text{(VIII-2)}$$

The Hydrodynamics Model Simulation: The hydrodynamics model used provides two alternate modes of dynamic behavior. The first deals with the responses of the core, two-phase system, and single phase recirculation system in concert as a loop. This analysis is referred to in the following as a loop stability analysis.

The second mode describes the dynamic response of flow in a single channel acting in parallel with a comparatively large flow path which establishes essentially an uncoupled channel. This analysis is referred to in the following as a parallel channel stability analysis.

Although the dynamic behavior of the loop hydrodynamics and the parallel channel hydrodynamics for the same reactor operating condition is generally quite different, the form of the mathematical description for the two hydrodynamic modes is identical and can be defined by a system of six linearized transient equations:

$$
\begin{aligned}
II^* &= K_1(S-W)^* + K_2(W)^* + K_4(V)^* + K_5 - (Q)^* + K_6(\alpha)^* \\
(S-W)^* &= -R^* + K_7(W)^* + K_8(V)^* + K_9(Q)^* + K_{10}(\alpha)^* \\
\frac{dw^*}{dt} &= K_{11}(R)^* + K_{12}(II)^* + K_{13}(Q)^* + K_{14}(V)^* + K_{15}(W)^* + K_{16}(\alpha)^* \\
\frac{dV^*}{dt} &= K_{17}(II)^* + K_{18}(Q)^* + K_{19}(V)^* + K_{20}(\alpha)^* \\
U^* &= K_{21}(W)^* + K_{22}(V)^* + K_{23}(Q)^* + K_{24}(\alpha)^* \\
\frac{d^2R^*}{dt^2} &= K_{25}(u)^* - K_{26}\frac{dR^*}{dt} - K_{27}(R)^* \qquad \text{(VIII-3)}
\end{aligned}
$$

The coefficients K_i's are functions of the geometry and the initial steady-state conditions. They are, in fact, coefficients which describe the slope of the non-linear transient hydrodynamic performance about the normalizing conditions. When the flow geometry and average steady-state conditions are varied widely, such as was accomplished during this study, a complete set of coefficients must be supplied for each steady-state condition of interest. This is a natural consequence of making a linear approximation of a non-linear system. Since it is a rather lengthy and laborious task to obtain a complete set of coefficients for this hydrodynamic model, and it is generally necessary in most reactor studies to supply not one but several complete hydrodynamic solutions, this model has been adopted to a digital computer code solution. This code (SATR-1) was written for the Philco 2000 computer. The input thermodynamic and geometric information for this code was obtained from the steady-state hydraulics code, COFFI. A detailed description of the above hydrodynamic model is provided in in GEAP-3975.[14] Additional information concerning the parallel flow channel mechanism can be found in GEAP-3508.[6]

Void Reactivity Model Simulation: The void reactivity model used was a linear relationship which describes the excess reactivity due to steam volume changes within the core (ΔK void) that are caused by reactor heat. This is a transport relation which averages the

core steam volume in time and assigns a void worth of reactivity to that average. The void reactivity gains were determined from reactivity calculations of the core employed for the tests.

$$\frac{\Delta K \text{ void}}{U^*} = \frac{\text{Void Worth}}{1 + \frac{\tau_c(S)}{2} + \frac{\tau_c^2(S)^2}{12}} \qquad \text{(VIII-4)}$$

Where: Void worth of Consumers element = 4.50
Void worth of Fuel Cycle element = 2.65
Void worth of lumped core = 2.65

The numberical values of the dollar void worths listed above were based upon physics calculations. The numberical value of core transit time (τ_c) in the above equations must be determined for each operating condition of the reactor because it, like the coefficients of the hydrodynamic model, is a linear approximation of a non-linear relationship.

2. Analytical Model Solution

Dynamic solutions were obtained from the aforementioned analytical model by the use of analogue computer techniques. Table VIII-2 summarizes the range of parametric reactor conditions considered in the pre-test analysis. One of the purposes of the pre-test analysis was to help establish the test conditions which would yield the most valuable data. The analysis indicated that the low flow, high power reactor condtions would be the most fruitful area for experimentation. It is for this reason that a large portion of the pre-test calculations were made in the core flow range of 3750 gpm. It was in this flow range that both loop and parallel channel hydrodynamics were studied. Also investigated in this range were the effects of power, flow, and inlet orificing upon the parallel flow channel mechanism. As can be seen from the table, each reactor condition was analyzed for the following characteristics:

Rod Oscillator Test (Reactor Power and Flow Transfer Function):
This portion of the analysis consisted of merely obtaining from the analogue computer the models response of reactor flux (N)* and inlet

water velocity (V)* to a $\pm$ 10¢ sinusoidal ΔK insertion spread over a frequency range of 0.03 to 8.0 cps.

Noise (Spectral Power and Flow Density

This portion of the analysis consisted of obtaining from the analogue computer a frequency spectrum of the neutron flux (N)* and inlet water velocity (V)* response to an assumed noise excitation. The noise excitation assumed for these predictions was an all-inclusive (0.03 to 8.0 cps) frequency spectrum in the temperature of the inlet water having an amplitude of $\pm$ 0.1° F.

It should be pointed out that the use of the analogue computer for analytical model solution introduces certain inherent inaccuracies in this study. The analogue solutions themselves are not precise solutions of the analytical model, in the sense that they are approximate at the equations. They also contain errors due to amplifier drift, recorder drift, chart reading, etc. These errors are beyond the inherent inaccuracies of the analytical model. If, however, the analytical model had been solved by digital computer techniques, the solutions would have represented precisely what the analytical model response was.

It is for the above reason that some of the analytical model solutions presented in this section do not appear to describe a smooth curve. A precise solution of the model would result in a smooth curve description of the reactor power and flow transfer functions and the spectral power and flow densities.

Pre-Test Analysis Predictions

The first object of the pre-test analysis was to help establish the test conditions which would yield the most valuable data. Predictions were made of the reactor characteristics based upon the results of this study to determine test conditions. These predictions represent only a portion of the technical content of the pre-test analysis, and portray only the more obvious implications made by the analytical model.

The following is a summary of these pre-test analysis predictions(16). Each summarizing statement is accompanied with a discussion of specific portions of the analysis results which led to these predictions.

a. <u>The external recirculation loop is insensitive to pressure changes across the reactor core and therefore cannot be driven in appreciable flow variation by the core</u>.

The core plus recirculation flow loop constitute an exceedingly stable hydrodynamic, two-phase flow loop, according to this prediction. It is possible, however, that external sources such as pump disturbances may be reflected in the recirculation loop which will, in turn, drive the core flow. In other words, if variations are observed in the recirculation loop flow, then it should not be concluded that the two-phase loop is oscillatory and driving the downcomer; rather, it should be considered an indicator to start looking for outside influences on the recirculation flow.

This prediction is a result of observing the inlet water velocity responses to the rod oscillator tests of Runs 37, 39, 41, and 43 (see Table VIII-2). These data are plotted graphically for discussion purposes in Figure VIII-2. These four runs represent four different recirculation flow loop geometries which could exist for a core flow rate of 3,750 gpm. It can be seen from Figure VIII-2 that none of these loop hydrodynamic responses exceeds $\pm$ 0.3 % variation in flow rate as a result of $\pm$ 10¢ cycle variation in ΔK. Since a ΔK disturbance results in a heat flux variation, and this in turn manifests itself as a core pressure difference variation, then it follows that: "The external recirculation loop is insensitive to pressure changes across the reactor core and therefore cannot be driven in appreciable flow variation by the core".

Also shown in Figure VIII-2 is a plot of the parallel flow channel response of a single uncoupled fuel cycle element (Run 27). The core conditions for this case are identical with those enumerated

for the four loop hydrodynamics cases. It can be seen by comparison of the parallel flow channel curve to the loop hydrodynamics curves that the inclusion of the external recirculation loop in the hydrodynamic analysis imposes strong restrictions on the two-phase flow loop, thus making it an exceedingly stable hydraulic system.

b. Changes in the recirculation loops' flow resistance within the range permitted by operations procedures will have no appreciable effect upon recirculation loop absolute stability.

It may be said, additionally, that small changes in the core bypass flow (three dummy fuel plugs removed) will represent no appreciable influence upon loop stability. Large changes in core bypass flow (baffle doors open), however, are expected to decrease loop stability.

This prediction is based upon observations of the pre-test analysis results for Runs 37, 39, 41, 43, and 27. The inlet water velocity responses of these runs have already been introduced in Figure VIII-2. Figure VIII-3 is a plot of the reactor flux responses for these runs. It can be seen by examination of these graphs that there is very little spread between the points that describe the four loop hydrodynamics cases. This is true for both inlet water velocity variations and reactor flux variation. In fact, it is likely that the only discernible difference between these curves is due to the already mentioned inherent errors of the analogue solutions. The significance of this slight difference between the four loop hydrodynamics cases is that changes in the recirculation loop's flow resistance, such as the difference between a constant pump speed, valve controlled flow and a variable pump speed-controlled flow, will have no appreciable effect upon recirculation loop stability. Furthermore, small changes in the core bypass flow (three dummy fuel plugs removed) will represent no appreciable influence upon loop stability.

Large changes in the core bypass flow (baffle doors open), however, tend to uncouple the individual elements from the rest of the core and the recirculation loop and instead couple them separately to an almost unrestrained, single-phase bypass flow path. This condition approaches the uncoupled, parallel flow channel condition which is presented in Figures VIII-2 and VIII-3, along with the loop hydrodynamics cases. It can be seen from these figures that there is a significant difference between the parallel flow channel response curves and the loop hydrodynamics response curves. The parallel flow channel curves are characterized by sharper peaks and valleys than are displayed by the loop hydrodynamics curves. These characteristics are a measure of the dynamic system response; i.e., the sharper the peaks and valleys in a frequency response curve, the more underdamped is the system, and, conversely, the flatter the frequency response, the more damped the system. Therefore, it follows from examination of Figures VIII-2 and VIII-3 that large changes in core bypass flow (baffle doors open), are expected to decrease loop stability.

c. <u>The effect of increased inlet orificing on the fuel elements is expected to have a significant damping effect upon parallel flow channel stability</u>.

This prediction is based upon observations of the pre-test analysis results for Runs 27, 29, 31, 33, and 35. Figure VIII-4 is a plot of the reactor flux responses for these runs. All of these runs represent the parallel flow channel mechanism for various degrees of inlet single-phase orificing with a core flow of 3,750 gpm, and a core power of 20 MWt. It is observed from this parametric display of reactor flux responses that there is a consistent flattening dendency in the response curves with increasing inlet orificing restraint. Applying the same logic as was outlined in the above discussion, it can be concluded that the effect of increased inlet orificing on the fuel elements is to have a signifi-

cant damping effect upon parallel flow channel stability.

d. Parallel flow channel stability is more sensitive to core flow changes than it is to core power changes.

This prediction is based upon observations of the pre-test analysis results for Runs 15, 11, and 23. Figure VIII-5 is a plot of the reactor flux responses for these runs. All three of the runs represent the parallel flow channel mechanism. Run 15 is a 7,650 gpm core flow and 10 MWt core power condition. Run 11 is a 7,650 gpm core flow and 20 MWt core power condition. Run 23 is a 4,675 gpm core flow and 10 MWt core power condition. It is observed by a comparison of the curves for Runs 15 and 11 that only a slight variation in parallel channel stability response occurs for a two-fold increase in reactor power. A comparison of the curves for Runs 15 and 23 shows, however, that a somewhat greater influence upon parallel channel stability is effected by roughly a one-half reduction in core flow. Therefore, it is concluded that parallel flow channel stability is more sensitive to core flow changes than it is to core power changes.

e. Flow oscillations within the individual elements for all test conditions will be of relatively small amplitude when compared to flux variations in response to reactivity oscillation.

It is expected, additionally, that somewhere during the test sequence, a change in the steady-state phase relationship between flow and power will be observed. i.e., A change from flow being in phase with power to flow being 180° out of phase with power in the steady-state.

The first portion of this prediction is based upon a comparison of the inlet water velocity responses and the reactor flux responses of all of the pre-test analysis results. It can be seen from Table VIII-2 that the inlet water velocity responses to the rod oscillator tests are, in general, less than 1/10 of the

reactor flux responses. This observation leads to the conclusion that flow oscillations within the individual fuel elements will be of relatively small amplitude when compared to flux variations in response to reactivity oscillation.

The second portion of this prediction, which is concerned with the phase between flow and power, is based upon the digital computer solutions of the hydrodynamics model. It was observed from these results that, for core flows between 2,980 gpm and 7,650 gpm at 20 MWt, an increase in power resulted in an increase in individual fuel element flow. On the other hand, it was found that in the high core flow condition (15,000 gpm) and slightly higher power (25 MWt), an increase in power resulted in a decrease in fuel element flow. At the point of flow reversal, the flow is 180° out of phase with the power. This behavior should not be unexpected. This reversal in the flow trend with power can be explained by recognizing that in the high flow condition elevation head due to voids is only a small contribution to the total pressure difference across the core. Therefore, even though an increase in heat added in the channel results in an increase available elevation head within the core, this effect is more than overshadowed by the incremental, two-phase friction which also increases with increased voids or power. The net result, then, is a decrease in fuel element flow which reaches equilibrium by the re-distribution of amount of two-phase friction loss to account for the interaction of two-phase and single-phase losses, both of which are rather substantial at the higher flows.

A similar effect can occur in a low flow, high power condition which results in a high void situation. In this situation, just as in the above case, the increased elevation head within the core caused by increased power is more than overshadowed by the incremental two-phase friction which also increases with power. In other words, two-phase friction outruns elevation head. For the

cases considered in the pre-test analysis, no reversal in the flow trend with power was observed in the low flow, high power regions. The analysis conditions did not go low enough in flow, or high enough in power, to display this effect.

B. COMPARISON OF ANALYSIS AND TEST RESULTS

A comparison of pre-test analysis to experimental results for the rod oscillator tests and the steady-state noise tests is presented in this section. No comparison is given for the transient tests, since there were no pre-test predictions made for this mode of operation. The following section presents three aspects in the following order:

1. A discussion of enumerated pre-test predictions of the previous section and their counterparts in experimental results.
2. A discussion of other significant experimental observations and their relationship with the pre-test analysis.
3. A comparison of measured power transfer functions and their predicted responses.

The actual operating conditions of the VBWR during test were not identical to the conditions assumed for the pre-test study. Therefore, a certain degree of rationalization and intuitive normalization is necessary in order to make a meaningful comparison. Subsequent analysis will allow calculations to be made with precise test conditions and, hence, provide an improved analysis. Such an analysis should yield more quantitative results.

1. Pre-Test Predictions and Experimental Results

a. Changes in the recirculation loop's flow resistance within the range permitted by operations procedures will have no appreciable effect upon recirculation loop stability.

(Refer to Section VIII-A-3a)

Experimental results verify this prediction very well. Two test cases which illustrate this condition are Runs 15-9 and 15-19.

Experimental results show that the high head, valve-controlled 4,000 gpm, forced circulation test(15-9) (Figure VII-46), and the low head, speed-controlled 4,000 gpm, forced circulation test (15-19) (Figure VII-47), have power transfer functions which are almost identical. This identity can be interpreted to indicate that the recirculation flow system is well-damped, even in the most frictionless condition which can be operationally produced, (15-19), and that additional recirculation flow loop friction, although large, (15-19), has no discernible effect because the hydraulic damping is already essentially saturated.

b. Small changes in the core bypass flow (three dummy fuel plugs removed) will represent no appreciable influence upon loop stability. Large changes in core bypass flow (baffle doors open), are expected, however, to decrease loop stability.

The first portion of this prediction, concerning small changes in bypass flow, cannot be answered from the test data directly since no such changes were made during the test series. This prediction can, however, be verified by an indirect interpretation of the test data. It is known that bypass or baffle leakage flow of a significant amount exists when the baffle doors are closed. Yet, the in-core fuel element flows did not display discernible resonances or consistent periodicities while the reactor was in this configuration. To be sure, the fuel element flows were noisy, but no resonant. This indicates that the normal bypass flow had not appreciably altered the coupling between the recirculation loop and the core channels and, thus, had little effect upon loop stability.

The second portion of this prediction, which states that large changes in bypass flow will decrease loop stability, is well verified by experiment. The forced circulation test with baffle doors open (15-16) illustrates this quite clearly. (Compare Figures VII-44, VII-45 and VII-48)

Experimental results show that resonant hydrodynamics at 0.4 - 0.5 cps were exhibited within the reactor core for both the natural circulation test and the forced circulation with baffle doors open test. This flow resonance was displayed two ways: First, by observation of the unorificed instrumented fuel assembly's turbine flow meter output, (Figure VII-10, Trace E-201 and Figure VII-9, Trace E-201); and second, by the existence of a characteristic dip in the power transfer functions of these two tests (see Figures VII-44 and VII-45).

The natural circulation test (15-18) (Figure VII-44) and the forced circulation test with baffle doors open test (15-16)(Figure VII-45) have power transfer functions of similar shape. This might well be expected since the core hydrodynamics of these two conditions are essentially the same. i.e., the baffle door passage is large enough that bypass flows, either positive or negative, do not appreciably alter the effective single-phase elevation head which exists across the core in natural circulation.

c. <u>The external recirculation loop is insensitive to pressure changes across the reactor core and therefore cannot be driven in appreciable flow variation by the core</u>.

The core plus recirculation flow loop constitute an exceedingly stable hydrodynamic two-phase flow loop, according to this prediction. It is possible, however, that external sources, such as pump disturbances, may be reflected in the recirculation loop which will, in turn, drive the core flow. In other words, if variations are observed in the recirculation loop flow, then it should not be concluded that the two-phase loop is oscillatory and driving the downcomer. Rather, it should be considered an indication to start looking for outside influences on the recirculation flow.

This prediction is well verified by experiment. The fact that a test condition which had a highly restricted recirculation flow

loop (15-9) (Figure VII-46) appeared essentially identical to a test condition which had considerably less flow restriction, (15-19)(Figure VII-47), suggests that the recirculation loop is well damped in both conditions. This observation was explained in (a) above. Other test conditions also verify this prediction.

No resonant hydraulics were observed in any of the closed flow circuit, forced circulation, rod oscillator tests.

d. <u>The effect of increased inlet orificing is expected to have a significant damping effect upon parallel flow channel stability.</u>

This prediction is well verified by experiment. The natural circulation experiment provided a test condition where the parallel flow channels were uncoupled or independent of one another in their flow behavior. The effect of orificing could, therefore, be observed by comparing the flow behavior of the orificed and unorificed instrumented assemblies during this test condition. (See Figure VII-10 and Figure VII-29)

The natural circulation test and the forced circulation with baffle doors open test are textbook examples of a reactor core with uncoupled, parallel flow channels and strong neutron coupling.

The effect of inlet orificing on fuel elements is to damp flow oscillations or resonance. This was observed from a comparison of the flow response of the unorificed and orificed instrumented assemblies during the natural circulation rod oscillator test.

e. <u>Parallel flow channel stability is more sensitive to core flow changes than it is to core power changes</u>.

This prediction has not been answered either pro or con by the experimental results thus far. As mentioned above, the natural circulation tests provide a flow condition with uncoupled parallel flow channels. Parametric variation of flow was obtained only

during forced circulation. The forced circulation tests do not provide an identifiable sensitivity to flow variation. This is due, at least in part, to the fact that in all the closed circuit forced circulation tests, the flow interdependence of individual channels appeared very tightly coupled. This tight hydraulic coupling, together with insufficient number of in-core flow measurements and high noise levels, make it doubtful if parallel channel effects can be determined in this instance. The stability of the lumped reactor system, however, was definitely observed to increase with increased core flow during the rod oscillator tests. The amplitude of the flux and flow noise measurements were concluded not to be good indicators of reactor system stability.

The amplitude of the steady-state flux noise is seen to increase with increasing recirculation flow (Figure VII-29). The stability of the reactor system, by rod oscillation test, however, is seen to increase with increasing flow. Thus, it is demonstrated that the consideration of peak-to-peak steady-state flux noise measurements as a prime indicator is inadequate. It was found in the VBWR that not only did the steady-state noise peaks fail to indicate a trend toward unstable operation, but, in fact, indicated the reverse trend.

f. Parallel flow oscillations within the individual elements for all test conditions will be of relatively small amplitude when compared to flux variation in response to reactivity oscillation.

It is expected, additionally, that somewhere during the test sequence a change in the steady-state phase relationship between flow and power will be observed; i.e., a change from flow being in phase with power, to flow being 180^{o} out of phase with power in the steady-state.

The first portion of this prediction, which relates to expected flow oscillations in response to reactivity oscillation, is well verified by experiment. The second portion of this prediction,

concerning the phase between power and flow, is neither answered pro nor con by the experimental results. Parallel channel flow response to power variation was only observed to exist conclusively in two test conditions: Natural circulation, and forced circulation with baffle doors open. These two conditions do not describe the entire range of the testing sequence and data are not complete. Therefore, the data thus far reduced are inconclusive about the predicted turn around in flow response to power change.

The in-core flow noise and the flow response to rod motion (when displayed) were always small compared to the flux response to rod motion. In all tests but 15-1, the flow noise was about 10% of the rod oscillation flux response. The flow noise in Test 15-1 (high flow) was approximately 25% of the flux response.

2. Test Observations and the Analytical Model

a. It may be observed that the worth of the oscillating rod appears to increase with decreasing average core voids.

This behavior should not necessarily be unexpected for a reactor with top entry control rods. Calculations have been made which predict this trend for the VBWR. The model used for this calculation was a specialized, 3-group diffusion code for use with one-dimensional slab geometry, which computes flux and void distribution accounting for control rod position.

b. The void coefficient of reactivity increases with increasing average core voids.

This same trend in the value of the regenerative void reactivity effect was predicted by physics calculations prior to the test. The model used for these calculations was the same model described above. It is extremely important that this effect be understood well enough so that it can be accurately predicted. As will be seen later, this effect is a large contributor to system stability.

This effect has thus far only been examined from a general trend point of view. A thorough and detailed examination is necessary and should be the subject of the future analytical program conducted with improved inputs.

c. The total power reactivity feedback gain increases with increasing average core voids.

This trend in the total regenerative reactivity feedback gain can be explained by analysis. The present results, however, are not thorough enough to have sound conclusions. This effect is exceedingly important to stability analysis, and is intimately related to the void coefficient of reactivity discussed above. The total regenerative power reactivity feedback gain is a result of the combined effects of doppler and power-generated void reactivity. It is known that the doppler coefficient (in per unit values) increases with increasing power. Also, as mentioned above, the void coefficient of reactivity was expected and was measured to increase with increasing power. But, the power-generated void reactivity is the product of this void coefficient and the power to void gain (see Analytical Model, Section VIII-A-1). Unfortunately, the power to void gains were not calculated previously in the pre-test analysis. The conditions assumed for the pre-test analysis thermal hydraulic calculations were considerably different, in most cases, than the actual test condition. The pre-test analysis should be recalculated for the precise test conditions and examined in depth with the experimental data. This will be necessary before a conclusive analytical understanding of the total feedback gain and its individual contributors can be resolved.

d. The importance of the observations and discussions of (b) and (c) above is dramatized by the test data of the 20,000 gpm and 4,000 gpm forced circulation rod oscillator tests.

Both of these reactor conditions are devoid of oscillatory hydraulic characteristics; yet, the reactor is observed to become less stable with decreasing recirculation flow. We observe, at the same time, an increase in the void coefficient of reactivity gain with decreasing flow. These two trends go hand in hand toward the direction of reactor instability. These data, therefore, demonstrate clearly the detrimental effect of increasing void reactivity coefficients upon reactor stability. It can be concluded that there are real design upper limits on the void-reactivity coefficients established by stability limitations. It is absolutely necessary for advanced reactor design that we understand and can predict these design upper limits. As was mentioned earlier, this will be the subject of continuing analysis.

e. <u>The stability gain margin is seen to decrease for increasing voids. Zero gain margin indicates an unstable reactor. Therefore, the stability of the VBWR system is seen to decrease with increasing voids.</u>

This trend was predicted in the pre-test analysis, and it should not be unexpected. This observation follows from (c) above; i.e., the gain margin decreases with increasing voids primarily because the total power reactivity feedback gain increases with increasing voids. The change in the frequency response of the system, of course, is also related to stability. But, its effect is not thought to be as large as the gain effect.

f. <u>The shapes of the power transfer functions, as measured by both the in-core ion chamber and the external μμA flux monitor, are essentially identical for a given test condition. However, the absolute flux levels and/or the percentage variations measured by any two given chambers or monitors may or may not be identical.</u>

The data are inconclusive about this. This observation is not surprising. Two effects which could cause differences in shapes

of the power transfer functions are:

1. Characteristic local dynamic responses or resonances combined with large spatial effects.

2. Spatial variation in the diffusion of nuclear effects from one part of the core to another.

Appreciably large core spatial effects were not expected, and the frequency resolution of the band pass filter is not adequate to discern the spatial diffusion effect. It would have been very interesting to compare the absolute levels of various flux chambers. Some noticeable spatial effects were expected to be present in this form. Unfortunately, however, the scale factors of the in-core ion chambers can probably never be resolved from the data. This is so because the signals were partially shorted (in undetermined amounts) by wet terminal strips in the reactor enclosure.

g. <u>It was observed that the flux response actually led the rod motion in phase during the low frequency portion of the rod oscillator tests. This phenomena should not be unexpected. This condition merely serves to dramatize the electrical reactive network analogy of a reactor system</u>.

Phase lead of power in response to rod motion has been observed before in BWR experiments.[8] [17] The pre-test analysis predicted this phase trend. The model proposed by Akcasu[4] also predicts this same general behavior.

h. <u>It was observed that the resonant frequency of the power transfer function increases with increasing flow. This flow dependence is not large. The system resonant frequency of the 4,000 gpm runs are about 1.2 cps, while the resonant frequency of the 20,000 gpm run is about 1.5 cps. (See Figures VII-44 and VII-46)</u>.

A trend similar to that shown above was predicted by the pre-test analysis, but was expected to be much more pronounced than was experimentally observed. It was predicted, based upon analogue computer simulation, that the system resonant frequency of the 4,000 gpm runs would be about 1.0 cps, while the resonant frequency of the 20,000 gpm run would be about 4.0 cps. This discrepancy should, and will, be examined in greater detail. Several factors may contribute to this disagreement. These are:

1. Analogue representation of the system produced drift and scale factor inaccuracies.
2. All the predictions (except for 3,750 gpm core flow) were made using the parallel channel hydraulics model. This model is known to represent an upper limit on frequency response and minimum hydraulic damping.
3. The hydrodynamic representation of the analytical model is single node. It is expected that multi-node representation of the system may contribute to reducing the disagreement between data and pre-test analysis.
4. The improvement of representation of steady-state gains (void coefficients, etc.) may also contribute to reducing the disagreement between data and pre-test analysis.

The pre-test predictions should be re-calculated, taking into account these effects, and then re-compared to the test data. A realistic evaluation of the model can then be obtained.

i. The natural circulation, rod oscillator test condition was shown to have a responsive or resonant hydraulic system. Thus, the effect of power or flux driving flow was displayed (Figure VII-35). Oscillation of the control rod caused a variation in power. This variation in power caused a corresponding change in core void content. And, finally, these changes in core void content caused the under-damped hydraulic system to respond with a fluctuation in the coolant flow. This observation has important implications to the noise disturbances of the system.

It should be pointed out, however, that the effects of power oscillation upon flow were only discernible near the resonant frequency of the hydraulic system. At all other frequencies, the flow noise was far greater than the flow response to power. The flow response to power, even at the hydraulic resonant frequency, was not to increase the amplitude of the flow noise by adding a sympathetic flow component to power, but rather, to cause the existing flow noise to become "ordered" with the power variations. i.e., The amplitude of the flow noise at this frequency was essentially the same during rod oscillation as it was just under the influence of steady-state noise. The foregoing observations lead to the following very important conclusion:

> If the relatively large scale power disturbances induced by rod oscillation just barely caused a noticeable ordering of the flow noise, then the equivalent noise disturbances must be at least as large as, if not larger than, those power-generated void disturbances which are caused by rod oscillation.

This observation is exceedingly important. It provides a significant step toward defining the noise excitation in the VBWR. This step does not define conclusively what the source(s) of noise is, but, rather, places a minimum limit upon the equivalent disturbance of that source(s). This step, therefore, allows us to eliminate from the possible courses of significant noise those proposed sources which cannot provide the minimum disturbances necessary for the observed reactor noise.

The implications of this observation are both good and bad: Bad because the existence of large noise disturbance(s) within the system indicate a plant condition which was certainly not intentional; good because, since the disturbance(s) is large, it is very possible that after it is located it can be reduced with minimum design changes. On the other hand, had the disturbance(s)

been small, or within normal design expectations, it would have been much more difficult to appreciably attenuate the excitation.

Two conclusions were made concerning the conduct of stability tests and the interpretation of data:

j. Meaningful results could not have been obtained from the steady-state noise and the rod oscillator data had they not been:
   1. Recorded on magnetic tape, and
   2. Subsequently subjected to effective filtering techniques.

   Due to the random nature of the noise components, it was necessary that the data be filtered and averaged over reasonably long time durations in order to secure accurate results. These restrictions were anticipated prior to the test. However, the program did not provide funding to do the needed work prior to the tests. Recent experience with the data handling has indicated a need for additional improvements in our data gathering and data reduction techniques:
   1. Even longer data recordings in order to resolve the low frequency data points, and
   2. More accurate data filtering techniques (such as one of several commercially available Fourier transform analyzers).

   The requirement for longer data recordings is purely academic as far as the VBWR tests are concerned, but should be borne in mind in future tests. The requirements for more effective data filtering techniques, however, can and will be met in the subsequent analysis of the VBWR tape recorded data.

k. The inadequacy of transient tests for reactor stability measurements is dramatized in the VBWR experiment by the combination of the presence of high noise components and the non-stationary character of that noise.

   In theory, the transient test will yield the same reactor information as will the rod oscillator test. Unfortunately, however,

the reactor information in a transient test is squeezed into the comparitively short time duration of the reactor transient. This short time interval is not sufficiently long to accurately obtain the reactor characteristics from the test data. Therefore, in reality, the transient test does not provide the same stability information as does the rod oscillator test. In the case of the VBWR, the transient tests did not provide comparable information to that obtained with the rod oscillator.

The fact that a rod oscillator test yields more accurate system data than does a transient test is generally accepted. The rod oscillator test, however, is comparatively expensive. The VBWR test results allow an assessment of the technical worth of the dollar difference between the two types of tests.

3. Predicted and Measured Power Transfer Functions

a. High Flow Forced Circulation

Figure VIII-6 presents a plot of the power transfer function of the 15-1 series test (December 5, 1961) as measured by the out-of-core micro-microammeter. The plant conditions were: 15 MWt, 20,000 gpm total recirculation flow, with both pumps running. No additional core bypass flow was introduced; i.e., dummy fuel elements removed or baffle doors opened. The power spectrum is normalized for a reactivity oscillation of $\pm$ 10¢ ΔK.

Pre-test analysis case No. 7 is also plotted on Figure VIII-6. The plant conditions analyzed for this prediction were: 25 MWt, 15,000 gpm core flow. The hydrodynamics model used in this analysis assumed that the whole core acted as an average Fuel Cycle AEC element uncoupled from the external loop, and acting as a parallel flow channel. The reactivity worth of voids used in this prediction was 2.65 ¢/% $(\Delta K/\beta)/(\Delta R_g/R_g)$ (per unit value). The doppler effect was omitted.

The peak magnitudes are about the same amplitude. The shapes are similar, but the resonant frequencies are considereably different.

It is observed from Figure VIII-6 that the predicted transfer function is faster in frequency response (displaced to the right) than the experimental data of Series 15-1. A large share of this discrepancy can probably be explained by the fact that the core hydraulics of the 15-1 test does not respond as an uncoupled parallel channel. The parallel channel hydraulic condition used in the prediction has a higher frequency response than the series core plus recirculation loop condition. This unrealistic appraisal of the coolant loop condition should have had a large effect. This is demonstrated in Figure VII-3 for a different condition. Another effect which may have contributed to the frequency discrepancy is the void coefficient of reactivity. If a lower value of the void reactivity coefficient were used in the prediction, the predicted curve would slow down in frequency response, and thus more closely approach the experimental curve. Experimental data (See Section VII-B) indicates that the predicted void coefficients are slightly high. A decrease in the void coefficient, however, not only reduces the speed of the frequency response somewhat, but also causes a <u>decrease</u> in the peak magnitude of the predicted transfer function. This effect is not in the direction of closer correlation since it is observed that the predicted peak magnitude is already less than the experimental peak magnitude. Therefore, the answer to both the frequency and peak magnitude discrepancies between the two curves cannot be found in the void coefficients alone. Additional effects, such as the hydraulics, hold the answer. It is probable that the omission of the doppler effect is a significant contribution. Multi-node representation of the fluid dynamics is known to reduce the speed of response of voids and, hence, the reactivity response.[5][18]

b. <u>Low Flow Forced Circulation - Loop Hydrodynamics</u>

Figure VIII-7 presents a plot of the power transfer function of the 15-9 series test (November 22, 1961) as measured by the out-of-core micro-microammeter. The plant conditions were: 15 MWt,

4,000 gpm total recirculation flow with pump number 1. The pump flow rate was controlled by exhaust valve throttling. No additional core bypass flow was introduced; i.e., dummy fuel elements removed or baffle doors opened. The power spectrum is normalized for a reactivity oscillation of $\pm$ 10¢ ΔK.

Pre-test analysis case No. 37 is also plotted on Figure VIII-7. The plant conditions analyzed for this prediction were: 20 MWt, 3,750 gpm core flow with valve flow control, and no additional core bypass flow introduced. The hydrodynamics model used in this analysis assumed that the whole core acted as an average Fuel Cycle AEC element coupled in series with the external recirculation flow loop. The reactivity worth of voids used in this prediction was 2.65 ¢/% $(\Delta K/\beta) \Big/ (\Delta R_g / R_g)$ (per unit value). The doppler effect was omitted.

The correlation between the two curves is good. The resonant frequencies are very close, the shapes are similar, and the peak magnitudes are of the same order. It can be observed from Figure VIII-7 that the predicted transfer function is of lower frequency response (displaced to the left) than the experimental data of Series 15-9. This can be explained in part by the difference between the flows of the two cases. However, it is felt that flow difference cannot account for all of the difference. It is also observed by a comparison of the two curves that the experimental curve peaks at a higher value than does the predicted curve. This could perhaps be explained by postulating that a low value of void reactivity coefficient was used for the pre-test analysis. Rod oscillator data show that the void reactivity coefficient of the VBWR core for this flow condition is nearly twice the 2.65 ¢/% value used in the pre-test analysis (see Section VII-B). An increase in the void coefficient not only affects the peak amplitude of the transfer function, but also will alter the magnitude of the low frequency end of the transfer function. This effect will also be in the direction of closer correlation. In addition,

as was mentioned earlier, an increased void coefficient will also cause an increase in the predicted function resonant frequency. This effect is also in the direction of closer correlation since the experimental curve is higher in resonant frequency than the predicted curve. Thus, it is seen that an adjustment or normalization for an increased void coefficient in the predicted results will cause a closer correlation in shape, resonant frequencies, and peak magnitudes. As in the previous case, it is probable that the omission of the doppler effect is a significant contribution.

c. Low Flow Forced Circulation - Parallel Channel Hydrodynamics

Figure VIII-7 contains a plot of the parallel channel pre-test analysis case No. 27. The plant conditions for this analysis are identical to those of the analysis already discussed (No. 37) except that the Fuel Cycle element was assumed to be hydrodynamically uncoupled from the rest of the core, and the external recirculation loop. The same experimental curve presented in Figure VIII-7 is plotted on this graph for reference. Rod oscillator test results (see Section VII-B) show that a comparison of the response of the instrumented assemblies in-core ion chambers with the out-of-core micro-microammeters presents no apparent difference. Therefore, for discussion purposes, the experimental curve of Figure VIII-8 can be considered to be an in-core flux response.

It is observed that the correlation between the parallel channel predicted and experimental power transfer functions is not nearly as well established as was the loop hydrodynamics correlation. Although the peak amplitudes appear to be close in frequency and peak magnitude, this is of relatively insignificant value. Noteworthy is the fact that the experimental curve shows no characteristic dip on the low frequency side of the resonant peak. This dip, which is displayed in the parallel channel prediction, is a hydrodynamic resonance.

A first speculation which can be drawn from this comparison is that resonant parallel channel mechanisms of significant contri-

bution do not exist in forced circulation. This is reasoned because the experimental curve does not show any sign of hydraulic resonance which, by prediction, would exist for uncoupled parallel channels. This speculation, however, is not conclusive. The VBWR core is small enough that the flux in any one channel is determined by some average or the weighted averages of the fluxes in the remainder of the core. In other words, the power transfer function of a single channel or small group of channels is not independent of the rest of the core. Therefore, the existence or non-existence of a parallel channel mechanism within the VBWR core cannot be proved by an experimental power transfer function alone. It is felt, however, that the flow transfer function for a single fuel element is not so closely coupled with the rest of the core and, therefore, can be used to investigate the behavior of the parallel channelmechanism. Thus far, no flow from power transfer functions have been established from closed circuit, forced circulation rod oscillator data.

The natural circulation test, however, showed some indications of a power driven flow behavior. This absence of power driven flow behavior gives reasonable credence to the earlier conclusion that parallel channel mechanisms of significant contribution do not exist in the VBWR. Thus, significant parallel flow channel mechanisms are seen to exist in natural circulation. Nevertheless, this parallel channel behavior is different than in forced circulation. Here, the separate flow channels are not primarily acting in parallel with each other, but for the most part, are individually acting in parallel with a common, almost unrestrained, recirculation flow path within the reactor vessel.

d. Natural Circulation

Figure VIII-9 presents a plot of the power transfer function of the 15-18 series test (December 11, 1961) as measured by the out-of-core micro-microammeter. The plant conditions were: 15 MWt, and natural circulation within the reactor vessel. The core

baffle doors were opened to allow this flow configuration. The power spectrum is normalized for a reactivity oscillation of $\pm$ 10¢ ΔK.

Pre-test analysis case No. 17 is also plotted in Figure VIII-9. The plant conditions analyzed for this prediction were: 20 MWt, and 4,675 gpm total core flow. Case No. 17 represents the responses of the Consumers High Power Density elements uncoupled from the external loop and acting as a freely floating parallel flow channel. The 4,675 gpm core flow pre-test condition was selected for comparison rather than the 3,750 gpm condition because it is considered to be nearer the experimental natural circulation condition (core flow during natural circulation is not known and can only be estimated). This element represents the response of a higher void coefficient (4.5 ¢/% $\Delta K/\beta$ / $\Delta R_g/R_g$) (per unit values) compared to the 2.65 ¢/% value for the Fuel Cycle element. The corresponding Fuel Cycle element may be compared by examining Case 19 of Table VIII-2. The Doppler effect is omitted.

The correlation between the two curves is very good. The resonant frequencies are very close, the shapes are quite similar, and the peak magnitudes are almost identical. It is observed from Figure VIII-9 that the experimental transfer function displays the characteristic dip on the low frequency side of the resonant peak which denotes the presence of under-damped core hydraulics. It is of great importance to note that the parallel channel pre-test analysis predicted this behavior. The implications of this correlation are two-fold:

1. The hydraulic component model used in the reactor dynamics model (see Section VIII-A) is capable of displaying a hydrodynamic resonance and does a reasonable job predicting where this condition will occur.
2. The VBWR core, in natural circulation, can be visualized as a

bank of flow channels acting in parallel with an essentially unrestrained downcomer.

If case No. 19, shown in Table VIII-2, were plotted on this curve, it would show the essential difference of a lower amplitude at the peak frequency. This points out that the average channel responses of the reactor have not been defined by this pre-test analysis. The advanced data analysis program will attempt improvement in the understanding of the average channel responses. This will be accomplished by analysis of the neutron physics and thermal hydraulic portions in a way that will provide weighted estimates of the contribution of various core areas upon responses. At least three areas of improvement are noted to be necessary, as pointed out previously. These are:

1. Use of a digital system analysis code
2. A multi-node hydraulics representation
3. Improved representation of the steady-state gains (void coefficient, Doppler effect).

e. Conclusions

In general, the correlation between predicted and experimental power transfer functions is good. Correlations for some test conditions are better than for others. The natural circulation prediction appears to provide the best correspondence, while the high flow, forced circulation prediction gave the poorest correspondence. In most cases, it is impossible to assess the degree of discrepancy that exists between prediction and experiment. This difficulty arises because of obvious inconsistencies and omissions which occur in the present model predictions. It is suggested that the omissions and inconsistencies be remedied and incorporated with a subsequent analysis and compared to the observed discrepancies reported here. There follows a discussion of the discrepancies, inconsistencies and omissions which were observed to exist between the analysis and experiment.

There is a trend concerning the fuel thermal time constants which is displayed consistently throughout all of the comparisons. This trend indicates that the predicted heat transmission of the fuel rods is slower in response than exist in experiment. This discrepancy can be observed by comparing the relative frequencies of the first "up-break" in the power transfer function as the curve passes from the low frequency end toward the high frequency end. This condition has been observed and reported before.[8]

It is generally concluded that the omission of the Doppler effect in the predictions may have introduced significant discrepancies between analysis and experiment. This effect should be included in subsequent analyses and predictions of the VBWR tests.

The hydraulic conditions assumed for the pre-test analysis were, at best, only "close" to the test conditions during experiment. This inconsistency is considered to have a considerable effect upon the correlation of analysis and experiment. New model predictions should be calculated for the VBWR tests. These predictions should include hydraulic model solutions for the actual test conditions of the experiment.

The void coefficients of reactivity used in the pre-test analysis appear to error by as much as a factor of two in some cases. This condition may be a discrepancy between analysis and experiment, or an inconsistency in the analysis, or a combination of both. An inconsistency in the analysis would occur if the reactivity coefficients were calculated for a core void configuration which is not consistent with the hydrodynamics model. This possibility is likely since the physics calculations were based upon a steady-state hydraulics model quite different in its scope, assumptions, and limitations from the hydrodynamics model used in the transfer function predictions. These models should be examined and normalized for subsequent analysis. A comparison of predictions, known to be devoid of void model inconsistency, and VBWR experiment would provide a good measure of the discrepancy between an-

alysis and experiment. No such comparison can be made at this time with the present predictions.

The void coefficient of reactivity does not, by itself, determine the total gain of the regenerative reactivity caused by power-produced voids. It just merely assigns a reactivity worth, or gain, to a void change. This void change, at the same time, is related to power variation by a separate gain relationship. The series combination of these two contributing effects constitute the total gain of the regenerative void reactivity. It is impossible to determine from reactor data alone what the relative contributions of these two effects are to the total feedback gain. This is one reason why out-of-pile, two-phase loop experiments are an absolute necessary supplement to reactor tests. Once the voids from power relationship is determined from two-phase loop data, the reactivity from voids can be established from reactor data.

The regenerative reactivity caused by power-produced voids is the dominant factor in boiling water reactor dynamics. Other considerations are, of course, important, but this effect is of prime importance; yet, it is probably the least understood. It is for this reason that it should be given the primary development effort in subsequent dynamic studies.

TABLE VIII - 2

PRE-TEST ANALYSIS RESULTS

RESULTS OBTAINED BY ANALOGUE SOLUTION OF THE ANALYTICAL MODEL

ROD OSCILLATOR TEST - CYCLICAL ΔK INSERTION OF $\pm$ 10¢

ASSUMED STEADY-STATE NOISE EXCITATION - CYCLICAL VARIATION IN INLET WATER TEMPERATURE OF $\pm$ 0.1° F.

REACTOR FLUX (N*) - % $\left(\frac{\text{PEAK TO AVERAGE}}{\text{AVERAGE}}\right)$ (PER UNIT VALUES)

INLET WATER VELOCITY (V*) - % $\left(\frac{\text{PEAK TO AVERAGE}}{\text{AVERAGE}}\right)$ (PER UNIT VALUES)

REACTOR CONDITION	RUN NO.	TYPE ANALYSIS	OUTPUT PARAMETER	DISTURBANCE FREQUENCY - CPS															
				0.04	0.08	0.1	0.2	0.4	0.6	0.7	0.8	0.9	1.0	1.2	1.5	2.0	3.0	4.0	8.0
PARALLEL FLOW CHANNEL	HYDRODYNAMICS ONLY		PARALLEL FLOW CHANNEL HYDRODYNAMICS ONLY																
Core Flow = 15,000 gpm, Core Power = 35 MWt	1	Rod Oscillator Test	N* - Reactor Flux	1.8	2.7	3.0	4.0	5.2			6.0		6.3		7.0	7.8	9.2	10.0	9.5
			V* - Inlet Water Velocity	0.0	0.5	0.5	0.5	0.5			0.4		0.3		0.2	0.2	0.05	0.0	0.0
Hottest Consumers instrumented assembly	2	Steady-State Noise	N*	1.0	1.8	2.0	2.9	3.9			4.9		5.4			6.5	6.2	5.3	1.9
			V*	0.0	0.0	0.0	0.2	0.3			0.4		0.5			0.65	0.6	0.5	0.3
Core Flow = 15,000 gpm, Core Power = 35 MWt	3	Rod Oscillator Test	N*	3.9	5.0	5.5	6.8	7.5			8.2		8.4			9.1		10.2	9.5
			V*	0.0	0.0	0.0	0.2	0.3			0.2		0.1			0.0		0.0	0.0
Hottest unorificed Fuel Cycle instrumented assembly	4	Steady-State Noise	N*	1.0	1.4	1.7	1.9	2.2			2.5		2.7			3.0	2.4	1.7	0.5
			V*	0.0	0.0	0.0	0.0	0.2			0.3		0.3			0.3	0.3	0.3	0.2
Core Flow = 15,000 gpm, Core Power = 25 MWt	5	Rod Oscillator Test	N*	3.5	4.6	5.0	6.6	7.3			8.1		8.5			9.4		10.9	9.6
			V*	0.0	0.0	0.0	0.0	0.0			0.0		0.0			0.0		0.0	0.0
Hottest Consumers instrumented assembly	6	Steady-State Noise	N*	1.5	1.9	2.0	2.4	2.9			3.8		4.2			4.6	3.7	2.6	0.7
			V*	0.0	0.0	0.0	0.0	0.1			0.2		0.3			0.3	0.3	0.3	0.3
Core Flow = 15,000 gpm, Core Power = 25 MWt	7	Rod Oscillator Test	N*	3.5	4.5	5.0	6.5	7.3			8.1		8.3			9.2		11.0	9.5
			V*	0.0	0.0	0.0	0.0	0.1			0.2		0.1			0.0		0.0	0.0
Hottest unorificed Fuel Cycle instrumented assembly.	8	Steady-State Noise	N*	1.5	1.8	2.0	2.5	2.9			3.7		4.1			4.5	3.7	2.8	0.7
			V*	0.0	0.0	0.0	0.0	0.1			0.2		0.3			0.3	0.3	0.3	0.3
Core Flow = 7,650 gpm, Core Power = 20 MWt	9	Rod Oscillator Test	N*	2.3	3.0	3.5	4.5	5.0			5.8		7.3			11.3		11.0	9.3
			V*	0.0	0.1	0.1	0.2	0.3			0.3		0.2			0.1		0.0	0.0
Hottest Consumers instrumented assembly	10	Steady-State Noise	N*	0.9	1.2	1.4	1.9	2.6			4.6		5.6		6.4	5.6	3.4	2.0	0.4
			V*	0.0	0.02	0.04	0.07				0.28		0.32		0.34	0.32	0.22	0.24	0.2
Core Flow = 7,650 gpm, Core Power = 20 MWt	11	Rod Oscillator Test	N*	4.0	5.0	5.8	6.8	7.0			8.3		9.5			11.0		9.5	8.8
			V*	0.15	0.25	0.3	0.3	0.25			0.25		0.2			0.1		0.05	0.0
Hottest unorificed Fuel Cycle instrumented assembly	12	Steady-State Noise	N*	0.8	1.0	1.2	1.4	1.7			3.1		3.5		3.3	2.3	1.2	0.6	0.2
			V*	0.02	0.04	0.05	0.06	0.12			0.20		0.22		0.24	0.22	0.20	0.20	0.18
Core Flow = 7,650 gpm, Core Power = 10 MWt	13	Rod Oscillator Test	N*	2.2	3.0	3.3	4.4	5.3			6.5		7.6			11.5	11.3	11.0	9.5
			V*	0.0	0.04	0.08	0.12	0.16			0.12		0.12			0.08	0.06	0.04	0.0
Hottest Consumers instrumented assembly	14	Steady-State Noise	N*	2.0	2.8	3.0	4.0	5.8			9.3		10.8		12.3	11.2	7.0	4.0	1.0
			V*	0.0	0.0	0.0	0.0	0.1			0.2		0.2		0.2	0.2	0.2	0.1	0.1
Core Flow = 7,650 gpm, Core Power = 10 MWt	15	Rod Oscillator Test	N*	3.7	4.9	5.1	6.5	7.0			9.0		10.5			11.0	10.0	10.0	9.5
			V*	0.2	0.2	0.2	0.2	0.2			0.2		0.15			0.1	0.08	0.06	0.04
Hottest unorificed Fuel Cycle instrumented assembly.	16	Steady-State Noise	N*	1.5	2.2	2.5	3.0	4.0			6.5		7.5		5.7	4.0		1.0	0.3
			V*	0.1	0.1	0.1	0.1	0.2			0.3		0.4		0.4	0.35		0.3	0.2

TABLE VIII - 2 (Continued)

REACTOR CONDITION	RUN NO.	TYPE ANALYSIS	OUTPUT PARAMETER	DISTURBANCE FREQUENCY - CPS														
				0.04	0.08	0.1	0.2	0.4	0.6	0.7	0.8	0.9	1.0	1.2	1.5	2.0	3.0	4.0	8.0
PARALLEL FLOW	CHANNEL	HYDRODYNAMICS ONLY	PARALLEL FLOW	CHANNEL HYDRODYNAMICS ONLY															
Core Flow = 4675 gpm Core Power = 20 MWt	17	Rod Oscillator Test	N* - Reactor Flux	3.2	4.2	4.8	5.2	4.8			7.0		11.2		14.5	12.5	10.5	9.5	9.0
			V* - Inlet Water Velocity	0.4	0.4	0.4	0.6	0.8			1.0		1.2		0.6	0.4	0.2	0.15	0.1
Hottest Consumers instrumented assembly	18	Steady-State Noise	N*	1.0	1.0	1.0	1.0	1.6			3.8		4.2		3.0	2.0		0.8	0.3
			V*	0.0	0.2	0.3	0.4	0.45			0.5		0.5		0.4	0.35		0.25	0.2
Core Flow = 4675 gpm Core Power = 20 MWt	19	Rod Oscillator Test	N*	5.3	6.2	6.7	7.0	6.5			10.5		12.0			10.5		9.8	9.3
			V*	1.2	1.0	0.9	0.8	0.7			0.7		0.6			0.4		0.3	0.2
Hottest unorificed Fuel Cycle instrumented assembly	20	Steady-State Noise	N*	0.4	0.5	0.6	0.7	1.2		2.4	2.8	2.7	2.5			0.8		0.3	0.1
			V*	0.1	0.15	0.2	0.2	0.3		0.4	0.4	0.4	0.4			0.3		0.2	0.15
Core Flow = 4675 gpm Core Power = 10 MWt	21	Rod Oscillator Test	N*	3.0	4.0	4.4	5.0	4.8			8.5		12.0			12.5		10.2	9.3
			V*	0.3	0.4	0.4	0.4	0.4			0.4		0.4			0.2		0.1	0.1
Hottest Consumers instrumented assembly	22	Steady-State Noise	N*	1.0	1.4	1.6	2.0	3.5	5.5		7.6		9.4		7.2	4.0		0.9	0.2
			V*	0.1	0.2	0.2	0.2	0.3	0.4		0.4		0.5		0.4	0.3		0.2	0.2
Core Flow = 4675 gpm Core Power = 10 MWt	23	Rod Oscillator Test	N*	5.0	6.0	6.0	6.5	6.2	9.5		13.0		13.5			10.7		10.0	9.1
			V*	1.0	0.8	0.7	0.6	0.5	0.5		0.45		0.35			0.2		0.15	0.1
Hottest unorificed Fuel Cycle instrumented assembly	24	Steady-State Noise	N*	0.8	1.2	1.2	1.6	2.9		5.3	5.5	4.8	4.3			1.0		0.2	0.2
			V*	0.1	0.2	0.2	0.25	0.35		0.4	0.4	0.4	0.35			0.3		0.2	0.2
Core Flow = 3750 gpm Core Power = 20 MWt	25	Rod Oscillator Test	N*	4.0	5.0	5.2	5.5	4.5			7.0		14.0	17.5	15.0	13.0	11.0	10.0	8.9
			V*	1.2	1.0	0.9	0.8	1.0			1.4		1.6	1.35	0.9	0.5	0.3	0.25	0.2
Hottest Consumers instrumented assembly	26	Steady-State Noise	N*	0.4	0.4	0.45	0.6	1.2	2.4		4.2		5.7	5.0	3.5	1.6		0.4	0.1
			V*	0.1	0.1	0.15	0.2	0.25	0.4		0.55		0.7	0.6	0.5	0.3		0.2	0.2
Core Flow = 3750 gpm Core Power = 20 MWt	27	Rod Oscillator Test	N*	6.0	6.9	7.1	7.0	5.5	7.2		12.5	13.8	14.1			10.5		9.4	9.3
			V*	2.6	1.8	1.6	1.2	1.1	1.28		1.24	1.1	0.84			0.4		0.3	0.2
Hottest unorificed Fuel Cycle instrumented assembly	28	Steady-State Noise	N*	0.2	0.25	0.3	0.4	1.0	1.9	2.3	2.4	2.2	2.0		0.8	0.5		0.2	0.0
			V*	0.1	0.16	0.18	0.2	0.24	0.34	0.4	0.4	0.4	0.36		0.26	0.24		0.2	0.2
Core Flow = 3750 gpm, Core Power = 20 MWt Hottest Fuel Cycle instrumented assembly - inlet orificing = 2X inlet loss with no orifice	29	Rod Oscillator Test	N*	6.0	7.0	7.0	7.0	6.5	10.0	11.5	12.5	12.5	12.0			10.3		9.7	9.2
			V*	2.2	1.6	1.4	1.1	0.9	1.0	1.0	0.86	0.76	0.64			0.4		0.3	0.2
	30	Steady-State Noise	N*	0.2	0.3	0.3	0.4	0.8	1.3	1.5	1.3	1.1	1.0		0.4	0.3		0.1	0.0
			V*	0.10	0.14	0.16	0.18	0.20	0.22	0.22	0.22	0.20	0.20		0.20	0.20		0.18	0.14
Core Flow = 3750 gpm, Core Power = 20 MWt Hottest Fuel Cycle instrumented assembly - inlet orificing = 3.5X inlet loss with no orifice	31	Rod Oscillator Test	N*	6.0	7.0	7.2	7.0	8.0	11.5	12.5	12.2	12.0	11.5			10.2		9.6	9.5
			V*	2.0	1.44	1.34	1.0	0.9	0.8	0.7	0.6	0.56	0.5			0.4		0.36	0.30
	32	Steady-State Noise	N*	0.2	0.3	0.3	0.4	0.7	0.9	0.8	0.7		0.5			0.2		0.1	
			V*	0.1	0.1	0.2	0.2	0.2	0.2	0.2	0.2		0.2			0.2		0.2	

TABLE VIII - 2 (Continued)

REACTOR CONDITION	RUN NO.	TYPE ANALYSIS	OUTPUT PARAMETER	DISTURBANCE FREQUENCY - CPS															
				0.04	0.08	0.1	0.2	0.4	0.6	0.7	0.8	0.9	1.0	1.2	1.5	2.0	3.0	4.0	8.0
PARALLEL FLOW CHANNEL	HYDRODYNAMICS	ONLY		PARALLEL FLOW CHANNEL HYDRODYNAMICS ONLY															
Core Flow = 3750 gpm, Core Power = 20 MWt Hottest Fuel Cycle instrumented assembly - inlet orificing = 5 X inlet loss with no orifice	33	Rod Oscillator Test	N*	6.2	7.0	7.6	7.5	9.2	12.2	12.2	12.0	11.5	11.2		10.3	10.0		10.0	9.4
			V*	2.0	1.5	1.3	1.0	0.85	0.65	0.55	0.5	0.45	0.4		0.35	0.3		0.3	0.3
	34	Steady-State Noise	N*	0.2	0.2	0.3	0.4	0.6	0.7		0.5		0.3			0.1		0.0	
			V*	0.1	0.15	0.15	0.2	0.2	0.15		0.1		0.1			0.15		0.15	
Core Flow = 3750 gpm, Core Power = 20 MWt Hottest Fuel Cycle instrumented assembly - Inlet orificing 7X inlet loss with no orifice	35	Rod Oscillator Test	N*	6.5	7.2	7.5	8.0	10.3	12.3		11.3		11.0			10.0		9.8	9.3
			V*	1.9	1.35	1.2	0.9	0.7	0.5		0.45		0.4			0.4		0.4	0.3
	36	Steady-State Noise	N*	0.2	0.2	0.2	0.35	0.55	0.50		0.35		0.20			0.1		0.0	
			V*	0.1	0.1	0.1	0.1	0.1	0.08		0.07		0.05			0.1		0.15	
LOOP DYNAMICS ONLY			LOOP	LOOP HYDRODYNAMICS ONLY							LOOP HYDRODYNAMICS ONLY								
Core Flow = 3750 gpm, Core Power = 20 MWt Valve controlled recirculation flow No dummy fuel plugs removed	37	Rod Oscillator Test	N*	3.7	4.8	5.0	6.0	8.3	11.0		12.5		12.7			10.5		9.8	9.2
			V*	0.1	0.1	0.1	0.1	0.1	0.1		0.1		0.1			0.1		0.1	0.1
	38	Steady-State Noise	N*	0.4	0.55	0.63	0.83	1.4	1.8	1.8	1.7		1.4			0.4		0.1	0.0
			V*	0.0	0.0	0.0	0.0	0.0	0.0	0.0	0.0		0.0			0.0		0.0	0.0
Core Flow = 3750 gpm, Core Power = 20 MWt Valve controlled recirculation flow 3 dummy fuel plugs removed.	39	Rod Oscillator Test	N*	4.0	5.0	5.3	6.0	7.5	10.5		12.0		12.5			10.3		9.9	9.1
			V*	0.2	0.2	0.2	0.2	0.15	0.15		0.12		0.1			0.1		0.1	0.1
	40	Steady-State Noise	N*	0.5	0.6	0.65	0.9	1.5	1.9		1.8		1.55			0.5		0.15	0.0
			V*	0.0	0.0	0.0	0.0	0.1	0.1		0.1		0.1			0.1		0.1	0.1
Core Flow = 3750 gpm Core Power = 20 MWt Pump speed controlled recirculation flow No dummy fuel plugs removed.	41	Rod Oscillator Test	N*	4.0	5.0	5.5	6.3	8.3	11.0		13.0		12.5			10.5		9.7	9.1
			V*	0.2	0.2	0.15	0.15	0.15	0.10		0.10		0.10			0.05		0.05	0.05
	42	Steady-State Noise	N*	0.4	0.55	0.6	0.83	1.35	1.7		1.65		1.35			0.4		0.1	0.0
			V*	0.0	0.0	0.0	0.0	0.0	0.0		0.0		0.0			0.0		0.0	0.0
Core Flow = 3750 gpm, Core Power = 20 MWt Pump speed controlled recirculation flow 3 dummy fuel plugs removed.	43	Rod Oscillator Test	N*	3.5	5.0	5.5	6.0	7.5	10.5		12.3		12.6			11.0		10.0	9.1
			V*	0.3	0.2	0.2	0.2	0.2	0.15		0.15		0.12			0.1		0.1	0.1
	44	Steady-State Noise	N*	0.4	0.6	0.7	0.9	1.5	1.9		1.85		1.6			0.5		0.15	0.05
			V*	0.0	0.0	0.0	0.05	0.05	0.05		0.05		0.05			0.05		0.1	0.1
PARALLEL FLOW CHANNEL HYDRODYNAMICS ONLY			PARALLEL FLOW CHANNEL HYDRODYNAMICS ONLY																
Core Flow = 2980 gpm, Core Power = 20 MWt Hottest Consumers instrumented assembly	45	Rod Oscillator Test	N*	5.0	5.8	6.0	6.0	4.5	2.0	4.5	9.0	15.5	19.5	19.0	15.0	12.0		9.7	9.1
			V*	2.0	1.6	1.5	1.2	1.3	1.55	1.85	2.2	2.5	2.5	1.6	1.0	0.7		0.4	0.3
	46	Steady-State Noise	N*	0.3	0.3	0.3	0.4	0.8	1.8		3.6		5.0		2.0	1.0		0.2	0.05
			V*	0.15	0.15	0.15	0.3	0.3	0.4		0.6		0.8		0.4	0.3		0.2	0.15
Core Flow = 2980 gpm, Core Power = 20 MWt Hottest unorificed Fuel Cycle instrumented assembly	47	Rod Oscillator Test	N*	7.5	7.5	7.5	7.0	5.5	8.5		14.5	15.0	13.3		11.3	10.2		10.0	9.4
			V*	3.8	2.5	2.3	1.6	1.5	1.8		1.6	1.3	1.1		0.6	0.45		0.40	0.30
	48	Steady-State Noise	N*	0.2	0.2	0.2	0.3	0.7	1.6	1.9	1.75		1.2			0.3		0.1	0.0
			V*	0.15	0.2	0.2	0.25	0.3	0.45	0.50	0.50		0.35			0.3		0.3	0.2
Core Flow = 2980 gpm, Core Power = 20 MWt Hottest Consumers instrumented assembly	49	Rod Oscillator Test	N*	4.5	5.3	5.3	4.8	2.0	6.0		18.0	21.5	20.0			11.0		10.0	9.3
			V*	2.2	1.7	1.55	1.2	0.9	1.0		1.5	1.3	0.9			0.3		0.2	0.2
	50	Steady-State Noise	N*	0.3	0.4	0.45	0.8	2.3	5.0	6.6	8.6	8.4	6.6		2.0	1.2		0.3	0.0
			V*	0.2	0.25	0.30	0.35	0.40	0.50	0.6	0.7	0.7	0.6		0.3	0.25		0.2	0.2
Core Flow = 2980 gpm, Core Power = 10 MWt Hottest unorificed Fuel Cycle instrumented assembly.	51	Rod Oscillator Test	N*	6.5	7.0	7.0	6.0	5.3	18.0	17.0	14.5		12.0			10.0		9.8	9.5
			V*	3.5	2.4	2.0	1.5	1.4	1.6	1.0	0.7		0.5			0.3		0.2	0.1
	52	Steady-State Noise	N*	0.3	0.4	0.4	0.6	2.2	4.1	3.0	2.0		1.2			0.3		0.1	0.0
			V*	0.25	0.3	0.3	0.35	0.43	0.6	0.5	0.4		0.3			0.25		0.25	0.2

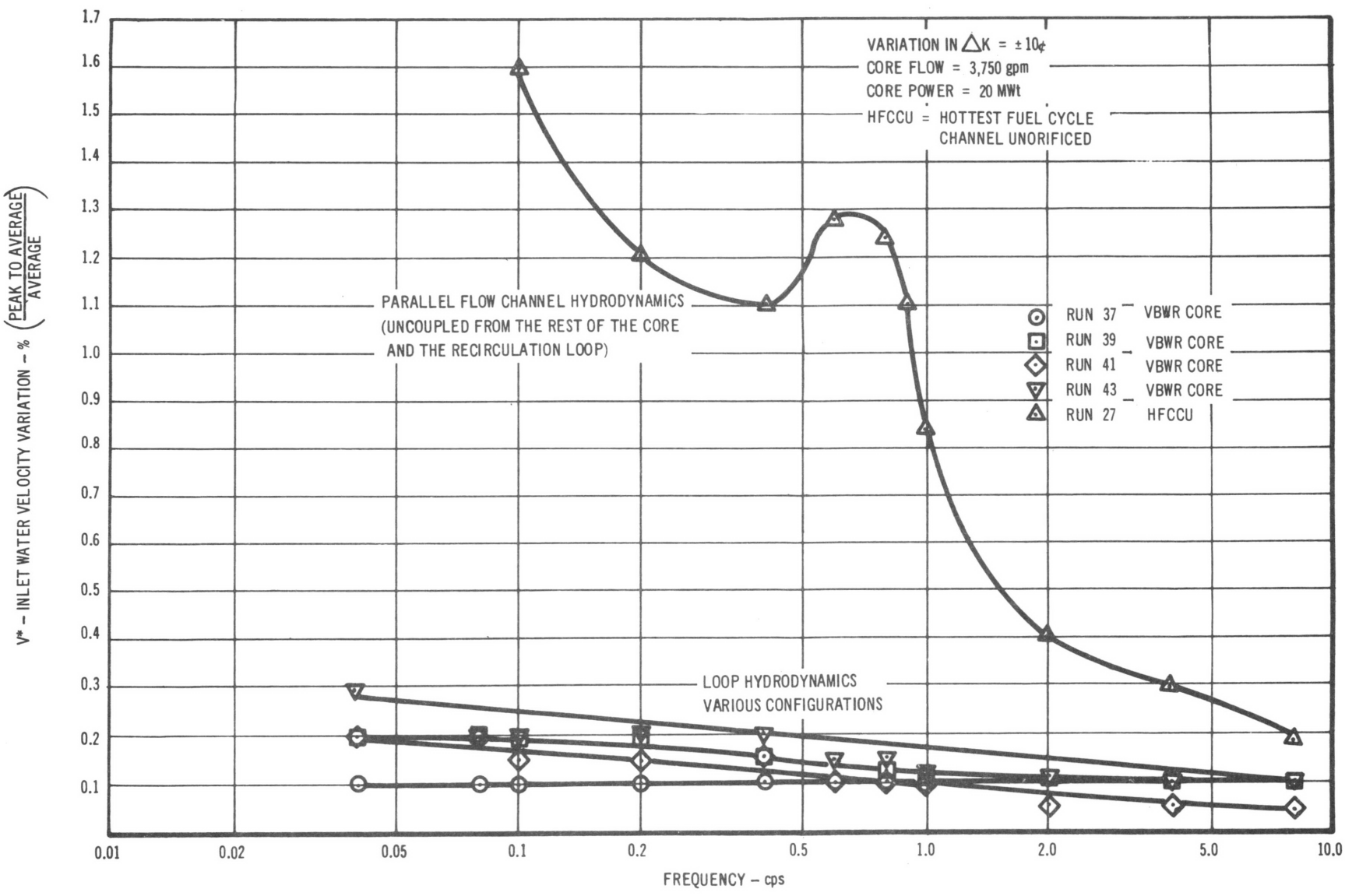

FIGURE VIII–2 FREQUENCY RESPONSE OF INLET WATER VELOCITY (V*) TO CYCLICAL VARIATION IN △K

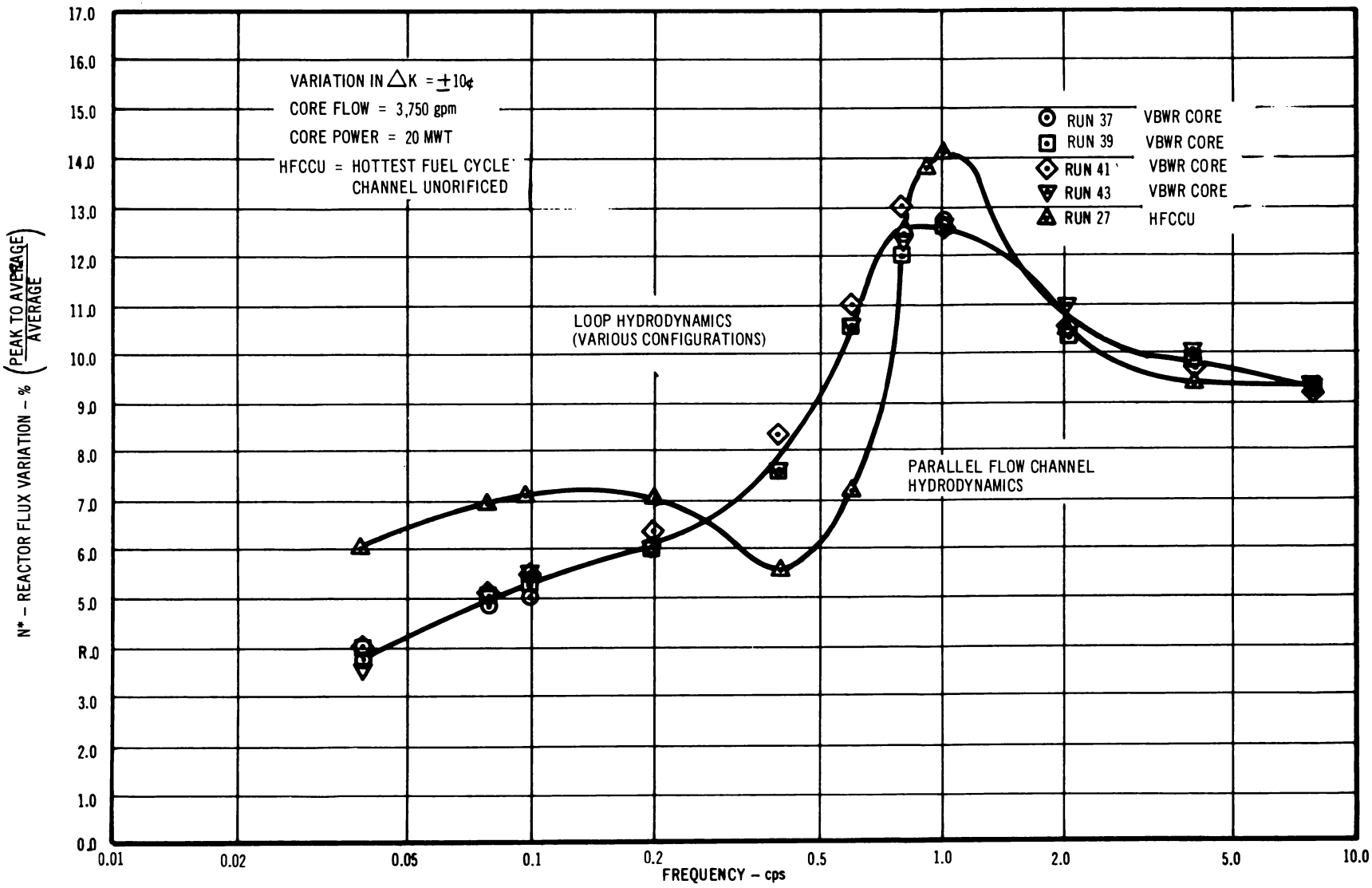

FIGURE VIII–3 FREQUENCY RESPONSE OF REACTOR FLUX (N*) TO CYCLICAL VARIATION IN △K

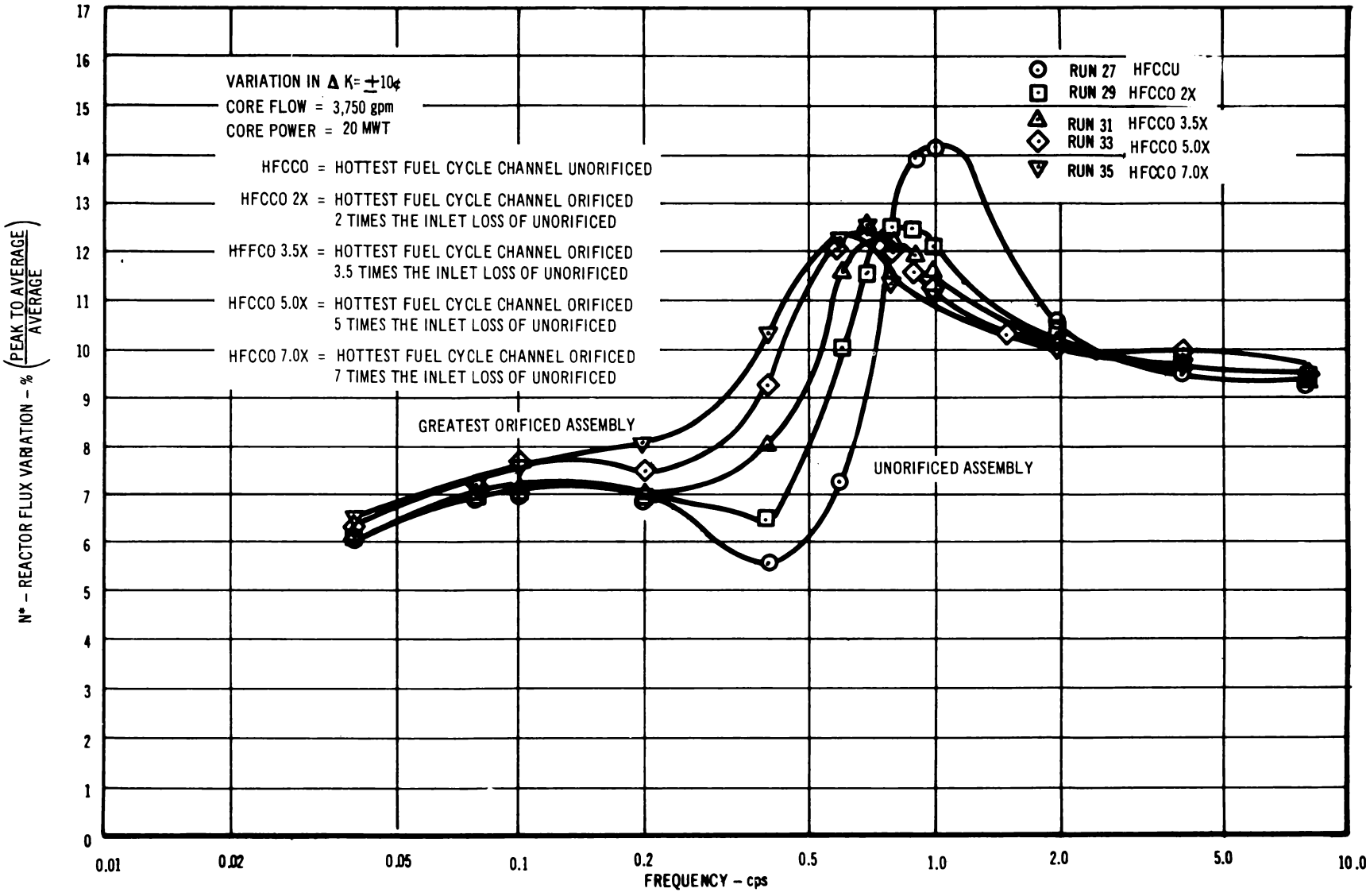

FIGURE VIII–4 FREQUENCY RESPONSE OF REACTOR FLUX (N*) TO CYCLICAL VARIATION IN △K
EFFECT OF INLET ORIFICING UPON PARALLEL FLOW CHANNEL STABILITY

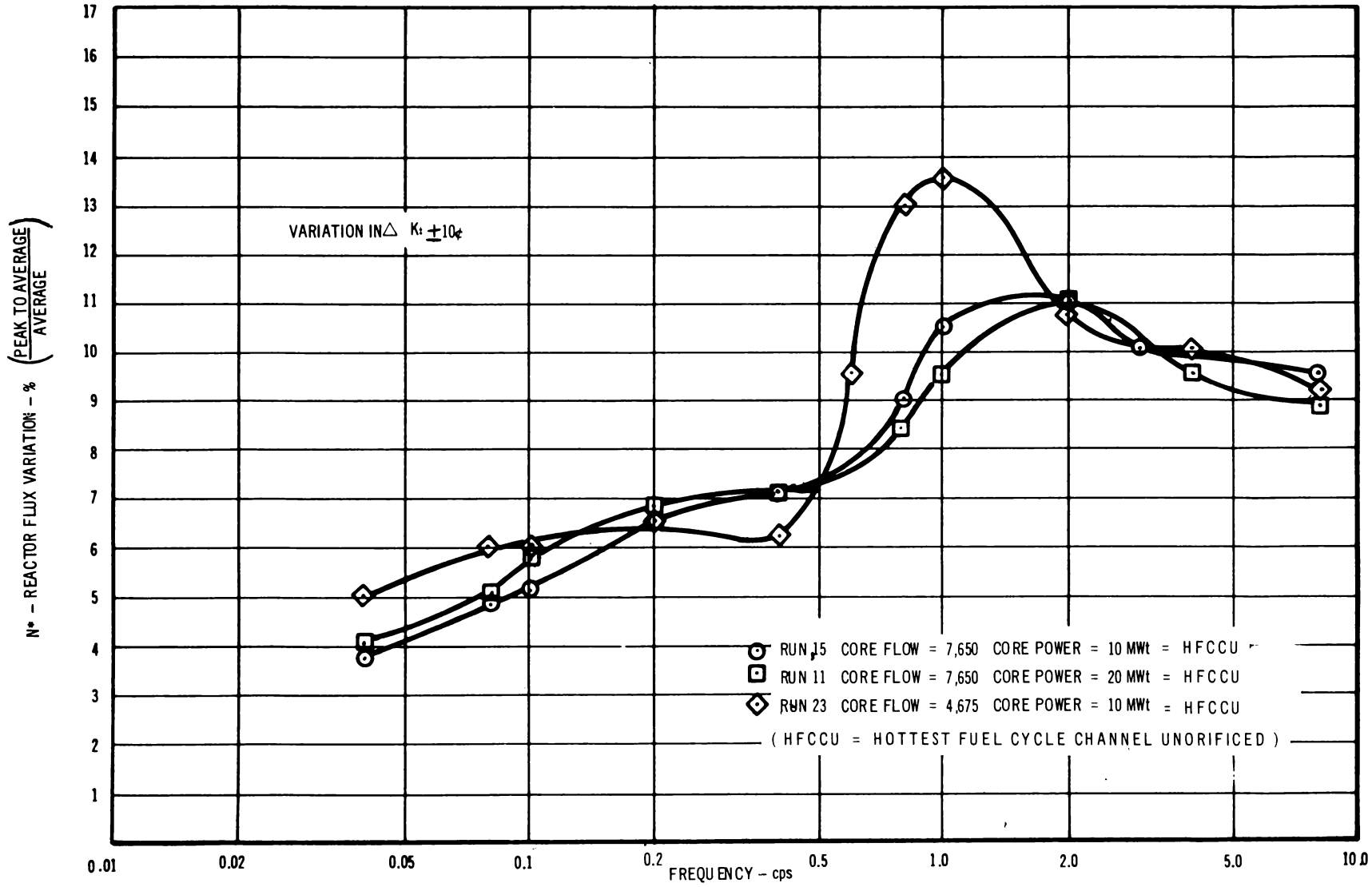

FIGURE VIII-5 FREQUENCY RESPONSE OF REACTOR FLUX (N*) TO CYCLICAL VARIATION IN △K
EFFECT OF POWER AND CORE FLOW UPON PARALLEL FLOW CHANNEL STABILITY

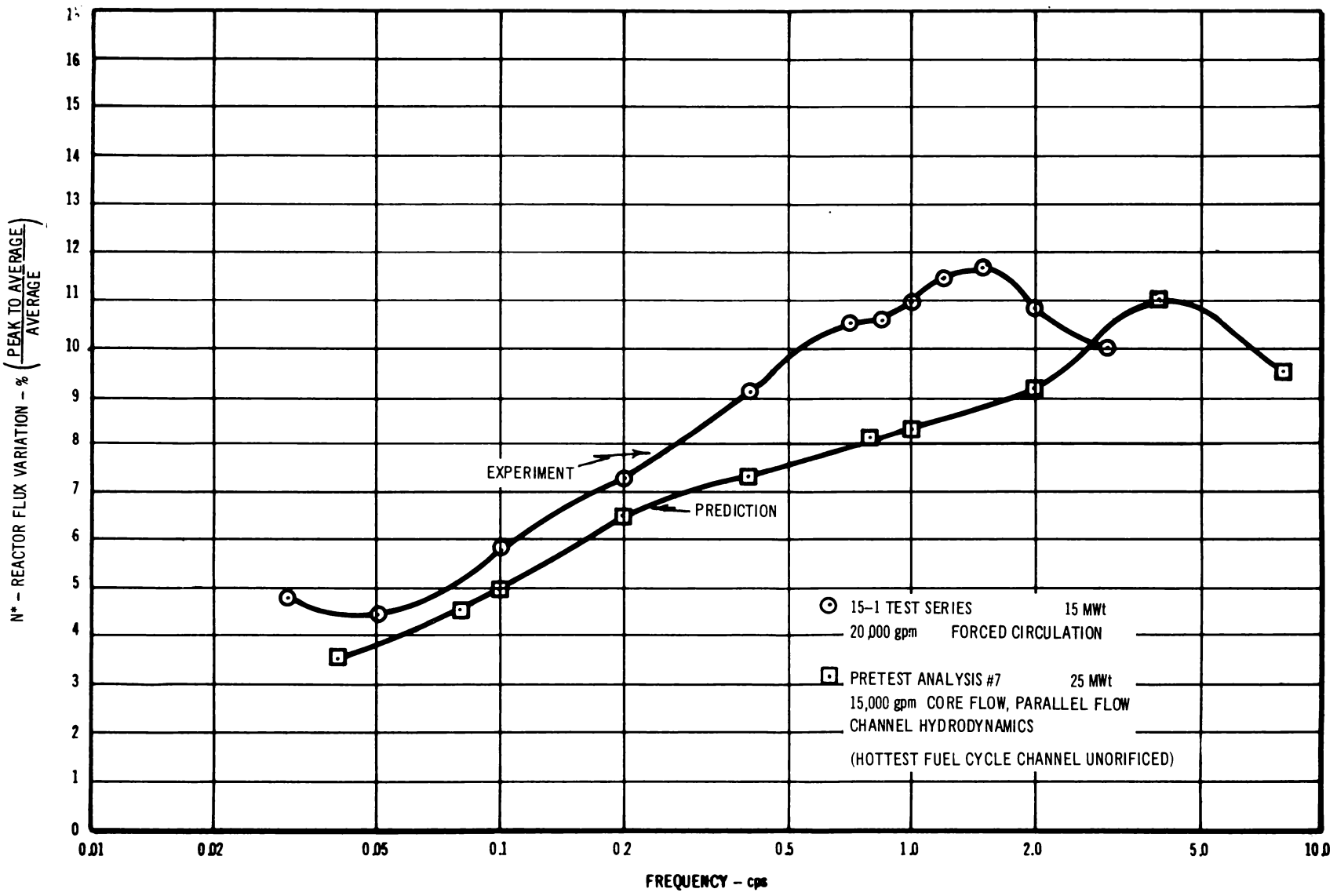

FIGURE VIII-6 **REACTOR POWER TRANSFER FUNCTION COMPARISON OF PREDICTION WITH EXPERIMENT HIGH FLOW - FORCED CIRCULATION**

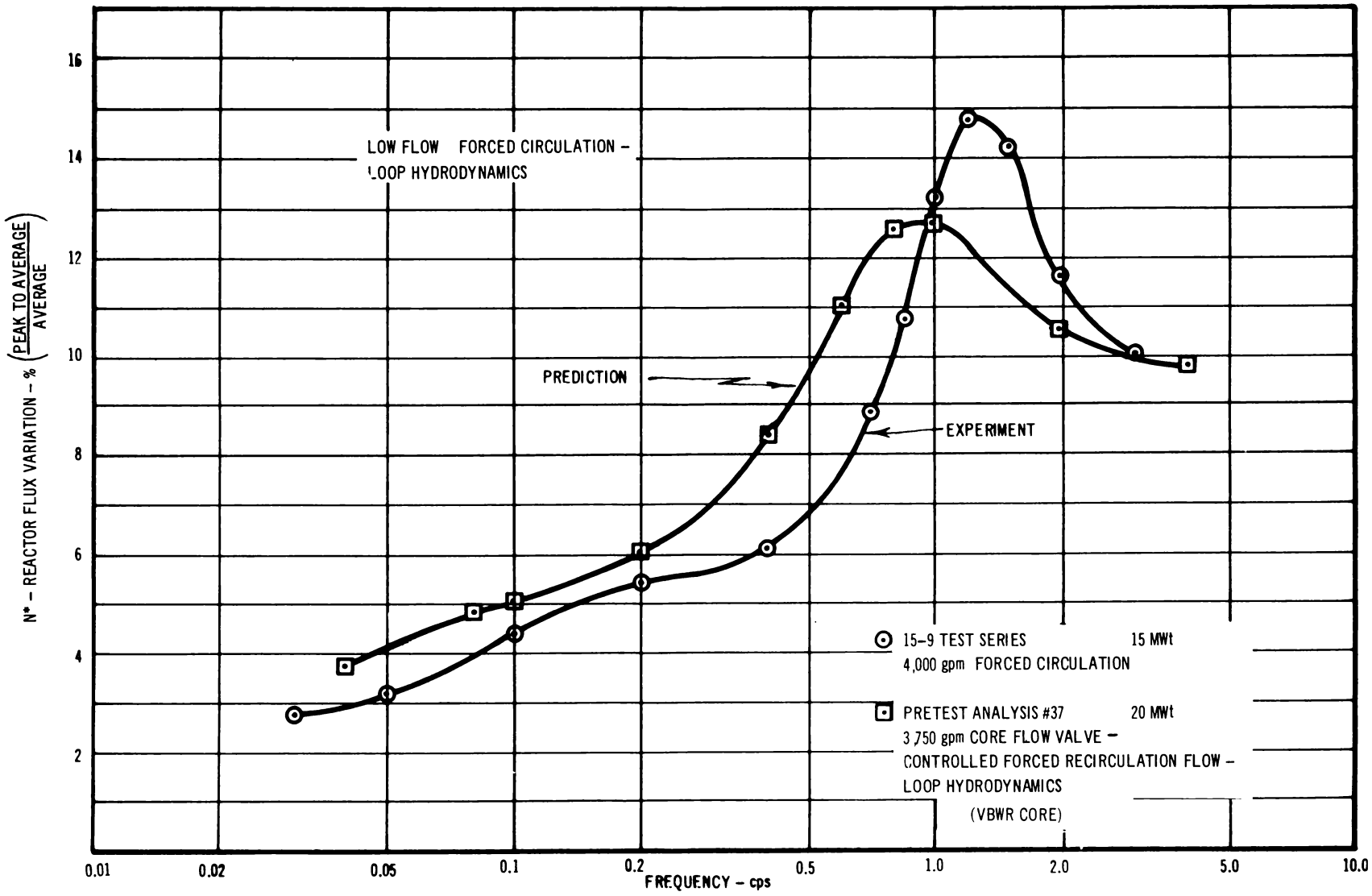

FIGURE VIII–7 REACTOR POWER TRANSFER FUNCTION COMPARISON OF PREDICTION WITH EXPERIMENT

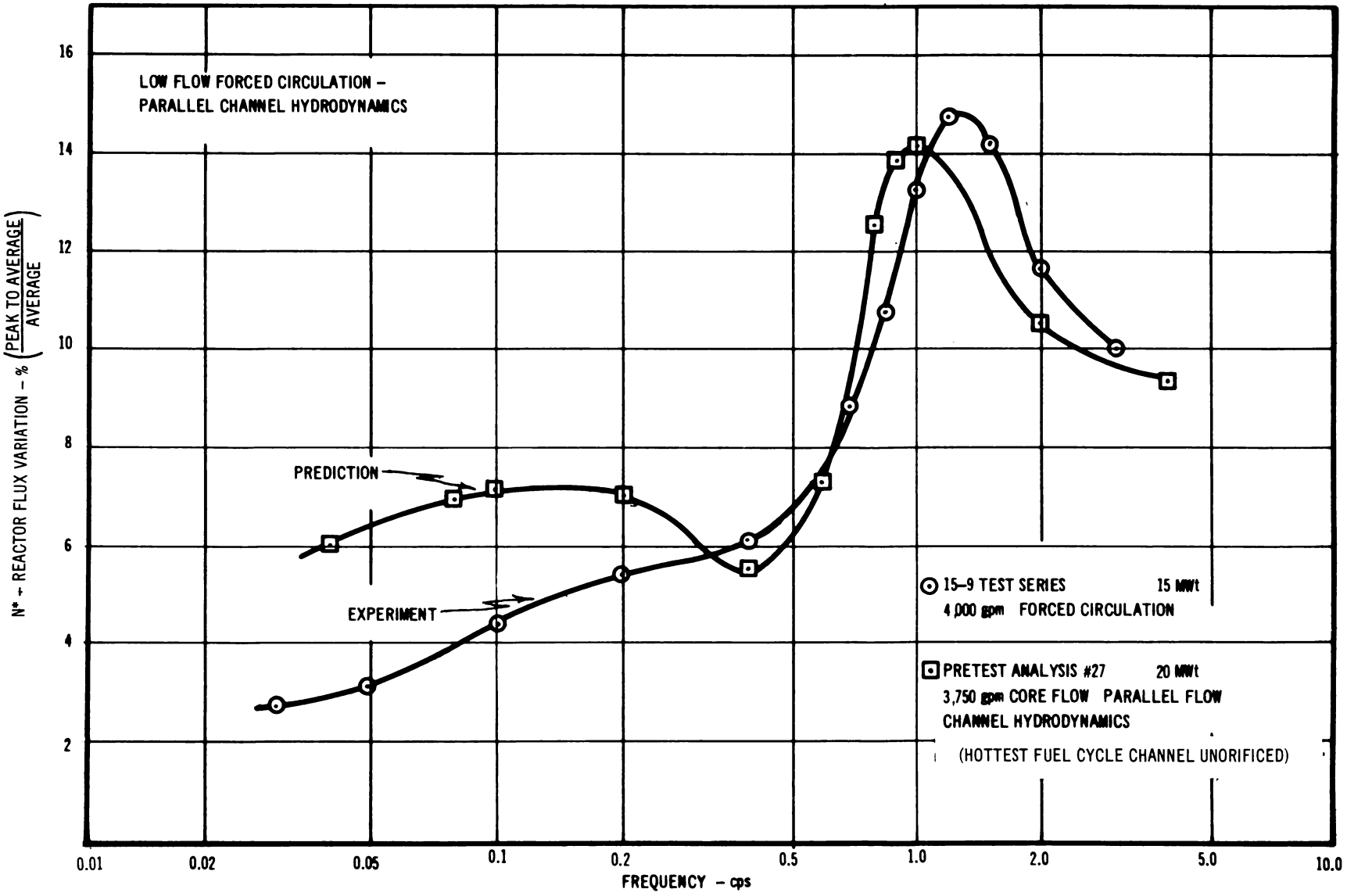

FIGURE VIII–8 **REACTOR POWER TRANSFER FUNCTION COMPARISON OF PREDICTION WITH EXPERIMENT**

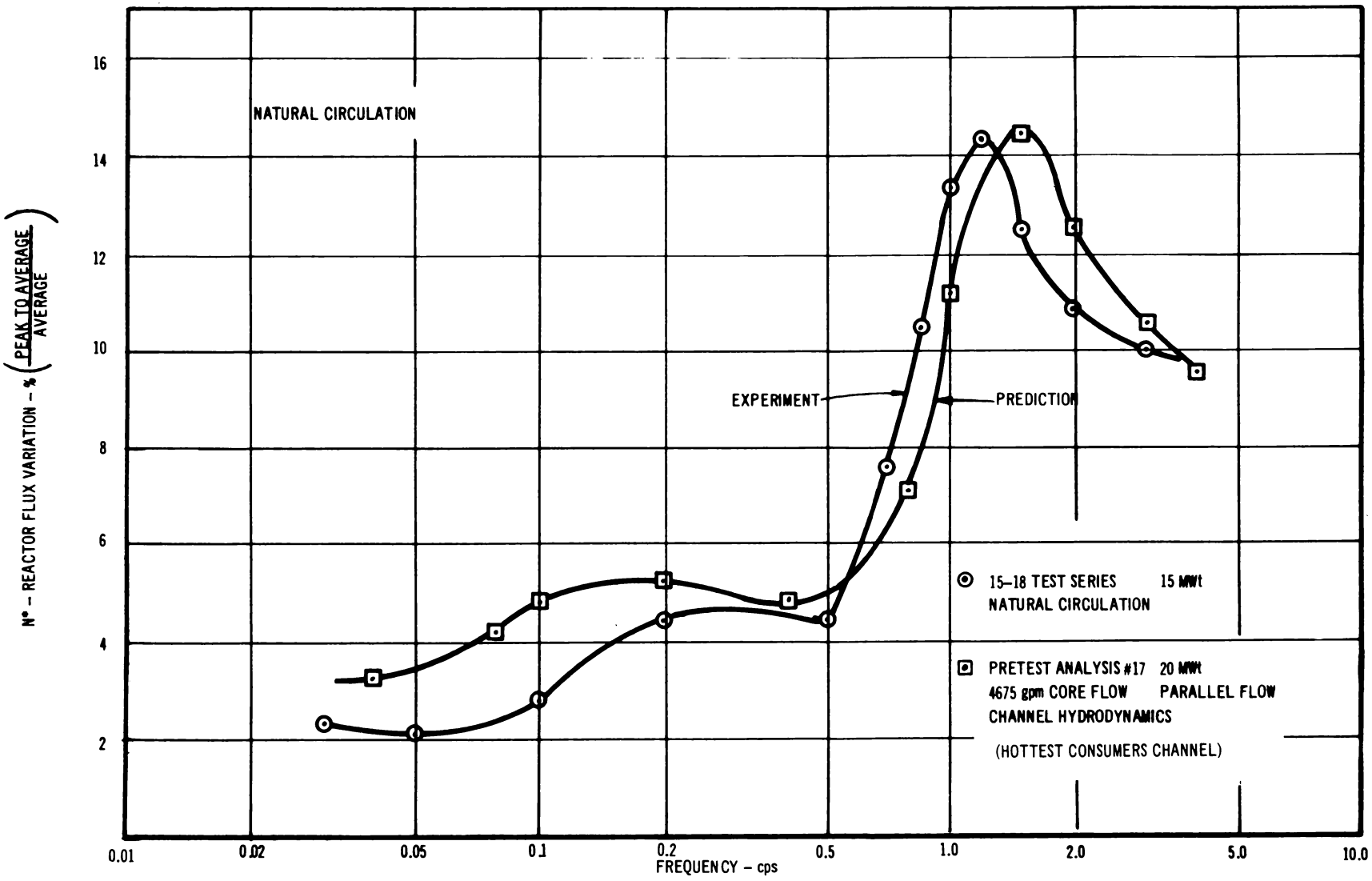

FIGURE VIII–9 **REACTOR POWER TRANSFER FUNCTION COMPARISON OF PREDICTION WITH EXPERIMENT**

SECTION IX

FUTURE WORK

Three types of tests, rod oscillator, transient, and steady-state noise, have been conducted in the VBWR to attain the objectives of the stability program. These objectives, which were discussed in Section III, resolve themselves to three when one considers only the retrieval and development of information from the reactor tests. These are:

1. Adequate description of the significant parameters of the reactor test.
2. A comparison of test and analytical model predictions that provides significant measures of the theories' adequacy, or inadequacy.
3. Analytical models must be improved in a manner where the significance of its predictions can be examined and reactor performance guided.

These three areas make up the areas of endeavor for future work which are important end products, useable directly in the development of improved boiling water reactors.

There are five specific work areas which go into the list of objectives above. These will be discussed in order and related to these major objectives. The work areas are:

1. Improved data retrieval.
2. Improved analysis of VBWR test points.
3. Data contributing to model analysis improvement derived from the hydraulic stability loop.
4. Improved analytical model.
5. Generalization to the design of large plants.

A. Improved Data Retrieval

Conclusions reached in Sections VII and VIII show that the preponderance of the quantitative measures of reactor performance have come from the control rod oscillation tests. No significant information was produced from the transient tests, and, although qualitative information is available from the noise tests, the uncertainties must be evaluated in order to have a well defined set of information. Improved techniques will, however, improve data retrieval from steady-state noise tests.

Data used in this report has been analyzed visually from the Brush recorder traces and by a band pass filtering operation on Ampex magnetic tape records. Discussion of these methods are found in Section VII and Appendix C. The data, on the basis of this analysis, is not considered to be refined data. There are several reasons for this:

a. The limitation of visual analysis is apparent and need not be commented upon.

b. The errors in the analytical methods stem from the nature of the traces examined and band pass filter characteristics which introduce overlap, transient response, and read out errors.

It was recognized at the time tests were conducted that improvements would be necessary. Basically, what is required is to obtain sufficient accuracy and statistical significance to data that the parametric effects of the reactor responses are shown with definition comparable to that obtained by analytical model predictions. When this is accomplished, objective (1) will be realized. Studies have been made of analytical methods and are summarized briefly in Appendix E. Two improved methods have been derived from these studies that are to be useful in analysis of test data. These are:

1. A digital code for auto correlation and cross correlation called DART.
2. A Fourier spectrum analyzer which performs precise mathematical operations by analogue methods.

Both of these methods are substantially improved methods over those used in the data retrieval shown in this report. Their development has been funded by APED. Some details of their properties are given in Appendix E.

A so-called advanced data program will be carried out on the significant runs from the stability test to provide the data refinement discussed earlier. The data analysis will be done primarily with the Fourier spectrum analyzer, which is able to accept Ampex tape records directly. Additional runs will be made, as necessary, with the digital auto correlation code to aid in identifying physical events which are significant to analytical model development.

The rod oscillator runs will be examined to obtain refined estimates of the power and flow transfer functions for the five runs which were examined in this report. Significantly, the output of the Fourier spectrum analyzer will not only provide amplitude responses, but phase responses as well. This will be of a great deal of value in detailed examination of the analytical models. Only amplitude data could be reduced from the traces by the previous methods of analyzing the data. The auto- and cross-correlation code will be used on specific runs for a reference for the Fourier spectrum analyzer, and for the purpose of identifying the specific influence of measured variables upon one another. This is discussed further in the next topic.

Additional information will be obtained from the University of Michigan, where auto- and cross-correlation studies of the VBWR data are being studied. Studies will include cross-correlation of up to 12 variables. This work, done at no cost to the AEC, will be reported when it is received. The work is being conducted, using the Chrysler Corporation analogue computer facilities.

B. Improved Analysis of VBWR Test Points

The objective of this work is to obtain analytical solutions for the specific reactor test conditions on an improved basis, and use them in the analysis and improvement of understanding of the VBWR tests. The improved

basis will attempt to obtain as nearly as possible a uniform consideration of void profiles, boiling lengths, and power distribution in the analysis of the following:

1. Thermal hydraulic, steady-state reference - COFFI Code.
2. Void coefficient of reactivity calculation by two-dimensional diffusion theory.
3. Stability and transient responses of the system, using the analytical models for thermal hydraulic responses and linearized system representation. Digital codes are written to handle these problems.

The above work will provide a basic point for comparing the model analysis with test data. There are several extremely important aspects of these analyses which have a bearing on the amount and type of information to be obtained from the improved, or advanced, analysis program. The first aspect is that analyses can now be made parametrically very accurately at very low cost, using the linear system analysis code. This was a major short-coming in the work reported in Section VIII, in that analogue system analysis, with its accompanying drift and reading errors, was employed.

A second consideration is the averaged channel responses can now be looked at in a more systematic and satisfying manner to obtain improved estimates of the average responses of neutron kinetics and of thermal-hydraulics. This is done by a succession of calculations that evaluate the responses of various regions of the core. A determination of average response is then made.

Two items will aid in identification of physical phenomena in both the model analysis and the reactor data. One of these is the fact that phase relationships are to be obtained both from the test data and the analysis. These may be compared, as well as amplitudes. Variations may be applied to the analytical model to determine the sensitivity of the theory to the influence of a variable, such as fuel thermal time constant, or void coefficient. The use of the auto- and cross-correlation code will also allow examination of the influence of various reactor measurements upon one

another, and will aid in understanding the physical events of interest in the model analysis comparison with data.

C. Data Contributing to Model Analysis Improvement - Derived from the APED Hydraulic Stability Loop

A series of hydraulic stability test loop studies have been conducted in the APED hydraulic stability test facility. These tests have examined the natural circulation flow stability responses of a single channel test loop for a parametric variation of power and subcooling. All completed studies have been made by investigating the responses to disturbance of power. Subsequent test work will be conducted using power oscillation and measurement of transient steam voids. The experimental results were compared with theory to provide a preliminary evaluation of the analytical models used in the stability and transient response analysis.

Test results showed a wide range of responses ranging from stable, to oscillatory with exponential decay, to unstable oscillations with divergent amplitude. It was observed that a two-phase pressure loss oscillation of 20 - 25 cps occurs during these tests. This is believed due to an exit loss variation resulting from the mechanisms of two-phase flow. During these tests, a pressure wave phenomena was shown to occur, making the fluid in the heater section act as a capacitance for an interval. This type of phenomena is not presently included in the theory.

A preliminary evaluation of the thermal-hydraulic model has been made from the tests. The evaluation shows that a multi-node representation of the fluid dynamics should be considered, and that some of the aspects of damping coefficients and subcooling parametric representation should be examined. The 20 - 25 cps pressure drop oscillation previously mentioned is expected to be a major contributor to noise in two-phase flow systems.

VBWR test data indicated that the analytical model needed improvement with respect to multi-node thermal hydraulics representation, and that void transfer function information is needed to evaluate both thermal hydraulic responses and the void reactivity effects. These data will be obtained

in the future effort portion of the hydraulic stability loop program.

Future efforts in the hydraulic stability loop area include:

a. Power oscillator test over a range of parameters significant to the VBWR with transient void measurements.

b. Tests to provide a basis for improvement of the thermal hydraulic analytical model. Included in this area are tests to provide a basis for a multi-node representation of responses and the revision of the code to include phenomena such as the capacitative effect, described above, and improved parallel channel considerations.

The future work which contributes specifically to the development of improved analytical models comes in the following areas.

a. Accurate void transfer functions will provide a means of improving predictions about test conditions.

b. The reactor test data has been compared to the theory which represents the reactor, based upon average channel responses. Examination of loop data for void transfer functions, and comparison with the same theory, will aid in establishing how well the reactor is represented by this average channel analysis.

c. Improvement of the multi-node thermal-hydraulics responses of the analytical model is directly related to the hydraulic stability test program results.

d. Evaluation of void transfer functions and transient power distribution properties are directly related to improved void coefficient determination.

D. Improved Analytical Model

The third objective of this program, which is the item of ultimate usefulness to the power reactor industry, is the development of improved analytical models for the prediction of stability and transient responses of advanced boiling water reactors. The improvement in model analysis from this program will be derived from two sources of information:

a. Comparison of the improved analysis of VBWR tests with existing theory.

b. Comparison of hydraulic stability loop data with the predictions of the analytical model.

The basic improvements stem from obtaining an understanding of:

a. Void transfer functions obtained from the hydraulic stability loop. This includes detailed understanding of the void shape and transient response over the parametric ranges which are of interest to the BWR designs.

b. An understanding, or identification, of the physical phenomena occurring in the VBWR test and hydraulic stability loop tests. This information is obtained from transfer function, and auto- and cross-correlation results for both VBWR and hydraulic stability loop data.

These two items must, then, be expressed in appropriate mathematical form for the analytical model.

There are a number of areas in which the analytical model used in the pre-test analysis, discussed in Sections VII and VIII, are considered to be in need of improvement. Basic to any of these improvements, however, is the assurance that the averaged parameter representation of the reactor and system are reliable in representing the responses of the system. The improved data analysis is expected to provide a better basis for determining this than is presently available. The improved analysis of VBWR test points discussed above has factored into it a more comprehensive way of arriving at the average response of the reactor than heretofore employed. The alternate to the average channel representation would be a complex and very expensive multi-dimensional representation. Such a representation does not seem technically feasible at this time.

VBWR tests have shown that the two parameters which most strongly influence the reactor stability and transient response are the gains of the system

(void coefficients, etc.) and the introduction of resonant thermal-hydraulics. The programs in items (1) and (2) above will ascertain if improvements in the void coefficient representation can be made which will be significant to the analysis. Improvement in the thermal-hydraulics is indicated to be required from the results of the VBWR test, and from hydraulic stability loop tests. The indications of this come both from VBWR tests and from the hydraulic stability loop tests conducted to date. VBWR tests and loop tests both show that the frequency responses of the system to changes in flow are not the same as predicted by the analytical model. Additionally, as discussed in item (3) above, a pressure wave phenomena was observed which causes the two-phase fluid to act as a capacitance during transient operations. This was not included in the model. Multinode representation and improved understanding of phase relationships, void transfer functions, and of specific phenomena observed in the hydraulic stability loop form a basis for this improvement.

There are several areas where it is felt that future work should not be emphasized. The most important of these are noise analysis, improvements in reactor kinetics, improvements in fuel thermal response methods. The VBWR tests show that a power oscillator test produces more well-defined results with present methods than noise analysis methods. There is an incentive to investigate noise to determine methods of reducing it, and to identify excitations which may contribute to the stability responses. Reactor kinetics models are well developed and suffice for the objectives of this work. Fuel thermal responses should be examined to determine the effect of varying the thermal conductivity or local conductances. Statistical variations in the condition of oxide fuel make it difficult to do more than this in improving analysis of thermal responses of fuel.

M. Generalizations to the Design of Large Plants

The improved model analysis can be generalized to an extent in order to make the results of this analysis program more useable. There is information from two large plants which could be used for this investigation. Rod oscillator tests were conducted on the Dresden Nuclear Power Station

and are being conducted on the Consumers Big Rock Station. A comparison of test results and the improved analysis should be made to demonstrate the ability of the model to predict plant performance.

These predictions should be based on discussion of the properties of the analytical model as applied to the specific design features of a large reactor. The most immediate items which should be considered are:

a. Spatial effects inherent in large cores, including the average channel representation of core response.

b. Variations in thermal hydraulic design of large reactors which introduce specific problems to the design.

c. Differences in fuel design.

d. Variation of stability and transient responses with fuel burn-up.

APPENDIX A

TEST FACILITY

Description of the test facility includes the reactor system, the core composition and characteristics, the rod oscillator mechanism, the instrumented fuel assemblies, and readout instrumentation.

1. Reactor System

The reactor is a water-moderated boiling reactor fueled with slightly enriched uranium dioxide rods. It is enclosed in a 7-foot diameter x 20-foot high pressure vessel operated at 1000 psi. Two pumps are provided for forced circulation operation. The reactor may be operated with natural circulation within the reactor vessel by opening four "baffle doors". A portion of the steam produced is utilized by a Pacific Gas and Electric Company turbine generator plant, rated at 5000 kw(e).

The reactor vessel is illustrated in Figure A-1, and a cross-sectional drawing is shown in Figure A-2.

Several aspects of the reactor structure and operation require further explanation.[19] Hinged "baffle doors" are located at the top of the core. These baffles block water from bypassing the core during forced circulation and may be opened for natural circulation operation of the reactor.

A "cone" is provided to direct the upward flow of water from the core until it has reached an elevation sufficiently near the reactor water level to prevent steam carryunder during forced circulation operation. The water then flows over the top of this cone and downward to the reactor outlet nozzles through the annulus formed by the outside surface of the cone and the pressure vessel wall. During natural circulation operation, the cone folds out of the circulating water path.

Reactor recirculation may be accomplished by means of either forced or natural circulation of the light-water coolant. In either case, water entering the

bottom of the fuel elements is heated as it passes upward through the core. At about one-third of its travel upward through the fuel, the water begins to boil. Water and steam continue to rise through the remainder of the active core height and through the chimneys which are provided as an extension of the fuel channels. Upon emergence from the chimneys, the upward flow of the water-steam mixture is bounded by the cone, which is a circular section above and bounding the reactor core. The water then flows over the top of this cone while the steam formed in the core continues its upward travel to the water surface. The steam leaves the reactor by way of the main steam line at the top of the reactor.

The water flows through the baffle doors back to the bottom of the reactor core during natural circulation operation. During forced circulation operation the direct flow path to the bottom of the core is blocked by the baffle doors. Water from the reactor enters the recirculating loop through four 10-inch nozzles in the pressure vessel. The 10-inch lines from these nozzles feed an 18-inch header which connects to the suction side of the two reactor circulating pumps. An 18-inch, manually-operated gate valve is included upstream of the suction nozzle of each pump. The discharge nozzle of each reactor circulating pump connects to a 14-inch line which leads to motor-operated throttle valves (gate type). The 14-inch discharge lines are joined for a short distance before branching into the two 10-inch lines which terminate at the reactor inlet nozzles. A 4-inch bypass valve around the discharge valve for Pump No. 1 permits experimental operation at flows of 2900 gallons per minute and less, which might cause excessive wear if the throttling were done with the 14-inch valve. The recirculating water returns to the reactor at the two inlet nozzles and flows to the bottom of the core via the diffusers located in the annulus formed by the outside surface of the core support structure and the inside surface of the reactor vessel.

The steam generator provided for dual-cycle operation of the plant was out of service during the test period because of tube leaks.

Feedwater is injected into the four reactor outlet lines. This condenses any steam which might be carried into the recirculation loop and increases the net

positive suction head of the pumps. The recirculation pumps operate with a low suction head, since the elevation difference between the reactor water level and the pump is only 14 feet. Extensive tests have shown that at the operating temperature, the pump head curve is not adversely affected by any vapor formulation which may occur in the pumps (cavitation).

The process variables that could be independently controlled during the tests include:

Forced Circulation

Recirculation flow rate

Recirculation pump head (Pump No. 2 has a variable-speed turbine drive)

Position of baffle doors. Opening the doors allows part of the flow to bypass the core. This also "decouples" the dynamic response of the core and the recirculation loop.

Reactor power

Reactor water level

Natural Circulation

Reactor power

Reactor water level

2. Core Composition and Characteristics

The fuel generally consists of pellatized UO_2 clad in either zircaloy or stainless steel. Rod diameters are 1/4 to 1/2 inch. Enrichments are 2.7 to 4.5 per cent for most of the fuel. Figure A-3 shows a typical fuel assembly in relation to the channels. A more detailed listing which shows some exceptions to the above, is given in Table A-1.

The fuel assemblies are placed in a checkerboard array of channels. The channels form a square grid having a spacing of 3.10 inches. Each fuel assembly is 3.00 inches on a side and the active fuel length is 37 inches. The channels have a wall thickness of 0.060 inches and are either stainless steel or zircaloy-2. The stainless steel channels are replaced by zircaloy channels to add reactivity as fuel burn-up occurs. The positions of the zircaloy

channels are shown in Figure A-5.

The control rods are box-shaped and are the same size as fuel assemblies (3" x 3"). The poison material consists of plates of boron steel which make up the sides of the boxes. The 14 control boxes are operated in pairs by 7 control rod drives. The two boxes in one pair are diagonally adjacent as shown in Figures A-4 and A-5. Each control box has a fuel follower attached to the bottom so that as the control rod is withdrawn the fuel follower comes up into the core. The fuel followers are designed to have the same characteristics as the fuel which is normally in the same region. The fuel follower characteristics are included with the other fuel in Table A-2. The steam-water mixture rising from a fuel follower flows upward through the control box.

The core arrangement used during most of the stability tests was shown in Figure A-4. The only deviations from this were for a few tests made before and after the main group of tests. The core compositions were as follows:

TABLE A-1

TABULATION OF FUEL ELEMENT CHANGES TO GRID PLAN FOR THE VBWR STABILITY TEST

November 1 to 7	Same as Figure A-4 except positions C-8 and C-9 were empty and positions D-9 was DF-5 instead of SADE-5A fuel.
November 13 through December 16	Figure A-4
December 27 and 28	Same as Figure A-4 except

Grid Position	Fuel Removed	Replaced By
F-5	17J	11I
G-5	18J	9I
K-4	11I	13I
L-5	9I	7I
E-10	DP-62	DF-1
J-12	DP-70	DF-29
F-11	DP-73	DF-34
H-14	DP-76	DF-3
O-9	DP-20	4-L
L-4	Empty	TC-1

TABLE A-2

CHARACTERISTICS OF FUEL

(All Fuel is UO_2)

PROGRAM	TYPE	NO. RODS	ROD O.D. (inches)	CLAD	ENRICHMENT	COMMENTS
CONSUMERS	A	16	0.42	s.s.	2.7	Control rod followers
	B	16	0.42	"	2.7	Control rod followers
	C,D,S	25	0.40	"	3.5	
	E,F,G,4S	25	0.38	"	4.5	
Fuel Cycle	H	16	0.42	"	2.7	Control rod followers
	I	16	0.41	"	3.2	
	J	16	0.42	Zy	2.7 - 4.3	
	L	8 - 16	.38-.51	ss - Zy	3.0 - 5.5	
Dresden	DP	9	0.57	ss - Zy	2.3	
	DP	16	.48-.55	ss - Zy	2.3 - 3.5	
N.S. Savannah	S-I	16	.50	s.s.	4.2 - 4.6	
	S-II	16	.57	s.s.	4.0	
Du Pont	DU	1	2.06	s.s.	5.0	Annular Boiling, I.D. 1.47 inch.
Superheat (SADE)	5A	1	1.50	s.s.	4.0	Annular, 2 flow passes, I.D. 1.02 inch
EURATOM	PBU	1	.60	s.s.	4.0 - 8.0	Pressure build-up test.
Driver	DF	16	.43	Zy	3.5	
G.E. Devel.	TC	8	.41	s.s.	8.0	Thermal cycler, non-rotating, has 2 half-cylinders of B_4C poison material. Depresses flux in adjacent fuel by 10%.

TABLE A-3

SUMMARY OF CORE PHYSICS DATA

30 MW Power, 15,000 GPM Core Flow

FUEL LOAD:

102 Elements, 3.1" center to center

41 KG U^{235}, 1170 KG U, Average enrichment, 3.5%

COMPOSITION:

68% H_2O, 21% UO^2, 5% Stainless Steel, 4% Zircalloy

FUEL ELEMENTS:

9 to 25 rods per bundle, Zircalloy and Stainless Steel clad,

2.3 to 6.5% Enriched.

CONTROL REQUIREMENTS:

Temperature	6%	ΔK/K	Cold to Hot
Voids	4%	"	(Core Average Void = 15%)
Xenon (Xe)	3%	"	
Samarium (Sm)	0.8%	"	
Burn-up Compensation	0.5%	"	

} Cold to Hot Reactivity Swing, Equilibrium Xe and Sm = 13.8%

ROD WORTH:

Total Control Rod Worth	19% ΔK/K
Worth of Strongest Rod	5% ΔK/K, Rod #7
Shutdown Margin	4.7% ΔK/K
Cold Excess Reactivity	14.3% (0.5% Held Above Stop on #7)
Thermal Flux	3.3×10^{13} Average, 7×10^{13} Peak

Vertical Peak to Average Flux Ratio: 1.4 to 1.7

TABLE A-3 (Cont'd)

FUEL OPERATING CONDITIONS

ELEMENT TYPE	No. RODS	KW	KW/ℓ	PEAK HEAT FLUX (BTU/HR.FT^2)	ORIFICE SIZE	FLOW RATES	
						GPM	FT/SEC
Fuel Follower	16	250	44	270×10^3	None	129	9.6
HPD-C,D,E,F,G	25	480	85	400×10^3	None	278	13.3
I, J	16	210	37	230×10^3	6	84	4.1
I, J	16	300	53	315×10^3	4	123	5.9
I, J	16	340	60	370×10^3	2	211	9.8
Dresden	9	136	24	215×10^3	6	83	3.8

The core power distribution was calculated by a two-dimensional diffusion theory method using three neutron energy groups. The results are the fuel assembly powers and peak heat fluxes shown in Figure A-4. The power and flow distributions are inter-dependent; only the final results of several iterations are shown. The results all include equilibrium xenon poisoning and the void content for 30 MW and maximum flow (20,000 gpm).

A summary of core physics characteristics is shown in Table A-3.

The worth of control rod #7 was calibrated on November 3, 1961, by a period and temperature coefficient technique. The temperature coefficient was measured as 0.027 per cent $\Delta k/k$ per ^{o}F for the range 520 to 550^{o}F, which agrees with previous measurements. The rod worth was as shown in Table A-4.

TABLE A-4

CONTROL ROD WORTH FOR

CONTROL ROD #7

Rod #7 Position*	Rods 1 - 6 Position *	Rod #7 Worth	
		Relative	% Δ k/k per Unit
600	320	1.0	0.00225
550	320	1.2	0.00270
500	330	1.5	0.00338
450	340	1.9	0.00427
400	350	2.4	0.00540
350	360	3.1	0.00696

* Units withdrawn. Total rod travel of 931 units corresponds to 31-1/4 inches. Then, there are 29.8 units per inch.

The above data has several limitations. First, the data were taken with no voids. Second, the results are dependent upon the position of the other six control rods. If rod #7 is below the other 6 rods, its worth will be 2 to 3 times greater. Rod worth at the operating condition is calculated from rod oscillator data in Section VII-B.

The core hydraulics calculations were made by means of a computer code which obtains simultaneous solutions for the flow and heat transfer equations for the various fuel types. The instrumented assemblies were included in the group shown in Table A-1. The core used for the hydraulics calculations had 105 assemblies compared to 102 assemblies in the actual test core (Figure A-4). These differences are considered within the calculational error. The core orifice configuration (Figure A-5) was optimized to give maximum burn-out heat flux.

The hydraulics calculations were made to (a) provide data needed for the pretest dynamic analysis (Section VIII), and (b) to determine the operating limits of the core. The core operating limit was, in each case, the burn-out heat flux at steady-state operation. The calculations were made for a loop flow rate equal to the low flow scram settings and the high flux scram settings. The operating conditions were as shown in Table A-5.

TABLE A-5

OPERATING LIMITS FOR TEST CORE

Type of Operation	Flow, 1000's gpm				Maximum Power, MW(t)	
	Pump #1		Pump #2			
	Operate	Scram	Operate	Scram	Operate	Scram at 125%
Forced Circ	10	8.5	10	3.2	25.8	32.2
" "	13	8.5	0	- -	19.8	24.7
" "	10	8.5	0	- -	19.8	24.7
" "	10	8.5	3	- -	19.8	24.8
" "	0	- -	4.	3.2	17.8	22.3
" "	0	- -	7	3.2	17.8	22.3
" "	2.5	2.0	- -	- -	14.8	18.4
Natural "	- -	- -	- -	- -	21.4	26.8
Forced Circ w/baffles open	- -	- -	- -	- -	21.4	26.8

3. Rod Oscillator System

a. General

The time variable inputs of reactivity dictated by the test procedures are applied to the core with the central VBWR control rod (#7) by a specially designed rod oscillator system (see Figure A-6). This system provided at any point of rod withdrawal, either a sinusoidal position displacement of the rod over a frequency range of 0.03 cps to 3.0 cps at amplitudes up to $\pm$ 1.0 inch, or a ramp change of rod position of up to 1 inch. The rod displacement is obtained with a double-acting hydraulic cylinder driving a lever arm in contact with the rod stop of the control rod drive line. Hydraulic fluid is supplied to the cylinder through an electronically controlled servo-valve to generate the desired reactivity variation. The system operated functionally independent of, and compatible with, the rod drive motor train, allowing normal operation and scram of the rod at any time.

b. Description of Equipment

The VBWR control rod system with the rod oscillator installed is shown in block diagram form in Figure A-7, and schematically in Figure A-8. The rod oscillator mechanism frame is solidly fastened to the motor driven stop and the lever arm extends under this stop to contact the rod drive line stop (Figure A-7). When the oscillator mechanism is not operating, the lever arm is in the full UP position and functions as an extension of the motor driven stop. The digicon rod position readout is adjusted to compensate for this extension.

As indicated in Figure A-7, the system may conveniently be separated into three functional units for purposes of description.

1. Normal operation and scram control.
2. Rod oscillator mechanism.
3. Rod oscillator control.

Normal Operation and Scram Control

Normal operation and scram control is not functionally changed by installation of the oscillator. Operating air is applied to the lower side of a double-acting air cylinder in the rod drive line, creating a contact force between the drive line rod stop and the lever arm. Rod withdrawal (vertically upward) from the core is achieved by raising the motor driven stop, contact between the stops being maintained by the pressure in the operating air cylinder. Should separation of the stops occur, two micro switches are actuated to initiate rod insertion; one actuates immediately, and the second at 2.1 inches of separation. (Figure A-8) Rod insertion is accomplished either by lowering the motor driven stop or, in the scram condition, by dropping out the voltage to the scram and operating air solenoid valve operation which vents the operating air cylinder to atmosphere and applies high pressure scram air to the upper side of the air cylinder. After the rod is scrammed, the motor driven stop is automatically lowered until contact is re-established between the lever arm and the drive line rod stop. Re-set of the operating air may, or may not, be automatic, depending on the cause of scram.

Rod Oscillator Mechanism

The rod oscillator mechanism (Figure A-9) frame is attached to, and positioned with, the motor driven stop. The actuator lever arm is pivoted from this frame to bear on the rod drive line stop. Placement of the lever arm pivot point and the shape of the cam surface provides essentially rolling, rather than sliding, contact between the lever arm and the rod drive line stop to minimize lateral forces. The hydraulic cylinder is pinned on one end to the frame and on the other end to the lever arm. Actuation of the hydraulic cylinder causes relative vertical motion between the rod drive line stop and the motor driven stop. This relative motion is mechanically limited to approximately 2-1/2 inches.

Rod Oscillator Control System

This system provides the desired function of rod position with time about a reference point. Energizing the hydraulic power control relay (Figure A-6) closes two sets of contacts; one, to bypass the contact separation switch to allow rod stop separation of up to 2.1 inches, and the second to start the wobbling plate piston hydraulic pump unit. Hydraulic fluid at 1800 psi is then supplied to the pressure post of the servo control valve where it is metered to the double-acting hydraulic cylinder according to the signal applied by the feedback amplifier to the servo-valve coil. Movement of the rod within the separation limit moves the wiper of the linerar motion feedback potentiometer which is pinned to the rod oscillator frame and lever arm. The power supply provides a constant 40 volt DC across this feedback potentiometer, hence, rod motion is seen as a voltage change between reference and the wiper of the potentiometer. This signal is fed back to the amplifier, generating a command to the servo-valve to re-position the rod at reference when no other signal is being fed to the amplifier. The reference, or mean rod position, is controlled with a vernier potentiometer in parallel with the feedback potentiometer. The ground leg of the servo-valve coil is connected to the wiper of this reference position potentiometer. This system provides an accurate calibration of mean rod position as a function of the graduations of the Vernier Reference Position Potentiometer, which is unaffected by other system variables, and allows the reference position to be established at any point on the available stroke of the control rod. The desired rod motion function about the reference is initiated as a voltage from the Krohnhite Pushbutton Oscillator or the ramp generator to the amplifier. It is compared to the voltage signal of rod position from the Feedback Potentiometer, and the resultant error generates a command to the servo-valve to re-position the control rod.

Provisions are incorporated in the system to automatically control and de-activate the oscillator in the event of reactor scram. The contact points SR1, SR2, and SR3 (Figure A-6) are controlled by the scram and

operating air solenois valve relay. When scram occurs, SR1 cuts AC power to the entire system, SR2 prevents application of amplifier switching transients to the servo-valve, and SR3 applies a full Up signal to the servo-valve to re-position the oscillator arm against the motor driven stop. The manually re-set scram dropout relay prevents automatic re-activation of the system when the reactor scram is cleared.

Monitoring of the control system is provided by oscillograph readout of the rod position and neutron flux tracer. This affords the operator a continuous reading of the relative reactivity input and power output of the reactor core upon which to base manipulation of the controls.

c. Pre-Test Operational Check-out

Extensive proof-testing of this system was performed prior to the initiation of the stability tests. Proof-testing was motivated by:

a. The importance of the system towards the overall success of the tests dictated that as trouble-free a system as possible be installed.

b. Safeguards considerations demand complete compatibility with the reactor control system of any installed test equipment functionally or mechanically connected to the control rod system.

The first phase of proof-testing was conducted on the spare control rod drive stand. The complete system was mocked up, except for the scram control provisions, and exercised throughout the range of test variables. Necessary modification were performed as required with subsequent re-testing. Initial calibration of the reference position control potentiometer was conducted. After successful completion of this pahse, the system was installed on the central rod of the VBWR. This was done coincident with a control rod modification program so that the second phase of testing could be done with the driver of rods #3 and #6 removed to facilitate observation and calibration. Once again, the system was exercised throughout the range of test variables to pinpoint any trouble areas

and perform necessary modifications. The final calibration of rod reference position control was completed.

The final check-out phase was performed after the reactor system had come up to pressure. With the core sub-critical, the system was again exercised completely and observed for proper operation. Successful completion of these proof tests proved fruitful, providing a system with extremely good reliability with a minimum of maintenance.

4. Instrumented Assemblies

Three instrumented assemblies were designed and built to measure in-core temperature, pressure drop, flow and neutron flux. The instrumentation consisted of the instrumented fuel assemblies, instrumentation leads which penetrate the reactor vessel and pass to readout panels, back flow panels for the pressure drop system, and readout panels. The read out panels were shared by the Fuel Cycle and High Power Density Research and Development Programs.

The design of the instrumented assemblies is shown in Figure A-10. All instrumentation is located on a probe that occupies two diagonally adjacent center fuel rod positions in the 4 x 4 fuel rod array. The instrument probe is anchored to the fuel assembly by means of a tie-plate located above the fuel. The design is such that when an instrument fails, the probe may be removed and appropriate repairs made on the instrument probe. The assembly consists of three pieces which can be handled separately in the reactor:

a. The instrument probe
b. The channel turbine flow meter
c. The fuel bundle.

Photographs of the instrumented assemblies, showing details of pressure taps, lead out cable, etc., are shown in Figures A-11 through A-16.

The flowmeters and ion chambers were generally successful in giving reliable test data. However, each type of instrument was subject to operating difficulties.

The flowmeters suffered from deterioration of the permanent magnets.

instrumented assemblies from the High Power Density Research and Development Program. For each instrumented assembly, a choice of seven parameters could be recorded:

1. Three in-core ion chambers
2. The inlet flow velocity
3. The pressure drop across the fuel bundle
4. The pressure drop across the riser located just above the fuel bundle.
5. A choice of either water inlet temperature, outlet temperature, or temperature rise across the fuel bundle.

The seven remaining parameters consisted of:

1. A signal originating from a gamma compensated ion chamber located outside the south face of the VBWR pressure vessel at a point half-way up the active core. The signal was fed through a micro-micro ammeter and thence to the readout system.
2. A signal representing the flow through the two recirculation pumps. The signals originated from Pace reluctance-type pressure transducers, located across flow nozzles in each flow loop.
3. Signals representing the reactor feedwater and main steam flows. Again, Pace reluctance-type pressure transducers were located across appropriate flow nozzles in each flow loop
4. The pressure in the steam dome of the reactor pressure vessel. A Pace reluctance-type transducer measured the gauge pressure of the steam.
5. The motion of the control rod oscillator mechanism. A linear potentiometer located on the mechanism produced the signal.

The choice of which 20 signals were recorded was made by use of a small switchboard arrangement. The switchboard was located on a switching center instrument rack. The rack is shown in the left center of Figure A-18a where the switchboard can be seen at the bottom of the rack.

Three small permanent magnets were located on the turbine rotor of the flowmeter such that, for each revolution of the rotor, three voltage pulses occurred in a small pickup coil. Thus, the flow rate through the flowmeter was proportional to the frequency of the pulses received at the readout circuitry. The pulse strength on all the assemblies gradually decreased and the signal became more difficult to distinguish from 60 cps noise picked up in the signal leads. Also, the loss in strength of the three magnets was unequal, thus resulting in a waveform that was not properly interpreted by the frequency-to-voltage converter. The converter sometimes counted two pulses per revolution and sometimes three pulses. Also, by mid-December, assembly D flowmeter pickup coil had partially shorted to ground. This was evidenced by a resistance to ground of 20 ohms on one lead, and about 40 on the other, compared to 500 ohms on each side when new.

The only difficulty experienced with the in-core ion chambers was that moisture (steam from leak in flange on head of reactor vessel) penetrated the junction box for electrical terminal strips located outside the reactor vessel. The moisture resulted in a leakage current which changed the effective calibration of the instruments. Otherwise, all ion chambers were operating satisfactorily when removed. Details of the calibration and procedures for use of the instrumented assemblies are given in Appendix C.

5. Readout Instrumentation

This section will describe the readout instrumentation indicating the choice of components, and design of the system.

a. Readout System Description

The fast readout system was located in the VBWR control room. It was designed to record simultaneously any 20 of 42 input signals. Figure A-17 shows a schematic diagram of the system and Figure A-18 shows the placement of the system components in the VBWR control room.

The 42 input signals consisted of 35 in-core parameters and 7 parameters from the reactor control rod and process system. The in-core parameters all originated from the three Fuel Cycle instrumented assemblies and two

Each signal was fed into a bucking voltage circuit arrangement located on the switching center rack just above the switchboard. Two types of bucking voltage circuits were used. The circuit for data channels 1 through 12 included a Kintel DC amplifier, a calibrated potentiometer in series with a 6-3/4 volt mercury battery and provision for including a low-pass filter. The circuits for data channels 13 through 20 were identical to channels 1 to 12 except that a DC amplifier was not used. (See Figure A-17)

Two types of recorders were used on the first twelve channels; a frequency-modulated tape recorder, and a direct-writing oscillograph. The tape recorder used was an Ampex Model FR100A instrument-grade FM recorder, having 12 data channels, a time channel, and a voice recording channel. It is shown to the right of the switching center instrument rack in Figure A-18a. A recording speed of 15 inches per second was used. The direct-writing oscillographs consisted of a Model 1684, 8-channel Brush recorder for channels 1 through 8 and a Model BL-256 Brush recorder for channels 9 through 12. The signals on Channels 13 through 20 were also recorded on Model BL-256 Brush recorders.

Each recorder was provided with a time channel. The Brush recorders had a built-in event marker which would mark 1-second intervals. The tape recorder was provided with direct-record amplifiers on two channels, one of which was used as a time channel. The time signal was a 10 K cps wave form. The time channels on all recorders were co-ordinated by means of a small stepping-relay circuit. At the beginning of each test run, the stepping-relay contacts were closed, actuating all time channels simultaneously.

At the beginning of each recording on the magnetic tape, a voice recording of the run number, type of run, date, time, and any other appropriate information was made. In addition, the back side of the recording tape was marked with a felt marking pencil at the start and end of each run to make it more convenient to locate a run on the tape.

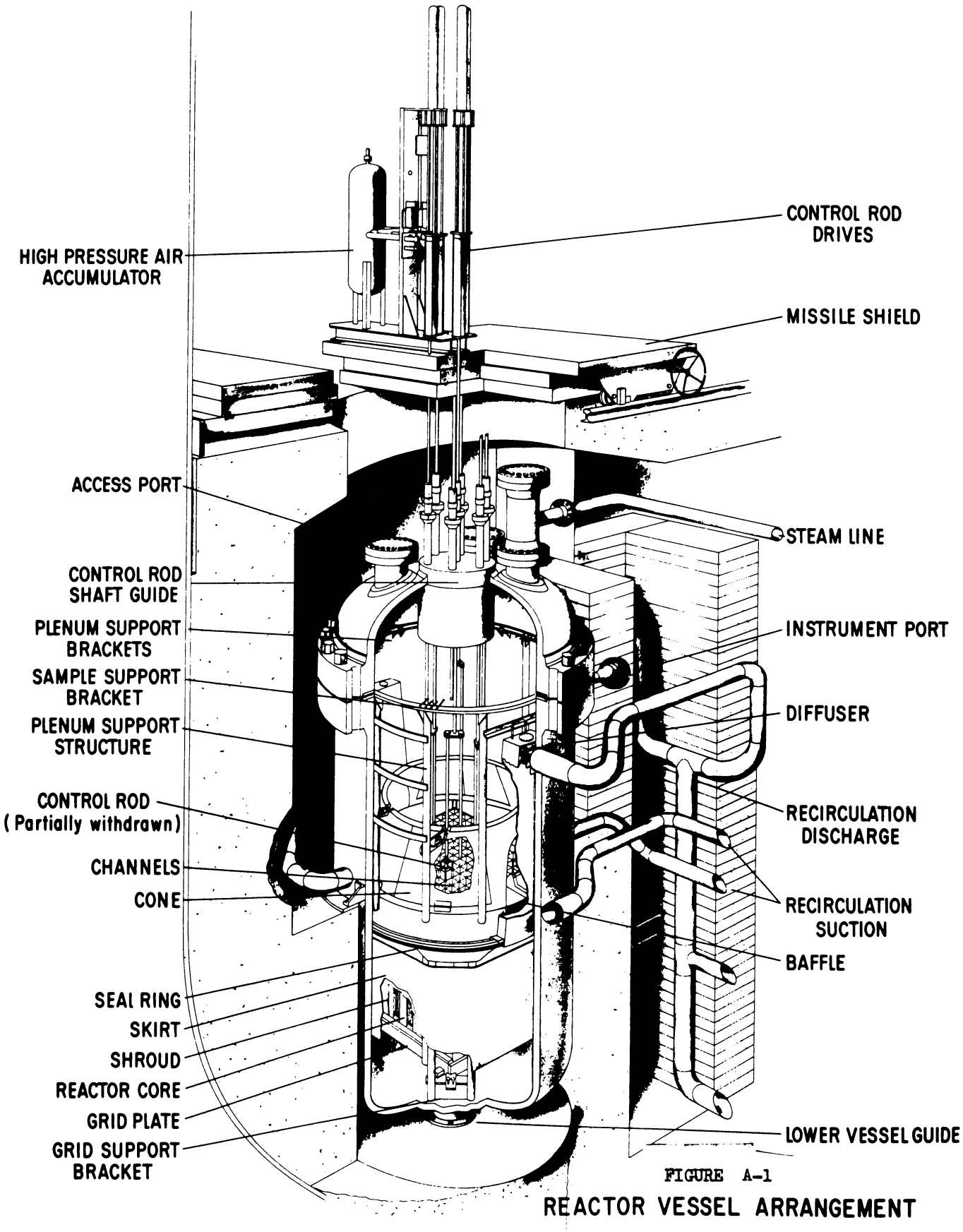

FIGURE A-1

REACTOR VESSEL ARRANGEMENT

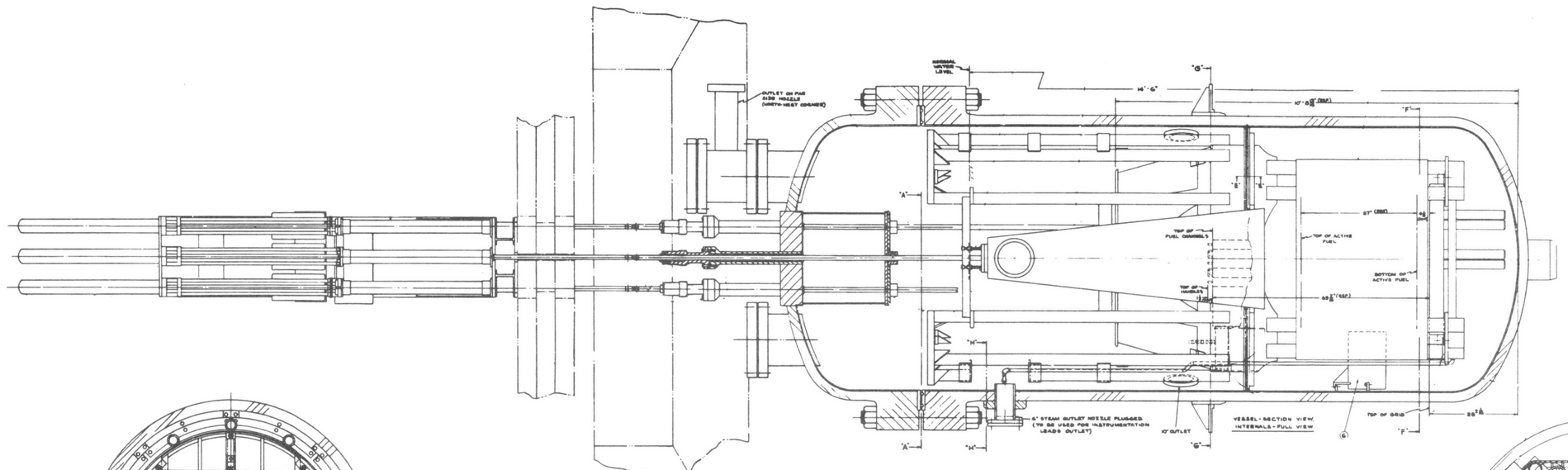

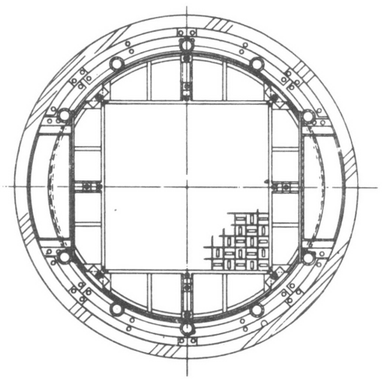

SECTION 'G-G'

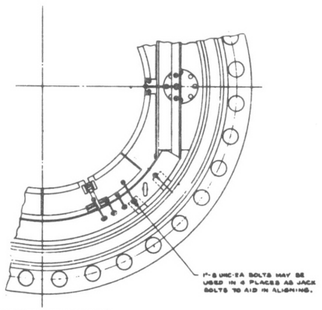

PARTIAL VIEW 'A-A'

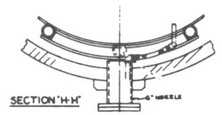

SECTION 'H-H'

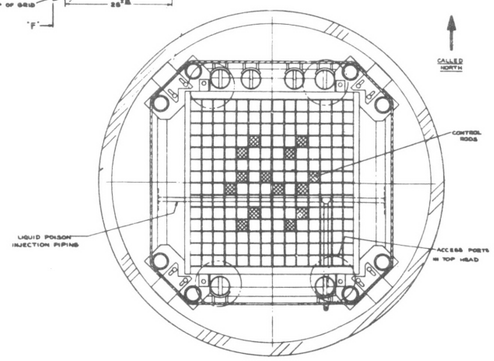

SECTION 'F-F'

FIGURE A-2

REACTOR ASSEMBLY

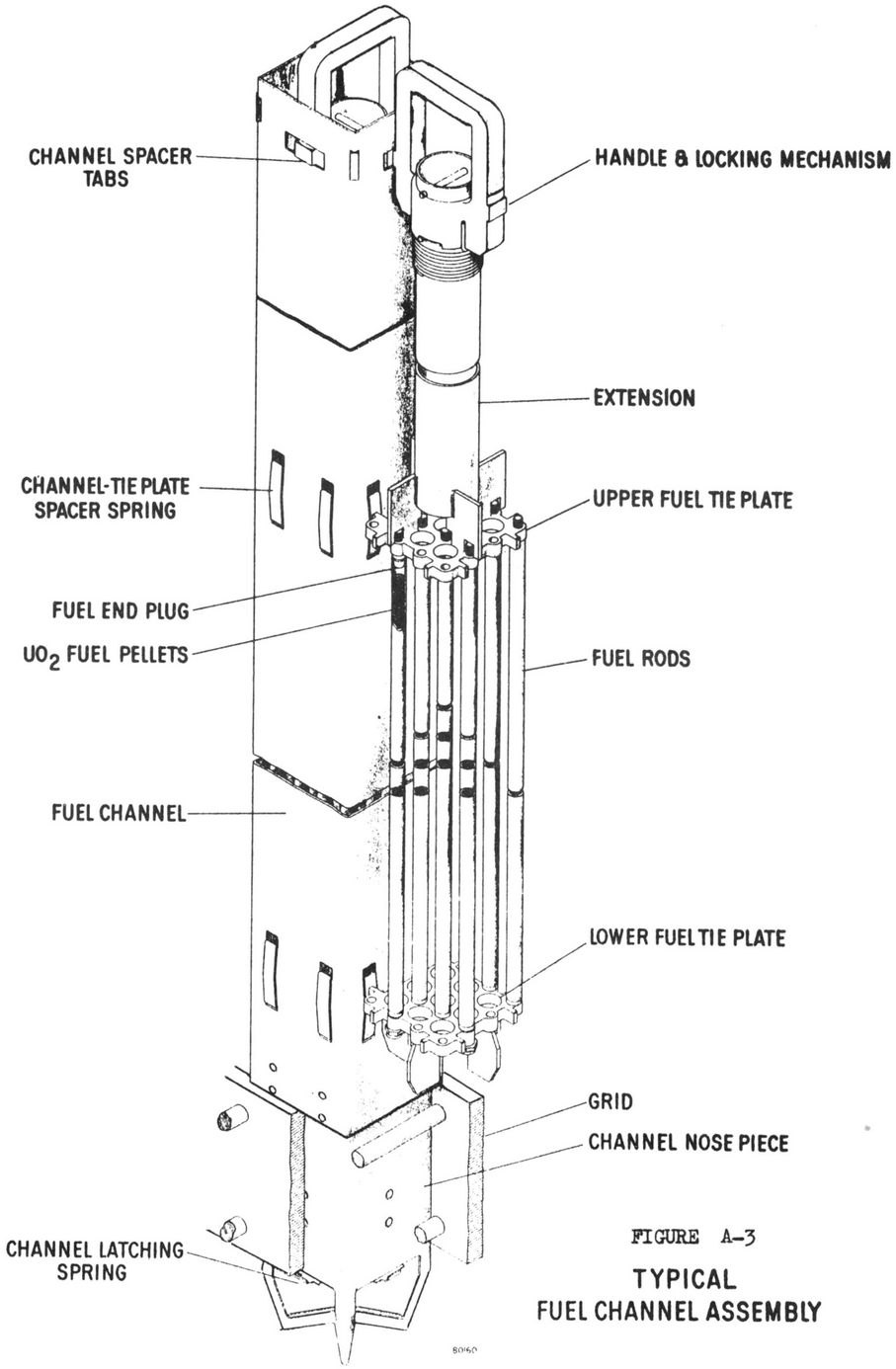

FIGURE A-3

TYPICAL FUEL CHANNEL ASSEMBLY

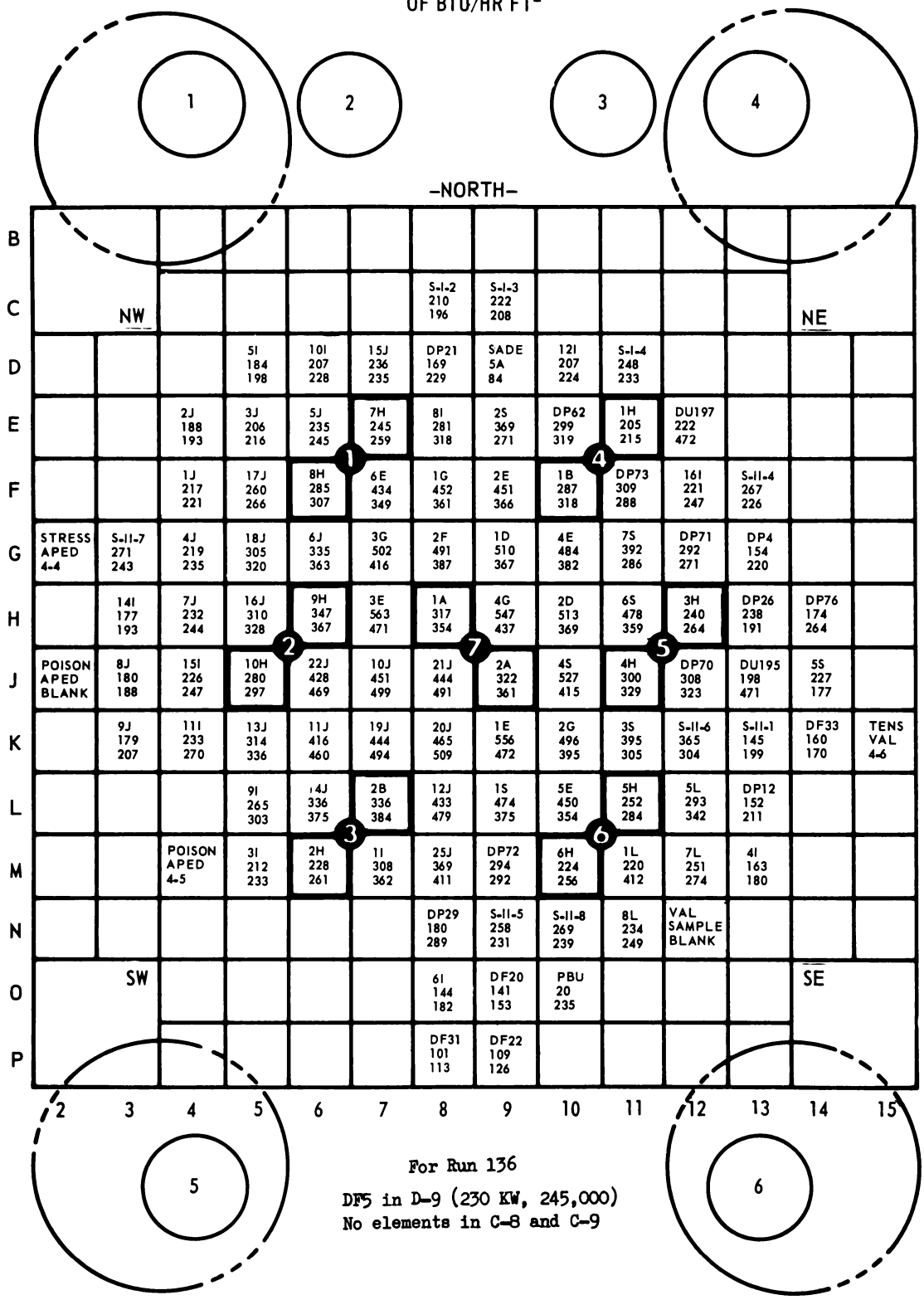

FIGURE A-4. CORE ARRANGEMENT VBWR TESTS

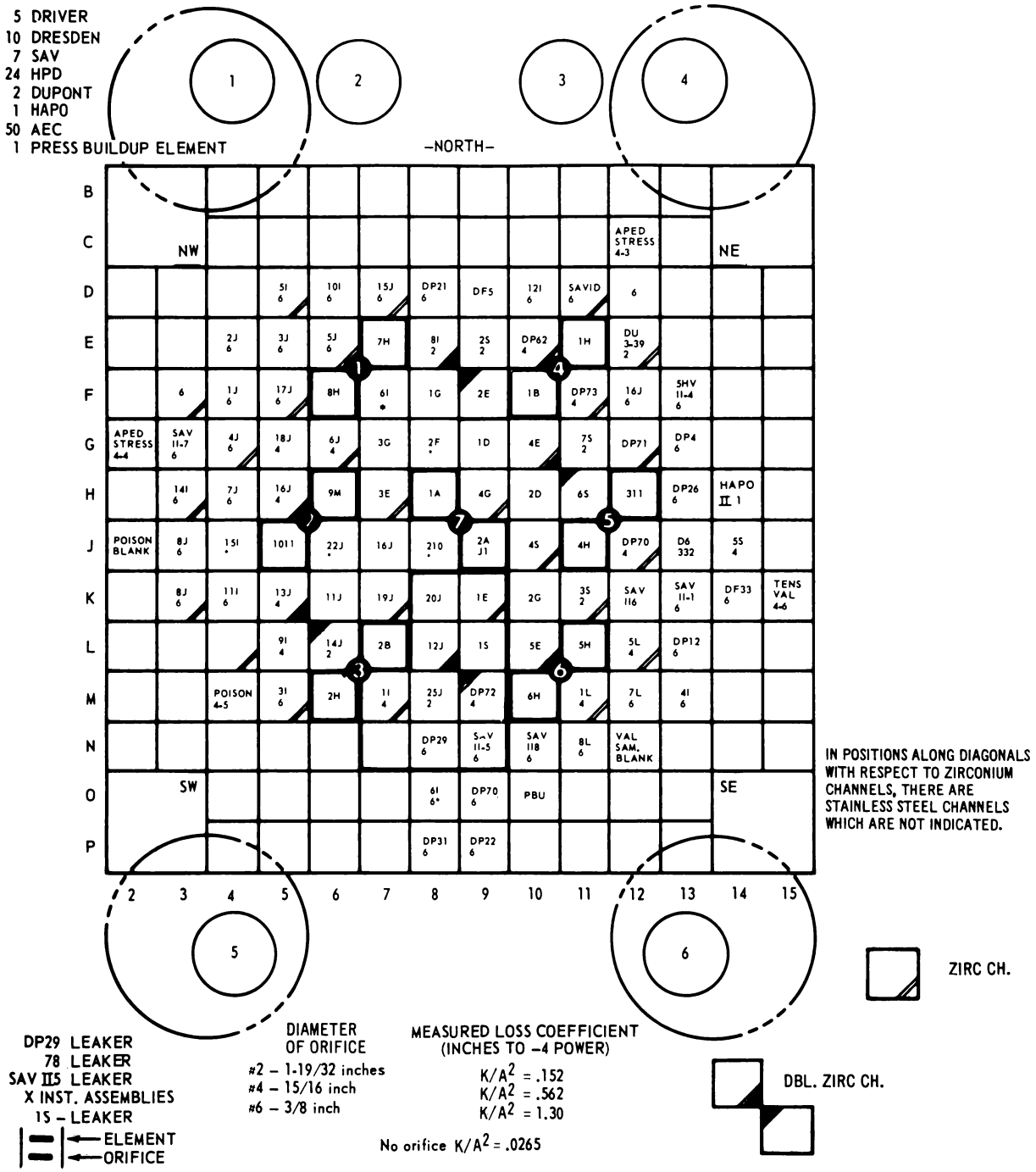

FIGURE A-5. CORE ORIFICING CONFIGURATION

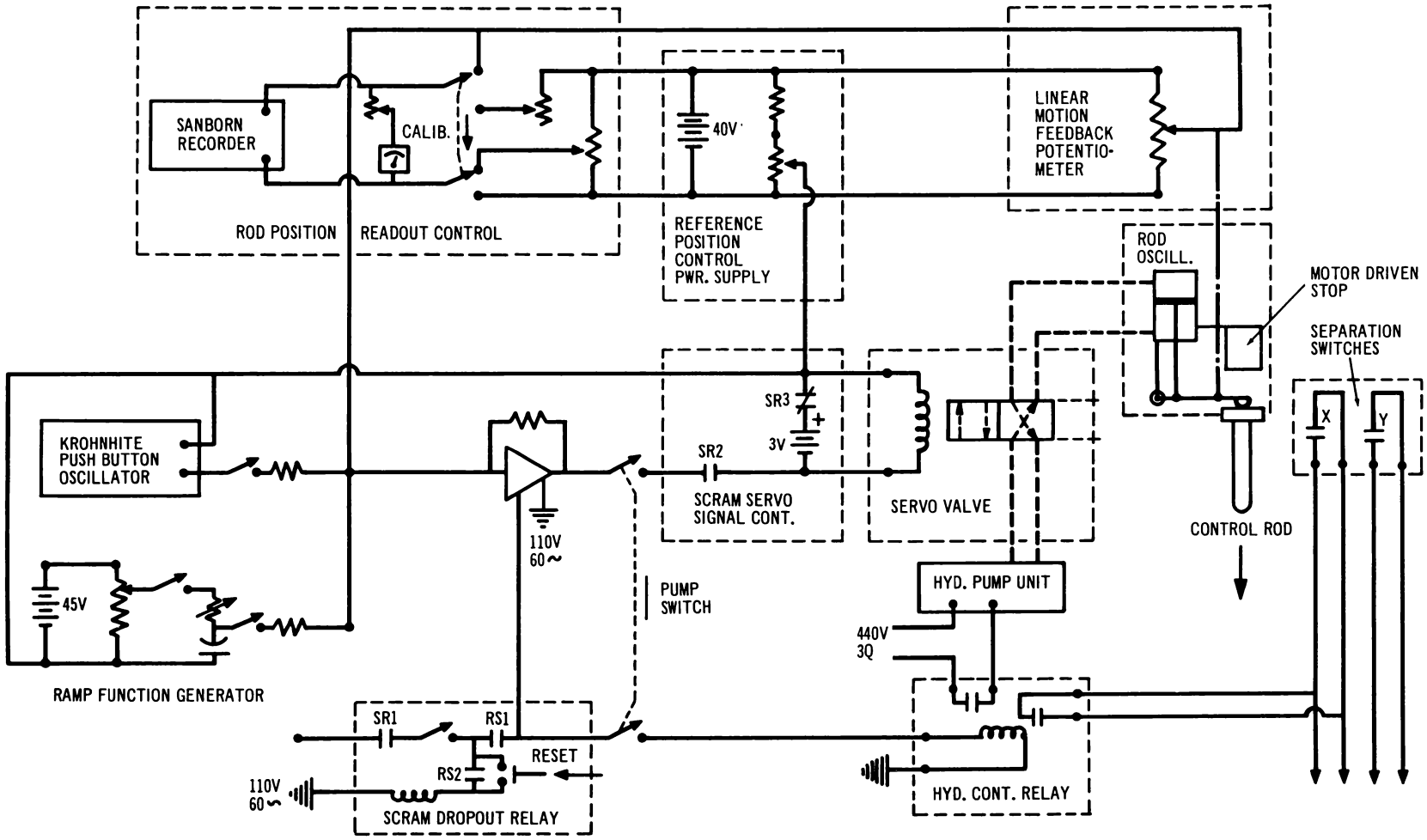

FIGURE A-6 ELECTRICAL HYDRAULIC DIAGRAM – VBWR ROD OSCILLATOR SYSTEM

1266–6

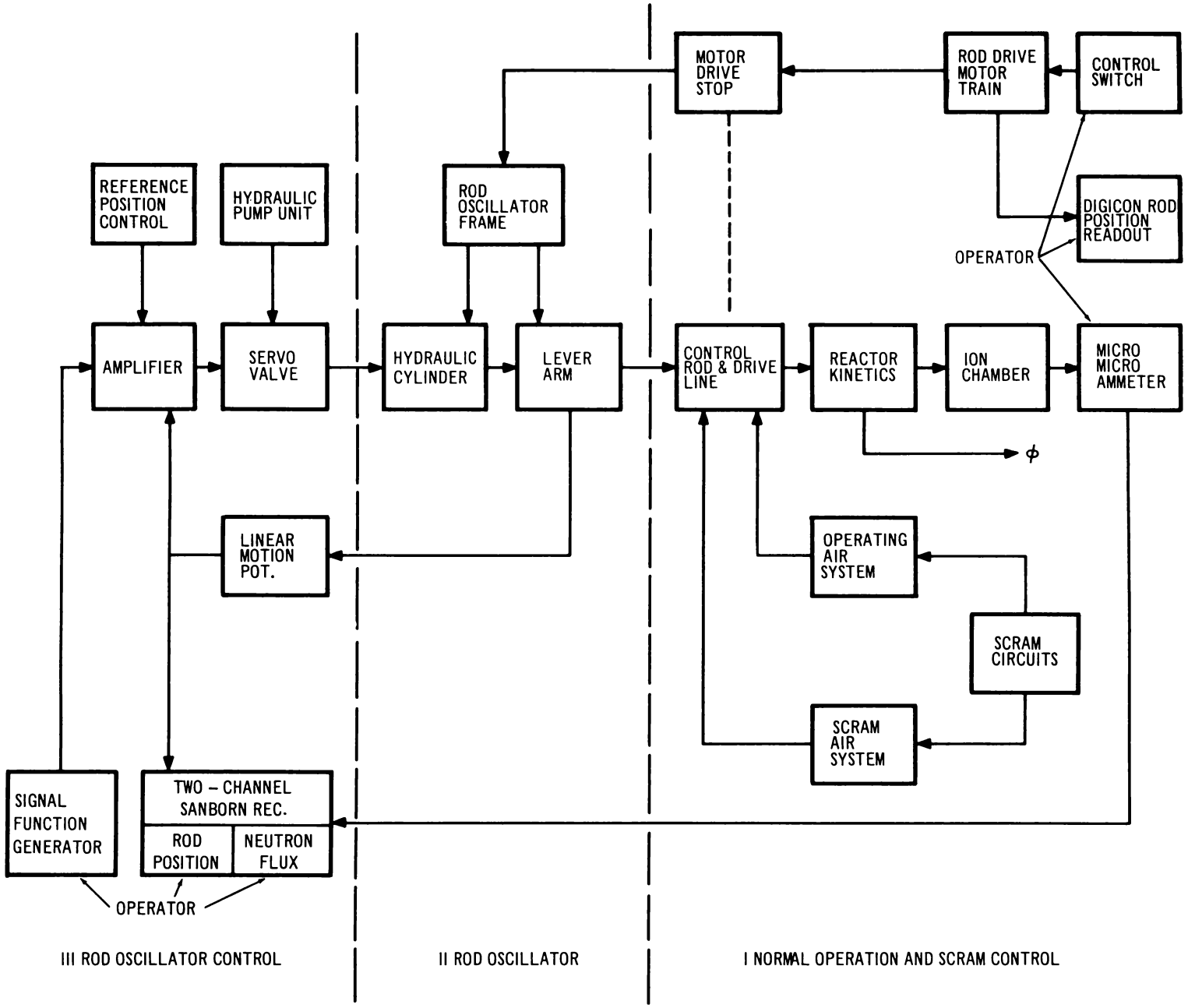

1266–8

FIGURE A-7 BLOCK DIAGRAM – CONTROL SYSTEM WITH ROD OSCILLATOR INSTALLED

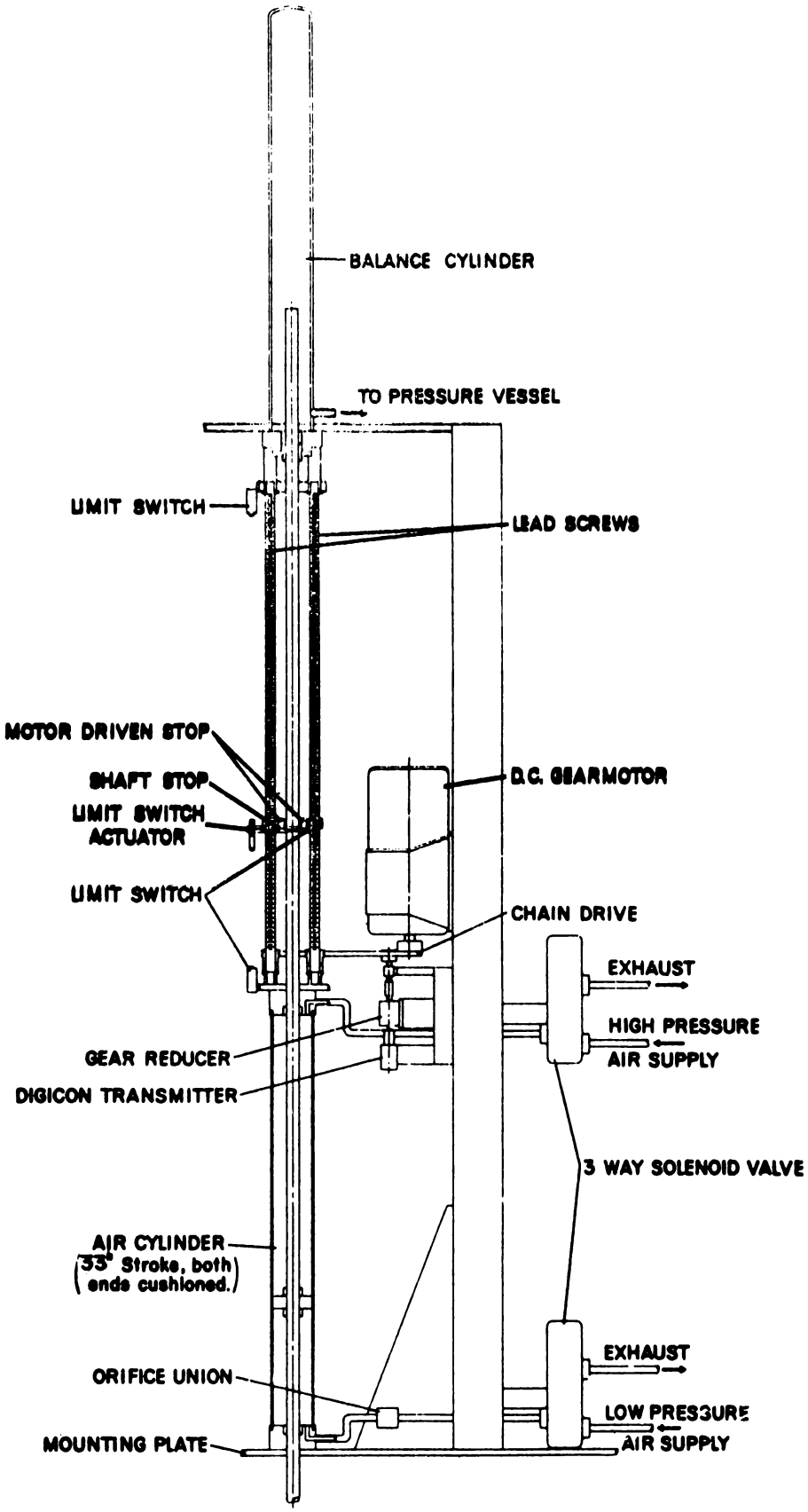

FIGURE A-8

CONTROL ROD DRIVE - SCHEMATIC

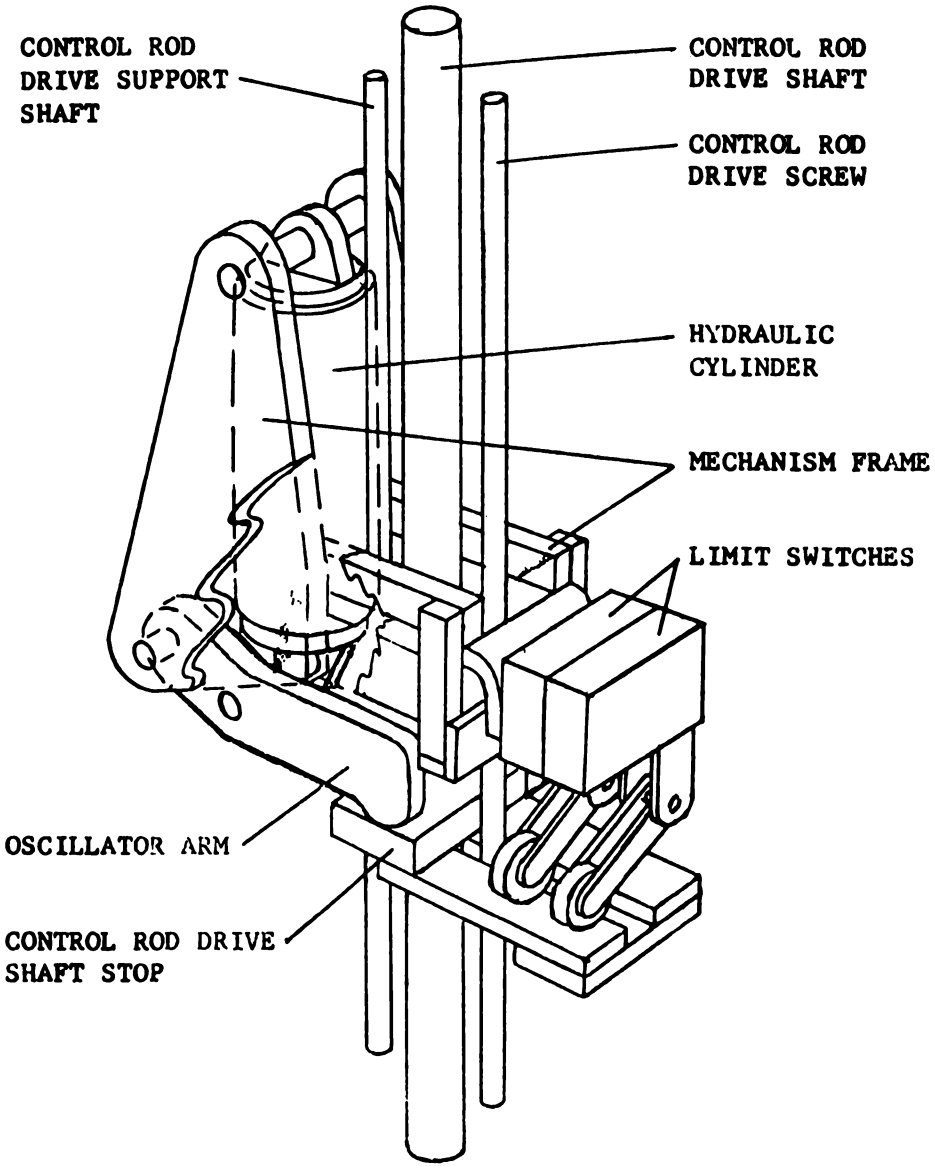

FIGURE A-9

CONTROL ROD OSCILLATOR MECHANISM

PL ISSUED

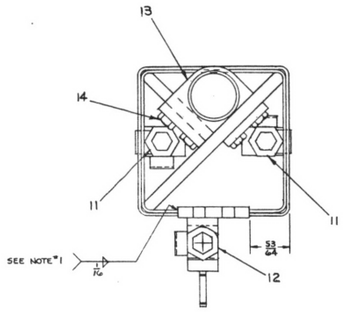

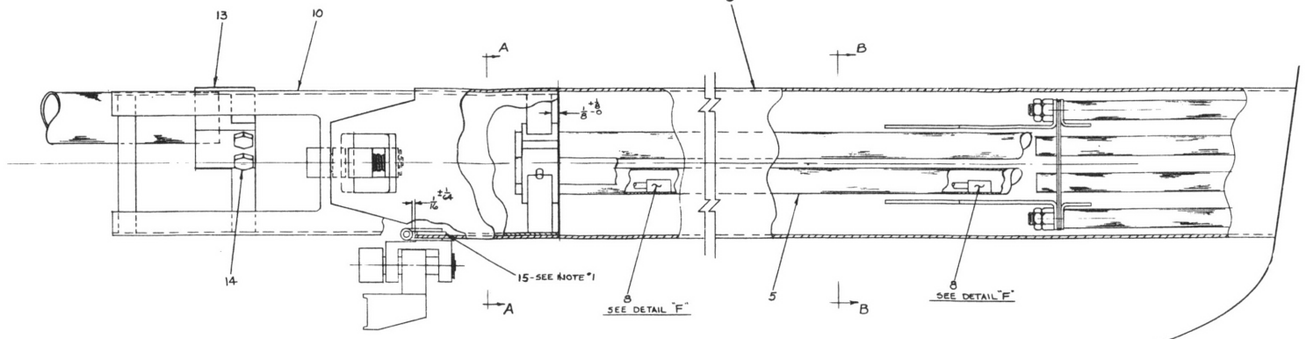

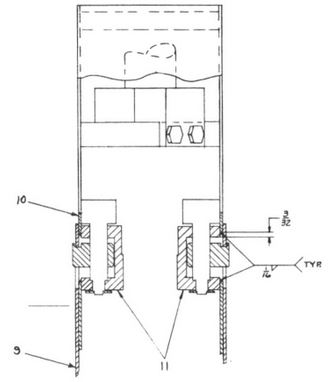

G1
G2 ZIRCALOY FUEL BUNDLE OTHERWISE SAME AS G1.

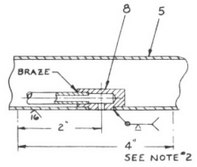

DETAIL "F"

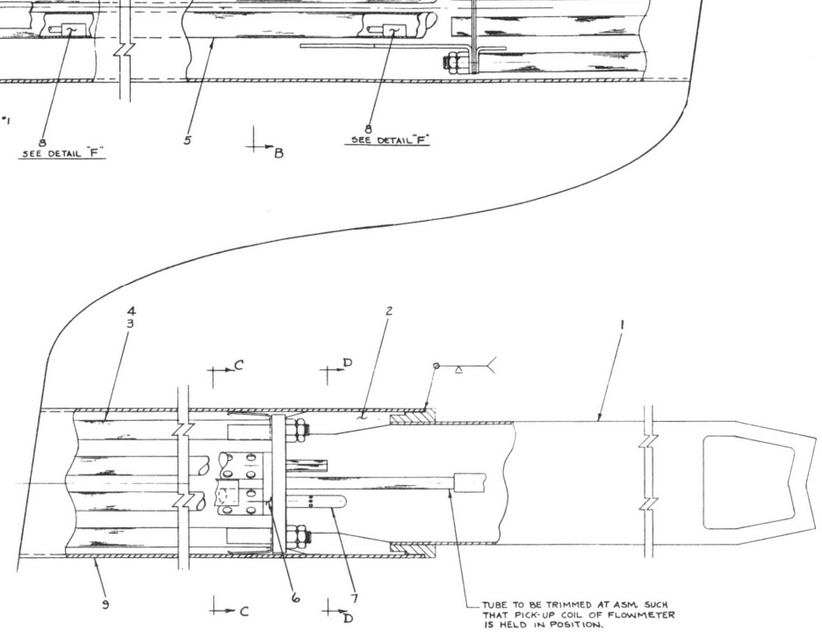

NOTES

1- SHIM AS REQ'D BETWEEN CHANNEL P9 AND LATCH P12 TO POSITION LATCH SCREW IN VERTICAL POSITION.

2- TUBE P5 TO HAVE A 63 FINISH FOR A DISTANCE OF 2" ABOVE AND 2" BELOW THE 1/16 DIA HOLE IN PRESSURE TAP P8. THIS FINISHED SURFACE SHALL BE BLENDED SMOOTHLY WITH O.D. OF TUBE.

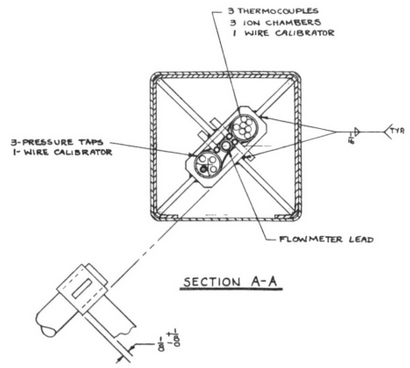

SECTION A-A

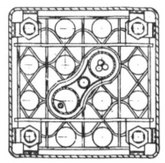

SECTION B-B

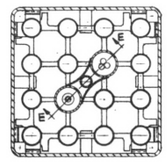

SECTION C-C

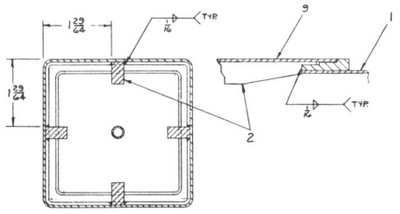

SECTION D-D

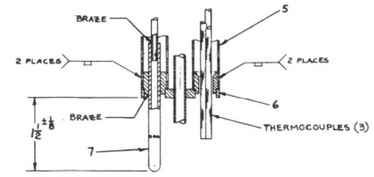

PARTIAL SECT. E-E

253

FIGURE A-10

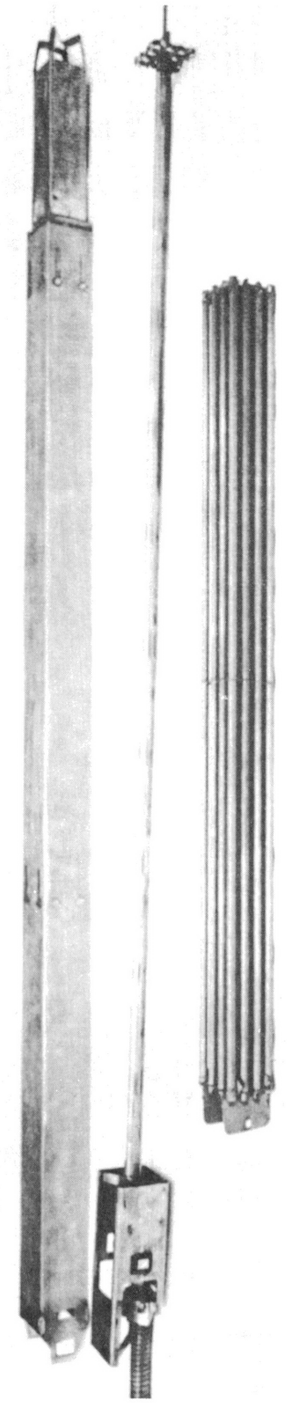

FIGURE A-11 - INSTRUMENTED ASSEMBLY SHOWING FUEL BUNDLES AND INSTRUMENT PROBE BEFORE ASSEMBLY

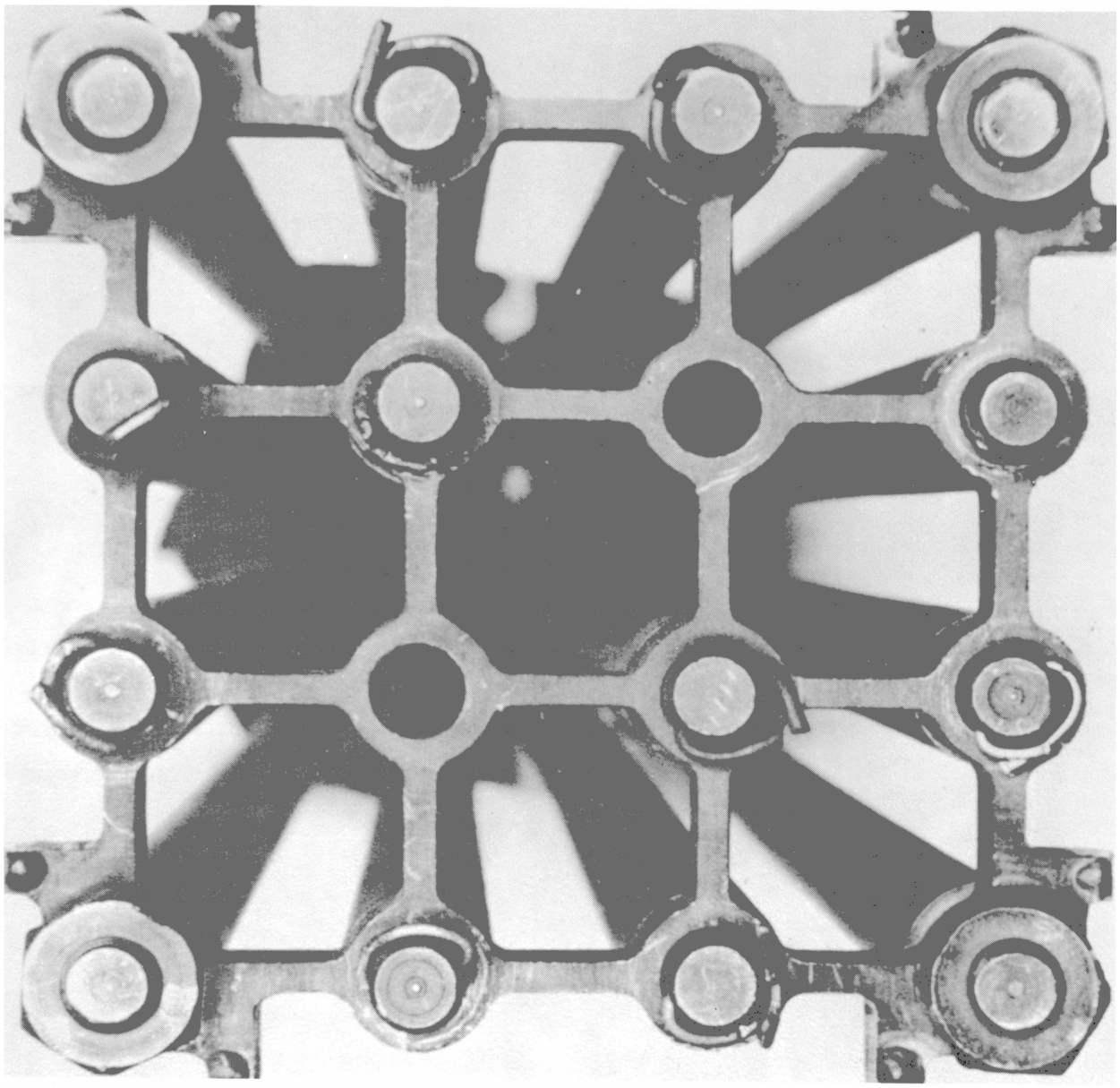

FIGURE A-12 - LOWER TIE PLATE INSTRUMENTED ASSEMBLY FOR FUEL BUNDLE

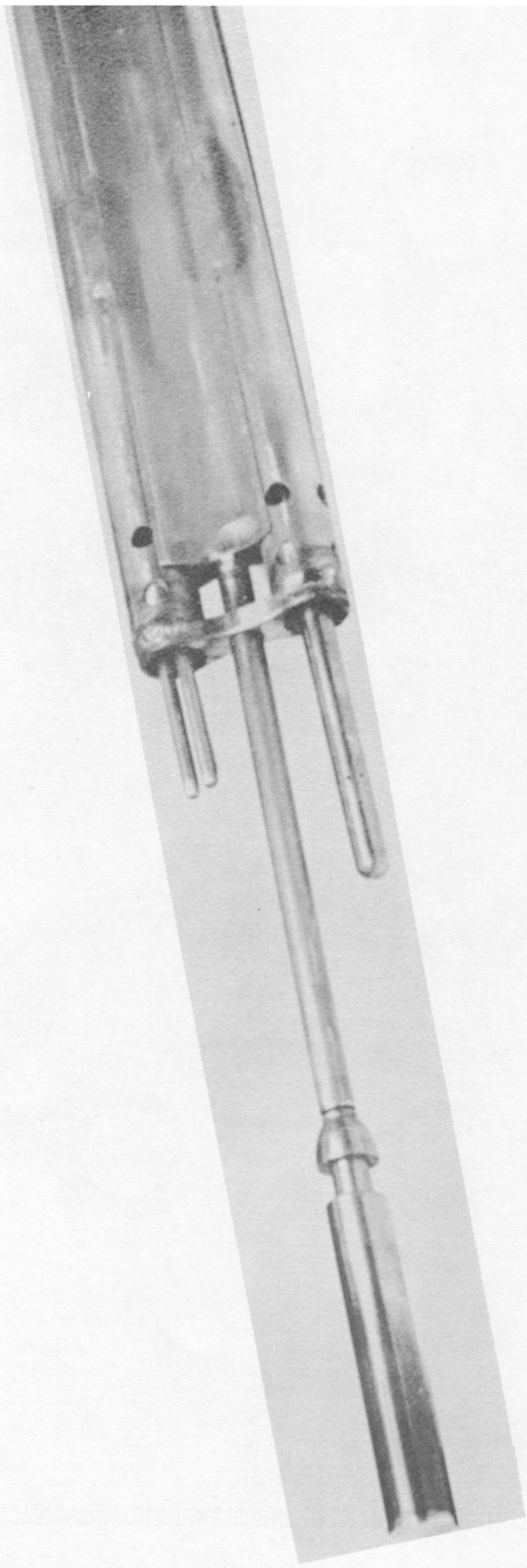

FIGURE A-13 - LOWER PORTION OF INSTRUMENTED PROBE FOR INSTRUMENTED ASSEMBLY

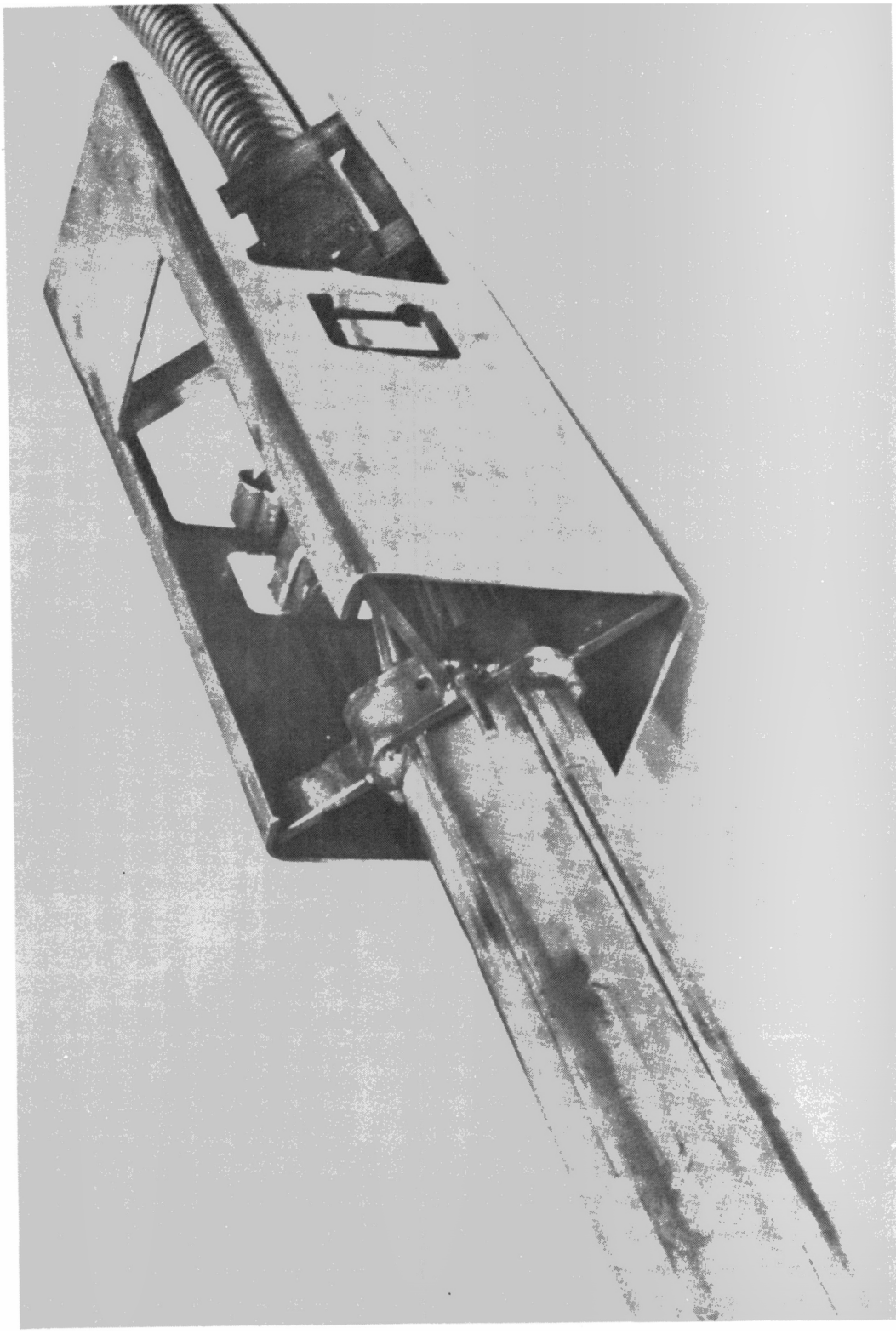

FIGURE A-14 - UPPER PORTION OF INSTRUMENTED PROBE FOR INSTRUMENTED ASSEMBLY

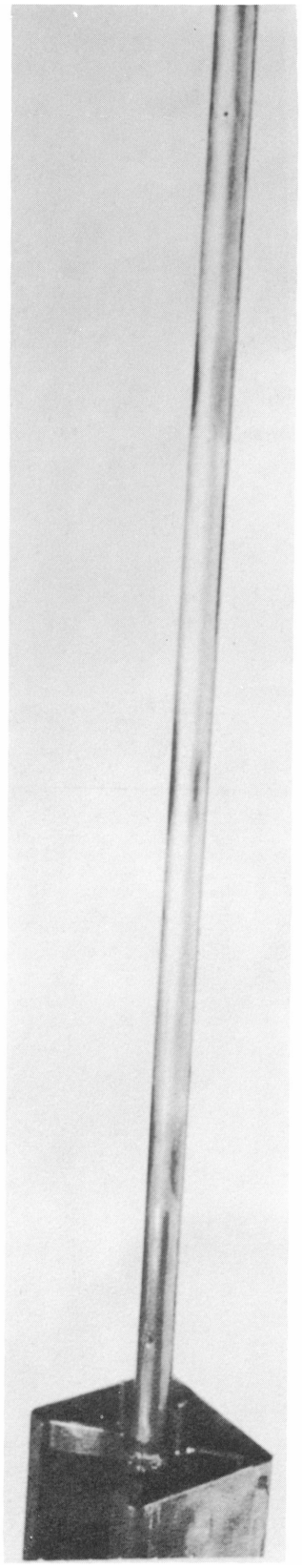

FIGURE A-15 - INSTRUMENT PROBE SHOWING STATIC PRESSURE TAPS

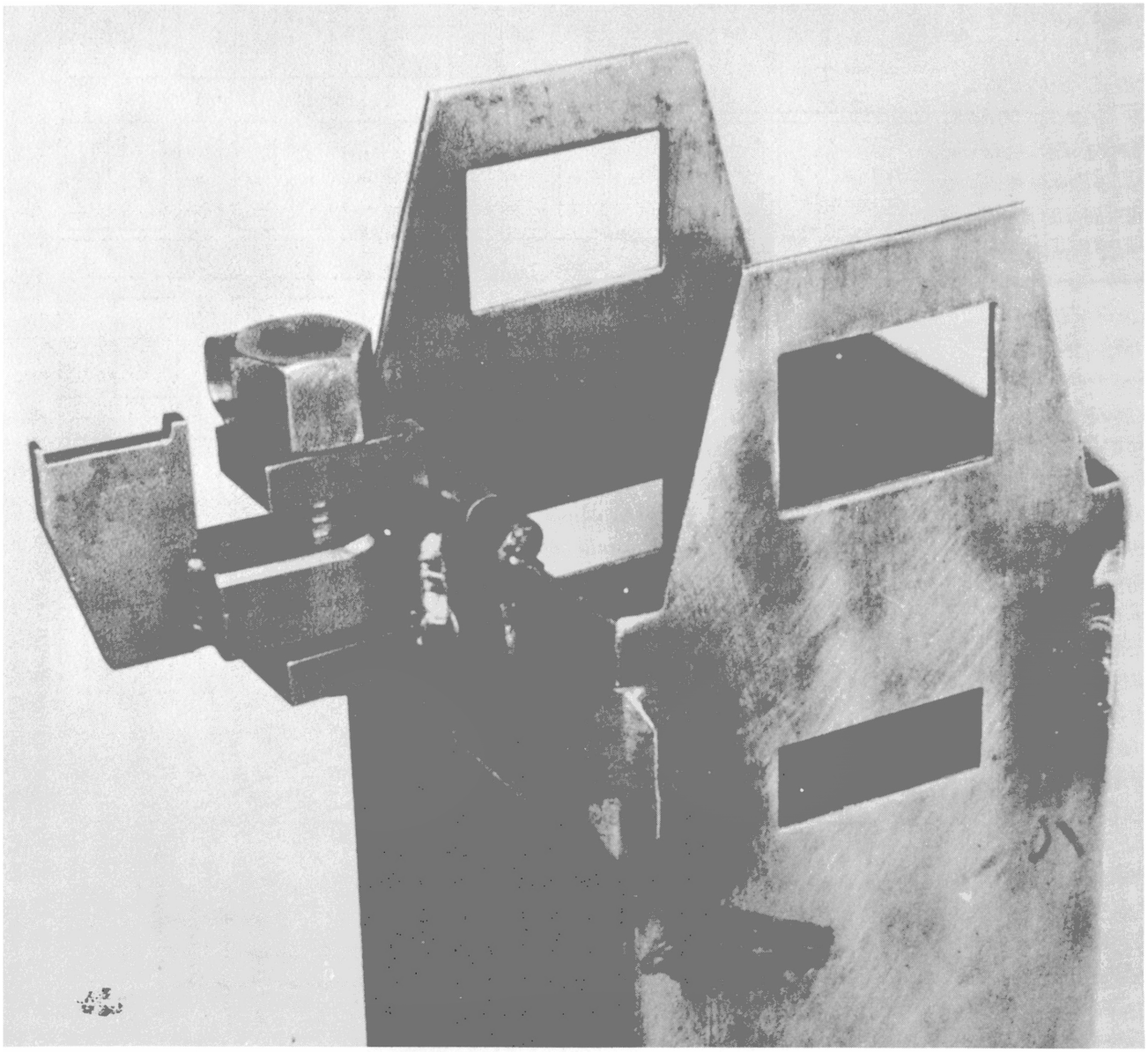

FIGURE A-16 - UPPER END OF INSTRUMENTED ASSEMBLY CHANNEL SHOWING DETAIL OF LOCK

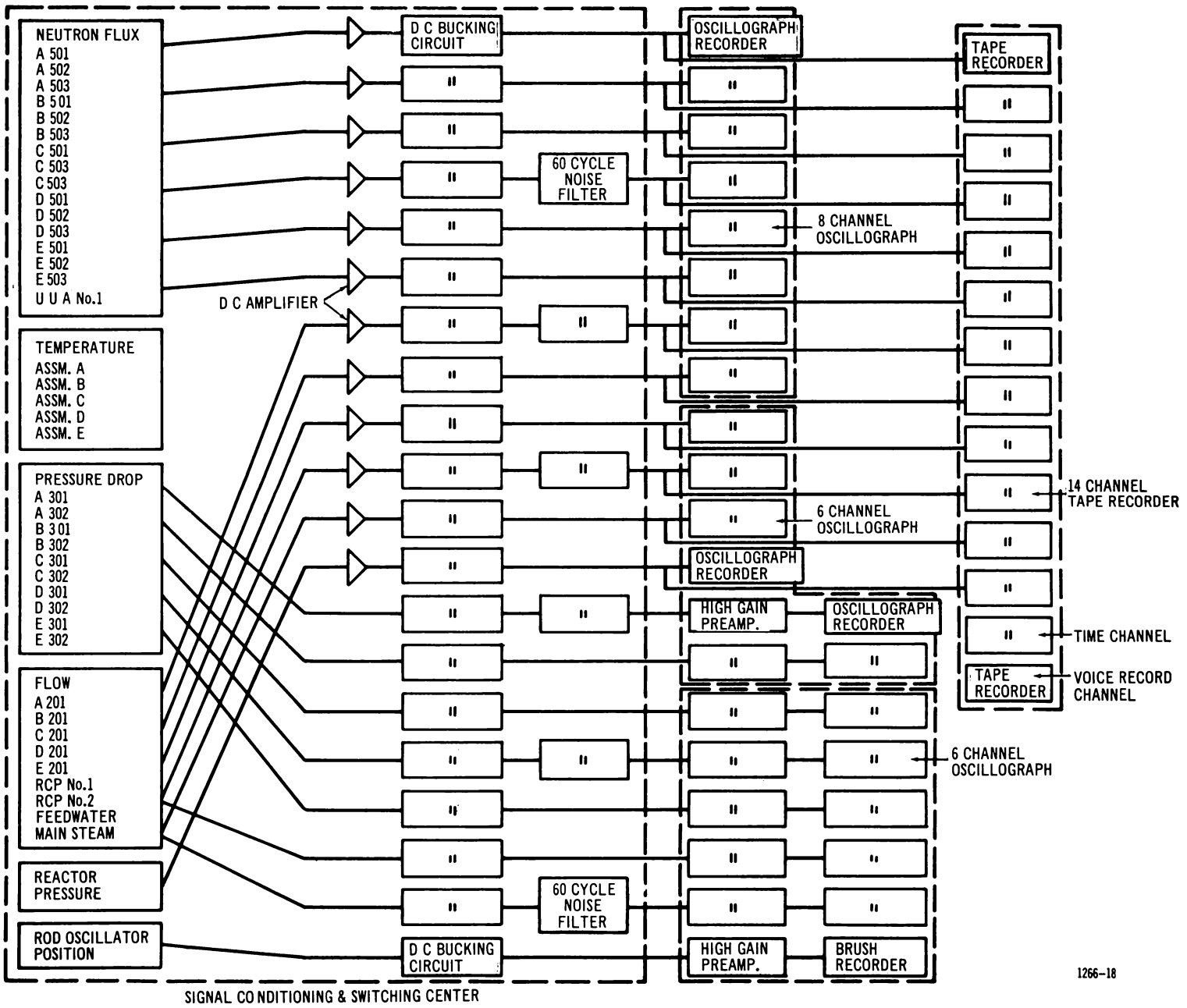

FIGURE A-17 SCHEMATIC DIAGRAM INSTRUMENTATION SYSTEM FUEL CYCLE STABILITY EXPERIMENT

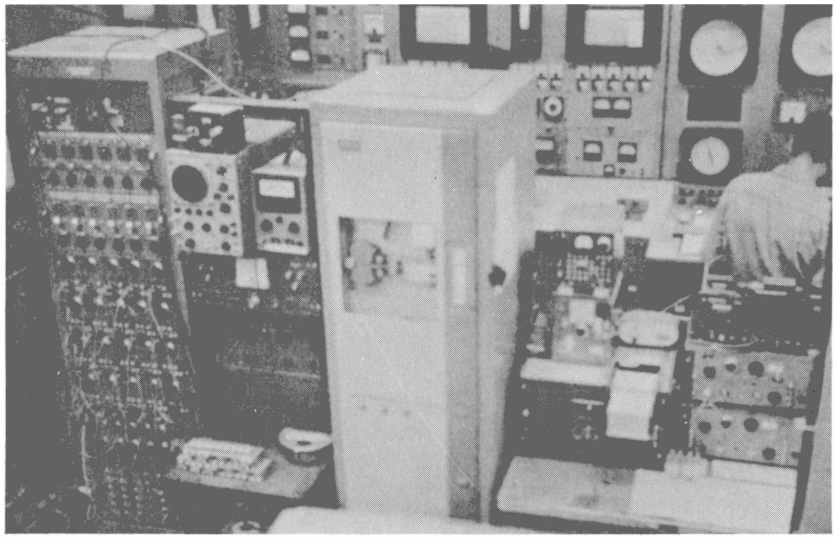

FIGURE A-18a GENERAL VIEW OF STABILITY TEST INSTRUMENTATION..

(Left side)

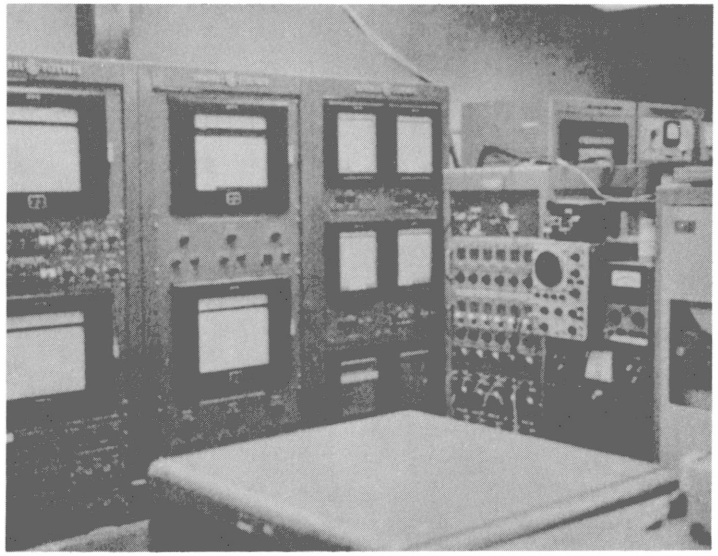

FIGURE A-18b STABILITY TEST INSTRUMENTATION LOCATED ADJACENT TO INSTRUMENTED ASSEMBLY READOUT PANELS..

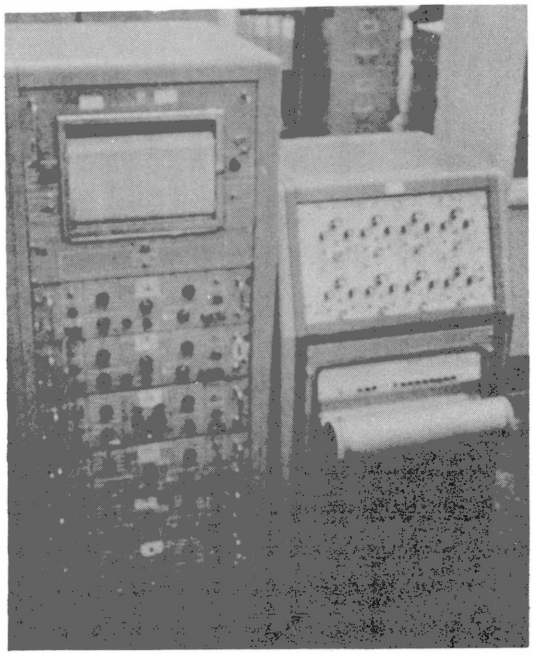

FIGURE A-18c VIEW SHOWING 14 OF 20 CHANNELS OF OSCILLOGRAPH RECORDERS.

522-7

APPENDIX B

TEST PROCEDURES

A. Overall Description

Written procedures for each type of test and the major items of test preparation and equipment installation were prepared and approved prior to conducting the experiment.

Safety criteria used throughout the procedures included the following:

1. The power-flow relationship combined with scram settings was such that a burnout margin of at least 1.5 was maintained at all times, including a pump loss accident.

2. Power changes or oscillations, as indicated by the external ion chambers, were always maintained within the range of $\pm$ 25 per cent of nominal test value. (High flux scram was set at $\pm$ 25 per cent; operation was limited to $\pm$ 17 per cent.)

3. Operation of any test equipment (particularly the rod oscillator) was only by persons specifically instructed in the operating requirements and authorized by the Reactor Test Program Engineer.

4. Operation of the rod oscillator was started only from a steady-state condition. The operator monitored at all times the recorder traces of rod position and reactor flux to insure that amplitude-frequency limits and reactor power oscillation limits were not exceeded. At each new test condition, rod oscillation amplitude was started at zero and increased to the desired value. Rod oscillator amplitude was limited to 10¢ reactivity, as determined by rod calibration on November 3, 1961.

5. The rod oscillator amplitude was limited to the following values:

Frequency cps	Amplitude inches	Limitation
Below 1	± 1	Stroke of hydraulic cylinder
1.4	± ½	Acceleration force *
2.0	± ¼	" "
3.0	± 1/8	" "

* Acceleration force available for upward stroke was limited by the permissible air pressure in the control rod operating air system.

B. Choice of Test Conditions

The test conditions were chosen to meet the experimental objectives by obtaining data over as wide a parametric range as possible. The range of operating conditions was limited in some cases by equipment performance, some by safety considerations, and in others, by reactor scheduling requirments.

The list of test conditions was then arranged in a sequence that:

1. Minimized the number of reactor shut-downs.
2. Maximized the average reactor power.
3. Minimized changes in low flow scram settings and high power scram settings.
4. Maximized spread of experimental conditions within the limits of the reactor system.

The list of desired conditions, and the steps for reaching them, constituted the Test Sequence Procedure. Failure of the seal on #2 Recirculation Pump necessitated revision of the sequence. The sequence used is shown briefly in the following.

At each of these experimental conditions, steady-state measurements were made, and, at most of the conditions, rod oscillator tests were made. Transient tests were made at a limited number of conditions only.

C. Steady-State Tests

The steady-state tests consisted of recording the signals from the various instruments. The recordings were made in several ways to indicate different types of phenomena.

First, an oscillograph recording was made at 2 mm/sec chart speed with no zero suppression. Second, the signals were zero-suppressed and amplified, and recordings were made at 2, 10, and 50 mm/sec. Magnetic tape recording of the zero-suppressed signal was also obtained at a tape speed of 15 inches per second. A one-second timing marker was used to indicate the speed of the oscillograph recorder. Duration of the recordings was chosen to provide adequate trace length for the various data analyses planned, and were as follows:

Recording	Minimum Duration
Oscillograph	
2 mm/sec	1 minute
10 mm/sec	1 minute
50 mm/sec	40 seconds
Tape	5 minutes

D. Rod Oscillator Tests

First, a steady-state recording was made as above. Then, with no changes in the instrument settings, the rod oscillator was started at the first frequency (0.03 cps). The resulting performance was recorded, using the same procedure as for a steady-state, zero-suppressed recording. The oscillator amplitude was decreased to zero, the frequency changed to the next value, and the amplitude increased to the desired value (limited by either mechanical design of oscillator, by flux variation of $\pm$ 17%, or by reactivity variation of $\pm$ 10¢). This condition was recorded and the procedure was repeated for each frequency up to 3.0 cps.

E. Transient Tests

First, a steady-state recording was made, as previously. Then, with the recording system operating, a "step" change was made in one variable. The transient was allowed to continue for one minute, or, until changes in power, water level, or pressure necessitated recovery to the initial conditions.

APPENDIX C

DATA REDUCTION

This section describes the following steps in data handling:

a. Instrument calibrations
b. Measurement errors
c. Frequency response of the instrumentation
d. Use of a band pass filter.

Digital analyses are described in Appendix E.

1. Instrument Calibrations

This section described the method of determining and maintaining the instrument calibrations during the testing.

a. Initial Transducer Calibrations

Prior to installation of the instrumentation on the VBWR process piping system and installation of the instrumented assemblies in the VBWR core, test-stand calibrations were performed on the transducers.

The transducers installed in the process piping system were Pace variable-reluctance type differential pressure cells. They were first bench-calibrated in the VBWR instrument shop against a Wallace and Tiernan, Model FA-145 mechanical pressure meter (0 to 200 inches H_2O). The accuracy of this latter meter was estimated to be better than $\pm$ 0.1 per cent of full scale when checked against water in a manometer. After installation in the VBWR process system, the calibrations of the differential pressure cells were checked. During the check after installation, the Wallace and Tiernan mechanical pressure meter was not available and another less accurate meter was used. The results of the calibrations on each transducer are plotted in Figures C-1 through C-5.

The instrumented assemblies were calibrated in the General Electric Heat Transfer Facility in San Jose, California. The procedures and equipment

used were described in GEAP-3898-AEC, "Sixth Quarterly Progress Report", October-December, 1961, Fuel Cycle Development Program.

The results of the pressure drop measurements are shown in Figures C-6, C-7 and C-8. Figure C-6 shows the nosepiece and flowmeter pressure drops for the three instrumented assemblies. Note that the nosepiece pressure drop in assembly 15-1 is over 9 times greater than in assemblies 21-J and 22-J, due to the orifice in the nosepiece of assembly 15-1 (nine 15/32-inch holes in a plate placed below the nosepiece). Figure C-7 shows the pressure drop across the fuel bundles of the instrumented assemblies. Figure C-8 shows the pressure drop across the fuel bundle and riser portion of the three assemblies. Note that the riser pressure drop is about 1/30 of the pressure drop across the fuel bundle.

Figure C-9 shows the calibration of the turbine type flowmeter. The data are tabulated in Table C-1.

The calibrations for the two instrumented assemblies from the High Power Density Research and Development Program were also done in the General Electric Heat Transfer Facility in San Jose, California. The complete results of the calibrations are being issued as GEAP-3896-AEC, "Calibration of Two Instrumented Reactor Fuel Assemblies for High Power Density Development Project", by E. Janssen and J. A. Kervinen. The calibration curves for the in-core flowmeters are shown in Figure C-10.

The thermocouples in the instrumented assembly were ungrounded chromel-alumel couples, embedded in magnesium oxide and swaged in a 304 stainless steel sheath to 1/8-inch outside diameter. During the tests, the reference junction was placed in a small furnace where the temperature was controlled to within + 0.3 F/- 0.6 F.

A summary of the transducer calibrations is shown in Table C-2.

b. Maintenance of Calibration

During the conduct of the tests, frequent checks of the calibrations of the instruments were made. Specifically, this included:

TABLE C-1

CALIBRATION OF TURBINE-TYPE FLOWMETERS

ASSEMBLY	LOOP DATA				ASSEMBLY DATA						
					Inlet Thermocouples			Inlet Flow-Meter			
	Run No.	Temp. ^{o}F	$\dot{w}$ (lb/sec)	$\dot{V}$ (gpm)	T_{101} ^{o}F	T_{102} ^{o}F	T_{103} ^{o}F	Q (gpm)	ΔP_1 "H_2O	ΔP_2 @	ΔP_3 75° F
21-J	1	109	6.05	43.95	107	110		44.2	3.43	5.91	5.85
	2	112	10.17	73.75	109	112		75.2	7.94	14.51	19.52
	3	109	14.41	104.6	110	110		105.6	11.99	27.42	28.79
	4	104	18.56	134.7	106	106		134.0	18.61	41.59	41.09
	5	545	12.78	123.9	549	557		125.0	30.30	42.30	44.40
	6	541	19.30	186.5	545	550		186.0			
	7	542	6.21	60.1	551	553		62.6			
22-J	1	113	10.13	73.6	113	114		74.6	6.55	9.85	12.04
	2	113	18.48	134.2	112	114		135.5	23.59	43.39	41.99
	3	545	12.86	124.8	554	556		124.4	24.60	39.10	37.60
	4	543	19.30	187.0	553	553		186.0	38.4	66.70	67.30
15-I	1	106	6.05	43.95	105	105		46.4			159.79
	1	88	6.07	43.95		99	99	44.0	28.81	31.31	32.31
	2	95	10.17	73.6		95	94	73.5	71.87	78.17	79.07
	3	97	14.43	104.6		98	98	103.5	139.07	151.07	152.57
	4	545	9.53	92.1		555	555	92.0	97.55	106.10	108.80
	5	541	12.82	123.9		548	553	123.0	163.60	174.00	175.00
	6	540	15.90	153.6		548	548	153.0	243.00	260.00	272.50

TABLE C-2

SUMMARY OF TRANSDUCER CALIBRATIONS

VARIABLE	TRANSDUCER	CALIBRATION
Reactor Pressure	Pace No. 4205	P = 0.495 (mV) - 90
Main Steam Flow	Pace No. 4203	0.099 in. H_2O/millivolt or 3350 lb/hr/$\sqrt{mV}$
Feedwater Flow	Pace No. 4201	.0654 in. H_2O/millivolt or 2550 lb/hr/$\sqrt{mV}$
Recirculation Flow:		
RCP No. 1	Pace No. 4202	0.0839 in. H_2O/millivolt or 265 gpm/$\sqrt{mV}$
RCP No. 2	Pace No. 4200	0.0720 in. H_2O/millivolt or 245 gpm/$\sqrt{mV}$
Assembly A Flow	A 201	103.7 gpm } Flow equivalent to 60 cps test frequency (Use scales of 400, 200, and 100 gpm On Pottermeter = 16 mV.)
Assembly B Flow	B 201	104.8 gpm
Assembly C Flow	C 201	113.5 gpm
Assembly D Flow	D 201	111.0 gpm
Assembly E Flow	E 201	111.3 gpm
Out-of-Core Flux	μμA	
In-Core Flux	501, 502, & 503 ion chambers	1.19×10^{11} nv/millivolt (Assumed calibration before flux-wire test.)
Fuel ΔP	301 Transducers	
Riser ΔP	302 Transducers	
Temperature	101, 102, & 103 thermocouples	REF. Jct. @ 291° F: T = 42.9(mV) + 300 REF. Jct. @ 499.7° F: T = 42.9(mV) + 500

1. Checking the balance of the Pace bridge-type carrier circuits once each day.

2. Re-balancing the Ampex tape recorder once each day.

3. Re-balancing the Brush direct-writing oscillograph recorders. This was done as often as necessary; for example, at the beginning of the day's operation, whenever a new instrument hook-up was made, whenever the chart paper was changed, when it was determined that excessive drift had occurred, or at the beginning of each new series of test runs.

4. At the beginning of each new series of test runs (i.e., at each new reactor operating point), one or more non-zero-suppressed, steady-state recording was made for calibration purposes. The Brush recorders were adjusted so that, in the balance condition, the recording styli were at the margin of the channel chart. The signal was introduced into the recorder and gain adjustments were made so that the signal would go as far full-scale as possible (see Figure C-15). The gains of the various circuit components and the reactor operating conditions were noted on appropriate data sheets. The "non-zero-suppressed" steady-state recording was immediately followed by a "zero-suppressed" steady-state recording. With the styli "zeroed" at the centerline of the channel chart, and with the sensitivity of the Brush recorder set at 0.05 volts per chart line on channels 1 to 12 (or some other appropriate sensitivity in the case of channels 13 to 20), a large percentage of the DC portion of the signal was suppressed off the channel chart. The Kintel amplifier gains were increased to cause the oscillating signal component to fill as much of the channel chart as possible. The gains of the various circuit components and the reactor operating conditions were again noted.

5. During testing, frequent spot checks were made to verify that the signals were not so large as to saturate the tape recorder amplifiers. This was done by reproducing the tape recorded signal on an oscilloscope. It was also accomplished by the "zero-suppressed" adjustments described in Item (d) above. The full scale peak-to-peak voltage on

the first twelve Brush recorder channels was 2.0 volts. The saturation voltage of the tape recorder was 2.8 volts peak-to-peak. As long as the stylus on a Brush recorder channel did not go off scale, the tape recorder amplifier was not saturated.

c. Calibration Equation

The calibration equation for the instrument system is

$$X = \frac{m K_3 N}{G_1 K_1 K_2 K_5} + \frac{m B}{K_1 K_2} + A + F(B,G_1)$$

In this equation

X = The value of the parameter measured

m = The calibration constant in Table C-2, units/millivolt

K_3 = Number of millivolts per chart line on Brush recorder

N = Number of chart lines deflection from balanced position

G_1 = DC attenuation of electrical noise suppression filter shown in Figure C-13.

K_1 = Attenuation of voltage divider, given in Table C-2

K_2 = Gain of Kintel DC amplifier

K_5 = Overall channel gain, shown in Figures C-11a through C-11c

B = Value of "bucking" voltage-millivolts

A = Constant correction factor

A = 90 psig for reactor pressure

A = Temperature of reference thermocouple junction - ^{o}F

$F(B,G)$ = Feedback voltage from Ampex (see Item d-5 below).

In practice during the data reduction, the complete calibration equation above was not used. Because the feedback factor from the Ampex recorder is a function of the bucking potentiometer setting and the 60-cycle filter, an alternate procedure was used in order to expedite the data reduction effort. Therefore, the following procedure was used.

1. Determine the number of lines of stylus deflection for the average value of the DC component of the signal.

2. Correct the number of lines in item (1) for any recorder drift.

3. Correct the number of lines in item (1) for feedback voltage from the Ampex tape recorder (obtained from Fig. C-12). The source of this feedback voltage is discussed in Item (d) below.

4. The scale factor for the non-zero-suppressed, steady-state trace in an example case is estimated as:

$$\text{Scale Factor} = \frac{100\%}{22.5 \text{ lines}} = 4.45\% \text{ per chart line} \qquad (C\text{-}1)$$

5. The scale factor for the zero-suppressed, steady-state trace is estimated by multiplying the scale factor for the non-zero-suppressed trace as follows:

$$SF_{ZS} = SF_{NZS} \cdot \left(\frac{(K_3)_{ZS}}{(K_3)_{NZS}}\right) \cdot \left(\frac{(G_1)_{NZS}}{(G_1)_{ZS}}\right)\left(\frac{(K_2)_{NZS}}{(K_2)_{ZS}}\right)\left(\frac{(K_5)_{NZS}}{(K_5)_{ZS}}\right) \qquad (C\text{-}2)$$

Where SF = Scale Factor,

The subscripts "ZS" and "NZS" indicate the value of the factor in the zero-suppressed and non-zero-suppressed case, respectively. Equation C-2 was obtained by considering the first term on the right-hand side of equation C-1 in the zero-suppressed and non-zero-suppressed cases. If a ratio of the value of this term in the zero-suppressed to the non-zero-suppressed case is taken, the result is the factor in equation C-2.

By this procedure, the oscillatory component of the signal can be expressed as a per cent of the mean signal. The analytical model also uses the per cent or fractional form for the model parameters. Comparison of the experimental and analytical models is thereby facilitated.

This procedure assumes linearity of the calibration curves of the primary sensing instruments. That is, the slope of the calibration curve at the operating point must equal the mean slope of the calibration curve from zero to the operating point. This assumption was

fairly accurate. In relative amplitude considerations, this does not introduce any error. Only in absolute magnitude analyses would correction be required.

d. Special Calibration Problems

During the testing, several problems of determining and maintaining calibrations and instrument operability were encountered. They were:

1. In-core Flowmeters

The flowmeters suffered from deterioration of the permanent magnets. Three small magnets were located on the turbine rotor of the flowmeter so that, for each revolution of the rotor, three voltage pulses occur in a small pickup coil. Thus, the flow rate through the flowmeter was proportional to the frequency of the pulses received at the read-out circuitry. The pulse strength on all the assemblies gradually decreased and the signal became more difficult to distinguish from the 60-cycle noise picked up in the signal leads. Also, the loss in strength of the three magnets was unequal, thus resulting in a wave form that was not properly interpreted by the frequency-to-voltage converter. The converter sometimes counted two pulses per revolution, and sometimes three pulses. Also, by mid-December, Assembly D flowmeter pickup coil had partially shorted to ground. This was evidenced by a resistance to ground of 20 ohm on one lead, and about 40 on the other, compared to 500 ohms on each side when new.

The flow signals from Assembly D (in the highest flux) became unuseable after 4 - 5 weeks, and from Assembly E became unuseable after 8 weeks. The signal from Assembly C were still useable at the end of two months of stability tests.

2. In-Core Ion Chambers

The only difficulty experienced with the in-core chamber was that moisture (steam from leak in flange on head of reactor vessel) penetrated the junction box for electrical terminal strips located outside the reactor vessel. The moisture resulted in a leakage current which changed the effective calibration of the instruments. Otherwise all ion chambers were operating satisfactorily when removed.

3. In-Core Thermocouples

A problem of calibration was encountered with the thermocouple system. Several times during the stability test, steady-state measurements of core inlet and outlet coolant temperatures were taken with the thermocouple system. The measured temperature difference was about 2 to 4° F. less than the temperature difference(subcooling) calculated from a heat balance. It was postulated that the difference is due to unequal gamma heating in the interiors of inlet and outlet thermocouples which caused a temperature gradient between the ungrounded couple and the coolant. The lower thermocouple is in a much higher radiation field than the upper.

4. Fuel and Riser Pressure Drop

The calibration of the pressure drop systems were found to be in error on several occasions due to several factors:

a. A zero shift in the variable-reluctance pressure transducers.
b. Errors caused by varying static pressure differences in two long vertical pressure lines connecting to the same transducer. These errors were caused by steam void accumulation within the pressure lines, and/or by transient temperature differences in the two lines. The back-purge system was able to reduce these effects but did not eliminate them.
c. The pressure signal had a large amplitude random variation of undetermined origin.

5. Overall Channel Gains

During the course of the readout system "de-bugging" and check-out, anomalous calibrations were observed. A check indicated that the output impedance of the bucking circuit was too large. A bias voltage on the grid of the first DC amplifier triode in the Ampex tape recorder was causing currents through the output impedance of the bucking circuit which resulted in rather substantial calibration errors. Data was accumulated on the magnitude of the errors and an analysis of the circuit was made. The results are shown in Figures C-11a through C-11c. The required correction to the calibration,

called overall channel gain, was found to be a function of the setting of the bucking voltage potentiometer. The magnitude of the bias voltage appearing at the input terminals of the tape recorder is shown, in Figure C-12, to be a function of the setting of the bucking voltage potentiometer.

6. Sixty-Cycle Filter

The insertion of a 60-cycle filter into the amplifier output circuit introduced a resistance in series with the bucking resistance. This produces a voltage reduction at the input to the recorders. This voltage reduction, which is a function of the bucking resistance setting, is shown in Figure C-13. The corrections were experimentally determined by measuring four filters. Since the filters were constructed with 1% tolerance resistors, the filter attenuations should be identical within 1%. The experimental data scatter was also of this order of magnitude. One correction curve was therefore used.

2. Frequency Response of Instrumentation

This section describes the frequency response of the various components of the readout system and the transducers.

a. Readout System

Figure C-14 presents an estimate of the frequency response of the Brush oscillograph recorders. The data in Figure C-14 was obtained after the Brush recorders were installed in the readout system in VBWR. A gain and phase shift of the electrical noise suppression filter exists in this circuit. In addition, there is an attenuation factor effective at all frequencies, and is due to the input grid voltage feedback from the Ampex recorder. (see Item 1 of this appendix). The filters were used only when needed to reduce 60 cps background noise.

The frequency response of the Kintel DC amplifiers and the Ampex tape recorder were assumed to be flat from DC to approximately 2 K cps, with negligible phase shift up to 1 K cps. This assumption is based on the manufacturer's specifications given in Table C-3.

TABLE C-3

MANUFACTURERS SPECIFICATIONS FOR KINTEL (MODEL 112A) AMPLIFIERS

Gain	Steps of 0, 20, 30, 50, 70, 100, 200, 300, 500, 1000
Gain Stability	0.1%
Input Impedance	100K Ohms
Output Impedance . . .	< 1 Ohm
Equivalent Input Drift	< $\pm$ 2 micro-volts
Equivalent Input Noise	< 5 micro-volts peak-to-peak in the 0 to 750 cps bandwidth
Linearity	Better than 0.05% to 1 KC
Frequency Response . .	$\pm$ 0.5% to 2 KC
Rise Time	< 10 micro-seconds
Phase Shift	< 5^{o} to 2 KC

b. Transducers

An estimate of the response rate of the Pottermeter turbine-type in-core flowmeters was made.[20] The readout instrumentation was experimentally determined by measuring the rise time. Assuming that the readout system can be simulated by a single time constant, the frequency response is obtained from the rise time. The curves shown in Figure C-15 also include the response rate of the frequency-to-analog converters in the readout system, but do not include the frequency response of the Brush oscillographs. The readout instrumentation contributes most of the response limitation.

Figure C-16 shows an estimate of the response of the recirculation flow transducers and their pressure lines. This estimate was based on the method of Iberall,[21] and indicates a flat response up to 100 cps. The frequency response of the ion chambers is estimated to be flat from DC to greater than 2 K cps. The out-of-core compensated ion chamber signal was taken through a micro-micro ammeter, the frequency response of which is flat from DC to greater than 2 K cps. All of the ion chamber signal frequency responses are, therefore, limited only by the readout system frequency response.

3. Experimental Accuracy

a. Approach to Error Analysis

Errors are usually broken into three categories; personal errors, fixed errors, and accidental errors.

1. Personal Errors

This type of error may be classed as operator bias or mistake. It is the tendency of one person to read the scales of an instrument or of a measure a trifle to one side of the line, for example, or to simply make an erroneous reading.

During the VBWR stability test, eight engineers were used to operate the instrumentation and take data. Two shift of data-taking were operated per day, each shift usually having three men. One man operated the control rod oscillator, and two men took data. Very few

actual readings were made during one test series.* Most of the testing consisted of recording transient signals. The readings that were made consisted of:

a. Reading the gain of the Brush oscillograph recorders,
b. Reading the gain of the Kintel DC amplifiers,
c. Reading the adjustment of the bucking voltage potentiometer,
d. Determining which signal was being recorded on each channel,
e. Where the "zero" of the oscillograph recorder channel was set,
f. Whether an electrical noise suppression filter was used.

The dial markings in items (a) and (b) were such that the Brush oscillograph gain took the values 10 volts/line, 5 volts/line, 2 volts/line, 1 volt/line, 0.5 volt/line, 0.2 volt/line, 0.1 volt/line, 0.05 volt/line, 0.02 volt/line, 0.01 volt/line, and the Kintel amplifier gain took the values of 0, 20, 30, 50, 70, 100, 200, 300, 500, 700, and 1000. Clearly, either the readings in items (a), (b), (d), (e) and (f) above were taken and noted correctly, or they were in error by a large percentage. In the latter case, the final results would be out of place and the data would be discarded.

The bucking voltage potentiometers in item (b) were the Helipot ten-turn type. It was possible to read them to 1/1000 of their full scale value, and to estimate to 1/2000 of their full scale value. However, the calibration of the "overall channel gain" described in section C-1 above was such that reading accuracies to 1/100 of the potentiometer full scale value wer adequate. Therefore, it is concluded that essentially no reading errors occurred during the data recording phase of the experiment, outside of actual mistakes.

2. Fixed Errors

Fixed errors, for the purposes of this experiment, were considered as errors inherent in the test equipment for which corrections were available. They included the following:

* The test series consisted of a non-zero-suppressed, steady-state recording, the zero-suppressed, steady-state recording, and the recordings at each rod oscillator frequency.

a. Frequency response of transducers and recorders.

b. Bias voltage from tape recorder.

c. Impedance mis-match between bucking circuit and tape recorder, corrected by "overall channel gain".

The appropriate corrections for these errors were presented and discussed in sections C-1 and C-2, above.

3. Accidental Errors

This type of error was considered as the residual error that occurred after all corrections for the other types of errors were made. Under the assumption that the accidental errors distributed themselves randomly about some mean value, the Gaussian or normal probability density function was used to describe the overall value of accidental errors. The following items were included under accidental errors:

a. Zero drift in readout system.

b. Noise level in readout system where appropriate.

c. Resolution in reading Brush oscillograph traces.

d. All other errors not included as personal and fixed errors.

b. In estimating the manner in which errors propagated through the readout system, the procedure suggested by Kline and McClintock[22] was used. Briefly, the procedure is:

1. A judgement is made as to which parameters contribute to the overall measurement uncertainty.

2. Estimate the "uncertainty" in each parameter as mean $\pm$ uncertainty interval (odds of 20 to 1).

3. Compute the uncertainty interval for the overall measurement from

$$w_R = \left[\left(\frac{\delta R}{\delta P_1} w_1 \right)^2 + \left(\frac{\delta R}{\delta P_2} w_2 \right)^2 + \ldots + \left(\frac{\delta R}{\delta P_n} w_n \right)^2 \right]^{\frac{1}{2}} \qquad (C\text{-}3)$$

where

w_R = Uncertainty interval for overall measurement

w_n = Uncertainty interval for nth parameter, P_n

R = Overall measurement value.

Equation C-3, above, assumes that the overall measurement value, R, is some function of the parameters V_1, V_2, V_3, —, V_n, i.e., that the partial derivatives $\partial R / \partial V_i$ exist. The uncertainty interval w_R for the overall measurement, thus, has the odds of 20 to 1 attached to it. Although the choice of these odds is arbitrary, the value 20 to 1 corresponds approximately to a spread of plus or minus two standard deviations of a normal distribution.

The method used to determine the calibrations for the runs of this experiment was described in Section C-1-c. It consisted of:

1. Computing the non-zero-suppressed scale factor for the Brush oscillograph recordings

$$(SF)_{NZS} = \frac{100\%}{N \pm C_1 \pm C_2} \quad (\% \text{ per chart line}) \qquad (C\text{-}4)$$

Where

N = Mean value of number of lines of pen deflection for the non-zero-suppressed signal (100% of mean signal value)

C_1 = Correction for feedback voltage from tape recorder, number of lines.

C_2 = Correction for recorder drift, number of lines

SF = Scale factor.

2. Computing the zero-suppressed scale factor for the Brush recorder,

$$(SF)_{ZS} = (SF)_{NZS} \cdot \left(\frac{(G_1)_{NZS}}{(G_1)_{ZS}}\right)\left(\frac{(K_2)_{NZS}}{(K_2)_{ZS}}\right)\left(\frac{(K_3)_{ZS}}{(K_3)_{NZS}}\right)\left(\frac{(K_5)_{NZS}}{(K_5)_{ZS}}\right)$$

(% per chart line) (C-5)

Where

G_1 = Gain of electrical noise suppression filter

K_2 = Gain of Kintel DC amplifier

K_3 = Gain of Brush oscillograph recorder, volts/line

K_5 = Overall channel gain,

and NZS and ZS represent the gains for the non-zero-suppressed and zero-suppressed runs, respectively.

3. Computing the tape recorder zero-suppressed scale factor,

$$\left(\begin{matrix}\text{Tape}\\ \text{Scale Factor}\end{matrix}\right)_{ZS} = \left(\begin{matrix}\text{Brush}\\ \text{Scale Factor}\end{matrix}\right)_{NZS} \quad \frac{(G_1)_{NZS}}{(G_1)_{ZS}} \quad \frac{(K_2)_{NZS}}{(K_2)_{ZS}}$$

$$\frac{1}{(K_3)_{NZS}} \quad \frac{(K_5)_{NZS}}{(K_5)_{ZS}} \quad (\% \text{ per volt}) \qquad (C\text{-}6)$$

4. Observing peak-to-peak amplitudes of the steady-state flux and flow noise from the oscillograph traces or from the tape recorded data.

These values, expressed as a number of chart lines or a number of volts of amplitude were then applied to the scale factors described in (1), (2), and (3) to determine amplitudes as a per cent of the mean values of the parameters. This is done by multiplying the number of chart lines (or volts) deflection by the appropriate scale factor. Thus, the overall results were calculated in the following manner. For the oscillograph recorder traces:

$$R = \frac{N^1\ 100\%}{N \pm C_1 \pm C_2} \frac{(G_1)_{NZS}}{(G_1)_{ZS}} \frac{(K_2)_{NZS}}{(K_2)_{ZS}} \frac{(K_3)_{ZS}}{(K_3)_{NZS}} \frac{(K_5)_{NZS}}{(K_5)_{ZS}} \quad \text{(per cent)} \qquad (C\text{-}7)$$

Where R = Percent of signal deviation from its mean value for a pen deflection of N^1 lines from its mean value.

And, for the tape recorded data:

(C-8)

$$R = V \frac{100\%}{N \pm C_1 \pm C_2} \frac{(G_1)_{NZS}}{(G_1)_{ZS}} \frac{(K_2)_{NZS}}{(K_2)_{ZS}} \frac{1}{(K_3)_{NZS}} \frac{(K_5)_{NZS}}{(K_5)_{ZS}} \quad \text{(per cent)}$$

Where R = Percent of signal deviation from its mean value for a recorded voltage deflection of V volts from its mean value.

The equations describing the overall measurement uncertainty interval was obtained by applying equations C-7 and C-8 to equation C-3. The results obtained were:

a. For the zero-suppressed oscillograph recorder traces: (C-9)

$$\frac{w_{(R)ZS}}{(R)_{ZS}} = \left[\left\langle \frac{(w_n)}{N^1} \right\rangle^2 + (w_n)^2 + \frac{(w_{c_1})^2 + (w_{c_2})^2}{(N \pm C_1 \pm C_2)^2} + \left\langle \frac{(w_{G_1})_{NZS}}{(G_1)_{NZS}} \right\rangle^2 + \left\langle \frac{(w_{G_1})_{ZS}}{(G_1)_{ZS}} \right\rangle^2 + \left\langle \frac{(w_{K_5})_{NZS}}{(K_5)_{NZS}} \right\rangle^2 + \left\langle \frac{(w_{K_5})_{ZS}}{(K_5)_{ZS}} \right\rangle^2 \right]^{\frac{1}{2}}$$

b. For the zero-suppressed recorder tape data: (C-10)

$$\frac{w(R)_{ZS}}{(R)_{ZS}} = \left[\left\langle \frac{wv}{V} \right\rangle^2 + \frac{(wn)^2 + (w_{c_1})^2 + (w_{o_2})^2}{(N \pm C_1 \pm C_2)^2} + \left\langle \frac{w_{G_1 NZS}}{(G_1)_{NZS}} \right\rangle^2 + \left\langle \frac{w_{G_1 ZS}}{(G_1)_{ZS}} \right\rangle^2 + \left\langle \frac{(w_{K_5})_{NZS}}{(K_5)_{NZS}} \right\rangle^2 + \left\langle \frac{(w_{K_5})_{ZS}}{(K_5)_{ZS}} \right\rangle^2 \right]^{\frac{1}{2}}$$

c. For the non-zero-suppressed oscillograph recorder traces and the non-zero-suppressed recorded tape data: (C-11)

$$\frac{w(R)_{NZS}}{(R)_{NZS}} = \left[\left\langle \frac{w_{n1}}{N^1} \right\rangle^2 + \frac{(w_n)^2 + (w_{c_1})^2 + (w_{c_2})^2}{(N \pm C_1 \pm C_2)^2} \right]^{\frac{1}{2}}$$

Table C-4 presents the values of the parameters occurring in equations C-9 to C-11, and the estimates (at 20 to 1 odds) of the uncertainty intervals for these parameters. Based on the numbers in Table C-4, the overall estimate of the uncertainty of the zero-suppressed scale factors computed for any variable was $\pm$ 9% of the value of the scale factor (20 to 1 odds).

After the scale factors were computed, they needed to be applied to the data by reading oscillograph pen deflections, or by performing some operation on the tape recorded data. In the case of the oscillograph data, an additional uncertainty occurred due to accuracy in reading of the oscillograph traces. Assuming a representative amplitude (peak-to-peak) on the trace of 10 chart lines, and an uncertainty in reading the trace of 1/2 chart line, the total uncertainty of the data derived from the oscillograph-recorded traces was computed to be $\pm$ 10% (20 to 1 odds).

c. Frequency Analysis

The data recorded on the tape recorder was frequency analyzed as described in Section C-4. Figure C-18 shows an example of the results of the frequency analyses. The following general statements can be made about the uncertainties:

1. The relative amplitudes have an error of 6% within a two-mean deviation spread about either side of the mean (95% confidence limit). The gain versus frequency curve for the band pass filter (Fig. C-22) showed the greatest spread in repeatability at the lower frequencies (about 0.03 to 1.0 cps). The repeatability was 5.7% for a two-mean deviation spread from the mean; calculation was performed at frequency of 0.2 cps. The data spread was calculated for Run 15-1-2 at a frequency of 0.1 cps and was 6.0% (95% confidence). The spread in the data is approximately equal to the uncertainty in the band pass gain.

2. The uncertainty in the absolute values of the tape recorded data is $\pm$ 10%, with two-mean deviations, or 95% confidence limits. This deviation is composed of contributions from the band pass analyzer (repeatability) and from the scale factor for the mean value in the zero-suppressed case. The potential gain in accuracy from improving the calculation of the scale factor for the mean value is 4 per cent.

TABLE C-4

ESTIMATE OF UNCERTAINTY INTERVALS FOR PARAMETERS

Parameter	Value of Parameter	Uncertainty Interval (20 to 1 odds)	Remarks
n and N	Assume $n_{ave.}$ = 10 lines $N_{ave.}$ = 20 lines	1/2 chart line for N 1/4 chart line for n	Value of parameter depends on value of the signal coming from transducer.
C_1	From 3/10 to 8/10 chart line depending on bucking potentiometer setting.	1/10 chart line	See Figure C-13
C_2	Mean value assumed to be zero.	1/2 chart line	Based on Brush recorder specifications.
$(G_1)NZS$	0.91	0.02	See Figure C-14
$(G_1)ZS$	From 0.91 to 0.86 depending on bucking potentiometer setting.	0.01	See Figure C-14
$(K_5)NZS$	From 0.46 to 0.53 depending on channel being considered.	0.01	See Figure C-12a - 12c
$(K_5)ZS$	From 0.46 to 0.87 depending on channel being considered and on bucking potentiometer setting. (Use .52 for calculation)	0.01	See Figure C-12a - 12c

4. Data Analysis Use of a Band Pass Filter Network

A band pass filter was used as the major technique of data reduction. The tape-recorded signals were analyzed for frequency content, using the circuit shown in Figure C-17, and discussed below. This analysis results in a plot of the amplitude of oscillation as a function of frequency. The technique was used on both the steady-state and rod oscillator data. The results are presented in Section VII.

The consistency of the results obtained for the present set of measurements is attributed to two factors: (1) Meticulous care in calibration and in experimental technique; and (2) use of a tape recorded input signal. This permits measurement of all frequencies from exactly the same input signal.

a. Equipment

The frequency analysis circuit consists of two amplifiers, a band pass filter, two more amplifiers, a full-wave rectifier circuit, and an integrator. The integration rate is a measure of the average amplitude of the signal at that frequency.

The circuit is shown in Figure C-17. The frequency analyzer circuit contains two operational amplifiers, D-10 and D-5, which amplify the signal before it goes through the band pass filter. The gains of the amplifiers are adjusted by changing the feedback resistors so that the maximum peak-to-peak voltage of the signal entering the band pass filter is less than 10 volts. The two band pass filters used are both "Kron-hite", Model 333A. The signal coming out of the filter is a sine wave of varying amplitude. The frequency of the band pass filter output is determined by setting the low and high cut-off frequency dials at the same desired frequency. Amplifier D-6 is used to increase the amplitude of the band pass output signal and to buck out the DC voltage present at the output of the band pass filter. The DC output of the band pass filter is about 50 ± 1 to 2 milivolts when the band pass power cord is connected to a regulated power supply. The 50 milivolts can be successfully bucked out, but the random variation of one to two milivolts cannot be eliminated. Since amplifiers D-6 and D-7 often have a combined gain of 100, an error volt-

age of 0.1 to 0.2 volts could exist at the input to the integrator. If the band pass is not connected to a regulated power supply, the DC output can be as large as 50 $\pm$ 10 milivolts. The gains of amplifiers D-6 and D-7 are adjusted to maintain a maximum signal amplitude of 10 to 30 volts which is large compared to the voltage drop of the diodes. The diodes of the full-wave rectifier have a forward drop of about 0.2 volts. The type IN91 germanium diodes were used because the forward drop is only 0.2 volt compared to a 0.6 volt forward drop for silicon diodes. As shown in the circuit, the integrator time constant can be adjusted by changing the input resistor.

b. Procedure

1. Steady-State Data

The procedure used in reducing the steady-state zero-suppressed runs which are recorded on magnetic tape can be divided into two parts. The first part is a trial run to adjust the input signal amplitude to the band pass filter so that it doesn't exceed 10 volts peak-to-peak and determine approximately the frequency when the output of the band pass is maximum. This is done by varying the dial setting of the band pass filter through the range of 0.2 to 2.0 cps during the trial run. During the trial run, the chart recorder is connected to the points shown in Figure C-17. The signals at the input and output of the rectifier, as recorded during the trial run, provides the necessary information for selecting the gains of amplifiers D-6 and D-7 to maintain 10 to 30 volts maximum signal amplitude at the input to the rectifier for all frequencies to be analyzed. The detailed procedure is as follows:

a. Balance the "Donner" operational amplifiers.
b. Calibrate chart recorder and position pens.
c. Position tape reel to start of steady-state, zero-suppressed run.
d. Position selectro switch of "Ampex" reproduce amplifier to the channel that contains the signal (i.e., flux, $\mu\mu$A) to be reproduced.

e. Connect chart recorder inputs to the points shown in Figure C-17 by closing switch S_1 .

f. Start chart recorder drive.

g. Push drive button on "Ampex" tape recorder to start reproducing the recorded signal.

h. Observe on oscillograph when timing signal starts and then close switch S_2 connecting the reproduced signal to the frequency analyzer circuit.

i. The band pass dials should be set initially at 1.0 cps and then varied up to 2.0 cps and down to .2 cps. (Peak amplitude usually occurred in this range.)

j. Adjust gain of amplifier D-5 or D-10 to obtain an input to the band pass filter of 10 volts peak-to-peak as determined from the chart recorder.

k. The steady-state recording is usually five minutes long. When switch S_2 is closed, the time must be recorded. About 10 seconds before the 5-minute run is completed, switch S_1 and then switch S_2 must be opened. Otherwise, the transient voltages generated by the band pass filter can damage the chart recorder pens by violently forcing the pens off scale.

l. Record the amplifier gains and chart recorder scale factors on the chart record for reference in subsequent runs.

m. Push stop button on "Ampex" tape recorder to stop reproducing at end of the run.

n. Stop chart recorder and cut off trial run chart record.

The procedure for conducting the subsequent steady-state data reduction runs is similar to that used in the trial run. The detailed procedure is as follows:

a. Position the tape reel to start of steady-state run.

b. Calibrate integrator chart recorder channel with a known external reference voltage and position pen to extreme edge of chart. (This step is done once, and need not be repeated for each

frequency analyzed).

c. Set the high and low dials of the band pass filter at the desired frequency. The frequencies analyzed from the VBWR data were 0.03, 0.05, 0.07, 0.1, 0.2, 0.4, 0.7, 1.0, 1.5, 2.0, 3.0, 5.0, 7.0, 10.0, and 20.0 cycles per second.

d. Switch the selector on the Donner analog computer to read the output of amplifier D-7 on the voltmeter. With the voltmeter on the two-volt scale, observe the reading. (It should be zero plus or minus the random variation of the DC output of the band pass.) Adjust the potentiometer so that variation is the same on either side of zero. This step has to be done three times; once for each decade change of the band pass filter range (0.02 to 0.2), (0.2 to 2.0), and (2.0 to 20.0) cps, respectively.

e. Adjust and record the gains of amplifiers D-10, D-5, D-6, and D-7, if necessary, by referring to the trial run. Select the input resistor of the integrator to obtain a maximum scale deflection on the chart record. This is usually 6 to 8 megohm with a 3 microfarad feedback capacitor.

f. Push drive button on "Ampex" tape recorder.

g. Observe start of timing signal (on tape recording) on oscilloscope; then close switch S_2.

h. Connect chart recorder by closing switch S_1. The chart recorder channels which are recording the input and output of the rectifier should be set at 20 or 50 volts/cm so that the pens are not driven off scale by the band pass filter transients at low frequencies.

i. After switch S_2 has been closed, wait 90 seconds; then switch the compute-reset switch to compute. Integrate for 200 seconds; then stop by switching to reset.

j. Open switch S_1 and then switch S_2.

k. Push stop button on "Ampex" tape recorder.

l. Repeat steps a to k for the next frequency to be analyzed.

The recorder chart from a typical steady-state data reduction run for three frequencies is shown in Figure C-18. It can be shown that the output of frequency analyzer is given by

$$e_o = \left(\frac{R_{f10}}{R_{i10}}\right)\left(\frac{R_{f5}}{R_{i5}}\right)\left(\begin{matrix}\text{BAND}\\ \text{PASS}\\ \text{GAIN}\end{matrix}\right)\left(\frac{R_{f6}}{R_{i6}}\right)\left(\frac{R_{f7}}{R_{i7}}\right)\left(\frac{1}{R_{i9}C_{f9}}\int_0^{T_{int}} e_{in}\,dt\right)$$

where

$\frac{R_f}{R_i}$ = Gain of "Donner" operational amplifiers, D-5,6,7, or 10

e_o = Output voltage

e_{in} = Input voltage signal from tape recorder

T_{int} = Integration time

R_f = Feedback resistor

R_i = Input resistor

The average magnitude of the voltage input at a certain frequency is given by

$$(e_{in})_{av} = \frac{e_o}{T_{int}}\left[\frac{R_{i9}\,C_{f9}}{\left(\frac{R_{f10}}{R_{i10}}\right)\left(\frac{R_{f5}}{R_{i5}}\right)\left(\begin{matrix}\text{BAND}\\ \text{PASS}\\ \text{GAIN}\end{matrix}\right)\left(\frac{R_{f6}}{R_{i6}}\right)\left(\frac{R_{f7}}{R_{i7}}\right)}\right]$$

The value of e_o and the corresponding integration time are taken from the chart recording and used to calculate $(e_{in})_{av}$. From the steady-state run, it can be seen that the value of $(e_{in})_{av}$ is good above 0.4 cps since the slope of the integrated voltage is fairly smooth. Below 0.4 cps, the value of $(e_{in})_{av}$ is not as accurate, due to filter transients which cause the curve to change slope rapidly. It should be noted that some rapid increases in the integrated signal result from a period of high amplitude oscillation in the original signal. Judgment is required in examining the charts to distinguish these two effects. A better value of $(e_{in})_{av}$ can be obtained by subtracting

from e_o the voltage due to the obvious filter transients. At 0.2 cps one very obvious filter transient can be seen in the trace showing the band pass output. The trace decays exponentially in about 15 seconds, which corresponds closely to the measured impulse response of the band pass at 0.2 cps. For an input pulse of 5.2 volts and 0.4 second width, it takes 13 to 14 seconds for the filter transient to decay at 0.2 cps.

It is difficult to estimate how much to subtract when a transient occurs. To bypass this problem, a minimum, or lower bound, can be obtained by determining the minimum slope of the integration curve. Most of the steady-state runs analyzed have transients below 0.4 cps so that the frequency spectrum is bounded by the average and minimum values of e_{in}. Both values are shown in the results section of this report.

2. Rod Oscillator Data - Amplitude

The rod oscillator frequency spectra are obtained by using the same procedure outlined for steady-state runs, with one exception. Each rod oscillator run is conducted in sequence starting at 0.03 cps, so it is not necessary to re-wind the tape reel. Also, the data for μμA and in-core flux are sinusoidal like the rod motion, so there are no filter transients to contend with. However, the flow data does not show the same sinusoidal characteristics, so filter transients do occur when the flow data is analyzed.

A typical rod oscillator run is shown in Figure C-19. The input data is from in-core flux chamber A502 during the forced circulation, baffle door open, Run 15-16.

The rod oscillator data reduction runs would have been easier if the length of time had been known. For instance, the length of the rod oscillator run at 1.0 cps was 55 seconds for natural circulation Run 15-18, while for 15-16, it was 125 seconds. For future rod oscillator tests, it is suggested that the following times should be used:

Frequency (cps)	Length (sec)
.03	300
.05	250
.10	200
.2	150
.4	150
.7	125
.85	125
1.0	100
1.2	100
1.5	100
2.0	100
3.0	100

3. Rod Oscillator Data - Phase Shift

The circuit used for obtaining phase shift is shown in Figure C-20. The circuit uses both reproduce amplifiers for simultaneously reproducing the data from two different tape tracks. The rod motion and μμA signals are filtered through identical "Kron-hite" band pass filters and recorded on adjacent channels of the Sanborn chart recorder, operated at an appropriately high chart speed. By comparing the adjacent signals, the phase shift can be determined.

The phase shift data reduction is easily done since no attention is devoted to recording gains, but only to obtain a full scale deflection of the recording pens by changing scales on the chart recorder. The chart speed is changed as the frequency is increased as follows: 0.03 cps, 2.5 mm/sec; .05 cps, 25 mm/sec; .1 cps, 5 mm/sec; .2 cps, 10 mm/sec; 0.4 cps, 25 mm/sec; 0.7 cps to 1.2 cps, 50 mm/sec; 1.5 cps to 3.0 cps, 100 mm/sec.

c. Calibrations

Before using the equipment shown in Figure C-17, several calibrations were made. Gain, bandwidth, phase shift and transient response were determined for the "Kron-hite" band pass filters. The gain of the filter

was determined as a function of frequency in the range of 0.03 to 20.0 cps. The calibration procedures were established for the chart recorders and the "Donner" integrating amplifiers.

1. Band Pass Filter Calibration

   a. Gain vs. Frequency Calibration

      The "Kron-hite" band pass filters were calibrated using a circuit which is very similar to that used for data reduction. (See Figure C-21.)

      The procedure for calibrating the band pass filters is as follows:

      1. Turn on equipment and allow 30 minutes for warm-up.
      2. Set high and low-pass dials of Kron-hite band pass filters at same frequency.
      3. Set input sine wave frequency at the same reading as the band pass filter.
      4. Turn on chart recorder and calibrate.
      5. Switch integrators to compute and integrate for 100 seconds.
      6. Switch integrators to reset and stop chart recorder.
      7. Repeat for next frequency.

      By taking the ratio of integrated output to integrated input, the gain is determined at each frequency. This procedure eliminates the attenuation characteristics of the pen motors in the chart recorders as the frequency is increased. This calibration circuit also contains the same possible sources of error that are present in the frequency analyzer circuit of Figure C-17. These are: integrating amplifier drift, chart recorder amplifier drift, and chart recorder calibration errors.

      Two calibration runs were made and are shown by the graphs of Figure C-22. After these calibrations were made, two circuits identical to Figure C-17 were set up. A frequency spectrum was obtained by sending the same signal from the tape recorder through the identical circuits. The results were compared using the gain

versus frequency calibrations for each band pass filter. When the spectra were compared, it was found that they differed by as much as eleven per cent at some frequencies down to one per cent at other frequencies. Due to error in results for the same input, it was decided to use only one band pass filter. This decision increases the data reduction time by almost a factor of two since only one frequency can be analyzed at a time on the steady-state runs.

A total of six calibrations were run on band pass filter No. 1544. The gain vs. frequency curve shows a maximum width of 5.1 per cent ($\pm$ 2.5%) as shown by the plotted data points listed in (c) below. If the other band pass filter has the same characteristic, it can be seen that putting the same signal through both band pass circuits could give the error of eleven per cent.

In future data reduction, both band pass filters can be used if the same signal is not put through both band pass filters. This can be accomplished by making use of both reproduce amplifiers to reduce and separate tape signals simultaneously. Two circuits, as shown in Figure C-17, are required. Using this procedure, the data reduction time could be reduced by nearly one-half. If more reproduce amplifiers and band pass filters were available, the data reduction time could be further decreased.

b. Filter Band Width

The filter band width at 1.0 cps was obtained using the circuit shown in Figure C-21. In this case, the high and low band pass dials were set at 1.0 cps and the input frequency was varied. The band width is determined by plotting the gain vs. input frequency as shown by the graph in Figure C-23. At other frequencies the results are similar. The band width at 1/2 the peak is 0.74 $\pm$ .02 times the center frequency. Therefore, when the frequency is plotted on a log scale, the filter band width does not change with frequency.

c. Transient Response

The transient response of the band pass filter was obtained using the circuit shown in Figure C-24.

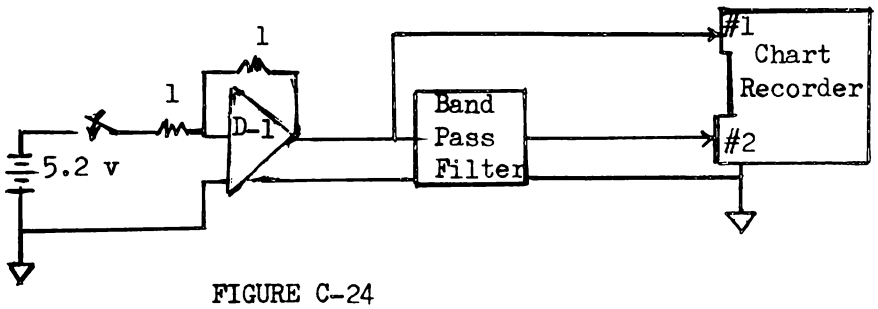

FIGURE C-24

BAND PASS FILTER TRANSIENT RESPONSE CIRCUIT

The band pass was subjected to a pulse input and a step input and the resulting time response was recorded. The data taken from the chart recording is tabulated below.

Frequency	Settling Time* for Step Input (Sec)	Pulse Input Response Time (Sec)	Pulse Width (Sec)
3.0	1.0	1.0	.2
2.0	1.4	1.6	.3
1.0	2.8	3.0	.3
0.7	4.0	4.4	.2
0.4	7.0	7.0	.3
0.2	14.0	13.2	.4
0.1	29.0	24.0	.3
.07	39.0	40.0	2.0
.05	57.0	59.0	1.8
.03	87.0	79.0	1.3

*Time from disturbance until output decays to essentially zero

From the transient response shown, it was decided to wait 90 sec. from the start of a steady-state data reduction run before the integration was begun. Thus, all of the frequencies analyzed during the steady-state data reduction are taken from the same piece of input data.

2. Chart Recorder Calibration

Both "Sanborn" and "Brush" oscillograph chart recorders contain internal calibration settings. To eliminate any errors in the internal calibration due to weak batteries in the "Brush" recorder or drift in the "Sanborn", the recorders were calibrated externally by applying a known voltage to the inputs. This known voltage was obtained by taking 100 volts DC from the regulated supply on the "Donner" analog computer and running it to the top of a 100 K ohm potentiometer. The potentiometer was set to obtain 70.00 volts using a "Beckman" digital voltmeter for measurement.

3. Integrating Amplifiers

The "Donner" amplifiers used are unstabilized and integration errors can result from drift. If the amplifiers are carefully balanced, it is found that no integration errors would be obtained. This effect is easily checked by balancing the amplifier, shorting the input, and then switching to compute. The integrating amplifiers were checked for balance twice during each steady-state run. They were checked at the beginning of the run and again after half of the desired frequencies were run.

d. Time Requirements

The time requirements for this type of frequency analysis are of interest to provide a basis for comparison with alternate methods. The entire band pass filter analysis for this report, including calibrations, required four man-months. After gaining experience in operating the equipment, the approximate time requirements are as follows:

	Analog Measurements	Calculation and Plotting
Steady-state data (15 frequencies)	2 per 8 hrs.	1 hr.
Rod oscillator amplitude (12 frequencies)	3 per 8 hrs.	1 hr.

Spectra from this work reported in Section VII.

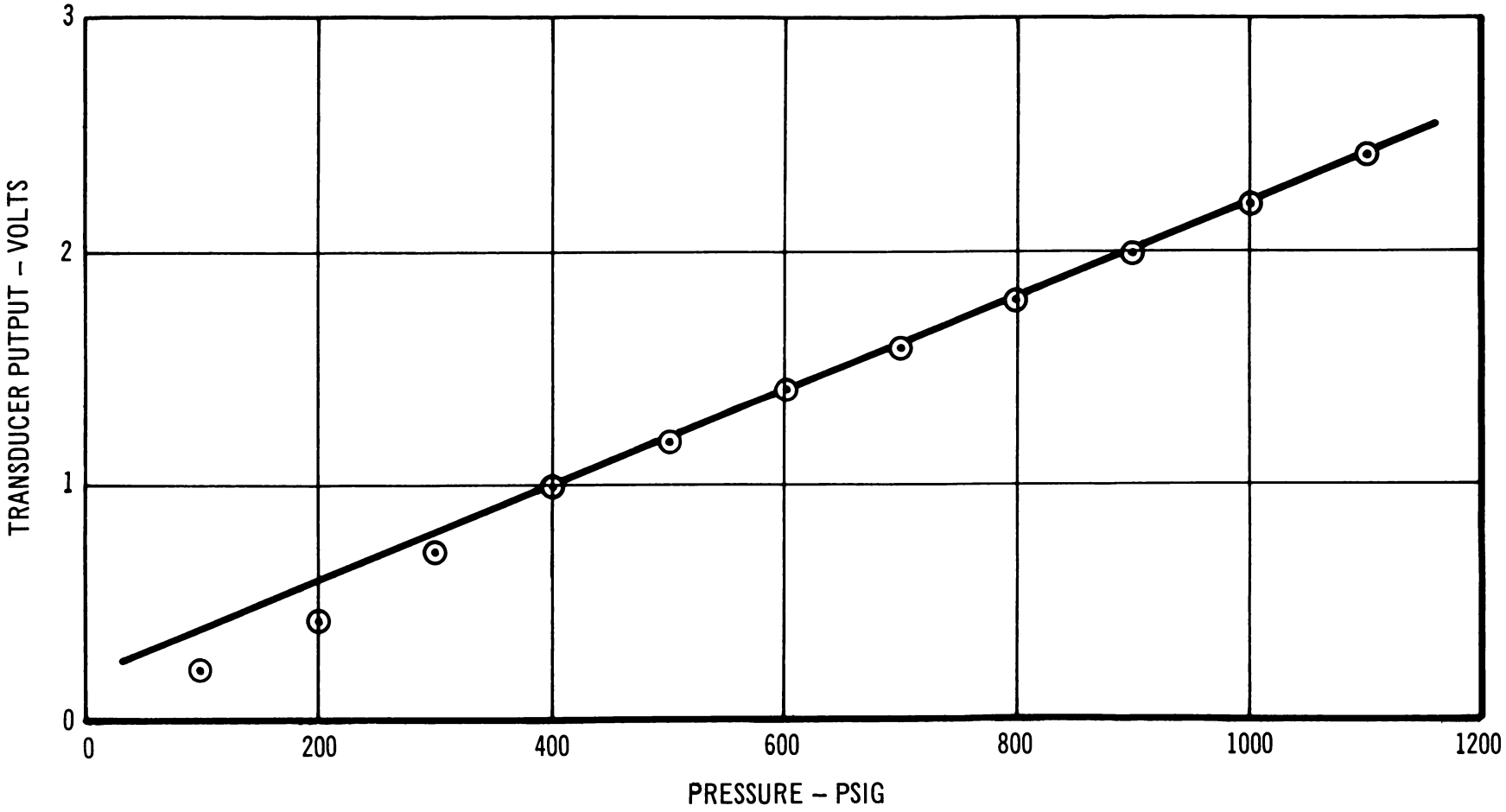

FIGURE C-1 FUEL CYCLE STABILITY TEST REACTOR PRESSURE CALIBRATION

1266-1

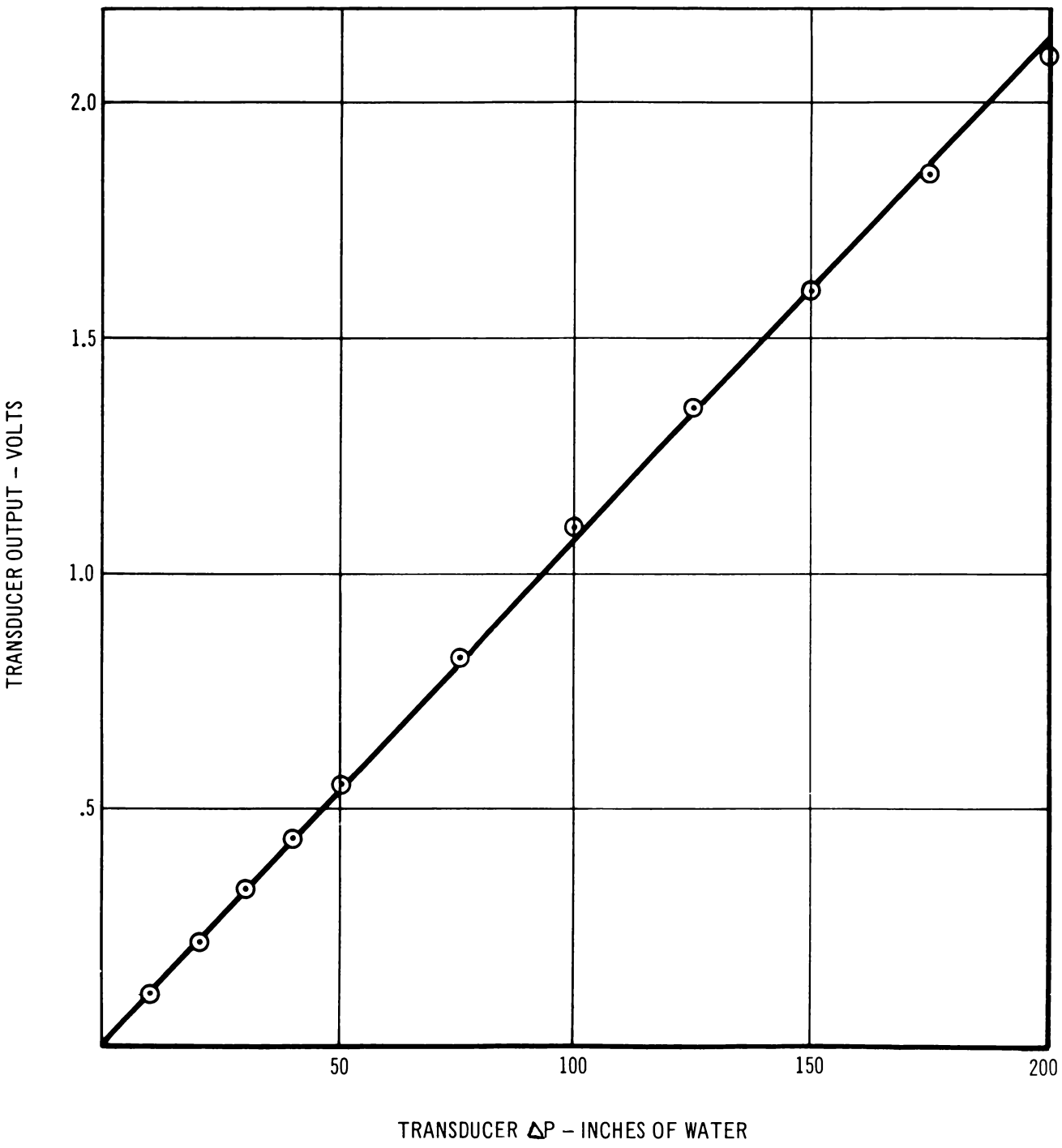

FIGURE C-2 FUEL CYCLE STABILITY TEST STEAM FLOW TRANSDUCER 1266-2

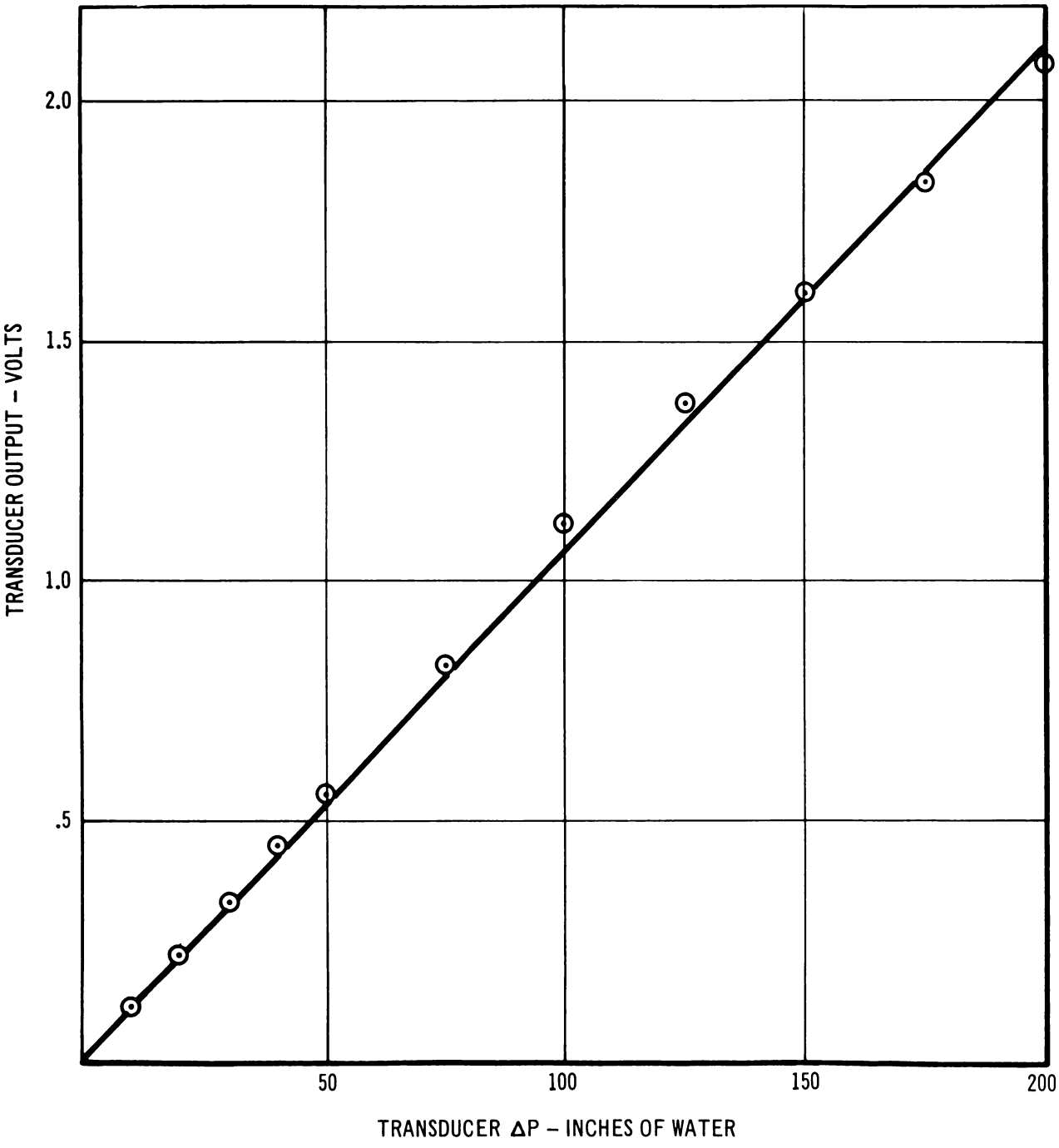

FIGURE C-3 FUEL CYCLE STABILITY TEST FEEDWATER FLOW TRANSDUCER 1266-3

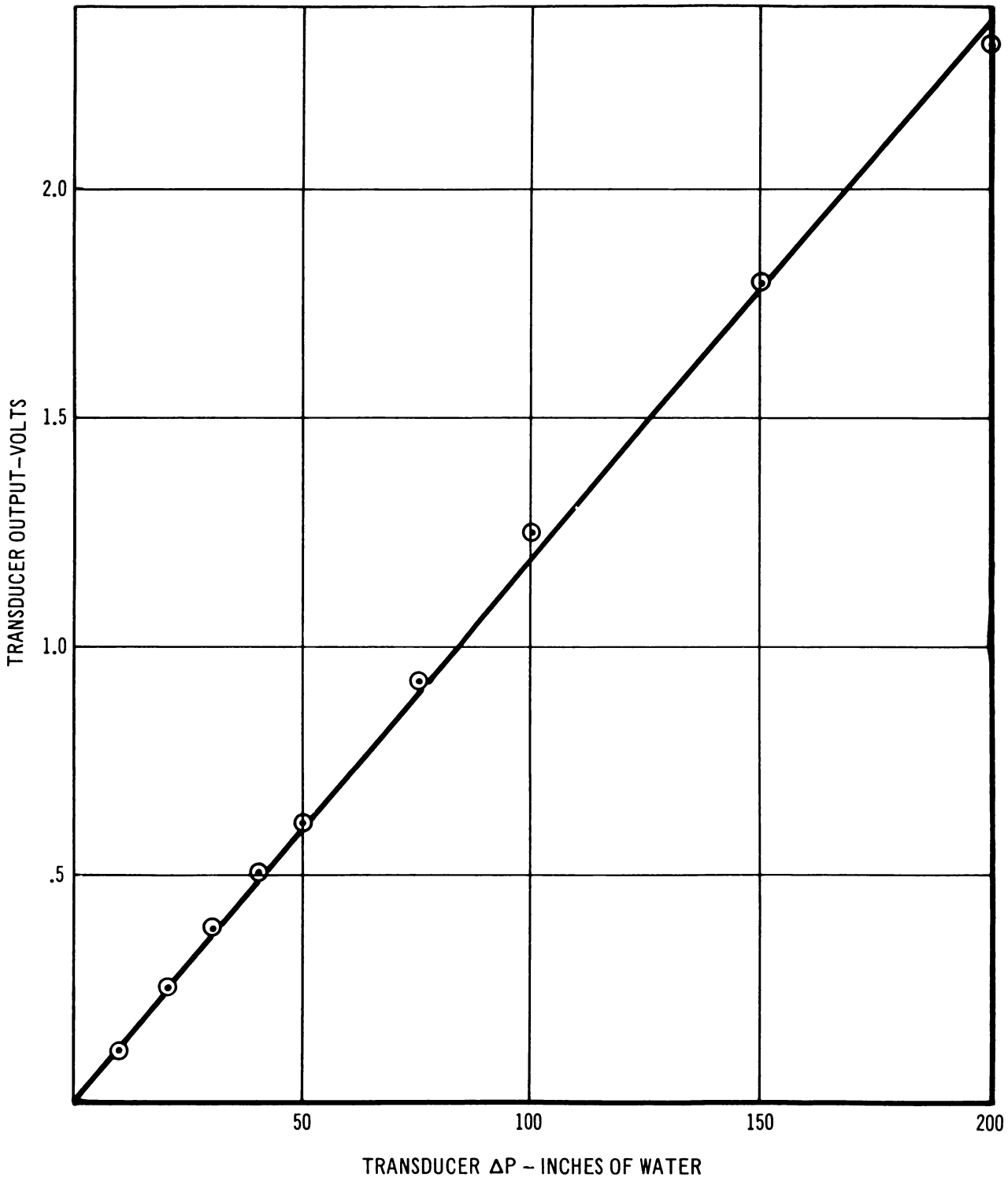

FIGURE C-4 FUEL CYCLE STABILITY TEST RECIRCULATION PUMP NO.1 TRANSDUCER 1266–4

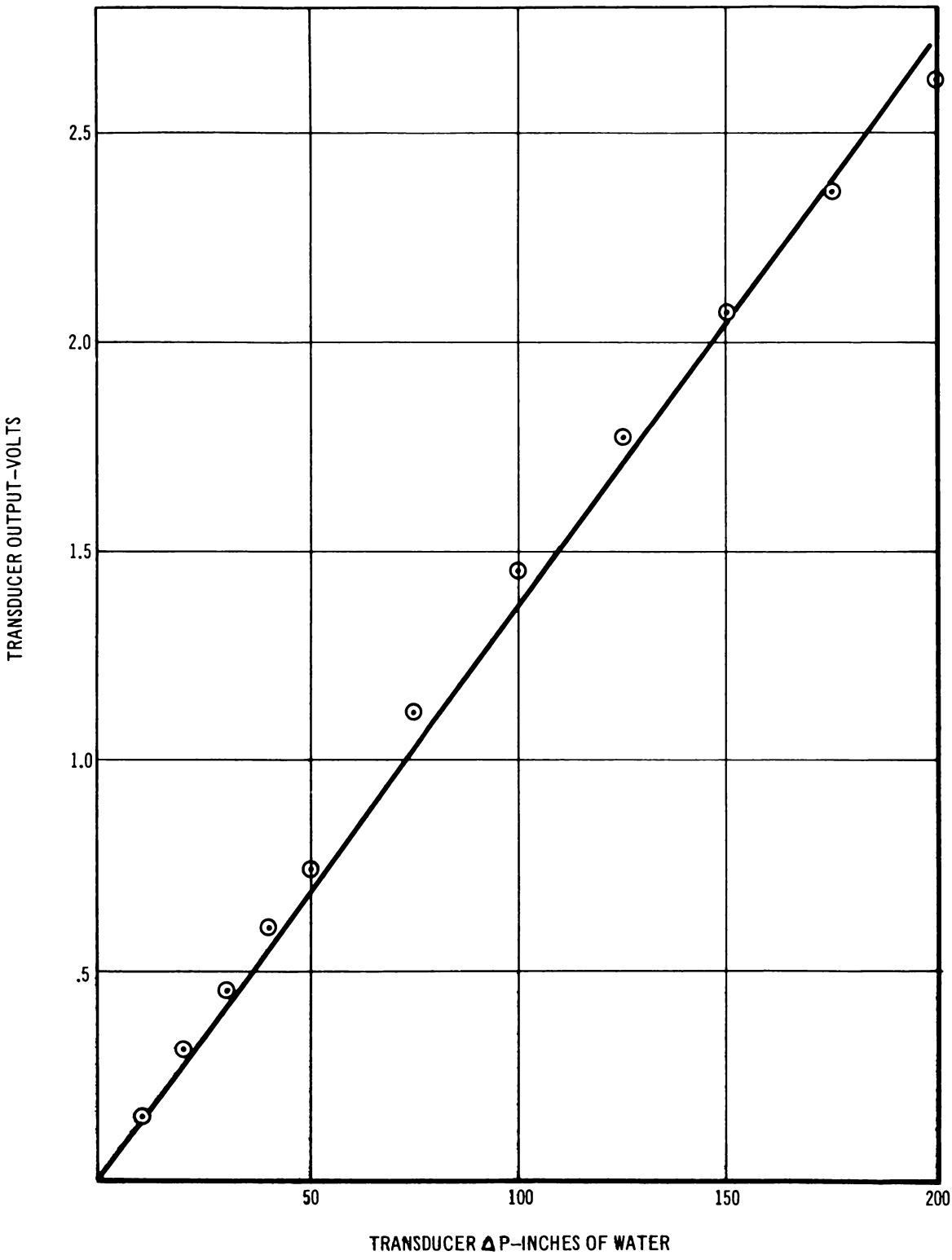

FIGURE C-5 FUEL CYCLE STABILITY TEST RECIRCULATION PUMP NO.2 TRANSDUCER 1266-5

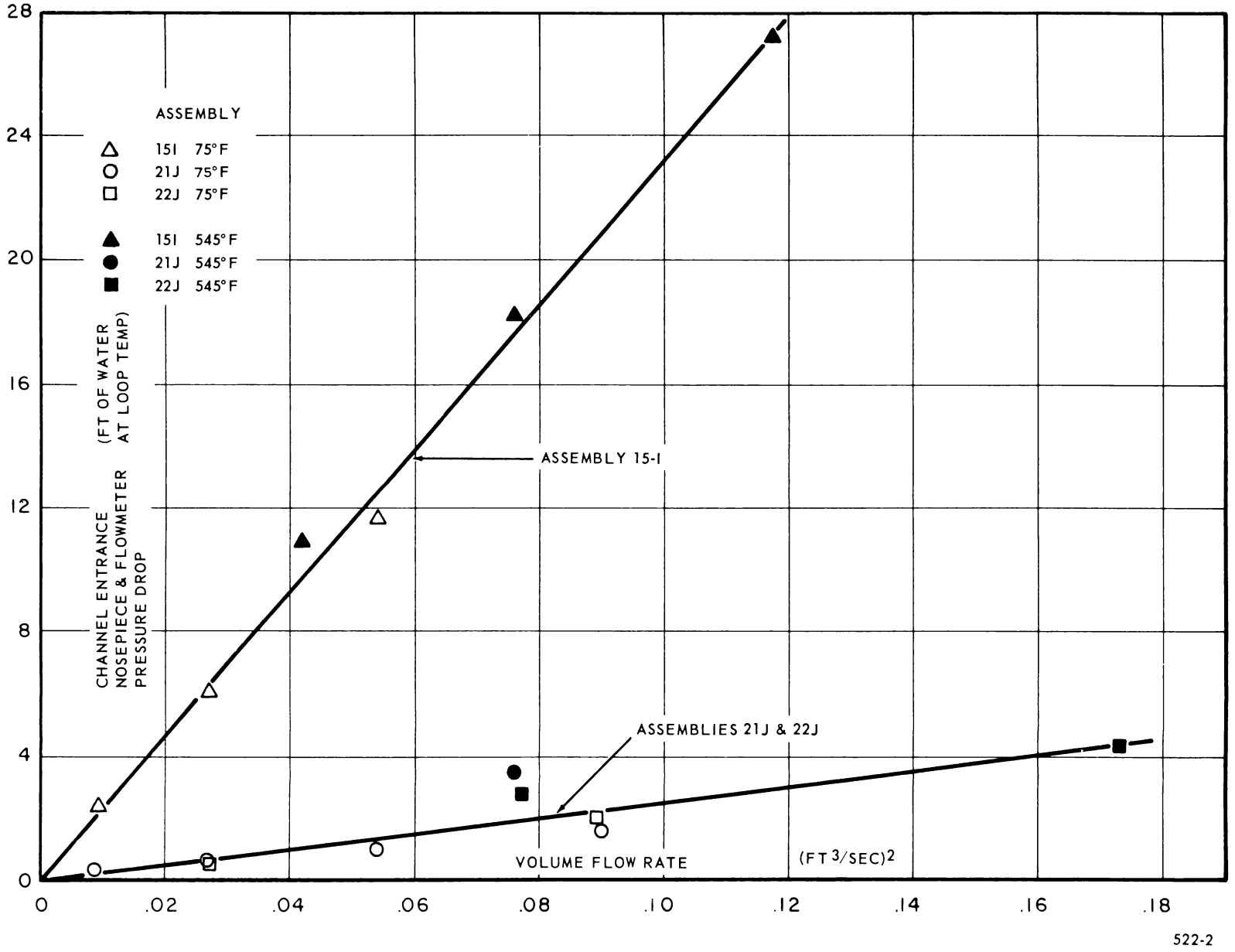

FIGURE C-6
NOSEPIECE & FLOWMETER PRESSURE DROP
INSTRUMENTED FUEL ASSEMBLIES

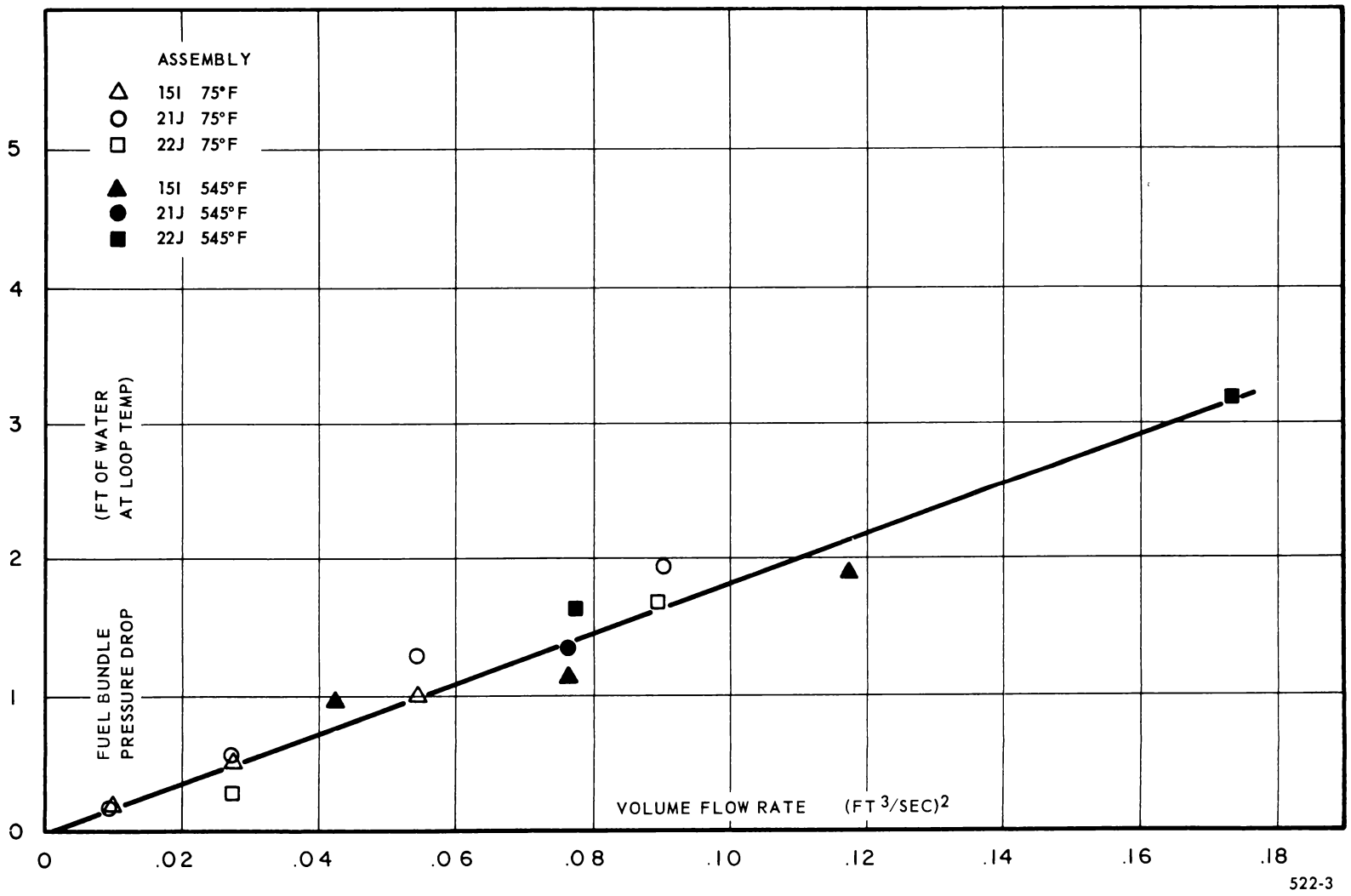

FIGURE C-7
FUEL BUNDLE PRESSURE DROP
INSTRUMENTED FUEL ASSEMBLIES

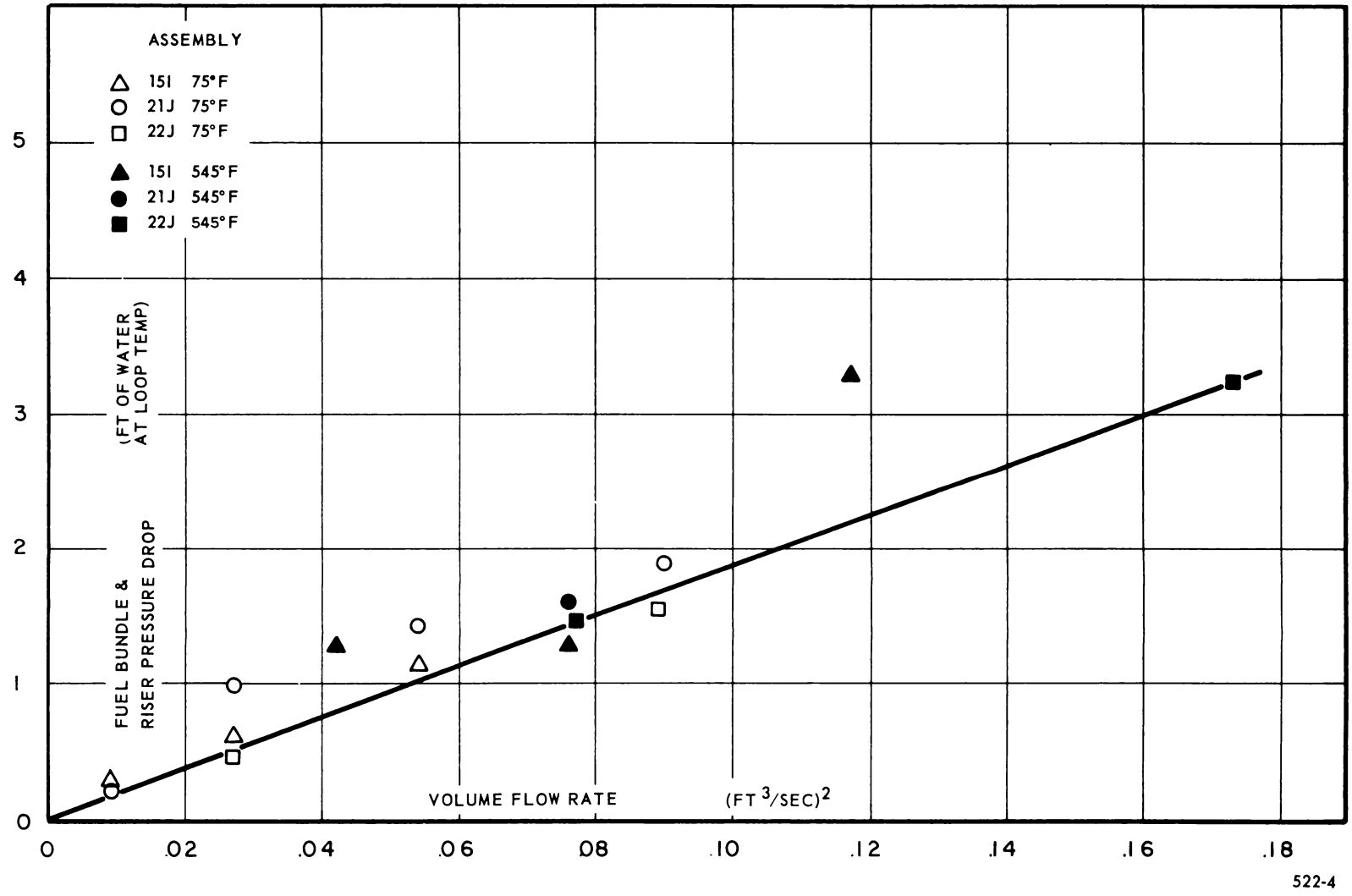

FIGURE C-8
FUEL BUNDLE & RISER PRESSURE DROP
INSTRUMENTED FUEL ASSEMBLIES

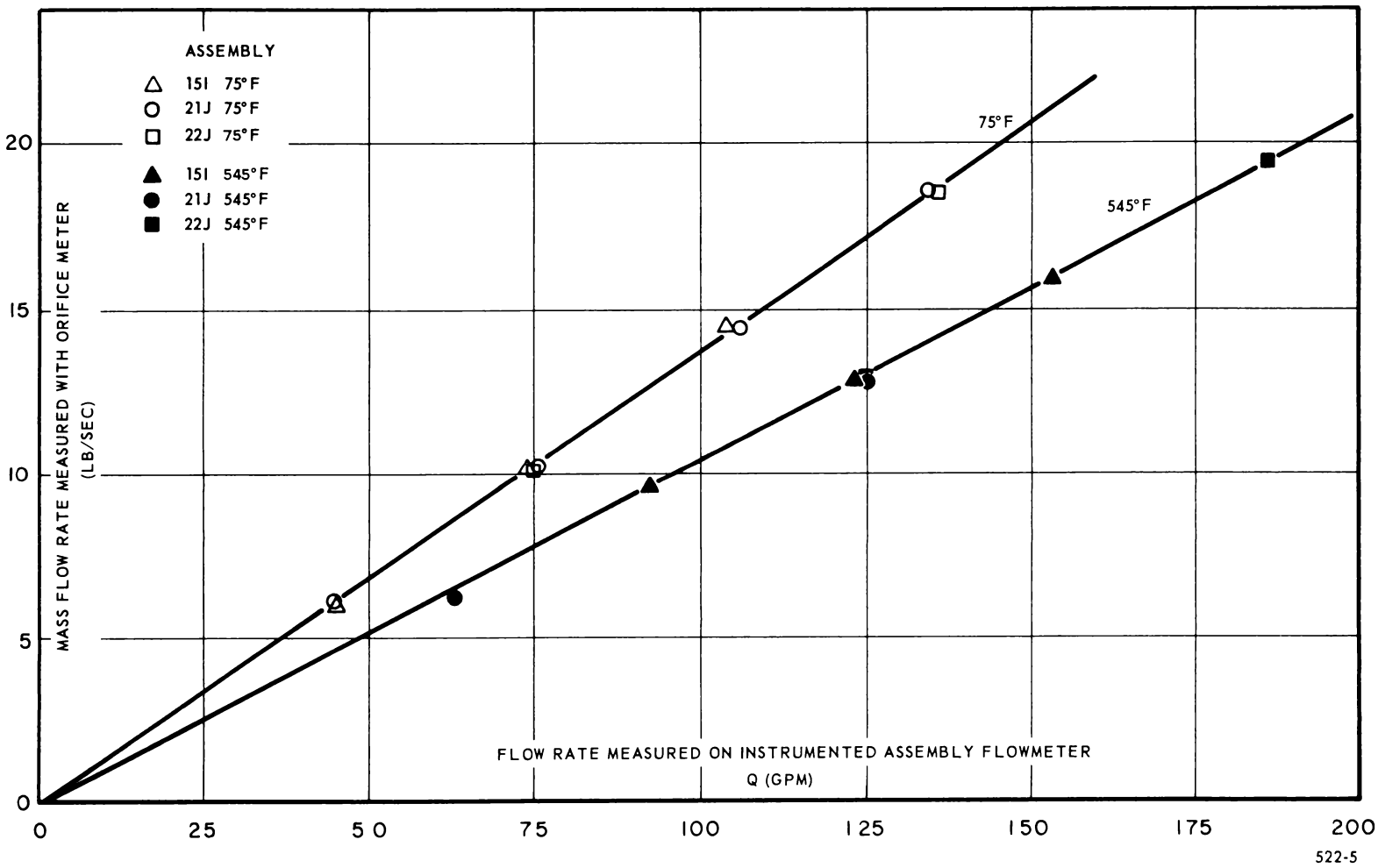

FIGURE C-9
INSTRUMENTED ASSEMBLY FLOWMETER CALIBRATION

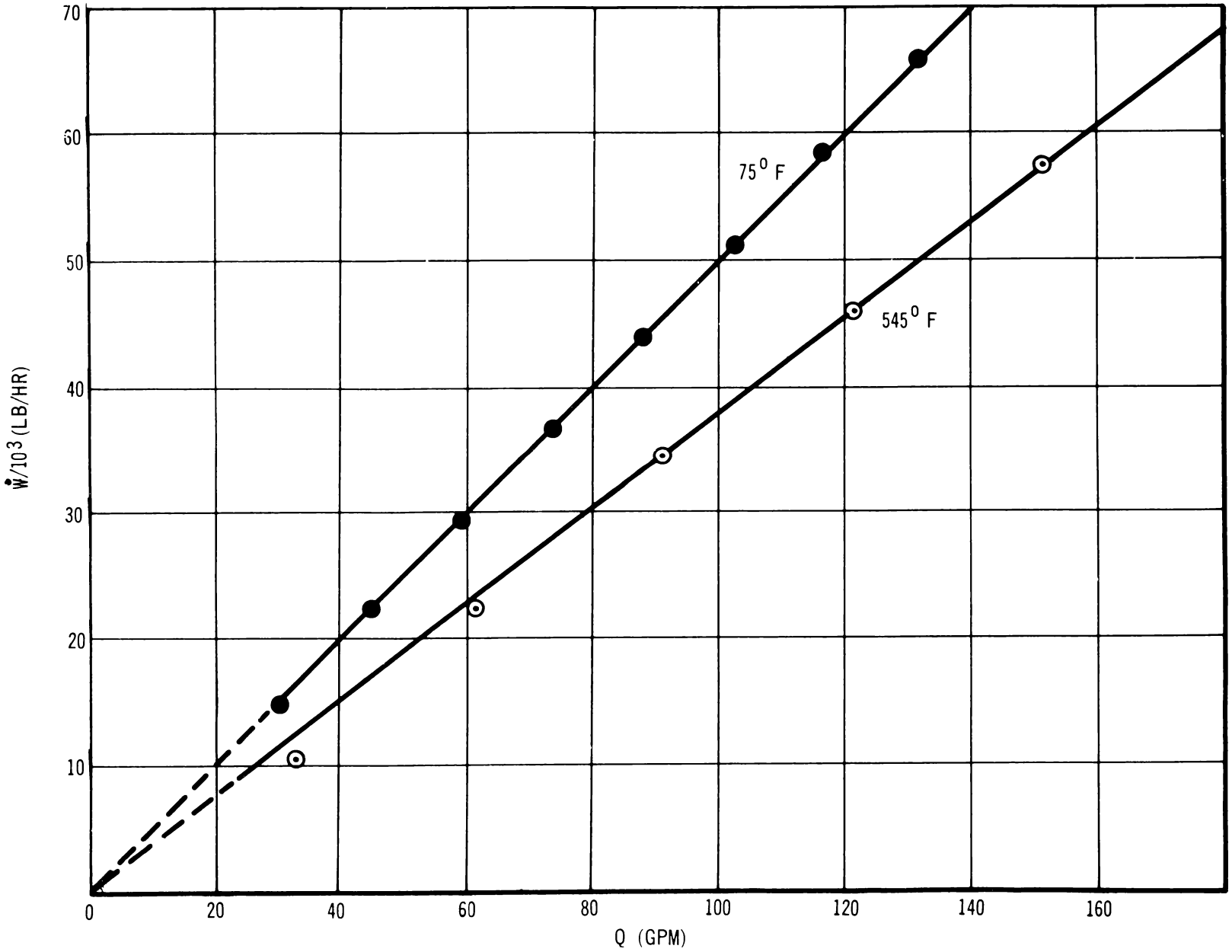

FIGURE C-10 CALIBRATION OF HIGH POWER DENSITY R&D PROGRAM IN – CORE FLOWMETERS 1266-21

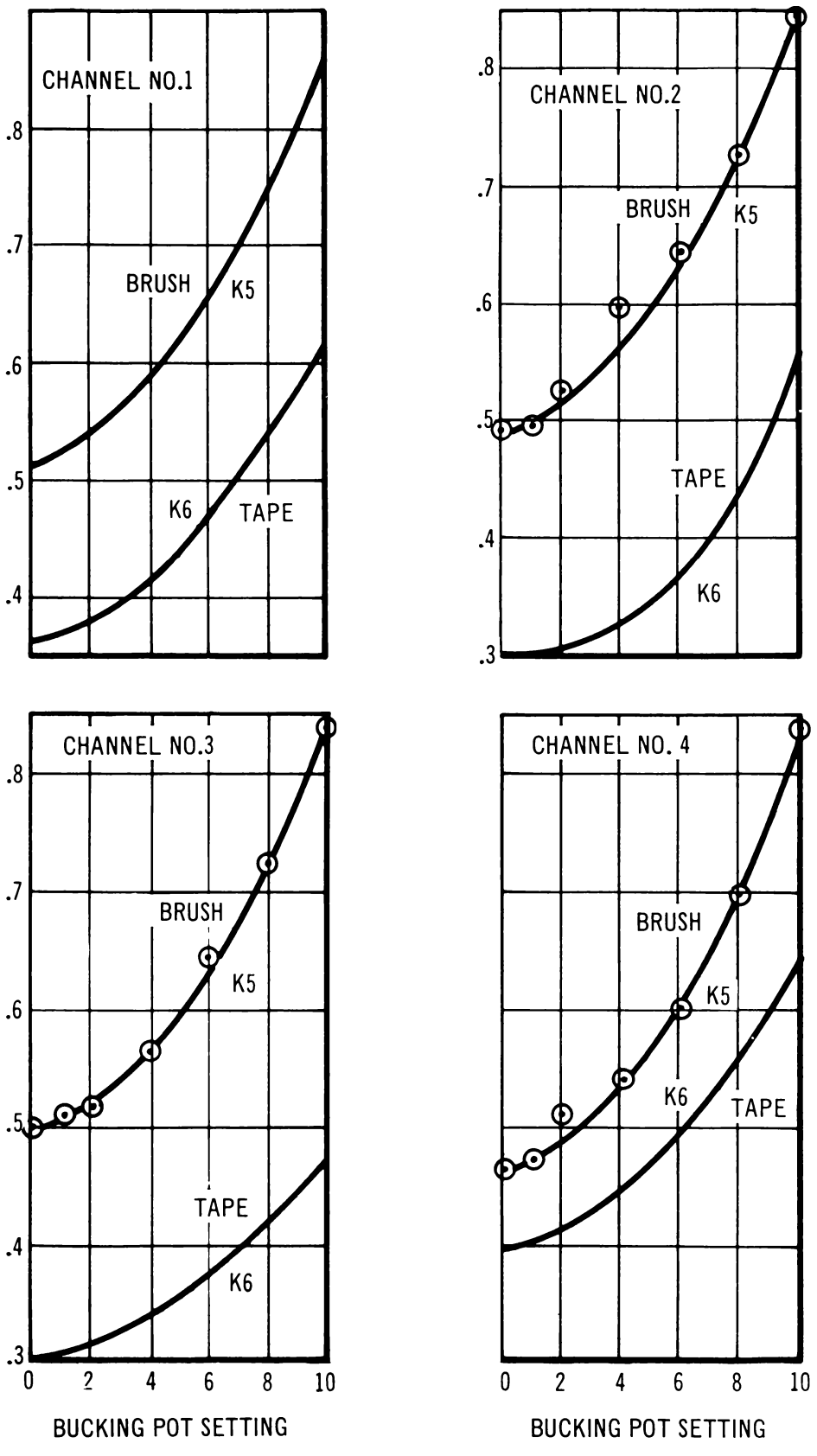

FIGURE C-11a OVERALL CHANNEL GAIN CALIBRATIONS 1266-12

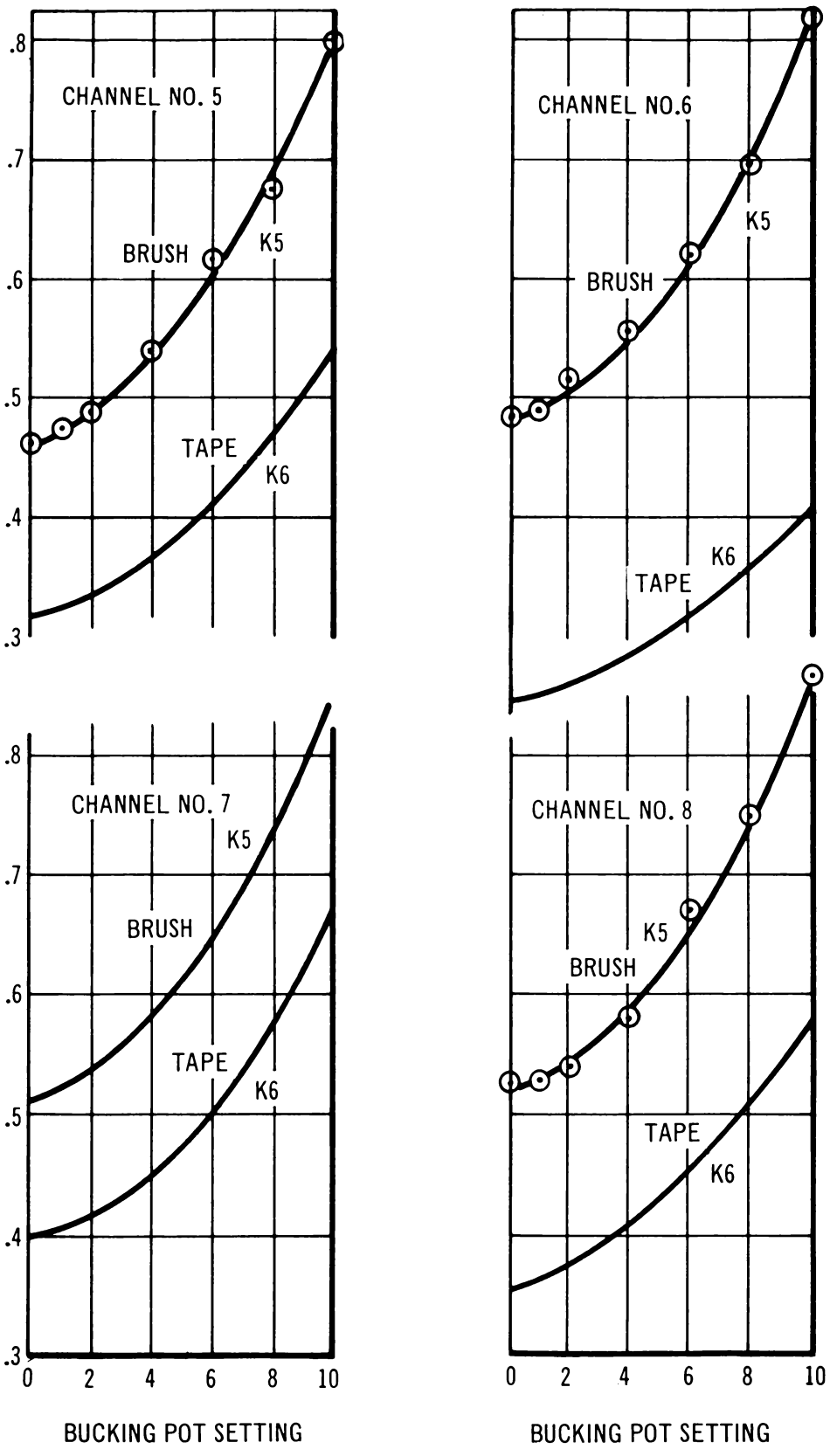

FIGURE C-11b OVERALL CHANNEL GAIN CALIBRATIONS 1266-11

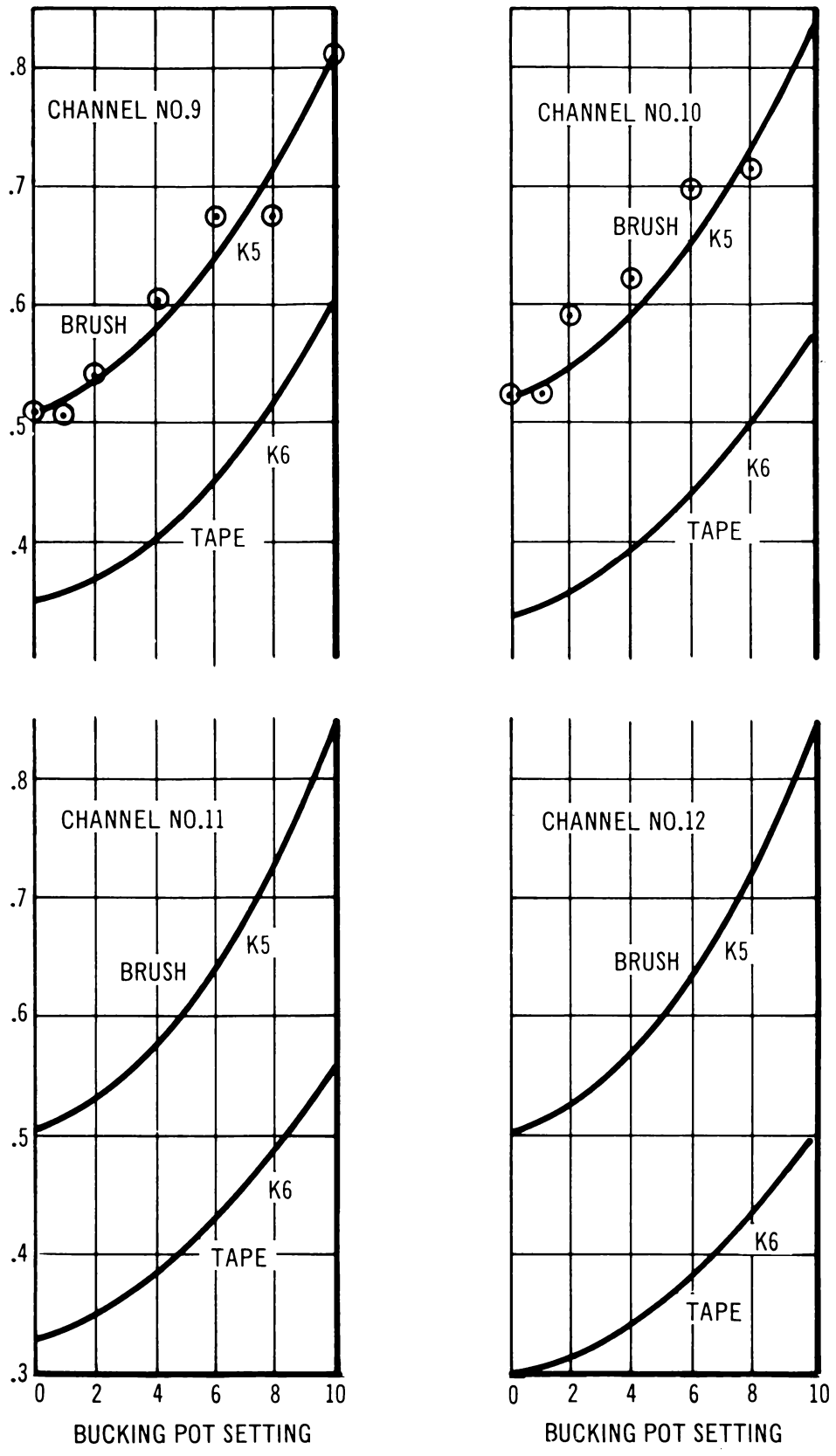

FIGURE G11c OVERALL CHANNEL GAIN CALIBRATIONS 1266-20

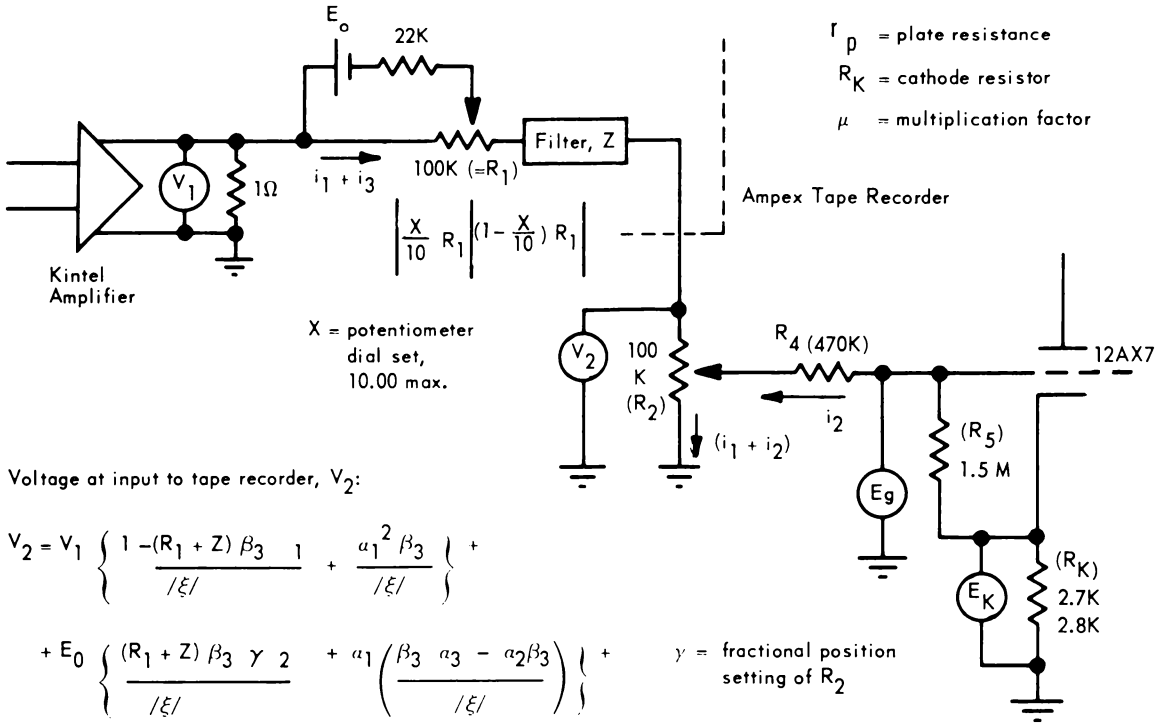

Voltage at input to tape recorder, V_2:

$$V_2 = V_1 \left\{ \frac{1 - (R_1 + Z)\,\beta_3}{/\xi/} \; 1 + \frac{\alpha_1^2\,\beta_3}{/\xi/} \right\} +$$

$$+ E_0 \left\{ \frac{(R_1 + Z)\,\beta_3\,\gamma_2}{/\xi/} + \alpha_1 \left(\frac{\beta_3\,\alpha_3 - \alpha_2\beta_3}{/\xi/} \right) \right\} +$$

$$+ \lambda \left\{ \frac{(R_1 + Z)\,\beta_2\,\gamma_1}{/\xi/} - \frac{\alpha_1^2\,\beta_2}{/\xi/} \right\}$$

γ = fractional position setting of R_2

A = 12AX7 gain

$$= \mu/(\mu + 1 + \frac{R_p}{R_K})$$

where: V_1 term is due to signal to be measured

E_0 term is due to bucking circuit voltage

λ term is due to cathode bias voltage

$$\alpha_1 = \frac{X}{10}\,R_1 \qquad \beta_1 = 0 \qquad \gamma_1 = R_3 + (X/10)\,R_1$$

$$\alpha_2 = R_1 + R_2 + Z \qquad \beta_2 = (1-\gamma)\,R_2 \qquad \gamma_2 = (X/10)\,R_1$$

$$\alpha_3 = (1-\gamma)\,R_2 \qquad \beta_3 = R_4 + \frac{R_5}{(1-A)} + (1-\gamma)\,R_2 \qquad \gamma_3 = 0$$

$$/\xi/ = \beta_3\,(\alpha\,\gamma_1 - \alpha_1\,\gamma_2) - \alpha_3\,\beta_2\,\gamma_1 \qquad \lambda = (E_K + E_g)/(1-A)$$

FIGURE C-12. BIAS VOLTAGE AT INPUT TERMINALS OF AMPEX RECORDER

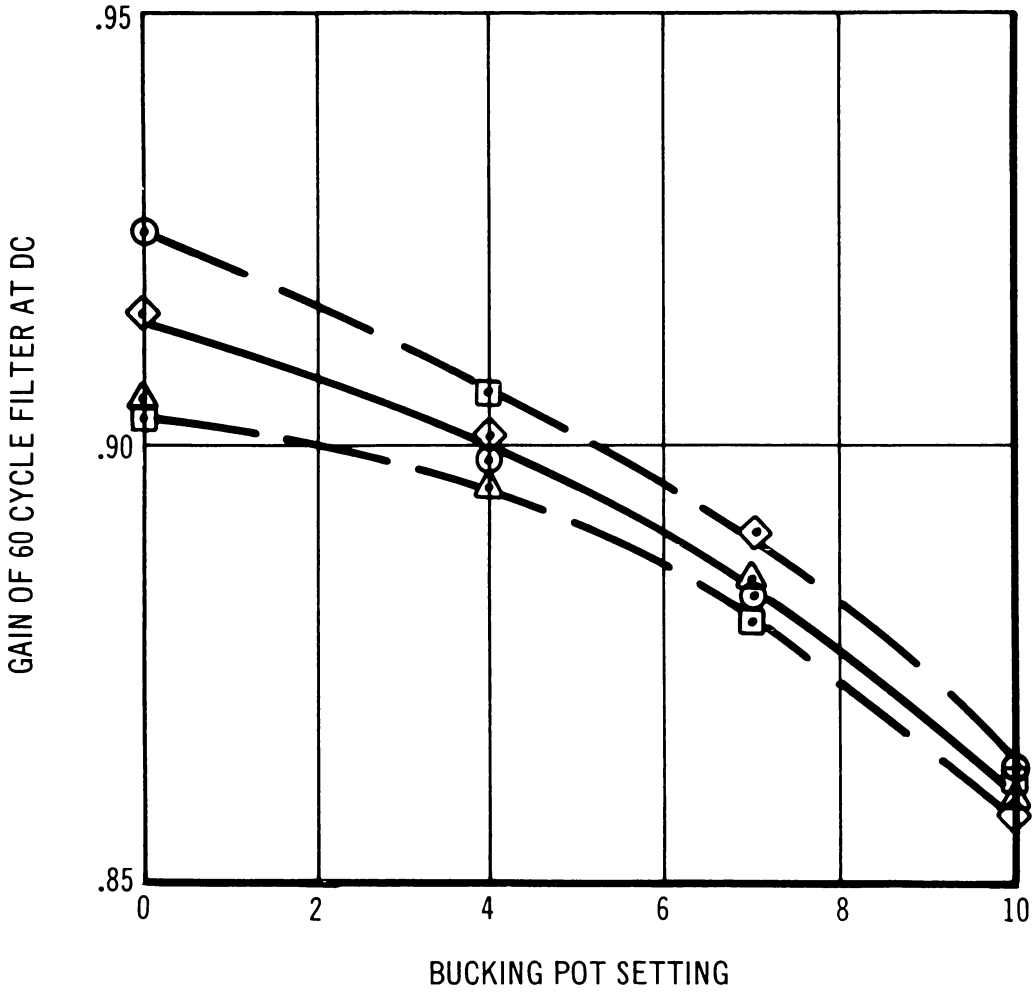

FIGURE G13 ATTENUATION OF 60 CYCLE FILTER 1266-19

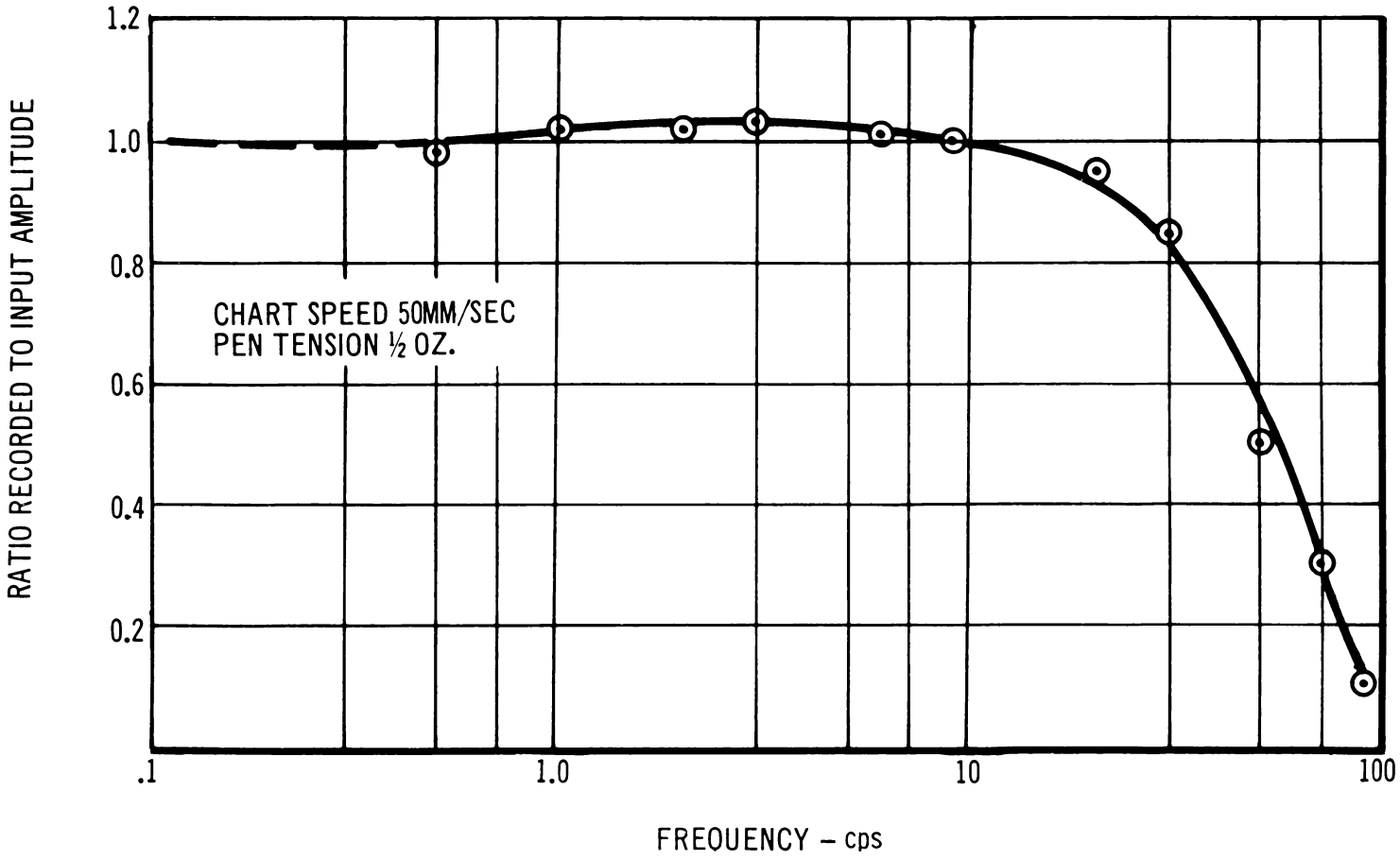

FIGURE C 14 FREQUENCY RESPONSE OF 8 CHANNEL BRUSH RECORDER 1266-15

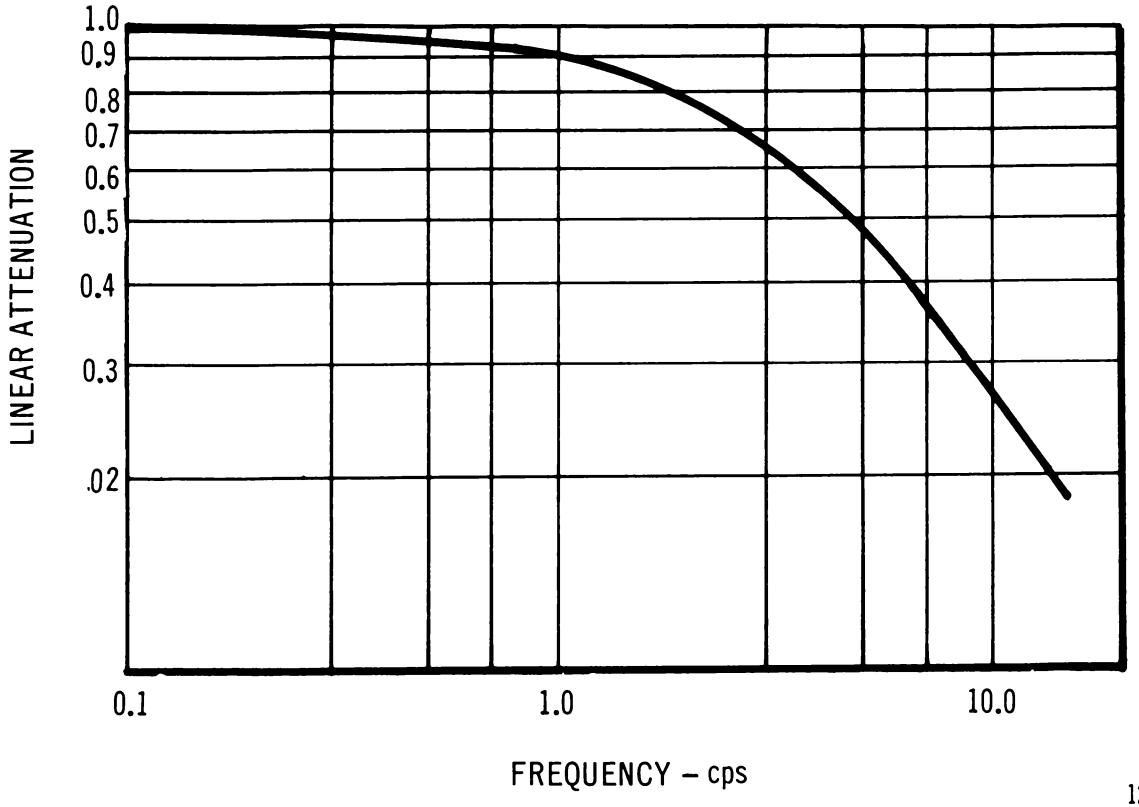

FIGURE C 15 FREQUENCY RESPONSE OF POTTER TURBINE–TYPE FLOWMETERS

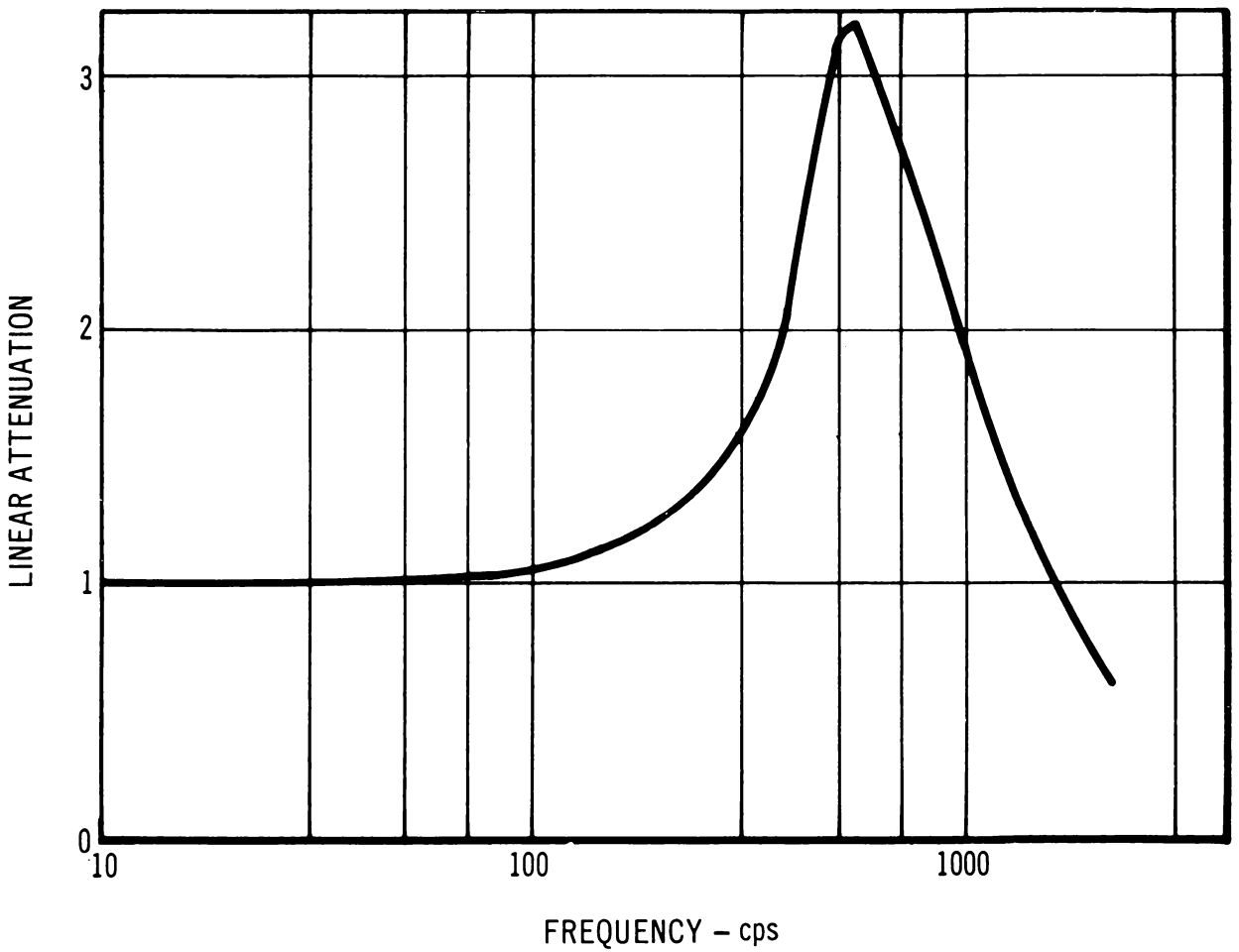

FIGURE C 16 FREQUENCE RESPONSE OF PACE VARIABLE RELUCTANCE TRANSDUCERS AS USED ON RECIRCULATION PUMP FLOWMETERS

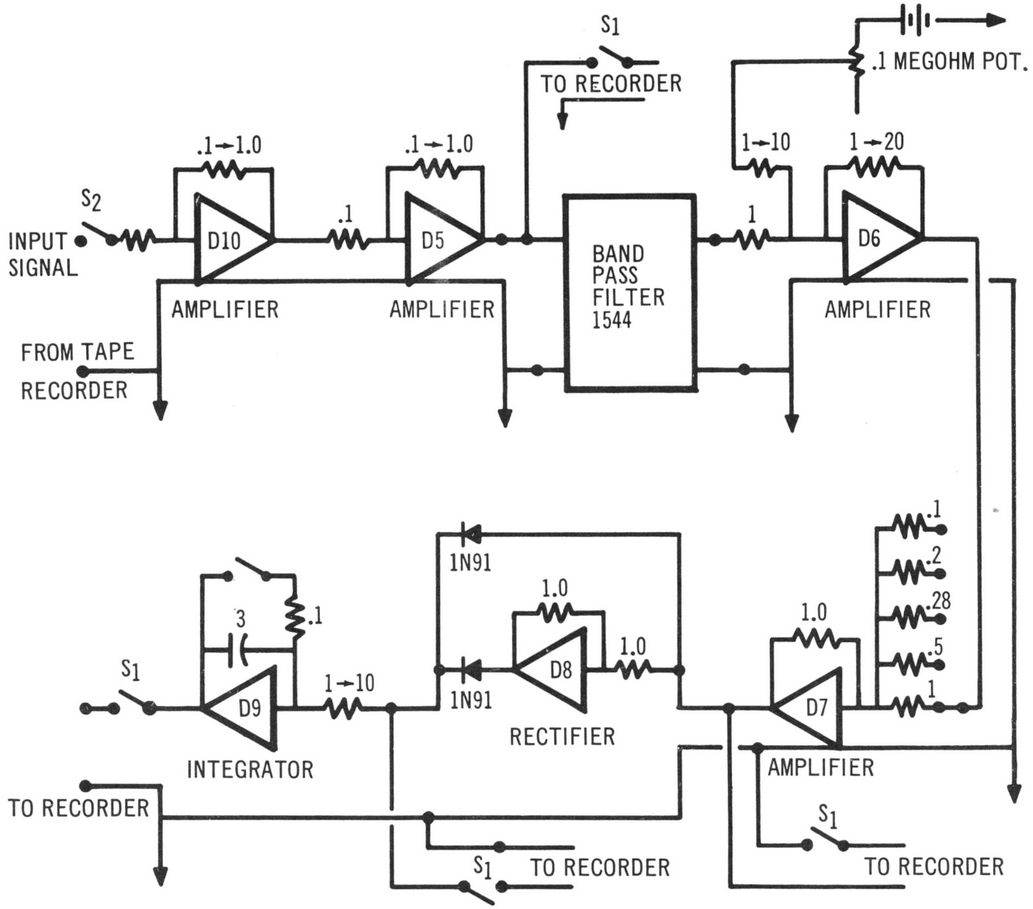

NOTE
D="DONNER" OPERATIONAL AMPLIFIER
ALL RESISTORS IN MEGOHMS AND CAPACITORS IN MICROFARADS

FIGURE C-17 ANALOG BAND PASS FREQUENCY ANALYZER 1266-10

RECTIFIED OUTPUT
OF
BAND PASS FILTER

INTEGRATED
OUTPUT OF RECTIFIER

AMPLIFIED OUTPUT
OF
BAND PASS FILTER

AMPLIFIED INPUT
TO BAND PASS FILTER
FROM AMPEX TAPE RECORDER

STEADY STATE NOISE

FIGURE C-18 BAND PASS FREQUENCY ANALYZER
CHART RECORDING

INPUT: IN CORE FLUX A502

RUN: 15-16-2
FORCED CIRCULATION BAFFLE
DOORS OPEN

CHART SPEED
1.0 mm/sec.

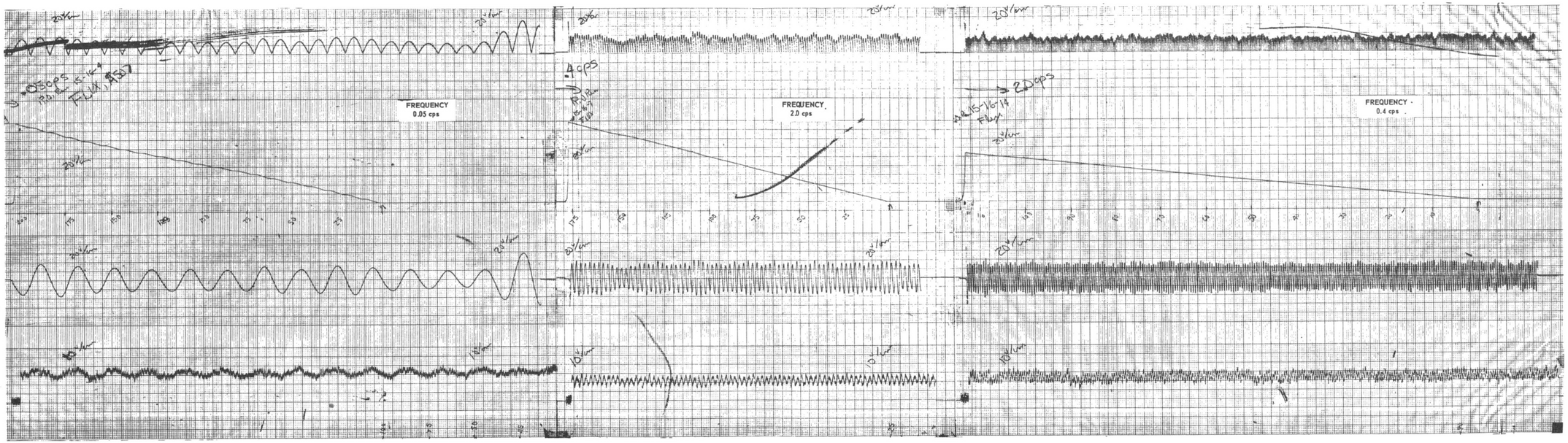

FIGURE C-19

ROD OSCILLATOR
BAND PASS FREQUENCY ANALYZER
CHART RECORDING
INPUT: IN CORE FLUX A502
RUN: 15-16
FORCED CIRCULATION
BAFFLE DOORS OPEN

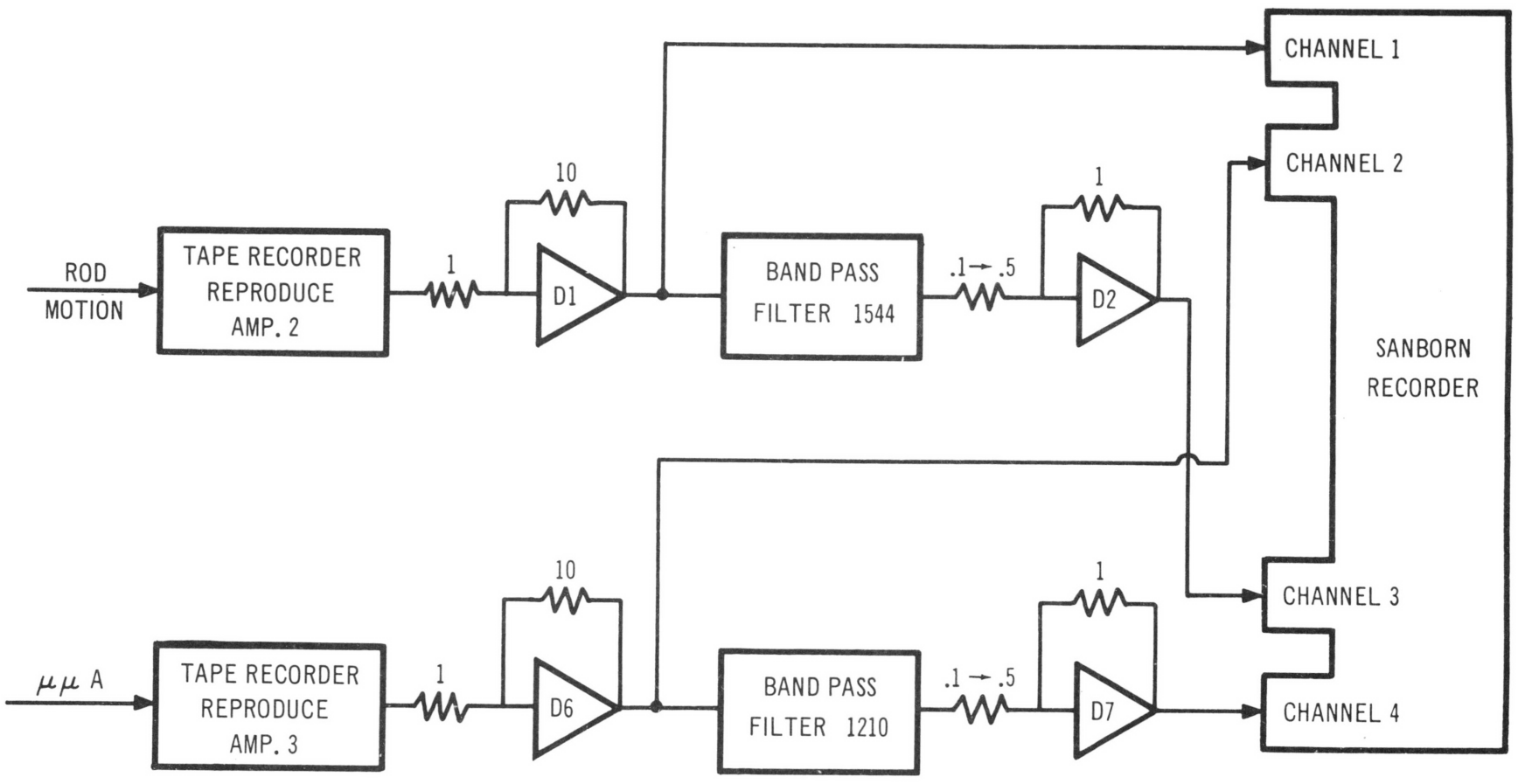

FIGURE C-20 PHASE SHIFT ANALYSIS CIRCUIT

1266-9

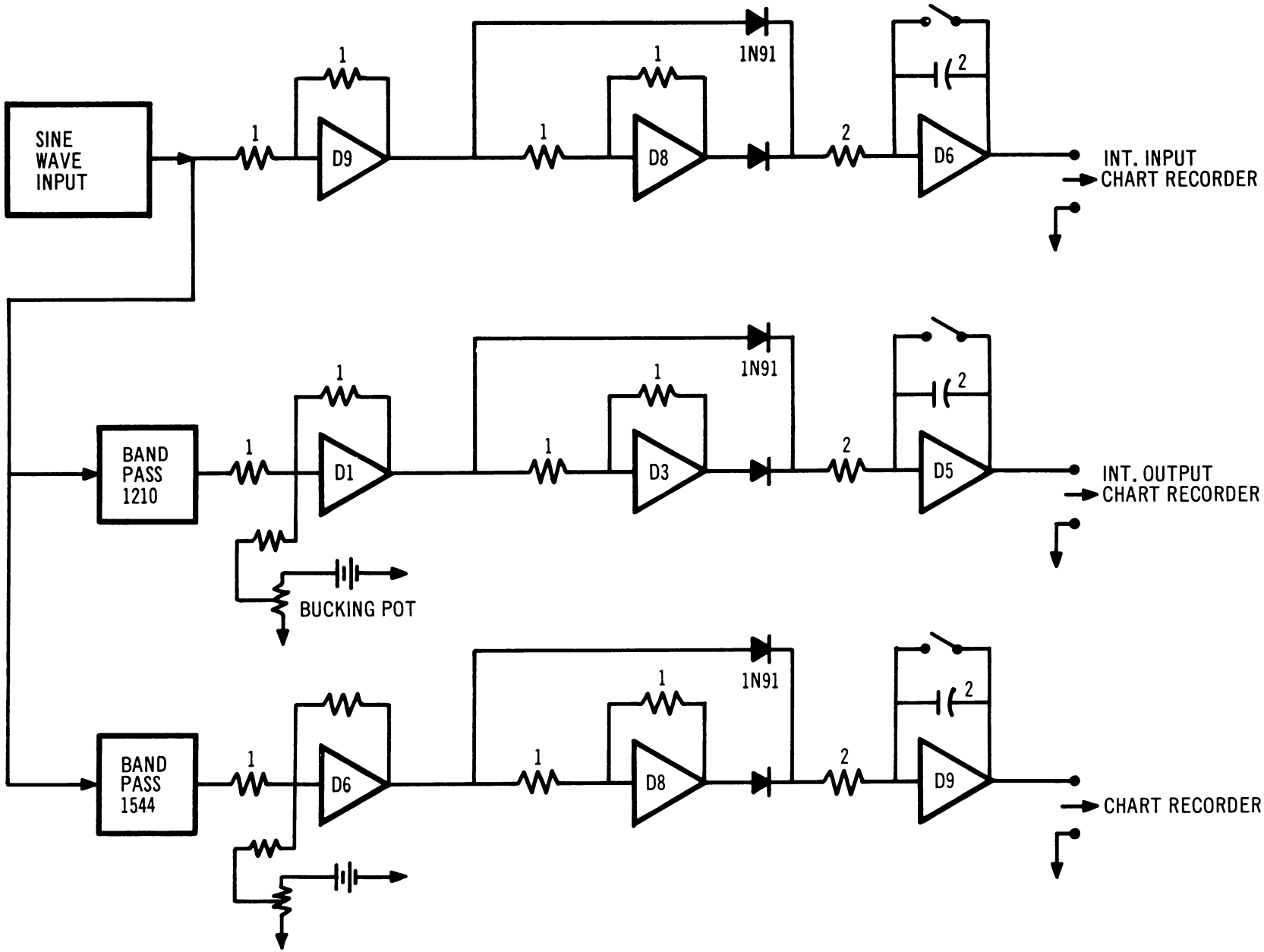

FIGURE G-21 BAND PASS FILTER CALIBRATION CIRCUIT

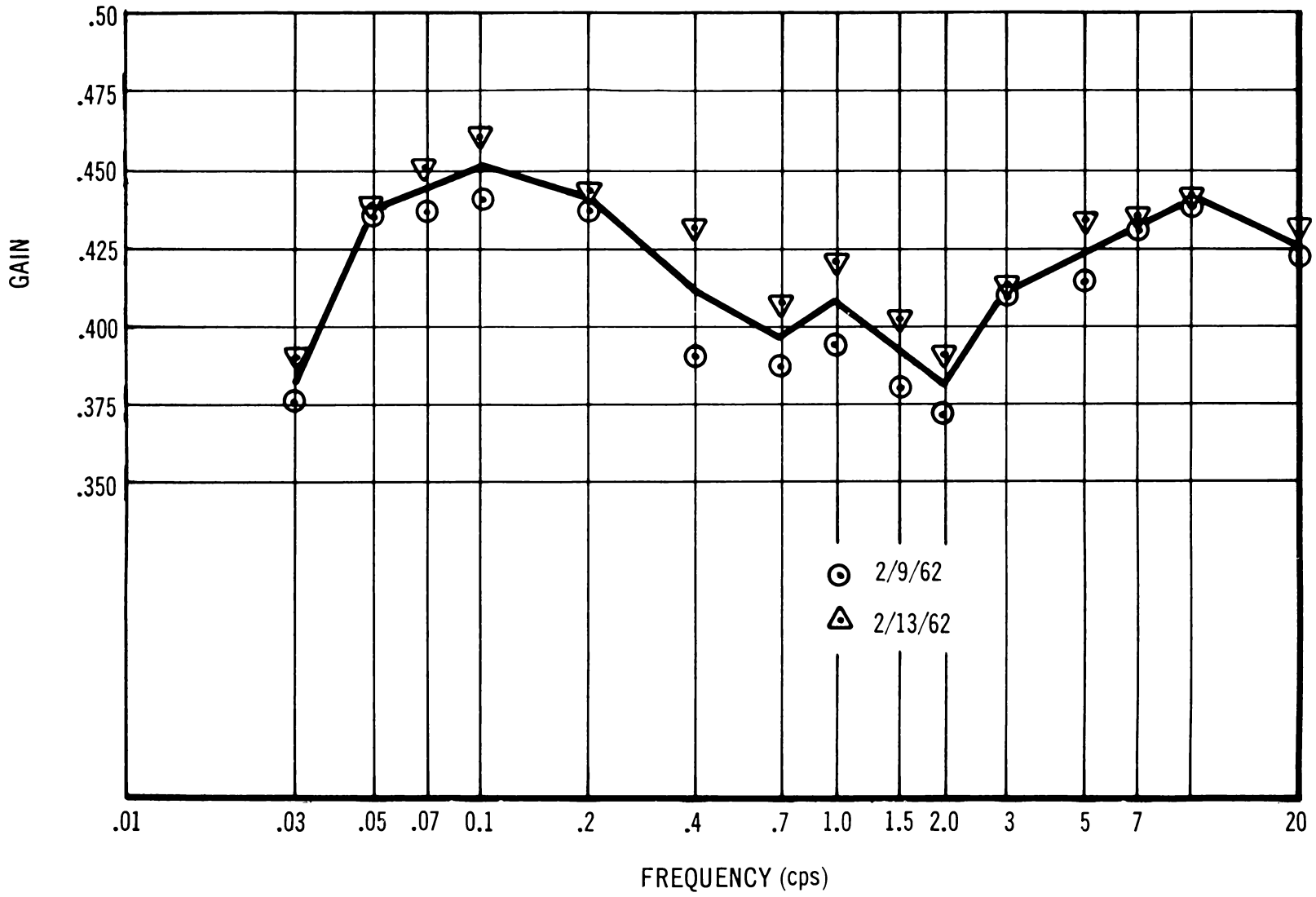

FIGURE C-22a BAND PASS FILTER CALIBRATION CURVES

1266–16

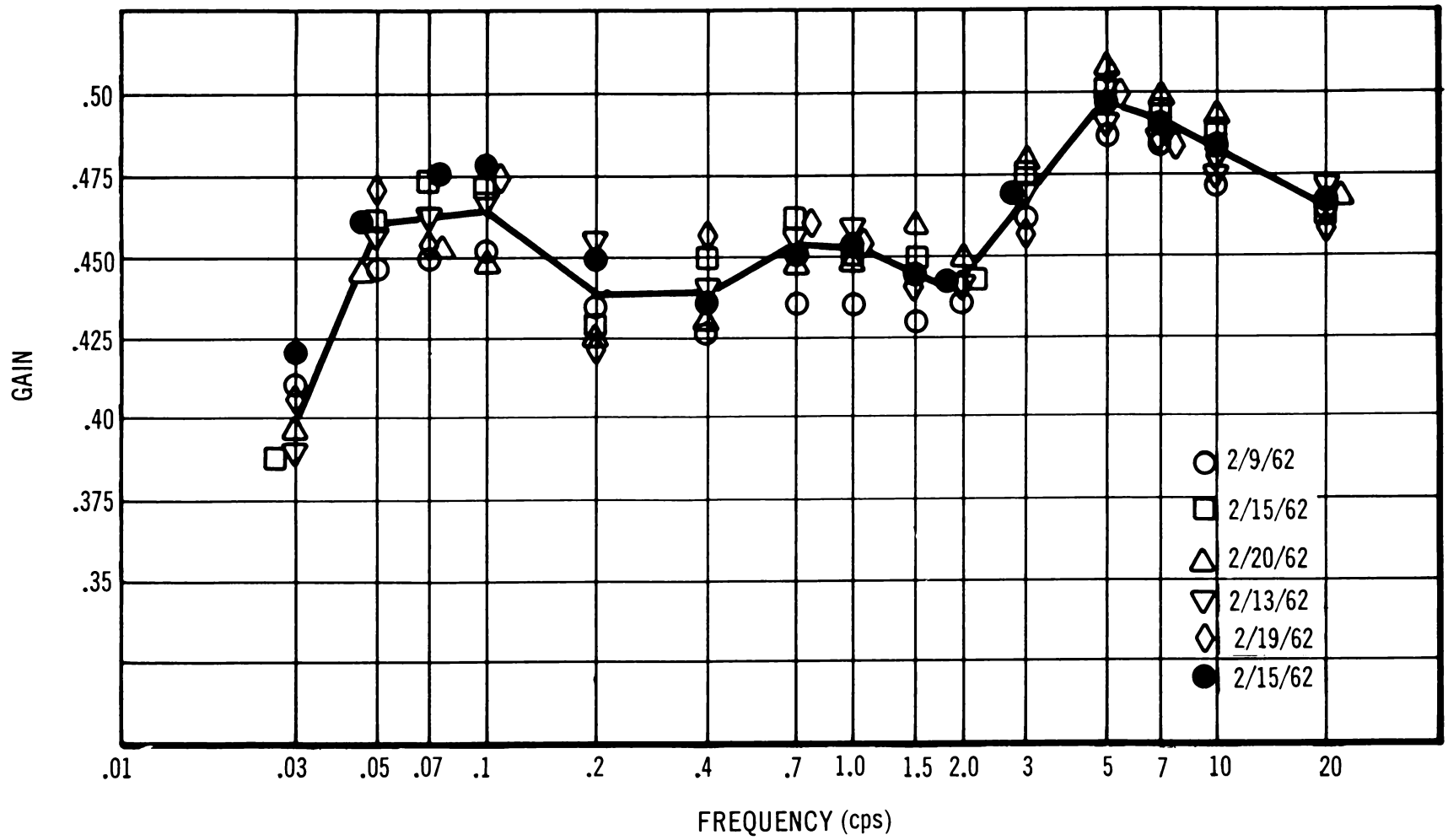

FIGURE C-22b BAND PASS FILTER CALIBRATION CURVES

1266–18

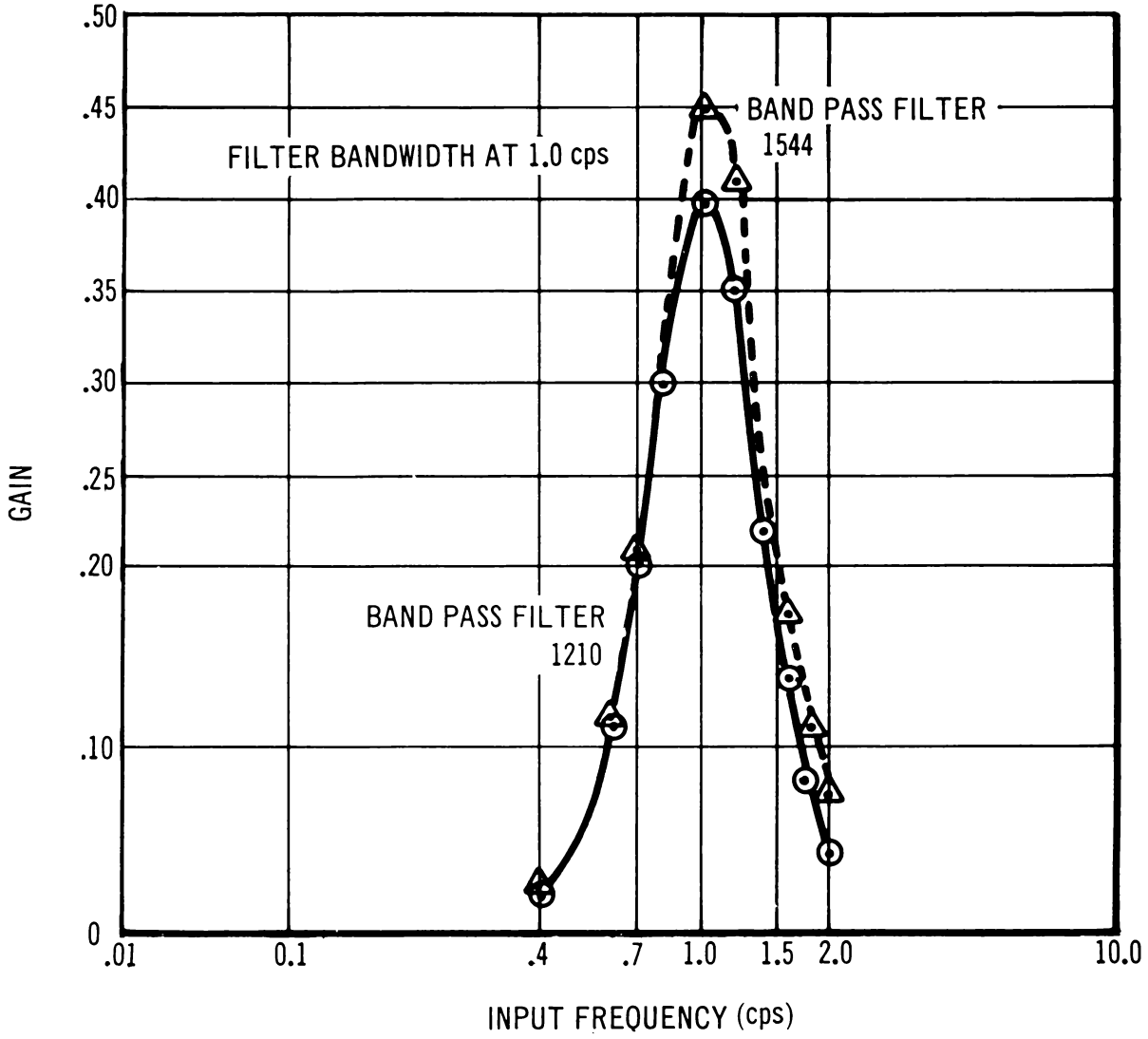

FIGURE C-23 BAND PASS FILTER BANDWIDTH 1266–17

APPENDIX D

PROPAGATION OF A FLOW DISTURBANCE

The approximation theory of Wallis and Heasley[10] is used to demonstrate the properties of the pre-test stability analysis when solved in time.

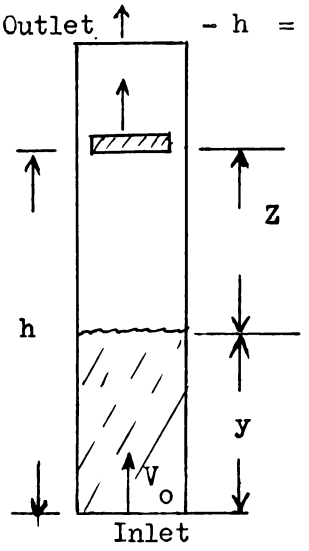

Assumptions:

Constant area tube
Uniform heat addition
No slip velocity
Constant subcooling
Fluid properties are constant

(1) Non-boiling length when V_o varies with time

$$y(t) \approx \int_{t - t_b}^{t} V_o(\tau)\, d\tau$$

(2) Determination of quality x for a time varying system.

Volume of element of mass m: $v_m = m(v_f + xv_{fg})$

Evaporation rate $= \frac{\phi v_m}{A_n} \frac{\rho_n}{h_{fg}}$

where notation of page is used.

$$\frac{dx}{dt} = \frac{\text{evaporation rate}}{m}$$

$$= \frac{\phi \rho_n}{A_n h_{fg}} (v_f + xv_{fg}) = \alpha \left(\frac{v_f}{V_{fg}} + x\right)$$

where $\alpha = \frac{\rho_n \phi v_{fg}}{A_n h_{fg}}$

integrating the above relation in $\frac{dx}{dt}$, x

$$x(t, t_o) = \frac{v_f}{V_{fg}} \left[e^{\alpha(t - t_o)} - 1 \right]$$

(3) Location of a control volume as a function of time.

Let Z be the coordinate of a fluid particle at t. Let length of volume be Z^1. Let lower boundary move with interface at y.

$Z = Z^1$ at time t.

Volume in control volume = $A_h\left(V_o - \frac{dy}{dt}\right)$

Volume flow out = $A_n \frac{dZ}{dt}$

Volume generated by boiling = $A_n \alpha Z^1 = A_n \alpha Z$

Volume balance for incompressible flow $\frac{dZ}{dt} = V_o - \frac{dy}{dt} + \alpha Z$

Substituting for y(t) in (1) above

$$\frac{dZ}{dt} = \alpha Z + V_o (t - t_o)$$

integrating $$Z(t, t_o) = e^{\alpha t} \int_{t_o}^{t} e^{-\alpha \tau} V_o (\tau - t_b)\, d\tau$$

where $Z = 0$ at $t = t_o$

(4) Position, quality, velocity and acceleration can be derived from (1) and (3) above.

(a) Fluid velocity at h $$V = \frac{\partial y}{\partial t} + \frac{\partial Z}{\partial t}$$

from (3) above $$V = \alpha Z + V_o (t) = \alpha h - \alpha y + V_o (t)$$

Substituting for y(t) from (1) above

$$V = \alpha h - \alpha \int_{t_b}^{t} V_o(\tau)\, d\tau + V_o(t)$$

(b) Fluid acceleration (a) at h

$$(a) = \frac{\partial^2 y}{\partial t^2} + \frac{\partial^2 Z}{\partial t^2}$$

from the expression for V above

$$(a) = \alpha^2 Z + \alpha V_o(t - t_b) + \frac{d V_o(t)}{dt}$$

Substituting $y(t)$ from (1) above

$$(a) = \alpha^2 h_1 - \alpha^2 \int_{t - t_b}^{t} V_o(\tau)\, d\tau + \alpha V_o(t - t_b) + \frac{d V_o(t)}{dt}$$

(c) Determination of density:

Using the quality relation from (2) above, density can be shown to be

$$\rho(t, t_o) = \rho_f e^{-\alpha (t - t_o)}$$

(5) Responses of the heater to a velocity perturbation

(a) inlet velocity with the perturbation

$$V_o + \epsilon e^{st}$$

(b) non-boiling and boiling heights y and Z

$$y = V_o t_b + \epsilon e^{st} \cdot \frac{1}{s} \cdot (1 - e^{-st_b})$$

$$Z = \frac{V_o}{\alpha} \left[e^{\alpha t_r} - 1 \right] + \epsilon e^{st} \frac{e^{-st_b}}{s - \alpha} \left[1 - e^{(\alpha - s) t_{tr}} \right]$$

where $t_{tr} = t - t_o$ is the time from the boiling boundary to the point considered.

(c) Velocity perturbation from equation (4-a) above

$$\Delta V = \left[- \frac{\alpha}{s}(1 - e^{- st_b}) + 1 \right] \epsilon e^{st} \quad \text{for} \quad h > y$$

this perturbation must be constant along the tube.

(d) Density perturbation from (4-c) above

$$\Delta \rho = \rho_f e^{- \alpha t_{tr}} (- \alpha \Delta t_{tr}) = - \alpha \rho \Delta t_{tr}$$

Substituting in a relationship for $H = y + Z$ from section (4) above, having first put in a perturbed form, Δt_{tr} may be eliminated from the relation for $\Delta \rho$ and H to give

$$\Delta \rho = \frac{\alpha \rho}{V_o e^{\alpha t_{tr}}} \left[\frac{1 - e^{- st_b}}{s} + \frac{e^{- st_b}}{s - \alpha} (1 - e^{(\alpha - s)t_{tr}}) \right] \epsilon e^{st}$$

(e) Perturbation of pressure drop F

Assume : (1) pressure drop varies as ρV^2 for small variations

(2) $t_{tr} = T_{tr}$ at exit.

$$\Delta F = F \left[\frac{\Delta \rho}{\rho} + 2 \frac{\Delta V}{V} \right]$$

Substituting in ΔV and $\Delta \rho$ terms. A final form is

$$\Delta F = \frac{F}{V_o e^{\alpha t_{tr}}} \left[\frac{\alpha e^{- st_b}}{s - \alpha} \left(1 - e^{(\alpha - s)T_{tr}} \right) - \frac{\alpha}{s}(1 - e^{- st_b}) + 2 \right] \epsilon e^{st}$$

The equations given in this section describe approximations of the time dependent equations from which the response to disturbances may be derived.

APPENDIX E

STATISTICAL AND MATHEMATICAL ASPECTS OF DATA ANALYSIS

1. OBJECTIVE

The objective of this discussion of the statistical and mathematical aspects of the experiment is to define the quantities measured, to describe the data in mathematically consistent terms, and to present the initial methods and thinking which is to be used in data handling. The over-riding objective of all the data handling is to obtain from time series traces of the measured variables, quantitative measurements of the amplitude responses, and phase angle responses of various parameters.

Amplitude responses are described as spectral density plots, a function of frequency, which can be compared with dynamic analysis of the system to obtain an understanding of the reactor responses and of the adequacy of the dynamical model in predicting its performance. Phase relationships are used, in a similar manner, for comparison with the dynamic model predictions. The real crux of the matter of comparing experiment and dynamic analysis lies in the fact that, for these experiments, maximum value is obtained from parametric study of variables. Hence, if the curves delineating response lie in orderly systems with changes in the ordinate or abscissa, and the changes are not large, the sensitivity of results to variance must be known. The sections that follow give definitions as used here for the fundamental variables, a description of the fundamental variables, and progress on methods of statistical description of the experimental data.

2. DEFINITIONS

a. Random process - This is also called a time series or a stochastic process, and denoted by the parameter $X(t)$. The trace in Figure VII-6 is an example.

b. Ensemble record - Time records of any measurement or sets of measurements. $^{K}_{X(t)}$ where K identifies a particular measurement.

c. Ensemble mean, any $K_{X(t)}$ - The average value of sets (K) of measurement in an ensemble.

d. Auto correlation function = $\dfrac{\sum_{K=1}^{N} K_{X(t_1)}\, K_{X(t_2)}}{N}$

This is a measure of the dependence of a function (t) upon what has gone on preceding it.

e. Power spectrum = $\int_{f_1}^{f_2} \dfrac{\left(\dfrac{\Delta P}{P}\right)^2}{\Delta f}\, df$

The expression for the second moments of an ensemble representation in terms of frequencies.

f. Power spectral density:
A value of the function whose integral over any frequency interval represents the contribution to variance from that frequency interval. This is the absolute value of the Fourier transform of the time series squared.

g. Stationary process - Time series in which the mean of any ensemble member is the same as any other member. An additional requirement is that the mean squared variance be the same for members of an ensemble.

h. Ergodic time series - Time series in which the time averages of a trace are the same as that of an ensemble.

3. METHODS OF APPROACH TO MATHEMATICAL HANDLING OF DATA

There are two basic approaches to handling of data which have been used; the auto correlation of time series signals, and filtering of time series for frequency response characteristics. The final objective for the use of either of the two methods are the same. At this time, only a few hand-picked data sets have been investigated. The results obtained thus far have been with an analogue band pass filter as described in Appendix C. Other methods are in the process of development. The alternatives possible are tabulated below:

TABLE E-1

Developed Methods	Methods Under Study
1. Analogue band pass	1. Revised auto correlation technique statistical description complete
2. Digital auto correlation code	2. Digital filtering code
	3. Analogue filtering of the tuned circuit type
	4. Analogue Fourier Spectrum Analyzer

As is often the case, alternatives which require the least amount of work to put in workable order have the most apparent undesirable properties. In this case, the analogue band pass filter equipment described in Appendix C has produced results after sufficient care in preparation of the circuits and calibration. It is, however, subject to the most problems, in that the minimum band width of frequencies obtainable is large compared to requirments. This induces overlap errors and a lack of precision in determining the frequency. In addition, there are filtering transients introduced which distort the response. It is felt that such errors have been minimized in the work reported here.

In order to obtain a method of handling data whose results are sufficiently well described for comparison with the dynamic analysis results, other approaches have been investigated. A digital code (AUTO) was worked on which computes the auto correlation function for discrete sampling of data. This code was found to give physically incorrect results, and a new code, DART, was written which appears to have corrected the apparent issues. The properties of the six methods tabulated in Table E-1 are listed in Table E-2 for comparison. Discussion of each of the alternatives follows this table.

TABLE E-2

COMPARISON OF PROPERTIES OF VARIOUS DATA HANDLING SYSTEMS FOR TIME SERIES

Developed Methods	Properties
Band Pass Filter (Kron-hite)	1. Direct method of obtaining responses from Ampex tape time traces. 2. Gives an average value of the traces contribution to the filter band shape. This quantity is $\left(\frac{\Delta P}{P_{av}}\right)$ over band pass. A correction can be applied for shape of the band pass. 3. An overlap error occurs in the signal output of the filter if the band pass width is sufficient. This error may be as large as the signal for sufficient overlaps. Overlap error for pass settings one octave apart is 12.5% for the Kronhite filter used. 4. The characteristics of the output of the band pass are such that different amplitude responses are obtained as a function of wave shapes. These are produced as a result of harmonics and filtering transients. The interpretation of the filter output amplitudes for variable wave shapes thus becomes uncertain. 5. No phase relationships or cross correlation is available.

TABLE E-2 (Cont'd)

Developed Methods	Properties
Digital Auto Correlation	1. Auto and cross correlation of stationary ergodic * traces.
	2. Computes time series mean and variance from mean. Normalty of distribution function examined.
	3. Spectral density $\left(\frac{\Delta P}{P} \right)^2 \frac{}{\Delta f}$ given in terms of the average of a specific trace. The best average comes from the longest trace.
	4. Phase lags can be inferred from auto correlation function plots.
	5. Smoothing techniques available.
	6. Loss of significance of results should be investigated. This occurs in that time domain errors and masking of errors occurs in compressing all time trace data into the time lags of the auto correlation plot.

(*) See definitions at the beginning of this section.

TABLE E-2 (Cont'd)

Methods Under Study	Properties
Revisions or additions to Digital Auto Correlation Code	Alternate (1) a. Retain the same properties as the developed digital auto correlation code. b. Adopt a procedure of extensive examination of traces for mean and mean-squared variation, performing these investigations for various lengths of trace. c. Examine the time average characteristics of the traces. d. Determine what traces, or portions thereof, obey stationary, ergodic hypotheses. Evaluate the usefulness of these traces and proceed with present auto correlation codes. This presents the probability of limiting considerably the number of traces from which data may be obtained, particularly that of interesting cases. Alternate (2) a. Retain the same properties as the developed auto correlation code. b. Determine trace characteristics as above. c. Compute variance of the spectral density function based upon the statistical errors introduced by finite time series lengths. d. Phase lag and cross correlations may be made using this method. Alternate (3) a. Re-write the auto correlation code for non-stationary processes. This will be useable with relatively few of the available traces. b. This would be extremely expensive and requires considerable data for adequate analysis.

TABLE E-2 (Cont'd)

Methods Under Study	Properties
Digital Filtering	a. Shape and band width of filter can be chosen to do a specific job.
	b. Filter has no memory, can be designed to have no overlap.
	c. Errors in filtering can be computed and the filter output optimized.
	d. Average and variance at any frequency can be determined directly.
	e. No phase lag estimates are made, or no cross correlation. Such a development may be possible, however, using the filter output signals of two traces.
Tuned Circuit Analogue Filter	a. Shape and band width of filter can be chosen.
	b. Overlap error is minimized.
	c. Average and variance at any frequency can be determined directly.
	d. No phase lag estimates are made except as noted in item (e) for digital filter.
	e. Equipment components are expected to make the filter sensitive to operational problems. Careful operation is necessary.
Analogue Fourier Spectrum Analyzer	a. Separates periodic signals from noisy steady-state time series leaving a white noise component.
	b. Separates periodic response of rod oscillator test data for transfer function evaluation and phase lag evaluation.
	c. May be adapted for auto and cross correlation of signals.
	d. Time series lengths effect statistically the errors of derived Fourier series coefficients.
	e. Devices capable of precise calibration and extreme accuracy in determination of periodic components even in the presence of large noise components.

a. Band Pass Filter

Band pass filter equipment is relatively easy to obtain. The operation and reduction of data from this device is discussed in Appendix C. The output of the band pass filter can be related in a simple and straight forward manner to the input signal and the resulting data is the most convenient form presently available for us in comparison of the results of dynamic analysis. Several errors are introduced to the data which are difficult to correct. These errors are the result of the mathematical characteristics of the filter and the input signal overlap errors due to filter width and amplifier drift and calibration problems. The statistical properties of the output may also be misleading due to amplitude uncertainties resulting from the mathematical characteristics of the filter.

Briefly, the nature of the errors introduced are:

1. Filtering transients are introduced when wave shapes are altered in the time series being examined. This can be demonstrated by examining the Fourier representation of a square wave

$$f(t) = \frac{4}{\pi} (\text{Sin } x + 1/3 \text{ Sin } 3x + 1/5 \text{ Sin } 5x)$$

From this, it can be seen that harmonics contribute to the amplitude of successive portions of the trace. These have been observed in VBWR and other time series data arising from wave shape changes, when analyzed with the band pass filter; examination of the variance of the signal from the mean signal would also be in error due to this, indicating a larger variance than actually exists.

2. Overlap errors are produced by the shape and width of the filter. As shown in Figure C-23, when the high and low pass bands of the Kronhite Model 330A filter are placed on the same frequency, an attenuation of 6 dg, or 0.5 amplitude exists. At the same settings, the attenuation for frequencies on octabe, or a factor of two below the set frequency, is approximately 18 db or .125. The filter output will thus have contributions from other frequencies. The Kronhite Model 330A filter can be shown to have a contribution due to

overlap of 12.5 per cent when the frequency settings are taken one octave apart.

3. Filter drift and calibration errors were minimized during the operations of the equipment. Individual component characteristics appear to be excellent in this respect. No errors of appreciable magnitude are expected from this source.

The band pass width of the Krohnite Model 330A filter produces the effect of smoothing the spectrum in the range of frequencies of interest for the VBWR data. This is due to the filter overlap discussed in (2) above. An iterative form of correction for overlap errors can be attempted for these spectra. It consists of an initial correction of output signal height followed by an iterative correction of the improved spectrum. Such a correction has not been made to the data of this report.

Similarly, for the filtering transients discussed in (1) above, graphical methods of correction of the rectified and integrated time traces can be devised. There is a question, however, about the correction itself. This is because of ambiguity in what makes up the wave shape of the stochastic process.

Conclusions with regard to the use of the band pass filter for analysis of magnetic tape time traces are, at this point:

1. Several uncertainties are introduced into the results such as filter overlap transients make this method of less final usefulness than desired. Complexity both to shape and amplitude of the spectrum resulting is added.

2. Smoothing of the spectrum may mask hydraulic resonances which would appear in power traces.

3. The make-up of random time series makes it difficult to correct the equations precisely. Because of this, corrections have not been applied to the output of the band pass for the data presented in this report.

b. Digital Auto Correlation Code

The initial efforts to develop a satisfactory auto correlation code resulted in the digital code AUTO. The AUTO program was written to compute the following:

1. The auto correlation function for one set of data.
2. The cross correlation function for two sets of data.
3. The power spectrum as the Fourier transform of the auto correlation function.
4. The frequency histogram of the raw data.
5. The mean value and standard deviation of the raw data.

Initial operation of this code showed a number of questionable properties, particularly with respect to the physical reality of the result. After a study of the mathematics of presentation of the code, it was determined that the mathematical procedures could be improved upon. Considerably better results have been obtained.

Digital analysis of noise data is now accomplished using the DART code, a revised version of AUTO. DART can calculate auto correlation, cross correlation, and power spectral density functions with a variety of useful options available. A complete description of DART and all the results obtained to date is in the last stages of writing.[23] The basic properties of DART can be described by five equations which follow.

Given equally spaced data points, y_i, the mean corrected data are:

$$1. \quad Y_i = y_i - \frac{1}{N}\sum_{j=1}^{N} y_j, \quad i = 1, 2, \ldots, N.$$

The normalized auto correlation function is defined,

$$2.\quad R_j = \frac{\frac{1}{N-j}\sum_{i=1}^{N-j} Y_i\, Y_{i+j}}{\frac{1}{N}\sum_{i=1}^{N} Y_i^2}, \quad j = 0, 1, \ldots, M$$

where the lag time is j times the time between data points, Defining the mean corrected data points for a second set of data, G_i, the normalized cross correlation function is defined:

$$3.\quad C_j = \frac{\frac{1}{N-j}\sum_{i=1}^{N-j} Y_i\, G_{i+j}}{\left[\frac{1}{N}\sum_{i=1}^{N} Y_i^2\right]^{\frac{1}{2}}\left[\frac{1}{N}\sum_{i=1}^{N} G_i^2\right]^{\frac{1}{2}}}$$

The unsmoothed estimate of the power spectral density function of the y_i data is

$$4.\quad P_\beta = 1 + 2\sum_{j=1}^{M} R_j \cos\left(\frac{\pi\beta j}{M}\right), \quad \beta = 1, 2, \ldots M-1.$$

$$P \equiv P\left(\frac{\beta}{2M\Delta}\right)$$

$\left(\frac{\beta}{2M\Delta}\right)$ defines the frequency at which the power spectral density function is identical to the argument of P.

The normalized smoothed estimate of the spectra which is of interest is obtained from the P_β as follows:

$$5. \quad G = \frac{0.5\,P_\beta + 0.25\left[P_{\beta-1} + P_{\beta+1}\right]}{0.5\,P_B + 0.25\left[P_{B-1} + P_{B+1}\right]},$$

where B is the value of β which determines the normalizing frequency.

The DART code has been carefully checked out against know functions, and is now on a production basis. The peculiarities of noise analysis and the considerations involved in the use and interpretation of DART results is given in detail in the report being completed.[23]

c. Basis for Further Revisions in Digital Auto Correlation Codes.

The code discussed in the preceding section is a basic tool for auto and cross correlation of random time series. The present code is designed to produce good results for stationary,* ergodic* processes. For these processes, the results should be superior to band pass filter.

The use of the code has been examined from the standpoint of mathematical basis, cost of operation, and operational characteristics in view of the time series which are being examined. A brief review of these considerations is contained in the paragraphs which follow.

The basic random time series which are being examined have been examined in detail by a number of investigators.[24][25][26][27] These time series are also called stochastic processes or random noise traces. Fundamental to the process is the trace recording a parameter of measurement as functions of time. Because the time series is in its simplest form, a record of events for which the next event is indeterminate, statistical measures must be used. The first measure of statistical significance is the mean value. A second is the variance about the mean.

---

* See Definitions, Appendix E (Table E-2).

There are several basic classifications of random time series. These classifications come from the time and statistical properties of the time series. The most general is a non-stationary random process. The property of these traces is that time translations from any t_1 to t_2 will change the average and the variance about the mean of the time series. Non-stationary time series require ensemble(*) representations. The ensemble average value is worked with rather than an individual time trace. Time series are classified as stationary series if they may be translated from time t_1 to time t_2 without changing the mean or the variance about the mean of the time series. Ensemble averages are required for these series. The third classification of time series is characteristic of ergodic(*) random processes. These processes have the property that each time record is statistically equivalent to every other, its mean and variance being the same. In addition, there is a significant difference in that ensemble records of a variable may also be shown to be equivalent to corresponding averages of a single time series. Detailed discussion of these characteristics is given in Reference (26). A primary conclusion of Bendat is that stationary ergodic processes are difficult, if not impossible, to justify in most physical problems.

It has been shown, Reference (26), that the equations used in the digital auto correlation code to compute the auto correlation function are sensitive to the nature of the approximation to ergodicity and stationarity of time series. In addition to these requirements, the time interval length used in computing the auto correlation function influences significantly the accuracy with which the auto correlation function can be determined. If these mathematical requirements are not met, the auto correlation function will not correctly represent the time series.

The significance of the auto correlation function is shown in Reference (26) to be in its measure of time lag relationship of the time series at time t and subsequent times. Its value at zero lag represents the variance as shown by the defining equation for the auto correlation function in section E-2. It is also a measure of the mean square effective output

(*) See Definitions.

of a linear constant parameter system to a random process set of inputs.

To summarize the requirements for a complete understanding of the responses of the system, it is necessary to know,

1. The mean value of the time series,
2. The variance of the time series,
3. The extent to which the series conforms, or does not conform, to the mathematical descriptions of non-stationarity, stationarity, and stationarity and ergodicity.
4. Obtain a value of the power spectral density function along with an evaluation of its variance due to (3) above, and to the fact that it is extracted from a time series of finite length.
5. Understand the contribution of harmonic effects in the equations' auto correlation equations upon the output of the program.

1. Consideration of Non-Stationary Code Development

The generalized approach to meeting the requirements outlined above would be to write a non-stationary time series analysis and code it for use in analysis of the data. To do this requires two things:

1. A considerable amount of money for code development and running time.
2. A sufficient time series data for ensemble representation. The tests run in VBWR were not designed with this eventuality in mind.

Development of this code does not appear the logical next step in the analysis of the VBWR test data. Other paths to improved data are available.

2. Digital Auto Correlation Program Usage with Modified Routines

A logical approach to improving the output of the auto correlation program can be obtained from modification of the routines of the program to obtain an increased understanding of the mathematical nature of the VBWR time series data. The steps are summarized as follows:

a. Select a series of runs which are considered representative for study.

b. Arrange for average and variance computations in the code to be printed out for study. Compute these for the runs in (a) above.

c. Examine these computations for stationarity conditions.

d. Divide the time series into subdivisions, re-compute the mean and variance of these new time series to examine further for stationarity and for ergodicity.

e. Choose from these new time series for which an understanding of the trace characteristics is known, and for which the existing auto program computations will have a measurable significance.

f. Compute the uncertainty in the auto correlation function and the corresponding spectral density function derived from steps (a) to (e) above.

It appears that such a program will be expensive and inflexible in operation. It must be said, however, that if steps (c) and (d) show that data satisfactorily approximates the requirements of stationarity and ergodicity, the process may be shortened. In any case, the process remains inflexible due to the necessity to contract for analogue to digital conversion of data outside the Atomic Power Equipment Department. Two analogue methods and a digital filtering method have been studied in addition to the above. One of these appears to be better suited to Atomic Power Equipment Department operation than the others. Brief reviews are given in subsequent paragraphs.

d. Digital Filtering

Digital filtering operations can be performed on random time series which operate in an analogous manner to the band pass filter, but have different properties. The major differences in properties arise from the fact that a filter shape of a specified mathematical form can be introduced, thus controlling the overlap errors of the band pass filter. In addition to this, the filter will have no memory of filtering transients as in the

case of analogue equipment. A tabulation of properties is given in Table E-2 for further details. The practical limitations of this method lie in the fact that analogue to digital conversion would be required for all data, placing an additional cost and inflexibility in the handling of data.

e. Tuned Circuit Analogue Filter

The properties of these filters are similar to those of the digital filter so far as the mathematical aspects are concerned. There will, however, be less desirable filter band width characteristics and filter transients, and harmonics must be considered when using this type of filter. Filters of this type have been shown to have improved characteristics compared to the band pass filters. No phase lags or cross correlation computations are possible with this technique.

f. Fourier Spectrum Analyzer

A study of possible electro-mechanical and analogue means of performing Fourier spectrum analyses has been made. An analogue device, shown schematically in Figure E-1, has been chosen. This device, manufactured by the Boonshaft-Fuchs Company, has been purchased by APED and placed in initial operation. An electro-mechanical device having similar properties has been developed and used by Space Technology Laboratories (Ref. 28).

Mathematically, the conversion of an aperiodic function requires the evaluation of the Fourier transform of the function,

$$F(j\omega) = \int_{-\infty}^{\infty} F(t)\, e^{-j\omega t}\, dt$$

Time series of interest in these considerations can be considered to have zero value at some initial time $t = 0$ and at $t = T$. The function will return to its zero value and remain there. The Fourier transform of such a function exists (over interval $0 < t < T$ for the practical case). It is:

$$F\left[f(t)\right] = \int_0^T f(t)\, e^{-j\omega t} dt$$

$$= \int_0^T f(t) \cos\omega t \, dt - i \int_0^t f(t) \sin\omega f \, dt$$

$$= A_n(t) + j\, B_n(t)$$

where

$$A_n = \int_0^T f(t) \cos\omega t \, dt$$

the real part of Fourier transform of $f(t)$ or the Fourier coefficient

$$B_n = \int_0^t f(t) \sin\omega t \, dt$$

the imaginary part of the Fourier transform $f(t)$.

Since the Fourier transform is a complex quantity, it will have a magnitude, $M_f(\omega)$ and phase $\phi f(\omega)$

$$M_f(\omega) = \sqrt{A_n^2(t) + B_n^2(t)}$$

and a phase

$$\phi = \tan^{-1} B_n / A_n$$

The schematic diagram of Figure E-1 shows how this is electronically accomplished. Additions to the equipment allow more complete statistical description, including auto correlation.

Such a device is indicated to be equally capable with the digital auto correlation code in handling time series. The ability and flexibility in handling non-stationary and non-ergodic time series is very favorable

compared to any of the other systems which have been studied. Calibration can be accomplished by a single measurement, therefore minimizing the introduction of scale factor errors. The technique for application of this device to time series is similar to that of the modified routine for digital code use. Understanding of the statistical characteristics of the traces are obtained by obtaining the mean, the variance, and the time averaging characteristics to establish stationarity and ergodicity conditions. Next, a choice must be made of traces which will produce significant results. Uncertainty in the output of the Fourier spectrum analysis may then be computed, based upon the output of individual frequencies upon the length of traced examined. There are a number of operational advantages to the use of the analogue technique. One particularly advantageous item is the fact that low frequency components, when identified as systematic transients, may be subtracted from the input to the detector, thus refining the time series input. The Fourier spectrum analyzer and Ampex magnetic tape recorder allow tape loop devices to be used, further improving results with respect to trace start-up errors.

4. CONCLUSIONS

a. The band pass filter, as set up for this test, has proven to be reliable, but has mathematical characteristics that make it extremely difficult to obtain refined data as an output.

b. The digital auto correlation code has improved filter characteristics with respect to the band pass filter, but has limitations in mathematically characterizing the time series. A practical limitation is imposed on its use at APED because an analogue to digital readout is not available.

c. Improvements in the digital auto correlation code could be made if a solution to the above practical limitation were found.

d. The digital filter has better filtering characteristics than auto correlation codes. The mathematical characteristics of its output should be the most desirable of the alternatives. It does not provide for cross correlation, and is subject to inflexibility of operation because of the analogue to digital conversion required.

e. The tuned circuit filter and the Fourier spectrum analyzer are the most direct methods to refined data handling. The electronic spectrum analyzer is able to perform all of the required operations on the data, and its mathematical characteristics are comparable to the digital filter. This device appears to be the logical method for subsequent refinement of data.

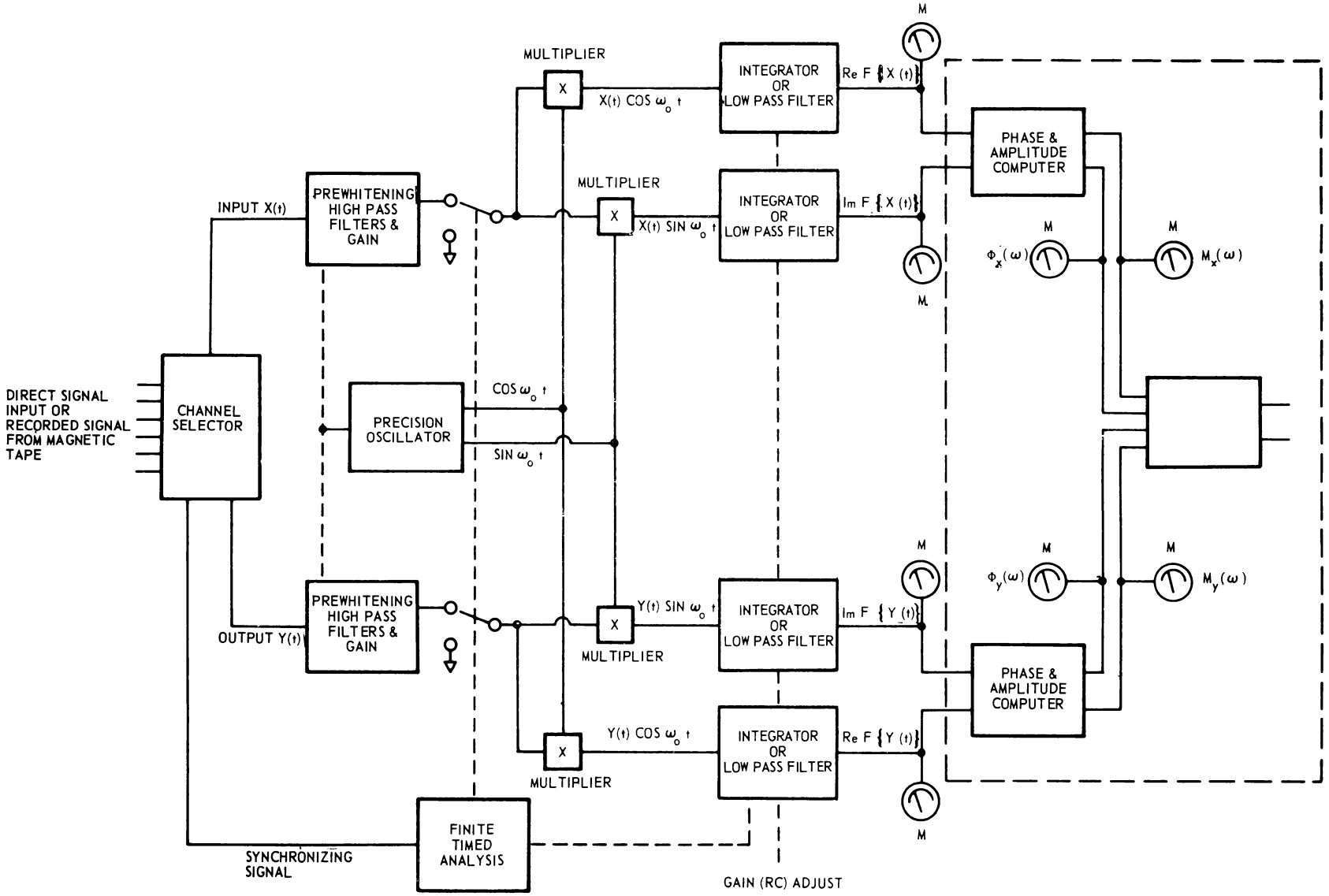

FIGURE E-1. FOURIER SIGNAL ANALYZER – TRANSFER FUNCTION ANALYZER

APPENDIX F

INDEX OF INSTRUMENT HOOK-UPS
FUEL CYCLE STABILITY TESTS

DATE	RUN NO.	CHANNEL NUMBERS 1	2	3	4	5	6	7	8	9*	10**	11	12	13	14	15	16	17	18	19	20
Nov. 3, 1961	0-1-4,6	A-201	B-201	C-201	D-201	E-201	A-501	B-501	D-501	E-501	μμA	Rod Osc.	Press.	RCP-1	RCP-2	FW	STM	C-501	B-503	D-502	E-503
4	0-1-7,21a	μμA	↓	↓	↓	↓	"	"	C-501	Press.	C-502	"	E-501	"	- - -	B-502	C-503	D-501	"	↓	- - -
6	R-1-1,17	STM	↓	↓	↓	↓	μμA	RCP-1	- - -	FW	- - -	RCP-2	Press.	A-301	E-301	D-501	A-501	B-501	C-501	↓	E-501
7	R-1-17a,23a	"	↓	↓	↓	↓	"	"	Rod Osc.	"	B-301	"	↓	"	"	"	"	"	"	↓	"
14	R-1-26,37	C-502	↓	↓	↓	↓	"	Rod Osc.	A-502	D-503	D-501	E-501	↓	RCP-1	RCP-2	FW	STM	C-501	B-503	↓	B-502
15	R-1-39,45	E-503	A-502	Rod Osc.	B-502	C-501	C-502	D-501	D-502	E-501	E-502	μμA	↓	- - -	B-201	B-503	D Temp.	A-503	D-503	D-201	E-201
16	R-1-48a	E-201	↓	A-503	E-201	E-502	E-503	μμA	RCP-1	RCP-2	FW	STM	↓	A-301	A-302	E-301	E-302	A △ T	E △ T	C-501	- - -
16	R-1-51	B-201	↓	"	B-501	B-502	B-503	"	"	"	"	"	↓	"	"	B-301	B-302	"	B △ T	"	- - -
16	R-1-59	FW	B-201	C-201	D-201	E-201	B-501	C-501	D-501	E-501	μμA	"	↓	RCP-1	RCP-2	A-502	D-502	D-503	D △ T	C △ T	- - -
16	R-1-49a,b	D-201	C-201	D-501	D-502	D Temp	C-501	C-502	C Temp	μμA	RCP-1	RCP-2	↓	B-201	E-201	D-503	D-301	D-302	A-301	A-302	- - -
17	20-1-1a,2	B-201	↓	D-201	E-201	Rod Osc.	μμA	B-502	D-501	B-501	C-501	Press.	RCP-1	RCP-2	FW	"	A-502	C-502	D-502	E-502	E-501
18	20-1-2a,9	↓	↓	↓	↓	"	↓	"	E-503	B-503	- - -	"	"	"	"	"	↓	"	"	"	↓
18	20-1-13,20	↓	↓	↓	↓	E-502	↓	RCP-1	RCP-2	FW	STM	D-503	Press.	E-503	D-301	D-501	↓	B-502	C-502	D-502	↓
18	20-3-14,16	↓	↓	↓	↓	"	↓	"	"	"	"	"	↓	"	"	"	↓	"	"	"	↓
21	20-1-1a,b	D Temp	↓	↓	↓	D-503	↓	D-501	D-502	C-502	E-501	E-502	↓	RCP-1	B-503	FW	↓	B-503	E-503	A-503	- - -
21	20-1-1c, 11a	"	↓	↓	↓	Rod Osc.	↓	↓	↓	"	D-503	"	↓	"	"	"	↓	B-502	"	"	- - -
21	15-2-1,12	FW	↓	↓	↓	↓	↓	↓	↓	D-503	- - -	C-502	↓	A-502	A-503	B-502	B-503	E-501	E-502	E-503	- - -
22	15-9-1,13	"	↓	↓	↓	↓	↓	↓	- - -	"	- - -	"	- - -	"	"	"	E-503	"	"	- - -	- - -
23	15-7-0,12	"	↓	↓	↓	↓	↓	↓	D-502	"	- - -	"	Press	"	"	"	"	"	"	- - -	STM
24	15-10-1a,14a	Press.	D-201	E-201	Rod Osc.	μμA	D-501	D-502	D-503	E-501	E-502	E-503	C-502	B-502	B-503	A-502	A-503	RCP-1	FW	- - -	↓
24	15-6a-1,1b	C-201	"	"	"	↓	"	"	"	"	"	"	"	"	"	"	"	"	"	- - -	↓
24	15-11-3a,15	"	"	"	RCP-1	↓	Rod Osc.	"	"	"	D-501	"	"	"	"	"	"	B-502	"	- - -	↓
25	20-3-17a,19	FW	RCP-1	STM	Press.	↓	C-201	D-201	E-201	A-502	B-502	C-502	D-502	E-502	D-501	D-503	D △ T	C △ T	B △ T	- - -	A △ T
25	15-3-14a,14c	"	"	"	"	↓	"	"	"	"	"	"	"	"	"	"	"	"	"	- - -	"
28	15-7a-1,2	C-201	D-201	E-201	RCP-2	Rod Osc	μμA	D-501	D-502	C-201 Pulse	D-503	D-201 Pulse	E-201 Pulse	Press.	A-503	E-501	E-502	E-503	C-502	- - -	B-503
28	15-7a-2a	↓	↓	↓	↓	↓	↓	↓	↓	- - -	- - -	- - -	- - -	- - -	- - -	- - -	- - -	- - -	- - -	- - -	- - -
29	15-7a-3,19	↓	↓	↓	↓	↓	↓	↓	↓	C-201 Pulse	- - -	D-201 Pulse	E-201 Pulse	- - -	B-501	C-501	C-502	C-503	E-501	- - -	E-503
29	15-6a-2,9	↓	A-501	↓	↓	↓	↓	↓	↓	"	- - -	A-502	"	- - -	↓	↓	↓	↓	↓	- - -	↓
30	15-6b-1,16	↓	D-201	↓	↓	Rod Pos.	↓	↓	↓	C Pulses	- - -	E Pulses	D Pulses	- - -	↓	↓	↓	↓	↓	- - -	↓
30	15-6a-9,23	↓	↓	↓	↓	↓	↓	↓	↓	↓	- - -	↓	↓	- - -	↓	↓	↓	↓	↓	- - -	↓
30	15-7-13,27	↓	↓	↓	↓	↓	↓	↓	↓	↓	- - -	↓	↓	- - -	↓	↓	↓	↓	↓	- - -	↓

FW = FEEDWATER

* Channel 9 Ampex Track

** Channel 10 Recorder

APPENDIX F

INDEX OF INSTRUMENT HOOK-UPS
FUEL CYCLE STABILITY TESTS

DATE	RUN NO.	CHANNEL NUMBERS 1	2	3	4	5	6	7	8	9 *	10 **	11	12	13	14	15	16	17	18	19	20
Dec. 1, 1961	15-4-1,4	C-201	D-201	E-201	RCP-2	Rod Pos.	μμA	D-501	D-502	C Pulses	- - -	E Pulses	D Pulses	Press.	B-501	C-501	C-502	C-503	E-501	- - -	E-503
1	15-6a-17,24					FW		STM Flow	Pressure		- - -			C-501	- - -	C-502	D-501	D-502		- - -	E-502
1	15-6b-17,18					"		" "	"		- - -			"	- - -					- - -	
1	15-7-28,29					"		" "	"		- - -			"	- - -					- - -	
1	15-2-1,17					Rod Pos		C-501	E-501		- - -			D-501	- - -		E-502	E-503	D-502	- - -	Press.
2	15-8-1,8				RCP-1				"		- - -				- - -	- - -				- - -	"
3	15-8-9,20								C-502		- - -				- - -	Press.				- - -	- - -
3	15-9-14,26		D-503								D Pulse		- - -		- - -					- - -	- - -
4	R-4-1,15		E-201	D-503							C-503 @		- - -		- - -					- - -	- - -
4	20-2-1,22			"		B-502 Rod Pos.					C-503 @		- - -		- - -					- - -	- - -
5	15-1-1,17			RCP-1	RCP-2	Rod Pos.				C-503	C Pulse		- - -	D-502	D-503				D-501	- - -	B-503
5	20-3-1,13			"	B-502	"				"			- - -	"	"				"	- - -	"
9	20-9-1,25			E-502	"	A-502 Rod Pos.				"			C-503	- - -	- - -	D-501	D-502	D-503	B-503	- - -	A-503
11	17.5-1-1,17			"	"	Rod Pos.				E-503			D-501	- - -	- - -	A-502	"			- - -	"
11	15-18-1,17a			D-501	Chan. Not Op.	"		C-502 Noisy	D-502	C-503			A-503	- - -	- - -	"	FW			- - -	C-502
	12-5-1 10-1 9-1																				
14	15-13a-1,16	C-201	E-201	μμA	Rod Pos	B-503 RCP-1	A-501	A-502	A-503	RCP-1 E-101	C-Pulse	E-Pulse	B-501	B-502	FW						
14	15-16-1,16					RCP-1				E-101											
15	15-14-1,15									"											
15	15-15-1,16									E-103											
15	15-12-1				RCP-2					"											
27	15-6a-2,16				Rod Pos.	RCP-2				C-502			- - -	- - -	- - -						
27	0-2-1,15					- - -							- - -	- - -	- - -						
28	15-19-2,17					RCP-2							- - -	- - -	- - -						

FW = FEEDWATER

* Channel 9 Ampex Track

** Channel 10 Recorder

● Channel 10 On Tape - Channel 12 On Brush

APPENDIX F

INDEX OF REACTOR OPERATING PARAMETERS

FUEL CYCLE STABILITY TEST

DATE	RUN NO.	POWER MW	μμA #1	μμA #2	RCP FLOW #1 10^3 GPM	RCP FLOW #2 10^3 GPM	RCP-2 D.P. FT.	FLOW FW 10^3 LB/HR	FLOW CLEAN UP GPM	CONTROL ROD POSITION 1	2	3	4	5	6	7	TESTS MADE S S NZS	S S ZS	R.O.	R.C	W.L.	T Re-Circ.	T F.W.	T STM	H.B.	Operating Conditions
Nov. 3, 1961	0-1-4,5,6	0	2.5^{-6}	1.1^{-6}	13.4	0	0	0	0	345	345	345	345	345	345	600		X	X							
4	0-1-7a,21a	0	2.7^{-6}	- - -	9.8	0	0	0	10	385	385	385	385	385	414	600			X	X						
6	R-1-1-14	26	2.9^{-5}	4.0^{-5}	9.9	10.1	225	99.9	0	775	775	770	766	751	751	576		X			X					
7	R-1-17-24a	26	2.8^{-5}	3.8^{-5}	10.15	9.5	218	81.0	0	948	900	937	947	915	958	588		X	X						X	
14	R-1-26,37	26	2.25^{-5}	- - -	9.6	9.8	215	85.0	10.2	905	905	905	905	905	905	594	X	X	X							
15	R-1-39,60	26	2.3^{-5}	3.4^{-5}	10.0	9.6	219	75.0	10.0	948	950	937	947	941	958	534	X	X	X					X	X	Flux Wire
16	R-1-48a,60	26	2.2^{-5}	2.4^{-5}	10.05	9.75	157	75.0	10	948	950	937	947	941	968	519	X	X						X	X	Irradiation
17	20-1-1a,11	20	1.65^{-5}	2.6^{-5}	10.8	9.7	218	59.0	3	948	950	937	947	941	966	462	X	X	X							
18	20-1-13,20	20	3.5^{-5}	2.4^{-5}	10.0	9.8	210	58.0	3	680	680	680	680	680	681	578					X					
18	20-3-14,16	20	3.5^{-5}	2.4^{-5}	10.0	0	- -	55.0	3	800	800	800	800	800	800	601					X					
21	20-1-1a,11a	20	3.6^{-5}	2.4^{-5}	10.2	0	- -	49.0	7	642	641	641	641	641	641	603	X	X	X							
21	15-2-1,13	15	2.7^{-5}	1.9^{-5}	10.1	0	- -	34.0	7	661	660	671	660	660	671	604	X	X	X						X	
22	15-9-1,13a	15	2.7^{-5}	1.95^{-5}	4.0	0	- -	38.0	7.5	703	708	700	696	781	701	604	X	X	X						X	
23	15-7-0,12	15	2.7^{-5}	1.9^{-5}	7.0	0	- -	37.5	14.5	771	771	775	775	775	775	603	X	X	X							
25	20-3-17a,20	20	3.5^{-5}	2.55^{-5}	10.05	0	- -	55.0	12	887	886	885	884	885	885	558	X	X				X	X	X	X	
25	15-3-14a,17	15	2.7^{-5}	1.95^{-5}	9.85	0	- -	37.5	12	749	749	749	749	749	749	567	X	X				X	X	X	X	
28	15-7a-1,2a	15	2.7^{-5}	1.95^{-5}	0	7.0	20	37.0	7.5	645	645	645	645	642	645	556	X	X								
29	15-7a-3,19	15	2.7^{-5}	1.9^{-5}	0	7.0	18	37.0	5	730	730	710	730	730	610	603	X	X	X						X	
29	15-6a-2,9	15	2.7^{-5}	1.9^{-5}	0	5.65	34	37.0	4	735	730	730	735	735	735	603	X	X	X						X	
30	15-6b-1,16	15	0.27^{-4}	0.195^{-4}	0	4.0	58	41	12	801	801	801	801	727	892	604	X	X	X							Forced Circulation
30	15-6a-9,23	15	0.27^{-4}	0.19^{-4}	0	5.55	36	40	11.5	841	841	842	841	842	842	603	X	X	X							"
30	15-7-13,27	15	0.27^{-4}	0.19^{-4}	0	7.05	19	39.5		825	812	800	800	800	801	603	X	X	X							"

APPENDIX F

INDEX OF REACTOR OPERATING PARAMETERS

FUEL CYCLE STABILITY TEST

DATE	RUN NO.	POWER MW	μμA #1	μμA #2	RCP FLOW #1 10^3 GPM	RCP FLOW #2 10^3 GPM	RCP-2 D.P. FT.	FLOW F.W. 10^3 LB/HR	FLOW CLEAN UP GPM	CONTROL ROD POSITION 1	2	3	4	5	6	7	TESTS MADE S S NZS	S S ZS	R.O.	R.C.	W.L.	T Re-Circ.	T F.W.	T STM	H.B.	Operating Conditions
Dec. 1, 1961	15-4-1,14	15	0.27^{-4}	- -	0	10.0	58	40.0	11.5	750	750	751	750	754	751	601	X	X	X							Forced Circulation
1	15-6a-17,24	15	0.27^{-4}	- -	0	5.55	42	41.0	11.5	835	835	835	835	835	831	603						X				"
1	15-6b-17,18	15	0.27^{-4}	- -	0	4.2	60	36.0	11.5	835	835	835	835	830	831	604	X					X				"
1	15-7-28,29	15	- -	0.19^{-4}	0	6.9	41	20.0		835	→					568	X					X				"
1	15-2-1,17	15	- -	0.19^{-4}	0	13.1	98	42.5	11.5	710	→					604	X	X	X							
2	15-8-1,8	15	0.27^{-4}	0.195^{-4}	5.4	0	0	43.	16	895	894	886	900	897	899	604	X	X	1/2							"
3	15-8-9,20	15	0.27^{-4}	- - -	5.4	0	0	40.	11	735	736	736	737	735	751	603	X	X	1/2							"
3	15-9-14,26	15	0.26^{-4}	- - -	3.95	0	0	39	11	752	752	752	752	752	752	603	X	X	X							"
4	R-4-1,15	(15) 26	0.32^{-4}	0.45^{-4}	10.1	9.9	162	73	11	890	890	888	882	882	882	603	X	X	X							"
4	20-2-1,22	20	0.37^{-4}	0.25^{-4}	13.1	0	0	56	11	948	950	937	947	941	965	590	X	X	X		X					"
5	15-1-1,17	15	0.27^{-4}	0.2^{-4}	10.2	9.3	158	44	10.7	709	706	706	709	709	709	602	X	X	X							"
5	20-3-1,13	20	0.34^{-4}	0.25^{-4}	10.3	0	0	55		948	950	937	947	941	948	570	X	X	X							"
9	20-9-1,26	20	0.35^{-4}	0.25^{-4}	Nat.	- -	- -	50	3	769	768	774	767	768	768	570	X	X	X		X				X	Natural Circulation
11	17.5-1-1,17	17.5	0.29^{-4}	- - -	Nat.	- -	- -	44	8.5	771	→					679	X	X	X							"
11	15-18-1,17a	15	0.26^{-4}	- - -	Nat.	- -	- -	37	8.5	760	→					679	X	X	X							"
11 11 11	12-5-1 10-1 9-1																									
14	15-13a-1,16	15	0.26^{-4}	0.2^{-4}	10.0	0	0	34	3	777	731	800	765	745	758	678	X	X	X							Forced Circulation W/Baffles
14	15-16-1,16	15	0.26^{-4}	0.19^{-4}	4.1	0	0	35	3	702	700	715	699	699	705	678	X	X	X							Open
15	15-14-1,15	15	0.26^{-4}	0.19^{-4}	6.9	0	0	34	5	810	→					678	X	X	X							"
15	15-15-1,16	15	0.25^{-4}	0.19^{-4}	5.4	0	0	34	4	790	→					678	X	X	X							"
15	15-12-1	15	0.25^{-4}	0.19^{-4}	5.6	4.6	113	33		831	→	→	833	831	844	678	X	X								"
27	15-6a-2,16	15	0.22^{-4}	0.17^{-4}	0	5.7	↳ 8	40	10	887	→					604	X	X	X							Forced Circulation Low Head (Core Rev.)
27	0-2-1,15	1	0.14^{-5}	0.195^{-5}	10	0	0	0		511	512	511	511	510	548	603	X	X	X							
28	15-19-2,17	15	0.21^{-4}		0	4.4	↳ 1 (?)	35		751	751	771	751	766	761	604	X	X	X							

D.P. = Differential Pressure (pump head)
F.W. = Feedwater
H.B. = Heat Balance
R.C. = Rod Calibration
R.O. = Rod Oscillator
RCP = Recirculation Pump

S.S. = Steady-State
STM = Steam
T = Transient
μμA = External Neutron Flux (Micro-microammeter)
W.L. = Water Level
Z.S. = Zero Suppressed

NZS = Non-Zero Suppressed
Nat. = Natural

NOMENCLATURE

π = Average two-phase pressure gradient divided by liquid density $\frac{1}{\rho_w}\left(\frac{\Delta P}{\Delta L}\right)$

S = Average steam velocity, ft/sec.

W = Average water velocity, ft/sec.

V = Inlet velocity at fuel element, ft/sec.

α = Subcooling factor = $\frac{h_w - h_{sc}}{h_{fg}}$ $\frac{\text{Subcooling enthalpy}}{\text{Vaporization enthalpy}}$, dimensionless.

Q = Heat factor = $\frac{Q}{A\rho_w h_{fg}}$ = heat input per unit flow area divided by the product of water density and vaporization enthalpy, ft/sec.

u = Void fraction at boiling boundry after heat input, dimensionless.

$\bar{u}$ = Average void fraction in the two-phase section of the core, dimensionless.

t = Time, seconds

τ_c = Core transient time, seconds

N = Power-neutron density, neutrons/cm

ΔK = Excess multiplication factor or delta K, dollars

ΔK voids, Delta K due to voids, dollars

ΔK rod, Delta K due to control rod, dollars

ℓ^* = Average neutron lifetime, sec.

t_i = Time constant of i^{th} delay group, sec.

β_i = Fraction of the delayed neutrons of the i^{th} group, dimensionless.

β = Total fraction of delayed neutron, dimensionless.

(s) = Complex place operator

NOMENCLATURE (Cont'd)

R = Average void fraction in total two-phase section, heater plus riser

$\mu\mu A$ = Micro-microammeter

ω = Frequency, rad/sec.

f_d = Damped frequency, cps

ζ = Quadratic damping coefficient

τ_o = ℓ^*/β

RCP = Recirculation pump

Superscripts

* normalized variation, = $\frac{\text{variation}}{\text{steady-state mean}}$

REFERENCES

SECTION I

1. ANL-6561, "Boiling Water Technology, Status of the Art Report", P. A. Lottes, et al. February, 1962.

SECTION VII-A

2. Internal Memorandum, Argonne National Laboratory, W. H. Cook.

3. ANL-6205 "Proceedings of the Conference on Transfer Function Measurement and Reactor Stability Analysis", May 2, 3, 1960. S. M. Zivi and Robert Wright.

4. ANL-6221, "Theoretical Feedback Analysis in Boiling Water Reactors", A. Z. Akcasu. October, 1960.

5. Personal Communication, L. Zettergren, Swedish Atomic Energy Authority.

SECTION VII-B

6. GEAP-3508, "Neutron and Parallel Flow Channel Coupling Effects on the T-7 Flux Trap Reactor", J. M. Case. August, 1960.

7. "Servo-Mechanisms and Regulating System Design", Vol. I, 2nd Edition, Harold Chestnut, Robert W. Mayer. John Wiley, 1959. pp 324-327.

8. GEAP-3550, "Dresden Reactor Stability Tests", E. S. Beckjord. Sept., 1960.

9. Transit Analysis of Nuclear Power Plants", A. B. Jones, ENGINEERING DATA BOOK, APED, May 13, 1959.

SECTION VII-C

10. ASME Paper 60 WA 209, "Oscillations in Two-Phase Flow Systems", Wallis and Heasley.

11. APDA-132, "Temperature Response to Power, Inlet Constant Temperature, and Flow Transients in Solid Fueled Reactors", F. Storrer, June 1959.

12. GEAP-4159, Fuel Cycle Development Program, 10th Quarterly Progress Report, Compiled by C. L. Howard. October - December, 1962.

    GEAP-4215, Fuel Cycle Development Program, 11th Quarterly Progress Report, Compiled by C. L. Howard. January - March, 1963.

REFERENCES (Cont'd)

SECTION VII-D

13. APDA-117, "Reactor Safety and Oscillator Tests", H.A. Bethe, October, 1956.

SECTION VIII

14. GEAP-3795, "Consumers Big Rock Point Nuclear Power Reactor Stability Analysis" J. M. Case, L. K. Holland.

15. GEAP-0805, "Heat Transfer from a Cylindrical Rod with Internal Heat Generation", L. K. Holland.

16. "VBWR Fuel Cycle Stability Test Predictions," Internal Memorandum, Nov. 10, 1961. J. M. Case, W. H. Cook, R. O. Niemi.

17. ANL-5798, "Power Transfer Functions of EBWR Obtained Using a Sinusoidal Reactivity Driving Function". J. A. De Shong, Jr., 1958.

18. ANL-6381, "Theoretical Study of Transient Operation and Stability of Two-Phase Natural Circulation Loops", K. Garlid, N. R. Amundson, H. S. Isbin.

Appendix A

19. SG VAL-2 "General Electric Vallecitos Boiling Water Reactor Final Hazards Summary Report", 3rd Edition, November 30, 1959. J. L. Murray, Editor.

Appendix C

20. "Transient Response of the Turbine Flowmeter", Jerry Gray, JET PROPULSION, February, 1956.

21. NBS Research Report RP-2116, "Attenuation of Oscillatory Pressures in Instrument Lines", Vol. 45, Washington, D. C., July, 1950. Arthur S. Iberall.

22. "Describing Uncertainties in Single Sample Experiments", S. J. Kline, F.A. McClintock, MECHANICAL ENGINEERING, January, 1953.

Appendix E

23. APED-4285, "VBWR Noise Analysis", P. R. Pluta.

24. "Some Comments on Spectral Analysis of Time Series", N. R. Goodman, pp 221 - 228, Vol. 3, No. 2, TECHNOMETRICS, May 1961.

REFERENCES (Cont'd)

25. "Selected Papers on Noise and Stochastic Processes", p. 137-294, S. O. Rice, Dover Publications.

26. "Principles and Applications of Random Noise Theory", Bendat, Wiley and Sons.

27. "The Measurement of Power Spectra", Blackman and Tuckey, Dover Publications.

28. RWD-RL-167, "Kinetic Studies of Heterogeneous Water Reactors", Technical Staff, Space Technology Laboratories, February, 1960.